
JSCSEN 80(8)971–1099(2015)

ISSN 1820-7421(Online)

Journal of the Serbian Chemical Society

Volume 80 :: 2015 :: 85 Years of the Journal

1930 Glasnik Hemिजkog Društva Kraljevine Jugoslavije

Journal of the Chemical Society of the Kingdom of Yugoslavia

1947 Glasnik hemijskog društva Beograd

Journal of the Chemical Society of Belgrade

1985 Journal of the Serbian Chemical Society

VOLUME 80

No 8

BELGRADE 2015

Available on line at



www.shd.org.rs/JSCS/

The full search of JSCS
is available through

DOAJ DIRECTORY OF
OPEN ACCESS
JOURNALS
www.doaj.org

The **Journal of the Serbian Chemical Society** (formerly Glasnik Hemijskog društva Beograd), one volume (12 issues) per year, publishes articles from the fields of chemistry. The **Journal** is financially supported by the **Ministry of Education, Science and Technological Development of the Republic of Serbia**.

Articles published in the **Journal** are indexed in **Thompson Reuters products: Science Citation Index-ExpandedTM** – accessed via **Web of Science[®]**, part of **ISI Web of KnowledgeSM** and **Journal of Citation Reports[®]**.

Impact Factor announced 2015: **0.871; 5-year Impact Factor: 1.009.**

Articles appearing in the **Journal** are also abstracted by: **Scopus, Chemical Abstracts Plus (CAplusSM), Directory of Open Access Journals, Referativni Zhurnal (VINITI), Analytical Abstracts and MINAS Online.**

Publisher:

Serbian Chemical Society, Karnegijeva 4/III, P. O. Box 36, 1120 Belgrade 35, Serbia
tel./fax: ++381–11–3370–467, E-mails: **Society** – shd@shd.org.rs; **Journal** – jscs@shd.org.rs

Internet Service:

Home Pages: **Society** – <http://www.shd.org.rs/>; **Journal** – <http://www.shd.org.rs/JSCS/>
Contents, Abstracts and full papers (from Vol 64, No. 1, 1999) are available in the electronic form at the Web Site of the **Journal** (<http://www.shd.org.rs/JSCS/>).

Former Editors:

Nikola A. Pušin (1930–1947), Aleksandar M. Leko (1948–1954), Panta S. Tutundžić (1955–1961), Miloš K. Mladenović (1962–1964), Đorđe M. Dimitrijević (1965–1969), Aleksandar R. Despić (1969–1975), Slobodan V. Ribnikar (1975–1985), Dragutin M. Dražić (1986–2006). BRANISLAV Ž. NIKOLIĆ, Serbian Chemical Society (E-mail: jscs-ed@shd.org.rs)

Editor-in-Chief:

DUŠAN SLADIĆ, Faculty of Chemistry, University of Belgrade

Deputy Editor:

Sub editors:

Organic Chemistry

DEJAN OPSENICA, Institute of Chemistry, Technology and Metallurgy, University of Belgrade
JÁNOS CSANÁDI, Faculty of Science, University of Novi Sad

Biochemistry and Biotechnology

OLGICA NEDIĆ, INEP – Institute for the Application of Nuclear Energy, University of Belgrade
MILOŠ ĐURAN, Faculty of Science, University of Kragujevac

Inorganic Chemistry

IVAN JURANIĆ, Serbian Chemical Society

Theoretical Chemistry

LJILJANA DAMJANOVIĆ, Faculty of Physical Chemistry, University of Belgrade

Physical Chemistry

SNEŽANA GOJKOVIĆ, Faculty of Technology and Metallurgy, University of Belgrade

Electrochemistry

SLAVICA RAŽIĆ, Faculty of Pharmacy, University of Belgrade

Analytical Chemistry

JASNA ĐONLAGIĆ, Faculty of Technology and Metallurgy, University of Belgrade

Polymers

MIRJANA KIJEVČANIN, Faculty of Technology and Metallurgy, University of Belgrade

Thermodynamics

MENKA PETKOVSKA, Faculty of Technology and Metallurgy, University of Belgrade

Chemical Engineering

RADA PETROVIĆ, Faculty of Technology and Metallurgy, University of Belgrade

Materials

NENAD RADOVIĆ, Faculty of Technology and Metallurgy, University of Belgrade

Metallic Materials and Metallurgy

BOJAN RADAK, Vinča Institute of Nuclear Science, University of Belgrade

Environmental and Geochemistry

History of and Education in Chemistry DRAGICA TRIVIĆ, Faculty of Chemistry, University of Belgrade

English Language Editor:

LYNNNE KATSIKAS, Faculty of Technology and Metallurgy, University of Belgrade

Technical Editors:

VLADIMIR PANIĆ, ALEKSANDAR DEKANSKI, Institute of Chemistry, Technology and Metallurgy, University of Belgrade

Journal Manager & Web Master:

ALEKSANDAR DEKANSKI, Institute of Chemistry, Technology and Metallurgy,

Office:

University of Belgrade
VERA ĆUSIĆ, Serbian Chemical Society, Karnegijeva 4/III, P. O. Box 36, 1120 Belgrade 35, Serbia (E-mail: jscs-info@shd.org.rs)

Editorial Board

From abroad: R. Adžić, Brookhaven National Laboratory (USA); A. Casini, University of Groningen (The Netherlands); G. Cobb, Baylor University (USA); D. Douglas, University of British Columbia (Canada); G. Inzelt, Etvos Lorand University (Hungary); A. R. Katritzky, FRS, University of Florida (USA); N. Katsaros, NCSR “Demokritos”, Institute of Physical Chemistry (Greece); J. Kenny, University of Perugia (Italy); Ya. I. Korenman, Voronezh Academy of Technology (Russian Federation); M. D. Lechner, University of Osnabrueck (Germany); S. Macura, Mayo Clinic (USA); M. Spitteler, INFU, Technical University Dortmund (Germany); M. Stratakis, University of Crete (Greece); M. Swart, University of Girona (Cataluna, Spain); G. Vunjak-Novaković, Columbia University (USA); P. Worsfold, University of Plymouth (UK); J. Zagal, Universidad de Santiago de Chile (Chile).

From Serbia: B. Abramović, T. Ast, J. Csanadi, Ž. Čeković, Lj. Damjanovic, A. Dekanski, V. Dondur, J. Đonlagić, B. Đorđević, M. Duran, M. J. Gašić, S. Gojković, I. Gutman, B. Jovančićević, M. Jovanović, I. Juranić, L. Katsikas, M. Kijevčanin, V. Leovac, S. Milonjić, U. Mioč, J. Nedeljković, O. Nedić, B. Nikolić, D. Opsenica, V. Panić, V. Pavlović, M. Petkovska, R. Petrović, I. Popović, P. Premović, B. Radak, N. Radović, S. Ražić, D. Sladić, S. Sovilj, M. Spasić, S. Serbanović, B. Solaja, Ž. Tešić, D. Trivić, D. Vitorović.

Subscription: The annual subscription rate is **150.00 €** including postage (surface mail) and handling. For Society members from abroad rate is **50.00 €**. For the proforma invoice with the instruction for bank payment contact the Society Office (E-mail: shd@shd.org.rs) or see JSCS Web Site: <http://www.shd.org.rs/JSCS/>, option Subscription.

Godišnja preplata: Za članove SHD: **2.500,00 RSD**, za penzionere i studente: **1000,00 RSD**, a za ostale: **3.500,00 RSD**:za organizacije i ustanove: **16.000,00 RSD**. Uplate se vrše na tekući račun Društva: **205-13815-62**, poziv na broj **320**, sa naznakom “preplata za JSCS”.

Nota: Radovi čiji su svi autori članovi SHD prioritetno se publikuju.

Odlukom Odbora za hemiju Republičkog fonda za nauku Srbije, br. 66788/1 od 22.11.1990. godine, koja je kasnije potvrđena odlukom Savjeta Fonda, časopis je uvršten u kategoriju međunarodnih časopisa (**M-23**). Takođe, aktom Ministarstva za nauku i tehnologiju Republike Srbije, 413-00-247/2000-01 od 15.06.2000. godine, ovaj časopis je proglašen za publikaciju od posebnog interesa za nauku. **Impact Factor** časopisa objavljen 2015. godine iznosi **0,871**, a petogodišnji **Impact Factor 1,009**.

INSTRUCTIONS FOR AUTHORS (2013)

GENERAL

The *Journal of the Serbian Chemical Society* is an international journal publishing papers from all fields of chemistry and related disciplines. Twelve issues are published annually. The Editorial Board expects the editors, reviewers and authors to respect the well-known standard of professional ethics.

Types of Contributions

<i>Original scientific papers</i>	(about 10 typewritten pages) report original research which must not have been previously published.
<i>Short communications</i>	(about 5 pages) report unpublished preliminary results of sufficient importance to merit rapid publication.
<i>Notes</i>	(about 3 pages) report unpublished results of short, but complete, original research.
<i>Authors' reviews</i>	(about 30 pages) present an overview of the author's current research with comparison to data of other scientists working in the field.
<i>Reviews</i>	(about 30 pages) present a concise and critical survey of a specific research area.
<i>Surveys</i>	(about 15 pages) communicate a short reviews of a specific research area.
<i>Book and Web site reviews</i>	(1–2 pages)
<i>Extended abstracts</i>	(about 3 pages) of Lectures given at meetings of the Serbian Chemical Society Divisions.

Generally, Authors' reviews, Reviews and Surveys are prepared at the invitation of the Editor.

Submission of manuscripts

Manuscripts should be submitted using the [OnLine Submission Form](#), available on the JSCS Web Site (www.shd.org.rs/JSCS/Form/). The manuscript must be uploaded as a Word.doc or .rtf file (tables and figures should follow the text, each on a separate page). Illustrations in TIF or EPS format (JPG format is acceptable for colour and greyscale photos, only), must be additionally uploaded as a separate archived (.zip, .rar or .arj) file. Figures and/or Schemes should be prepared according to the [Artwork Instructions](#).

Manuscripts must be accompanied by a cover letter in which the type of the submitted manuscript and a warranty as given below are given. The Author warranties that the manuscript submitted to the *Journal* for review is original, has been written by the stated authors and has not been published elsewhere; is currently not being considered for publication by any other journal and will not be submitted for such a review while under review by the *Journal*; the manuscript contains no libellous or other unlawful statements and does not contain any materials that violate any personal or proprietary rights of any other person or entity. All manuscripts will be acknowledged on receipt (by e-mail) and given a reference number, which should be quoted in all subsequent correspondence. A password for "Article Tracking" (www.shd.org.rs/JSCS/) will also be supplied.

A MANUSCRIPT NOT PREPARED ACCORDING TO THESE INSTRUCTIONS WILL BE RETURNED FOR RESUBMISSION WITHOUT BEING ASSIGNED A REFERENCE NUMBER.

Conflict-of-Interest Statement*: Public trust in the peer review process and the credibility of published articles depend in part on how well conflict of interest is handled during writing, peer review, and editorial decision making. Conflict of interest exists when an author (or the author's institution), reviewer, or editor has financial or personal relationships that inappropriately influence (bias) his or her actions (such relationships are also known as dual commitments, competing interests, or competing loyalties). These relationships vary from those with negligible potential to those with great potential to influence judgment, and not all relationships represent true conflict of interest. The potential for conflict of interest can exist whether or not an individual believes that the relationship affects his or her scientific judgment. Financial relationships (such as employment, consultancies, stock ownership, honoraria, paid expert testimony) are the most easily identifiable conflicts of interest and the most likely to undermine the credibility of the journal, the authors, and of science itself. However, conflicts can occur for other reasons, such as personal relationships, academic competition, and intellectual passion.

Informed Consent Statement*: Patients have a right to privacy that should not be infringed without informed consent. Identifying information, including patients' names, initials, or hospital numbers, should not be published in written descriptions, photographs, and pedigrees unless the information is essential for scientific purposes and the patient (or parent or guardian) gives written informed consent for publication. Informed consent for this purpose requires that a patient who is identifiable be shown the manuscript to be published. Authors should identify individuals who provide writing assistance and disclose the funding source for this assistance. Identifying details should be omitted if they are not essential. Complete anonymity is difficult to achieve, however, and informed consent should be obtained if there is any doubt. For example, masking the eye region in photographs of patients is inadequate protection of anonymity. If identifying characteristics are altered to protect anonymity, such as in genetic pedigrees, authors should provide assurance that alterations do not distort scientific meaning and editors should so note. The requirement for informed consent should be included in the journal's instructions for authors. When informed consent has been obtained it should be indicated in the published article.

Human and Animal Rights Statement*: When reporting experiments on human subjects, authors should indicate whether the procedures followed were in accordance with the ethical standards of the responsible committee on human experimentation (institutional and national) and with the Helsinki Declaration of 1975, as revised in 2000 (5). If doubt exists whether the research was conducted in accordance with the Helsinki Declaration, the authors must explain the rationale for their approach, and demonstrate that the institutional review body explicitly approved the doubtful aspects of the study. When reporting experiments on animals, authors should be asked to indicate whether the institutional and national guide for the care and use of laboratory animals was followed.

**For detailed instructions please visit the JSCS website:
<http://www.shd.org.rs/JSCS/JSCS-instruction.HTM>**

* International Committee of Medical Journal Editors ("Uniform Requirements for Manuscripts Submitted to Biomedical Journals") -- February 2006

PROCEDURE

All contributions will be peer reviewed and only those deemed worthy will be accepted for publication. The Editor has the final decision. To facilitate the reviewing process, authors are encouraged to suggest up to three persons competent to review their manuscript. Such suggestions will be taken into consideration but not always accepted.

Manuscripts requiring revision should be returned according to the requirement of the Editor, within 60 days or the manuscript will be considered as having been withdrawn. Later, the manuscript would have to be resubmitted.

The *Journal* maintains its policy and takes the liberty of correcting the English of manuscripts scientifically accepted for publication.

When a manuscript is ready for printing, the corresponding author will receive a PDF-formatted manuscript for proof reading, which should be returned to the *Journal* within 2 days. Failure to do so will be taken as the authors are in agreement with any alteration which may have occurred during the preparation of the manuscript.

Accepted manuscripts of active members of the Serbian Chemical Society (all authors) have publishing priority.

The corresponding author will receive by e-mail a PDF-formatted version of the paper as published in the journal.

MANUSCRIPT PRESENTATION

Manuscripts should be typed in English (either standard British or American English, but consistent throughout) with 1.5 spacing (12 points Times New Roman; Greek letters in the character font Symbol) in A4 format leaving 2.5 cm for margins. For Regional specific, non-standard save documents with Embed fonts Word option: *Save as -> (Tools) -> Save Options... -> Embed fonts in the text*.

The authors are requested to seek the assistance of competent English language expert, if necessary, to ensure their English is of a reasonable standard. The Serbian Chemical Society can provide this service in advance of submission of the manuscript. If this service is required, please contact the office of the Society by e-mail (jscs-info@shd.org.rs).

Tables and figures and/or schemes should not be embedded in the manuscript but their position in the text indicated. In electronic version (Word.doc document) tables and figures and/or schemes should follow the text, each on a separate page. Please number all pages of the manuscript including separate lists of references, tables and figures and their captions.

IUPAC recommendations for the naming of compounds should be followed. SI units, or other permissible units, should be employed. The designation of physical quantities must be in italic throughout the text (including figures, tables and equations), whereas the units are in upright letters. They should be in Times New Roman font. In graphs and tables, a slash should be used to separate the designation of a physical quantity from the unit (example: p / kPa , $t / ^\circ\text{C}$, T / K , $\tau / \text{h}...$). Designations such as: $p (\text{kPa})$, $t [\text{min}]...$, are not acceptable. However, if the full name of a physical quantity is unavoidable, it should be given in upright letters and separated from the unit by a comma (example: Pressure, kPa, Temperature, K...). Please do not use the axes of graphs for additional explanations; these should be mentioned in the figure captions and/or the manuscript (example: "pressure at the inlet of the system, kPa" should be avoided). The axis name should follow the direction of the axis (the name of y-axis should be rotated by 90°). Top and right axes should be avoided in diagrams, unless they are absolutely necessary.

Latin words, as well as the names of species, should be in *italic*, as for example: *i.e.*, *e.g.*, *in vivo*, *ibid*, *Calendula officinalis L.*, etc. The branching of organic compound should also be indicated in *italic*, for example, *n*-butanol, *tert*-butanol, etc.

Decimal numbers must have decimal points and not commas in the text (except in the Serbian abstract), tables and axis labels in graphical presentations of results.

Title page.

Title in bold letters, should be clear and concise, preferably 12 words or less. The use of non-standard abbreviations, symbols and formulae is discouraged.

AUTHORS' NAMES in capital letters with the full first name, initials of further names separated by a space and surname. Commas should separate the author's names except for the last two names when 'and' is to be used. In multi-affiliation manuscripts, the author's affiliation should be indicated by an Arabic number placed in superscript after the name and before the affiliation. Use * to denote the corresponding author(s).

Affiliations should be written in italic. The e-mail address of the corresponding author should be given after the affiliation(s).

Abstract: A one-paragraph abstract written of 150–200 words in an impersonal form indicating the aims of the work, the main results and conclusions should be given and clearly set off from the text. Domestic authors should also submit, on a separate page, an Abstract – Izvod, the author's name(s) and affiliation(s) in Serbian (Latin letters). For authors outside Serbia, the Editorial Board will provide a Serbian translation of their English abstract.

Keywords: Up to 6 keywords should be given. Do not use words appearing in the manuscript title

RUNNING TITLE: A one line (maximum five words) short title in capital letters should be provided.

Main text.

The main text should have the form: INTRODUCTION, EXPERIMENTAL (RESULTS AND DISCUSSION), RESULTS AND DISCUSSION (EXPERIMENTAL), CONCLUSIONS, NOMENCLATURE (optional), Acknowledgements: If any, REFERENCES (Citation of recent papers published in chemistry journals that highlight the significance of work to the general readership is encouraged.)

The sections should be arranged in a sequence generally accepted for publication in the respective fields. They subtitles should be in capital letters, centred and NOT numbered.

The INTRODUCTION should include the aim of the research and a concise description of background information and related studies directly connected to the paper.

The EXPERIMENTAL section should give the purity and source of all employed materials, as well as details of the instruments used. The employed methods should be described in sufficient detail to enable experienced persons to repeat them. Standard procedures should be referenced and only modifications described in detail. On no account should results be included in the experimental section.

The RESULTS AND DISCUSSION should include concisely presented results and their significance discussed and compared to relevant literature data. The results and discussion may be combined or kept separate.

The inclusion of a CONCLUSION section, which briefly summarizes the principal conclusions, is highly recommended. NOMENCLATURE is optional but, if the authors wish, a list of employed symbols may be included.

REFERENCES should be numbered sequentially as they appear in the text. When cited in the text, the reference number should be superscripted in Font 12, following any punctuation mark. In the reference list, they should be in normal position followed by a full stop. Reference entry must not be formatted using Carriage returns (enter key; ↵ key) or multiple space key. The formatting of references to published work should follow the *Journal's* style as follows:

- | | |
|---------------------|---|
| Journals*: | 1. A. B. Surname1, C. D. Surname2, <i>J. Serb. Chem. Soc.</i> Vol. (Year) first page Number |
| Books: | 2. A. B. Surname1, C. D. Surname2, <i>Name of Book</i> , Publisher, City, Year, p. 100 |
| Compilations: | 3. A. B. Surname1, C. D. Surname2, in: <i>Name of Compilation</i> , A. B. Editor1, C. D. Editor2, Ed(s), Publisher, City, Year, p. 100 |
| Proceedings: | 4. A. B. Surname1, C. D. Surname2, , in: <i>Proceeding of Name of the Conference or Symposium, Title of the Proceeding</i> , (Year of publishing), Place of the Conference, Country, Year, p. 100 |
| Patents: | 5. A. B. Inventor1, C. D. Inventor2, (Holder), Country Code and patent number (registration year) |
| Chemical Abstracts: | 6. A. B. Surname1, C. D. Surname2, Chem. Abstr. CA 234 567a
For non-readily available literature, the Chemical Abstracts reference should be given in square brackets: [C.A. 139/2003 357348t] after the reference |
| Standards: | 7. EN ISO 250: <i>Name of the Standard</i> (Year) |
| Websites: | 8. Title of the website, URL in full (date accessed) |

* International Library Journal abbreviation is required. Please consult e.g. <http://www.library.ubc.ca/scieng/coden.html>

Only the last entry in the reference list should end with a full stop.

The names of all authors should be given in the list of references; the abbreviation *et al.* may only be used in the text. The original journal title is to be retained in the case of publications published in any language other than English (please denote the language in parenthesis after the reference). Titles of publications in non-Latin alphabets should be transliterated. Russian references are to be transliterated using the following transcriptions:

к→zh, х→kh, ү→ts, ң→ch, ى→sh, ە→sheh, ы→y, ى→yu, я→ya, ә→e, ى→i, ې→’.

Table Captions. A separate list of table captions, which makes the tables comprehensible without reference to the text, should be provided in numerical order on a separate page.

Tables. Tables are part of the text but must be given on separate pages. The tables should be numbered consequently in Roman numbers. Quantities should be separated from units by a slash (/). Footnotes to tables, in size 10 font, are to be indicated consequently (line-by-line) in superscript letters. Tables should be prepared with the aid of the WORD table function, without vertical lines. The minimum size of the font in the tables should be 10 pt. Table columns must not be formatted using multiple spaces. Table rows must not be formatted using Carriage returns (enter key; ↵ key). Tables should not be incorporated as graphical objects. In setting up tables, Authors should keep in mind the area of the *Journal's* page (12.5 cm × 19 cm) and should make tables conform to the limitations of these dimensions.

Figure and/or Scheme Captions. A separate list of figure and/or scheme captions, which makes the figures and/or schemes comprehensible without reference to the text, should be provided in numerical order on a separate page.

Figures and/or Schemes. Figures and/or Schemes (of moderate resolution) should follow the captions, each on a separate page of the manuscript. High resolution illustrations in TIF or EPS format (JPG format is acceptable for colour and greyscale photos, only) must be uploaded as a separate archived (.zip, .rar or .arj) file.

Mathematical and chemical equations must be numbered, Arabic numbers, consecutively in parenthesis at the end of the line. All equations should be embedded in the text except when they contain graphical elements (tables, figures, schemes and formulae). Complex equations (fractions, integrals, matrix...) should be prepared with the aid of the WORD Equation editor.

Reporting analytic and spectral data: Adequate evidence to enable the identity and purity of all newly synthesized compounds should be provided. The styles for the presentation of analytical and spectral data, which should be strictly adhered to (including the order), are as follows:

Compound (3a). Yield: 60 %; m.p. 120 °C. Anal. Calcd. for C₃₀H₂₃N₃O₅: C, 71.27; H 4.58; N, 8.31. Found: C, 71.30, H, 4.54, N, 8.70. IR (KBr, cm⁻¹): 1535, 1469 (C=C stretching of aromatic ring), 1680s (-C=O stretching of -COOH group), 3128 (-NH stretching of secondary amine). ¹H-NMR (200 MHz, DMSO-d₆, δ / ppm): 1.38 (3H, t, J = 7.2 Hz, -CH₂-CH₃), 4.15 (2H, q, J = 7.2 Hz, -CH₂-CH₃), 10.92 (1H, s, -NH, D₂O exchangeable), 7.75 (2H, t, J = 7.8 Hz, aromatic), 2.26–2.75 (2H, m, -CH₂). ¹³C-NMR (100 MHz, CDCl₃, δ / ppm): 157.76 (C₁), 146.89 (C₂), 177.69 (-COO), 33.44 (-CH), 38.55 (-CH₂). MS (m/z, (relative abundance, %)): 252 (M+, 32.5) 225, 213, 211 (BP, 100). UV-Vis (EtOH) (λ_{max} / nm, eV or cm⁻¹ (ε / L mol⁻¹ cm⁻¹)): 205 (2300), 243 (1800). Optical rotation values, α (589 nm, 20 °C, 10 g dm⁻³ in H₂O, 10 cm): +66.470°. Specific rotation [α]²⁰₅₈₉ / deg dm⁻¹ g⁻¹ cm³. Magnetic moment, μ_{eff} / μ_B: 3.1.

Deposition of crystallographic data

Prior to submission, the crystallographic data included in a manuscript presenting such data should be deposited at the appropriate database. Crystallographic data associated with organic and metal-organic structures should be deposited at the Cambridge Crystallographic Data Centre (CCDC) by e-mail to deposit@ccdc.cam.ac.uk

Crystallographic data associated with inorganic structures should be deposited with the Fachinformationszentrum Karlsruhe (FIZ) by e-mail to crysdata@fiz-karlsruhe.de. A deposition number will then be provided, which should be added to the reference section of the manuscript.

ARTWORK INSTRUCTIONS

JSCS accepts only **TIFF** or **EPS** formats, as well as **JPEG** format (only for colour and greyscale photographs) for electronic artwork and graphic files. **MS files** (Word, PowerPoint, Excel, Visio) **NOT acceptable**. Generally, scanned instrument data sheets should be avoided. Authors are responsible for the quality of their submitted artwork. Every single Figure or Scheme, as well as any part of the Figure (A, B, C...) should be prepared according to following instructions (every part of the figure, A, B, C..., must be submitted as an independent single graphic file).

TIFF - Virtually all common artwork and graphic creation software is capable of saving files in TIFF format. This “option” can normally be found under the “Save As...” or “Export...” commands in the “File” menu. TIFF (Tagged Image File Format) is the recommended file format for bitmap, greyscale and colour images. Colour images should be in the RGB mode. When supplying TIFF files, please ensure that the files are supplied at the correct resolution: Line artwork: minimum of 1000 dpi, RGB image: minimum of 300 dpi, Greyscale image: minimum of 300 dpi, Combination artwork (line/greyscale/RGB): minimum of 500 dpi, Images should be tightly cropped.

If applicable, please re-label artwork with a font supported by JSCS (Arial, Helvetica, Times, Symbol) and ensure it is of an appropriate font size. Save an image in TIFF format with LZW compression applied. It is recommended to remove Alpha channels before submitting TIFF files. It is recommended to flatten layers before submitting TIFF files.

EPS - Virtually all common artwork creation software, such as Canvas, ChemDraw, CorelDraw, SigmaPlot, Origin Lab..., are capable of saving files in EPS format. This “option” can normally be found under the “Save As...” or “Export...” commands in the “File” menu. For vector graphics, EPS (Encapsulated PostScript) files are the preferred format as long as they are provided in accordance with the following conditions: when they contain bitmap images, the bitmaps should be of good resolution (see instructions for TIFF files).

JPEG - (Joint Photographic Experts Group) is the acceptable file format only for colour and greyscale photographs. JPEG can be created with respect to photo quality (low, medium, high; from 1 to 10), ensuring file sizes are kept to a minimum to aid easy file transfer. Images should have a minimum resolution of 300 dpi. Image width: minimum 8.0 cm; maximum 12.0 cm.

When colour is involved, it should be encoded as RGB. An 8-bit preview/header at a resolution of 72 dpi should always be included. Embed fonts should be always included and only the following fonts should be used in artwork: Arial, Helvetica, Times, Symbol. The vertical space between the parts of an illustration should be limited to the bare necessity for visual clarity. No data should be present outside the actual illustration area. Line weights should range from 1 pt to 2 pt. When using layers, they should be reduced to one layer before saving the image (Flatten Artwork).

Sizing of artwork

JSCS aspires to have a uniform look for all artwork contained in a single article. Hence, it is important to be aware of the style of the journal. Figures should be submitted in black and white or, if required, colour (charged). If coloured figures or photographs are required, this must be stated in the cover letter and arrangements made for payment through the office of the Serbian Chemical Society. As a general rule, the lettering on an artwork should have a finished, printed size of 11 pt for normal text and no smaller than 7 pt for subscript and superscript characters. Smaller lettering will yield a text that is barely legible. This is a rule-of-thumb rather than a strict rule. There are instances where other factors in the artwork, (for example, tints and shadings) dictate a finished size of perhaps 10 pt. Lines should be of at least 1 pt thickness. When deciding on the size of a line art graphic, in addition to the lettering, there are several other factors to address. These all have a bearing on the reproducibility/readability of the final artwork. Tints and shadings have to be printable at the finished size. All relevant detail in the illustration, the graph symbols (squares, triangles, circles, etc.) and a key to the diagram (to explain the explanation of the graph symbols used) must be discernible. The sizing of halftones (photographs, micrographs,...) normally causes more problems than line art. It is sometimes difficult to know what an author is trying to emphasize on a photograph, so you can help us by identifying the important parts of the image, perhaps by highlighting the relevant areas on a photocopy. The best advice that can be given to graphics suppliers is not to over-reduce halftones. Attention should also be paid to magnification factors or scale bars on the artwork and they should be compared with the details inside. If a set of artwork contains more than one halftone, again please ensure that there is consistency in size between similar diagrams.

THE GRAPHS AND ARTWORK SHOULD BE **10 cm WIDE AT LEAST**.



Journal of the Serbian Chemical Society

JSCS-info@shd.org.rs • www.shd.org.rs/JSCS

J. Serb. Chem. Soc. Vol. 80, No. 8 (2015)

CONTENTS

Organic Chemistry

- S. Z. Hejazi, A. F. Shojaei, K. Tabatabaeian and F. Shirini: Preparation and characterization of ZrO_2 -supported Fe_3O_4 -MNPs as an effective and reusable superparamagnetic catalyst for the Friedländer synthesis of quinoline derivatives 971

Biochemistry and Biotechnology

- D. S. Milojković, D. H. Andelković, G. M. Kocić and T. D. Andelković: Evaluation of a method for phthalate extraction from milk related to the milk dilution ratio 983

Inorganic Chemistry

- M. Dehestani and L. Zeidabadinejad: QTAIM investigation of a dipyrazol-1-ylmethane derivative and its Zn(II) complexes ($ZnLX_2$, X = Cl, Br or I) 997

Theoretical Chemistry

- I. Gutman, B. Furtula and X. Li: Multicenter Wiener indices and their applications 1009

Physical Chemistry

- P. Subramaniam and N. Thamil Selvi: Dynamics of cetyltrimethylammonium bromide-mediated reaction of phenylsulfinylacetic acid with Cr(VI): Treatment of pseudo-phase models 1019

Electrochemistry

- K. Nikolić, M. M. Aleksić, V. Kapetanović and D. Agbaba: Voltammetric and theoretical studies of the electrochemical behavior of cephalosporins at a mercury electrode 1035

Analytical Chemistry

- L. Liu, M. Chen and X. Chen: Analysis of alcohol dehydrogenase inhibitors from *Desmodium styracifolium* using centrifugal ultrafiltration coupled with HPLC–MS 1051

Polymers

- C. Kizilkaya, M. Bicen, S. Karatas and A. Gungor: Structural effects of the monomer type on the properties of copolyimides and copolyimide–silica hybrid materials 1061

Thermodynamics

- G. R. Ivaniš, A. Ž. Tasić, I. R. Radović, B. D. Djordjević, S. P. Šerbanović and M. Lj. Kijevčanin: An apparatus proposed for density measurements in compressed liquid regions at pressures of 0.1–60 MPa and temperatures of 288.15–413.15 K 1073

Environmental

- T. Perunović, K. Stojanović, M. Kašanin-Grubin, A. Šajnović, V. Simić, B. Jovančićević and I. Brčeski: Geochemical investigation as a tool in the determination of the potential hazard for soil contamination (Kremna Basin, Serbia) 1087

Published by the Serbian Chemical Society
Karnegijeva 4/III, P.O. Box 36, 11120 Belgrade, Serbia
Printed by the Faculty of Technology and Metallurgy
Karnegijeva 4, P.O. Box 35-03, 11120 Belgrade, Serbia



Preparation and characterization of ZrO_2 -supported Fe_3O_4 -MNPs as an effective and reusable superparamagnetic catalyst for the Friedländer synthesis of quinoline derivatives

SEYYEDEH ZOHA HEJAZI, ABDOLLAH FALLAH SHOJAEI*,
KHALIL TABATABAEIAN and FARHAD SHIRINI

Department of Chemistry, Faculty of Sciences, University of Guilan,
P. O. Box 41335-1914, Rasht, Iran

(Received 23 October 2014, revised 4 March, accepted 27 March 2015)

Abstract: In this study, a convenient, appropriate and eco-friendly method for the synthesis of quinoline derivatives *via* a Friedländer reaction was developed using $\text{ZrO}_2/\text{Fe}_3\text{O}_4$ -MNPs as an effective and reusable heterogeneous catalyst. The morphology of $\text{ZrO}_2/\text{Fe}_3\text{O}_4$ -MNPs was studied by the XRD, FT-IR, SEM, TEM and VSM techniques. Green reactions, straight and easy work-up, high yields of the products and good reaction times are the benefits of this procedure. Further, the catalyst could be recovered using an external magnetic field and reused at least three times without a considerable decrease in its catalytic activity.

Keywords: quinoline derivatives; Friedländer reaction; $\text{ZrO}_2/\text{Fe}_3\text{O}_4$ -MNPs; heterogeneous catalyst; green procedure.

INTRODUCTION

Quinoline and its derivatives are very important intermediates in organic and medicinal chemistry that show various physiological and pharmacological activities, such as antimalarial, anti-inflammatory, anti-asthmatic, antibacterial, anti-hypertensive, and are tyrosine kinase inhibiting agents.^{1–3} These heterocycles are valuable compounds for the preparation of nano- and meso-structures with enhanced electronic and photonic properties.^{4,5} Furthermore, quinoline derivatives have been employed in the study of bio-organic and bio-organometallic processes.^{6,7} Due to the importance of the use of quinolines in the fields of medicinal, bioorganic, industrial and synthetic organic chemistry, there is immense interest in the development of effective procedures for their synthesis. Thus, several methods, such as the Skraup, Doebner–von Miller, Friedländer and

*Corresponding author. E-mail: a.f.shojaie@guilan.ac.ir
doi: 10.2298/JSC141023031H

Combes, have been mentioned in the literature for the creation of quinoline derivatives.^{8–11}

Among various methodologies suggested for the preparation of quinolines, the Friedländer annulation^{12,13} is one of the most frequently used pathways for the synthesis of polysubstituted quinolines. This method involves an acid- or base-catalyzed or thermal condensation between an aromatic 2-aminoaldehyde or ketone with a carbonyl compounds containing a reactive α -methylene group followed by a cyclodehydration.^{14,15}

In general, Friedländer reactions are carried out either by refluxing an aqueous or alcoholic solution of reactants in the presence of a base or by heating a mixture of the reactants at high temperatures ranging from 150 to 220 °C in the absence of a catalyst.¹⁶ However, under thermal or basic catalysis conditions, 2-aminobenzophenone does not react with simple ketones, such as cyclohexanone and β -keto esters.¹⁷ Subsequent work showed better yields of quinolines were achieved under acid catalysis.¹⁷ Several acid catalysts, such as Brønsted acids including hydrochloric acid in water,¹⁸ sulfamic acid,¹⁹ sulfuric acid,²⁰ silica sulfuric acid,²¹ dodecylphosphonic acid,²² PEG-supported sulfonic acid,²³ arylidene pyruvic acids (APAs),²⁴ oxalic acid,²⁵ Lewis acids containing Zr(NO₃)₄ or Zr(HSO₄)₄,²⁶ zirconium tetrakis(dodecyl sulfate) Zr(DS)₄,²⁷ GdCl₃·6H₂O,²⁸ BiCl₃,²⁹ SnCl₂,³⁰ FeCl₃,³¹ Y(OTf)₃³², NiCl₂³³, Ag₃PW₁₂O₄₀³⁴ and ZnCl₂³⁵ have been reported for this conversion.

However, most of the previously reported procedures suffer from different drawbacks, such as low yields of the products, poor selectivity, long reaction times, harsh conditions, high temperatures, usage of hazardous, corrosive and relatively expensive catalysts, tedious work-up procedures and using toxic/polar solvent leading to complex isolation and recovery procedures. Moreover, the main disadvantage of a number of previous methods is that the catalyst cannot be recovered. Therefore, the development of a simple, efficient and environmentally friendly method for the synthesis of quinoline derivatives is still a challenging task.

Recently, the applications of heterogeneous nanocatalysts have attracted remarkable attention as inexpensive, non-toxic and eco-friendly catalysts for various organic transformations under mild and convenient conditions. The catalysts have advantages over conventional homogeneous catalysts, including simple recovery from the reaction mixture by easy filtration, higher surface activity and reusability.^{36–38}

Among heterogeneous catalysts, inorganic oxides especially zirconia have different physical and chemical properties and have gained much consideration by researchers. Good chemical and dimensional stability, high electrical resistivity, high refractive index, mechanical strength and toughness, biocompatibility and low cost are the origin of the interest in using the zirconia as a catalyst.^{39,40}

However, the specific surface area and thermal stability of pure ZrO₂ is low⁴¹ and it shows weak catalytic activity in a number of chemical transformations.⁴²

In order to enhance the catalytic performance of zirconia-based catalysts, many endeavors have been inducted by introducing various metal oxides where-upon zirconia acts as a support for the preparation of the solid catalysts.^{43–48} Although the doping of appropriate cations with specific concentration into zirconia improves thermal stability, surface area and acidity of solid acids, the separation and recovery of mixed oxide catalysts from the reaction products are still difficult and require a large amount of separation energy and cost. For this reason, a material immobilized onto the solid support plays a fundamental role in the efficiency of the resulting supported reagent catalyst. Among the different modified zirconia materials, Fe₃O₄ magnetic nanoparticles (MNPs) are widely used due to easy handling, a simple work-up procedure, nontoxicity, enhanced catalytic activity and chemical selectivity in various organic synthesis.^{49,50} In addition, ZrO₂-supported Fe₃O₄-MNPs can be easily separated from the reaction media by applying an external magnetic field.

In continuation of ongoing studies on metal oxides as catalysts,⁵¹ herein, a simple and eco-friendly procedure is demonstrated for the synthesis of quinoline derivatives using the Friedländer heteroannulation method in the presence of ZrO₂/Fe₃O₄-MNPs as catalyst.

EXPERIMENTAL

Chemicals and apparatus

All materials and solvents were purchased from Merck and Fluka, and used without further purification. Yields refer to isolated products. Products were characterized by their physical constants, comparison with authentic samples, and IR and NMR spectroscopy. The IR spectra were obtained in KBr discs on a Perkin–Elmer model Spectrum One FT-IR spectrometer.

The structures of the synthesized catalysts were characterized by X-ray diffraction analysis (XRD Equinox 3000, INEL, France). The XRD patterns were obtained using CuK_α radiation (wavelength 1.54056 Å) at a current of 200 mA and a voltage of 40 kV in the 2θ range of 10–100 at a scanning rate of 8° min⁻¹. The surface microscopic morphologies of the ZrO₂-supported Fe₃O₄-MNPs were visualized by scanning electron microscopy (SEM MIRAI II TESCAN). The size of Fe₃O₄-MNPs was investigated by transmission electron microscopy (TEM Philips MC 10) with an acceleration voltage of 80 kV. A magnetic study was performed using a vibrating sample magnetometer at room temperature (VSM JDM-13).

Reaction progress was checked by thin-layer chromatography (TLC) with detection by UV light. The ¹H-NMR spectra were obtained on a Bruker DRX-400 Avance spectrometer, while the ¹³C-NMR spectra were obtained on a Bruker DRX-100 Avance spectrometer. Samples were analyzed in CDCl₃ and chemical shift values are reported in ppm relative to tetramethylsilane (TMS) as the internal reference. Melting points were measured on an electrothermal apparatus and are uncorrected. Elemental analyses were realized using a Carlo Erba EA1110 CHNS-O analyzer and the values agreed with the calculated ones.



Preparation of the catalyst (ZrO_2/Fe_3O_4 -MNPs)

Firstly, 96 mg of ZrO_2 nano particles were well dispersed in 30 mL of distilled water in a two-necked round bottom flask (100 mL) by ultrasonic irradiation for 30 min. After adding 81 mg of $FeCl_3 \cdot 6H_2O$, the solution was stirred vigorously for 30 min. Subsequently, 120 mg $FeCl_2 \cdot 4H_2O$ was slowly added into the mixture under stirring for 30 min. The whole process was performed under an argon atmosphere. Then, 8 mL of a concentrated aqueous solution of NH_3 was added into the solution dropwise over 1 h. Thereafter, the mixture was stirred at 60 °C for 2 h. After cooling the solution to room temperature, the black magnetic ZrO_2/Fe_3O_4 -MNPs were recovered by centrifugation at 6000 rpm, rinsed several times with deionized water and dried at 60 °C for 24 h. It was expected that the positive ferrous and ferric ions would be in proximity with the oxygen atoms of ZrO_2 and that they would be converted to Fe_3O_4 -MNPs after the dropwise addition of the concentrated aqueous solution of NH_3 into the solution.

General procedure for the synthesis of quinolines catalyzed by ZrO_2/Fe_3O_4 -MNPs

A mixture of 2-amino-5-chlorobenzophenone (1 mmol), a ketone or β -diketone (1.5 mmol) and ZrO_2/Fe_3O_4 -MNPs (20 mg) in ethanol (5 mL) was stirred magnetically and heated at 70 °C. After completion of the reaction, confirmed by TLC, the catalyst was collected by magnetic separation using an external magnet and washed repeatedly with warm ethanol. The aqueous phase was filtrated and cooled to room temperature. Then the solid product was collected and washed with cold water to afford the pure product. In some cases, further purification was achieved by recrystallization in ethanol to give the pure product.

RESULT AND DISCUSSION

Catalyst characterization

X-Ray diffraction studies. To confirm the synthesis of the catalyst, first, the XRD patterns of the pure ZrO_2 nanoparticles and ZrO_2/Fe_3O_4 magnetic nanoparticles were studied. All the diffraction peaks in the XRD patterns of the pure ZrO_2 imply the monoclinic phase of pure ZrO_2 nanoparticles (*m-ZrO₂*, JCPDS NO 24-1165). The additional diffraction peaks at θ 30.6, 36.5, 43.7, 53.9, 57.6, and 62.8° appearing in the XRD patterns of the ZrO_2/Fe_3O_4 -MNPs correspond to the standard XRD data for the cubic Fe_3O_4 phase of inverse spinel crystal structure (JCPDS file No. 19-0629).⁵² No peaks corresponding to impurities were present. The average diameter of the crystallites (*D*) of the synthesized catalyst was calculated using the Scherrer formula and found to be 21 nm, as confirmed by TEM analysis.

Fourier transform infrared spectroscopy. The FT-IR spectrum of pure zirconia was compared with the synthesized ZrO_2/Fe_3O_4 -MNPs. The pure zirconia spectrum exhibited bands at 734, 581 and 508 cm^{-1} , which could be attributed to the Zr–O stretching vibration of ZrO_2 . These bands were not distinctly found in the spectrum of ZrO_2/Fe_3O_4 -MNPs. They are related to the broad band at around 579 cm^{-1} , which was assigned to the Fe–O stretching vibration of Fe_3O_4 -MNPs that may overlap with the Zr–O peaks. Moreover, the absorption bands in the

region 3435 and 1630 cm^{-1} may be related to the stretching and bending vibrations of the O–H bond due to physically adsorbed water molecules.

SEM and TEM analysis. The morphology and size of the synthesized $\text{ZrO}_2/\text{Fe}_3\text{O}_4$ -MNPs were examined by scanning electron microscopy (SEM) and transmission electron microscopy (TEM). From the SEM image (Fig. 1a), it can be seen that the loaded Fe_3O_4 -MNPs were uniform in shape and size distribution and had a porous structure. The particles sizes derived from TEM analysis (Fig. 1b) were in the range 5–25 nm, which is comparable with the crystallite size calculated from the X-ray spectrum.

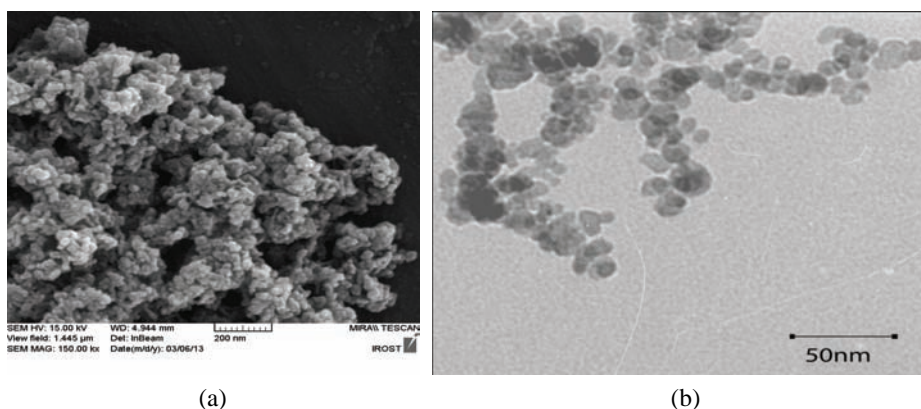


Fig. 1. a) SEM and b) TEM image of $\text{ZrO}_2/\text{Fe}_3\text{O}_4$ -MNPs.

Vibrating sample magnetometer (VSM) analysis

The magnetic properties of $\text{ZrO}_2/\text{Fe}_3\text{O}_4$ magnetic nanoparticles were investigated by the most common method of examining the magnetic properties of a material, using a vibrating sample magnetometer (VSM). The results showed that the synthesized nanoparticles exhibit superparamagnetic behavior at room temperature and the hysteresis loops of the samples exhibited no coercivity and retentivity. The saturation magnetization (M_s) values of the synthesized catalysts were 33 emu g⁻¹, which is mainly attributed to a high weight ratio of Fe_3O_4 magnetic nanoparticles that were loaded onto the ZrO_2 .

Catalyst synthesis optimization

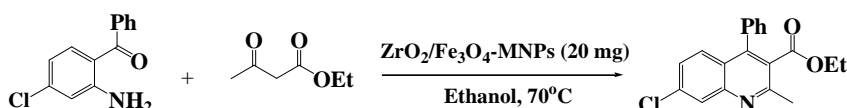
At the beginning of the investigations on the usage of $\text{ZrO}_2/\text{Fe}_3\text{O}_4$ -MNPs as a green and efficient heterogeneous nanocatalyst, the reaction of 2-amino-5-chlorobenzophenone and ethyl acetoacetate (EAA) was selected as a model for determining the optimal conditions. For this reason, several reactions were performed using diverse amounts of catalyst at various temperatures in different solvents to achieve a good yield of the desired products. The results are summarized in Table I.

TABLE I. Optimization of the conditions for the synthesis of ethyl 2-methyl-4-phenylquinoline-3-carboxylate; reaction conditions: 2-amino-5-chlorobenzophenone (1 mmol), EAA (1.5 mmol) in different solvents at different temperatures with different amount of catalyst

Entry	Catalyst [amount, mg]	Solvent	<i>t</i> / °C	<i>τ</i> / min	Yield ^a , %
1	—	Ethanol	Reflux	300	Trace
2	ZrO ₂ -NPs [300]	Ethanol	Reflux	240	18
3	ZrO ₂ /Fe ₃ O ₄ -MNPs [10]	Ethanol	Reflux	60	88
4	ZrO ₂ /Fe ₃ O ₄ -MNPs [20]	Ethanol	Reflux	24	91
5	ZrO ₂ /Fe ₃ O ₄ -MNPs [30]	Ethanol	Reflux	25	90
6	ZrO ₂ /Fe ₃ O ₄ -MNPs [20]	Ethanol	25	320	Trace
7	ZrO ₂ /Fe ₃ O ₄ -MNPs [20]	Ethanol	50	300	51
8	ZrO ₂ /Fe ₃ O ₄ -MNPs [20]	Ethanol	70	25	92
9	ZrO ₂ /Fe ₃ O ₄ -MNPs [20]	Methanol	Reflux	30	86
10	ZrO ₂ /Fe ₃ O ₄ -MNPs [20]	Acetonitrile	70	120	22
11	ZrO ₂ /Fe ₃ O ₄ -MNPs [20]	<i>n</i> -Hexane	Reflux	120	Trace

^aIsolated yield

As can be seen in Table I, the best result was obtained when the reaction was performed at 70 °C, with a relative ratio of the substrate: EAA:ZrO₂/Fe₃O₄-MNPs of 1 mmol:1.5 mmol:20 mg, respectively (Table I, entry 8). In this procedure, any further increase in temperature and amount of catalyst did not lead to considerable improvement in the reaction times and yields. Moreover, when the same procedure was run at room temperature, the yield of the product was poor after 320 min (Table I, entry 6). It is noteworthy that without any catalyst at reflux, the product was isolated in low yield after a long reaction time (Table I, entry 1). Moreover, it can be seen that the pure *m*-zirconia as the catalyst led to a lower yield of the product (Table I, entry 2). In order to examine the effect of the solvent, the reaction was explored in different solvents, *i.e.*, ethanol, methanol, acetonitrile and *n*-hexane (Table I, entries 8–11) and ethanol was selected as the best solvent. Under the optimized conditions, the model reaction gave 92 % yield of the corresponding product after 25 min (Table I, entry 8 and Scheme 1).



Scheme 1. ZrO₂/Fe₃O₄-MNPs catalyzed synthesis of ethyl 2-methyl-4-phenylquinoline-3-carboxylate.

Subsequently, in order to evaluate the generality of this methodology, a series of *ortho*-aminoaryl ketones were reacted with different 1,3-dicarbonyl compounds under the optimum conditions and the results are reported in Table II.

TABLE II. Synthesis of various quinolines using $\text{ZrO}_2/\text{Fe}_3\text{O}_4$ -MNPs as the catalyst; reaction condition: 2-aminoaryl ketone (1 mmol), ketone or β -diketone (1.5 mmol) and $\text{ZrO}_2/\text{Fe}_3\text{O}_4$ -MNPs (20 mg) at 70 °C in ethanol (5 mL)

Entry	Substrate	Ketone or β -diketone	Quinoline	τ min	Yield ^a %	M.p., °C	
						Measured	Reported
1				40	89	109–111	111–112 ²⁵
2				30	91	98–100	100–101 ²⁵
3				35	90	99–100	98–100 ⁵³
4				60	86	191–194	190–192 ³⁴
5				45	90	154–156	155–156 ³⁴
6				50	89	129–131	130–132 ³⁴
7				60	87	153–156	156–157 ³⁴
8				45	90	151–153	150–151 ³⁴
9				25	92	101–103	102–104 ²²
10				30	90	134–136	133–135 ²⁵
11				45	89	207–209	208–209 ³⁴
12				35	92	184–186	185–186 ³⁴
13				45	90	107–108	106–107 ²⁵

TABLE II. Continued

Entry	Substrate	Ketone or β -diketone	Quinoline	τ min	Yield ^a %	m.p., °C	
						Measured	Reported
14				60	89	165–167	164–165 ³⁴
15				65	87	239–241	240–243 ⁵⁴

^aIsolated yield

According to Table II, both cyclic and acyclic diketones such as 5,5-dimethylcyclohexanedione and acetylacetone, cyclic ketones including cyclohexanone and cyclopentanone and β -ketoesters such as EAA reacted with 2-amino-5-chlorobenzophenone and 2-aminobenzophenone to afford the corresponding quinolines. It can easily be seen that in all cases, the Friedländer annulation proceeded smoothly and gave good to high yields ranging from 86 to 92 %. The reactions were remarkably clean and no chromatographic separation was necessary to obtain spectra-pure compounds. Furthermore, the work-up of present method was easy and the process is beneficial in avoiding the application of strong acids, high temperatures and volatile and/or toxic reactants. All of the synthesized products are known compounds and were characterized by comparing their melting points, IR, ¹H- and ¹³C-NMR spectra with those of authentic samples.

The possibility of reusing the catalyst is one of the most significant benefits of heterogeneous catalysts over homogeneous systems. Thus, the recovery and reusability of ZrO₂/Fe₃O₄-MNPs was investigated in the model reaction under the optimized condition. After completion of the reaction, the catalyst was easily separated from the reaction mixture by an external magnetic field and reused in subsequent runs. The results of continuous runs showed that the recovered catalyst could be reused three times without any appreciable decrease in its activity (Table III). The strength of catalyst is emphasized *via* measurement of Fe ions leaching by atomic absorption spectroscopy and trace metal ions were detected in the filtrate of this reaction.

TABLE III. Reusability of the ZrO₂/Fe₃O₄-MNPs in the model reaction (Table II, entry 8)

Run No.	τ / min	Yield, %
1	25	92
2	25	92
3	27	90
4	30	88

Moreover, in order to demonstrate the excellent catalytic activity of ZrO₂/Fe₃O₄-MNPs and the performance of this method, some of the results obtained

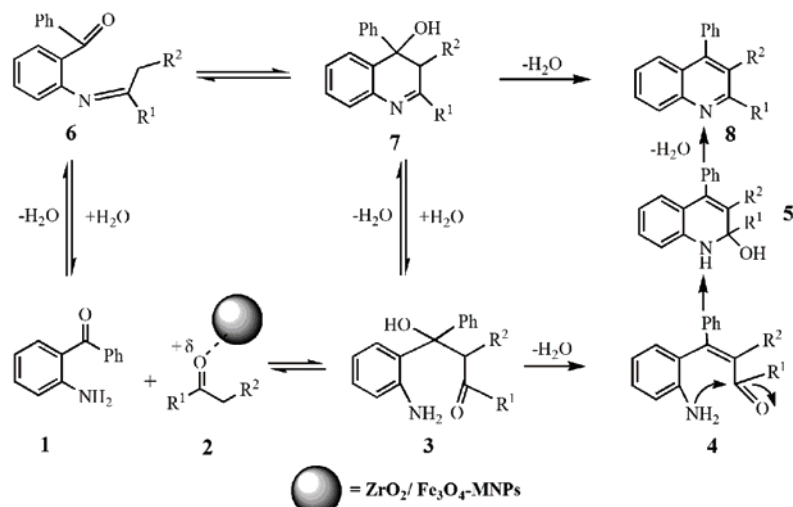
by the presented procedure were compared with other previously reported heterogeneous catalytic systems in the literature. As shown in Table IV, the obtained results show the advantage of the present protocol in terms of catalyst amount, yields or reaction times.

TABLE IV. Comparison of the result obtained for the synthesis of model reaction (Table II, entry 8) using $\text{ZrO}_2/\text{Fe}_3\text{O}_4$ -MNPs with other catalysts reported in the literature

Entry	Catalyst amount	Solvent	$t / ^\circ\text{C}$	τ / min	Yield ^a , %	Reference
1	(BSPY) $\text{HSO}_4/\text{MCM}-41$ (70 mg)	—	100	80	94	55
2	$\text{NH}_2\text{SO}_3\text{H}$ (5 mol %)	—	70	45	89	56
3	SiO_2/I_2 (100 mg/50 mg)	—	60	120	80	57
4	Amberlyst-15 (10 % w/w)	$\text{C}_2\text{H}_5\text{OH}$	Reflux	150	87	58
5	Nano-Flake ZnO (10 mol %)	—	100	120	92	59
6	$\text{ZrO}_2/\text{Fe}_3\text{O}_4$ -MNPs (20 mg)	$\text{C}_2\text{H}_5\text{OH}$	70	25	92	This Work

^aIsolated yield

Two possible mechanisms exist for the Friedländer synthesis of quinolines that are shown in Scheme 2. Based on these mechanisms and in the first step, the carbonyl group is activated by $\text{ZrO}_2/\text{Fe}_3\text{O}_4$ -MNPs. Then, 2-amino-5-chloro substituted carbonyl compound **1** and carbonyl compound **2** react in a rate-limiting step to the aldol adduct **3**. This intermediate loses water in an elimination reaction to the unsaturated carbonyl compound **4** and then loses water again in imine formation to quinoline **5**. In the second mechanism, the first step is Schiff base formation to **6** followed by an aldol reaction to **7** and elimination to **8**.



Scheme 2. Proposed mechanism for the synthesis of quinoline derivatives in the presence of $\text{ZrO}_2/\text{Fe}_3\text{O}_4$ -MNPs.

CONCLUSIONS

In conclusion, a green, one-pot, effective and environmentally friendly approach has been explained for the synthesis of quinoline derivatives *via* Friedländer annulation using ZrO₂/Fe₃O₄-MNPs as a convenient, mild and reusable catalyst. The remarkable benefit of the described method include good substrate generality, mild reaction conditions, high yields, good reaction times, simple experimental procedure, the use of a low cost catalyst, easy work-up, clean reaction profiles and green conditions by avoiding the usage of toxic organic solvents. Furthermore, the catalyst was successfully recovered and reused at least for four runs without significant loss in its activity, which make the presented procedure an interesting alternative to previously reported methods.

Acknowledgement. The authors are thankful to the Guilan University Research Council for the partial support of this work.

ИЗВОД

ДОБИЈАЊЕ И КАРАКТЕРИЗАЦИЈА ZrO₂/Fe₃O₄ МАГНЕТНИХ НАНОЧЕСТИЦА (MNPs)
КАО ЕФИКАСНОГ СУПЕРПАРАМAGНЕТНОГ КАТАЛИЗATORA ЗА ФРИДЛЕНДЕРОВУ
СИНТЕЗУ ДЕРИВАТА ХИНОЛИНА

SEYYEDEH ZOHA HEJAZI, ABDOLLAH FALLAH SHOJAEI, KHALIL TABATABAEIAN и FARHAD SHIRINI

Department of Chemistry, Faculty of Sciences, University of Guilan, P. O. Box 41335-1914, Rasht, Iran

Током истраживања развијен је приступачан и еколошки прихватљив поступак синтезе деривата хинолина Фридлендеровом реакцијом, употребом ZrO₂/Fe₃O₄-MNPs као ефикасног хетерогеног катализатора. Морфологија ZrO₂/Fe₃O₄-MNPs је испитана XRD, FT-IR, SEM, TEM и VSM аналитичким техникама. Предности овог поступка су лака обрада реакционе смеше, висок принос производа и кратко реакционо време. Употребљен катализатор се уклања спољашњим магнетним пољем и може се поново употребити најмање три пута без значајнијег смањивања каталитичке активности. Током синтезе и обраде реакционе смеше избегава се употреба органских растворача што целокупан процес чини еколошки прихватљивим.

(Примљено 23. октобра 2014, ревидирано 4. марта, прихваћено 27. марта 2015)

REFERENCES

- Y. L. Chen, K. C. Fang, J. Y. Sheu, S. L. Hsu, C. C. Tzeng, *J. Med. Chem.* **44** (2001) 2374
- G. Roma, M. D. Braccio, G. Grossi, M. Chia, *Eur. J. Med. Chem.* **35** (2000) 1021
- O. Billker, V. Lindo, M. Panico, A. E. Etiene, T. Paxton, A. Dell, M. Rogers, R. E. Sinden, H. R. Morris, *Nature* **392** (1998) 289
- X. Zhang, S. A. Jenekhe, *Macromolecules* **33** (2000) 2069
- S. A. Jenekhe, L. Lu, M. M. Alam, *Macromolecules* **34** (2001) 7315
- I. Saito, S. Sando, K. Nakatani, *Bioorg. Med. Chem.* **9** (2001) 2381
- C. He, S. J. Lippard, *Inorg. Chem.* **40** (2001) 1414
- G. Jones, in *Comprehensive Heterocyclic Chemistry II*, Vol. 5, A. R. Katritzky, C. W. Rees, E. F. V. Scriven, Pergamon, New York, USA, 1996, pp. 167–243
- H. Skraup, *Chem. Ber.* **13** (1880) 2086



10. P. Friedländer, *Chem. Ber.* **15** (1882) 2572
11. R. H. F. Mansake, M. Kulka, *Org. React.* **7** (1953) 59
12. J. Marco-Contelles, M. D. Carreiras, *The Friedlander Reaction*; Lambert Academic, Saarbrücken, Germany, 2010
13. J. Marco-Contelles, E. Perez-Mayoral, A. Samadi, M. D. Carreiras, E. Soriano, *Chem. Rev.* **109** (2009) 2652
14. R. C. Elderfield, in *The Chemistry of Heterocyclic Compounds*, Vol. 4, Wiley, 1952, pp. 45–47
15. G. Jones, in *The Chemistry of Heterocyclic Compounds, Quinoline*, Vol. 32, Wiley, 1977, pp. 137–151
16. C. C. Cheng, S. J. Yan, *Org. React.* **28** (1982) 37
17. E. A. Fehnel, *J. Heterocycl. Chem.* **4** (1967) 565
18. G. W. Wang, C. S. Jia, Y. W. Dong, *Tetrahedron Lett.* **47** (2006) 1059
19. J. S. Yadav, P. Purushothama Rao, D. Sreenu, R. Srinivasa Rao, V. Naveen Kumar, K. Nagaiah, A. R. Prasad, *Tetrahedron Lett.* **46** (2005) 7249
20. L. Strekowski, A. Czarny, H. J. Lee, *Fluorine Chem.* **104** (2000) 281
21. M. A. Zolfigol, P. Salehi, M. Shiri, T. Rastegar, A. Ghaderi, *J. Iran. Chem. Soc.* **5** (2008) 490
22. S. Ghassamipour, A. R. Sardarian, *Tetrahedron Lett.* **50** (2009) 514
23. X. L. Zhang, Q. Y. Wang, S. R. Sheng, Q. Wang, X. L. Liu, *Synth. Commun.* **39** (2009) 3293
24. M. Shiri, M. M. Heravi, B. Soleymanifard, *Tetrahedron* **68** (2012) 6593
25. M. Dabiri, M. Baghbanzadeh, M. S. Nikcheh, *Monatsh. Chem.* **138** (2007) 1249
26. M. A. Zolfigol, P. Salehi, A. Ghaderi, M. Shiri, *Catal. Commun.* **8** (2007) 1214
27. M. A. Zolfigol, P. Salehi, A. Ghaderi, M. Shiri, Z. Tanbakouchian, *J. Mol. Catal., A* **259** (2006) 253
28. P. Prabhakar Reddy, B. China Rayu, J. Madhusudana Rao, *J. Chem. Res.* **12** (2008) 679
29. C. S. Jia, G. W. Wang, *Lett. Org. Chem.* **3** (2006) 289
30. P. Arumugam, G. Karthikeyan, R. Atchudan, D. Murlidharan, P. T. Perumal, *Chem. Lett.* **34** (2005) 314
31. J. Wu, L. Zhang, T. N. Diao, *Synlett* **17** (2005) 2653
32. M. Dabiri, M. Baghbanzadeh, E. Arzroomchilar, *Heterocycles* **75** (2008) 397
33. J. Wu, H. G. Xia, K. Gao, *Org. Biomol. Chem.* **4** (2006) 126
34. J. S. Yadav, B. V. S. Reddy, P. Sreedhar, R. S. Rao, K. Nagaiah, *Synthesis* **14** (2004) 2381
35. B. R. McNaughton, B. L. Miller, *Org. Lett.* **5** (2003) 4257
36. F. M. Menger, C. Lee, *J. Org. Chem.* **44** (1979) 3446
37. K. Smith, *Solid Supports and Catalysts in Organic Synthesis*, Ellis Horwood and PTR Prentice Hall, New York, 1992
38. P. Laszlo, in *Comprehensive Organic Synthesis*, Vol. 7, B. M. Trost, I. Fleming, Eds, Pergamon, New York, 1991, p. 839
39. A. H. Heuer, L. W. Hobbs, *Advances in ceramics*, Vol. 3, *Science and technology of zirconia*, American Ceramic Society, Westerville, OH, 1981
40. N. Claussen, M. Ruhle, A. H. Heuer, *Advances in ceramics*, Vol. 11, *Science and technology of zirconia II*, American Ceramic Society, Westerville, OH, 1984
41. G. D. Yadav, A. D. Murkute, *Langmuir* **20** (2004) 11607
42. V. K. Smith, H. Suja, J. Jacob, S. Sugunan, *Indian J. Chem., A* **42** (2003) 300
43. G. D. Yadav, A. D. Murkute, *J. Phys. Chem., A* **108** (2004) 9557



44. T. Lei, J. S. Xu, Y. Tang, W. M. Hua, Z. Gao, *Appl. Catal., A* **192** (2000) 181
45. B. M. Reddy, P. M. Sreekanth, Y. Yamada, T. Kobayashi, *J. Mol. Catal., A* **227** (2005) 81
46. D. J. Rosenberg, F. Coloma, J. A. Anderson, *J. Catal.* **210** (2002) 218
47. Y. Xia, W. Hua, Z. Gao, *Appl. Catal., A* **185** (1999) 293
48. P. D. L. Mercera, J. G. Van Ommen, E. B. M. Doesburg, A. J. Burggraaf, J. R. H. Ross, *Appl. Catal.* **71** (1991) 363
49. A. Kong, P. Wang, H. Zhang, F. Yang, S. P. Huang, Y. Shan, *Appl. Catal., A* **417–418** (2012) 183
50. M. Z. Kassaei, H. Masrouri, F. Movahedi, *Appl. Catal., A* **395** (2011) 28
51. A. Fallah-Shojaei, K. Tabatabaeian, F. Shirini, S. Z. Hejazi, *RSC Adv.* **4** (2014) 9509
52. Y. Chen, H. Gu, *Mater. Lett.* **67** (2012) 49
53. K. Niknam, M. A. Zolfigol, A. Dehghani, *Heterocycles* **75** (2008) 2513
54. F. Shirini, A. Yahyazadeh, K. Mohammadi, N. Ghaffari Khaligh, *C. R. Chim.* **17** (2014) 370
55. M. Abdollahi-Alibeik, M. Pouriyaveali, *Catal. Commun.* **22** (2012) 13
56. J. S. Yadav, P. Purushothama Rao, D. Sreenu, R. Srinivasa Rao, V. Naveen Kumar, K. Nagaiah, A. R. Prasad, *Tetrahedron Lett.* **46** (2005) 7249
57. M. A. Zolfigol, P. Salehi, A. Ghaderi, M. Shiri, *J. Chin. Chem. Soc.* **54** (2007) 267
58. B. Das, K. Damodar, N. Chowdhury, R. Aravind Kumar, *J. Mol. Catal., A* **274** (2007) 148
59. S. Genovese, F. Epifano, M. C. Marcotullio, C. Pelucchini, M. Curini, *Tetrahedron Lett.* **52** (2011) 3474.



Evaluation of a method for phthalate extraction from milk related to the milk dilution ratio

DANICA S. MILOJKOVIĆ^{1#}, DARKO H. ANDELKOVIĆ^{1#}, GORDANA M. KOČIĆ²
and TATJANA D. ANDELKOVIĆ^{1#*}

¹Faculty of Sciences and Mathematics, University of Niš, Višegradska 33, 18000 Niš, Serbia
and ²Faculty of Medicine, University of Niš, Bulevar dr Zorana Đindića 81, 18000 Niš, Serbia

(Received 4 December 2014, revised 26 February, accepted 19 March 2015)

Abstract: Liquid–liquid extraction techniques coupled with gas chromatography–mass spectrometry (GC–MS) were compared for the extraction and the determination of four phthalates: dimethyl phthalate (DMP), di-*n*-butyl phthalate (DBP), benzyl butyl phthalate (BBP) and di-(2-ethylhexyl) phthalate (DEHP) in six different kinds of milk-based samples. Extraction factors: sample preparation, organic solvent type and volume, salt effect, agitation and the extraction time were optimized. The ions of the base peak (*m/z* 149 for DBP, BBP and DEHP and *m/z* 163 for DMP) for the investigated phthalates were selected for the screening studies. The acquisition was performed in the selected ion-monitoring mode. The response of the mass selective detector (MSD) for GC–MS phthalate calibration standards was linear between 0.25 and 2.50 µg mL⁻¹ with calculated limit of detection (*LOD*) values between 0.01 to 0.04 µg mL⁻¹ and limit of quantitation (*LOQ*) values of 0.05 to 0.12 µg mL⁻¹, while repeatability was between 1.7 to 4.9 % relative standard deviation (*RSD*). The study demonstrated an increase in the recovery of less polar phthalates in matrix milk standards on matrix dilution. Recovery for hydrophilic phthalates, such as DMP, was not changed by matrix dilution and it was continuously low for the investigated method. Two spiking levels, tested for the influence of matrix dilution on phthalate recovery, showed the same trend.

Keywords: extraction efficiency; phthalate esters; gas chromatography-mass spectrometry; milk samples.

INTRODUCTION

Phthalates present one of the ubiquitous chemicals in the environment. Since their usage is mainly as plasticizers for polymers, such as poly(vinyl chloride) (PVC), over one million tons of phthalates are produced in western Europe each year.¹ The most important congeners are: di-2-ethylhexyl phthalate (DEHP),

* Corresponding author. E-mail: tatjanaan@gmail.com

Serbian Chemical Society member.

doi: 10.2298/JSC141204028M

which accounts for about 50 % of the world production of phthalates,¹ dimethyl phthalate (DMP), di-*n*-butyl phthalate (DBP) and benzyl butyl phthalate (BBP), which is prohibited by the EU in toys and childcare articles if they could be placed in the mouth by children.² Phthalates have long been considered to be potential endocrine disrupters, and several of them have shown reproductive effects in animals.^{3–5}

The structures of the four studied phthalates as the most commonly used phthalate esters based on the 1,2-benzenedicarboxylic acid are given in Fig. S-1 of the Supplementary material to this paper.

The permanence of phthalates in polymer materials is low because phthalates are not chemically bound to the polymer. Their migration from food-packaging materials was reported as a route for food contamination with phthalates. Since food is one of the major sources of human exposure to phthalates, in order to assess human exposure to these substances, monitoring of phthalates levels in various foods should be performed. Fatty and oily foods are primarily contaminated with phthalates due to their lipophilic character.⁶ Although human intake of phthalates may originate from many food sources and routes, there is a special interest in monitoring the contamination of milk and milk products because they constitute a primary food source, especially for children. Tolerable daily intakes (*TDI*) were specified by the European Food Safety Authority (EFSA) for several phthalates, and they are 0.01, 0.05 and 0.5 mg kg^{−1} body weight day^{−1} for DBP, DEHP and BBP, respectively.^{7–9} The physicochemical properties of phthalates (Table S-I of the Supplementary material) and their amount and frequency of usage in food-packaging materials could determine their migration and leaching levels and thus the possibility of food contamination and human exposure.

The majority of publications deal with phthalate determination in simple matrices, such as water^{10–12} or biological fluids,¹³ while publications about phthalates in food samples with fatty matrices^{14–16} are less frequent. Due to usually low level of phthalates and generally high complexity of the matrices of food sample, extraction and clean up of the sample are usually considered as necessary and critical steps in phthalate determination.

However, as indicated in this paper, the crucial point in phthalate extraction from complex milk matrices is considered the choice of solvent for the extraction and sample dilution step. The influence and importance of these two aspects on the recovery of phthalates, as well as analytical methodology (agitation method, extraction time, *etc.*) are considered herein.

When sample extraction is performed with solvent mixtures of low polarity, fats are co-extracted together with the phthalates and thus, the fats must be removed and the membranes of milk fat globules should be disrupted before the chromatographic analysis. Otherwise, phthalates may not be effectively extracted, yielding low recoveries. The optimization of extraction efficiency of phthalates

from milk could alternatively be achieved by precipitation of milk proteins by addition of NaCl for salting-out followed by the addition of acetonitrile¹⁷ or through primary addition of acetone or an alcohol.¹⁸ Gel permeation chromatography (GPC) is often used for this purpose.^{6,19} When the sample is extracted with polar solvents, such as methanol or acetonitrile, the extract contains other interfering organic impurities in addition to fat. These may require solid-phase extraction (SPE) on different sorbents.^{20–22} In each of these sample preparation steps, the possibility of contamination of the sample is high because even in pure solvents, solid phase extractants, laboratory water, laboratory air and laboratory glassware, phthalates could be detected.²³ This can be negligible source of contamination that could be reduced by establishing whether the reduction of the accuracy of phthalate determination is higher due to phthalate contamination of the sample by using clean-up procedures or due to the complexity of co-eluting substances, which could influence the sensitivity of phthalate determination by MS analysis.

Since the extraction procedure could be the source of a matrix effect and is an essential step in the evaluation process of phthalate determination, different liquid solvents and solvent mixtures were investigated in this study regarding the extraction efficiency of phthalates, the possibility of phase separation, visibility of phase separation, clearness of the extracts, formation of emulsions, availability of reagents and duration of the extraction. In addition to the selection of the solvent type, different methods/procedures for extraction were also investigated in order to obtain the most optimal method for the extraction phthalates from milk and dairy products.

Bearing in mind that in milk with high fat content, phthalates cannot be easily extracted due to phospholipid–protein membranes that encapsulate the fat droplets containing lipophilic phthalate, dilution of milk samples prior to the analysis could enable a better extraction efficiency of phthalates and relatively clean extracts to be obtained. Moreover, sample dilution is an easy and effective method to reduce interfering compounds and to diminish the matrix effect. The obtained extracts, even without a clean-up step, could be used for GC–MS analysis, as shown herein.

EXPERIMENTAL

Reagents and materials

All solvents (HPLC grade) were purchased from Sigma–Aldrich (St. Louis, MO, USA), except *n*-hexane that was purchased from Fisher Scientific (Pittsburgh, PA, USA). Dimethyl phthalate (DMP), di-*n*-butyl phthalate (DBP), benzyl butyl phthalate (BBP) and di-(2-ethylhexyl) phthalate (DEHP) were purchased, in the highest available purity, from Sigma–Aldrich (St. Louis, MO, USA). Dibutyl adipate (DBA) was purchased from Fluka (Buchs, Switzerland) and used as an internal standard. Water from a Milli-Q system (Millipore, Bedford, MA, USA) was used.

All reagents and water used for the analyses were checked for contamination with phthalates. To avoid phthalate contamination, all the employed laboratory dishes were made of glass, previously washed with water and soap, tap and ultrapure water, rinsed with acetone and *n*-hexane and dried at 200 °C in a clean oven for 4 h.²³

All stock, intermediate and working solutions were prepared in *n*-hexane. Individual stock solutions of each phthalate were prepared at a concentration of 1000 µg mL⁻¹ and stored at 4 °C. The stock solutions were stable for up to one month. A mixed stock solution of phthalates was prepared at a concentration of 100 µg mL⁻¹ for each phthalate. With stepwise dilutions, individual working solutions of 1 µg mL⁻¹ were obtained for each phthalate to identify their retention times. The working solutions were stable for 10 days. Furthermore, the mixed working solutions of all phthalates at 0.25, 0.50, 1.00, 1.50 and 2.50 µg mL⁻¹ were also prepared as calibration standards with DBA as the internal standard at a concentration of 1 µg mL⁻¹. Between some other commonly used internal standards, such as benzyl benzoate²⁰ or isotope-labeled standards, DBA was adopted as an internal standard being approved for this purpose according to our findings and literature data.²⁴

The calibration curves were linear in the range from 0.25 to 2.5 µg mL⁻¹ with correlation coefficients higher than 0.990. The linear dynamic range was broader and covered the range from 2.50 to 50 µg mL⁻¹. Samples of nine systems of commercial milk-based samples diluted with water, from 0 to 50 vol. %, were all spiked phthalates at two concentration levels, 3.0 and 6.0 µg mL⁻¹.

Dairy samples

Optimization of the phthalate liquid–liquid extraction procedure was realized using six samples of dairy products: raw bovine milk, commercial (pasteurized) milk, thawed milk, whey, human milk and yogurt. Samples of raw bovine milk were collected in glass bottles from a dairy farm in south Serbia avoiding any contact with plastic materials. This milk had not been pasteurized before analysis and was used as collected. Samples of commercial milk from a Serbian dairy were purchased at Serbian market and used as received. The commercial milk was bottled in a plastic (polyethylene terephthalate, PET) bottle.⁶ The shelf life of milk is 10 days after packaging and the milk was used within this period. Thawed commercial milk was obtained after thawing overnight the milk that had been frozen for 24 h in the original packing. Whey produced in a cheese manufacturing process was purchased from the same dairy farm as the raw bovine milk. Samples of human milk were collected in three successive days by a postpartum 35-year old woman (5th week postpartum). Milking was carried out manually, with previously cleaned breasts and hands, directly into a glass container that was intended for this purpose. The yogurt used in this study was made from cow's milk, commercially available from a Serbian market and stored in a plastic (PET) bottle.

All nine systems of commercial milk-based samples diluted with water were used for the selection of optimum solvent type as extractant considering the possibility of phase separation, visibility of phase separation, clearness of the extracts, formation of emulsion, availability of the reagents and duration of extraction. In addition to selection of the solvent type, different methods/procedures for extraction were also investigated in order to obtain the most optimal method for the extraction of phthalates from milk and dairy products.

For the determination of extraction efficiency of phthalates in milk, only the commercial milk was used. The milk was diluted with water from 0 to 50 vol. %.

Before the analysis, samples of raw bovine milk, thawed milk and human milk were stored in a glass bottle in a refrigerator at 4 °C.

GC-MS analysis

Gas chromatographic analysis was performed on a gas chromatograph 6890 (Hewlett-Packard) equipped with a mass selective detector (MSD) 5973 (Agilent) and a DB-5 MS capillary column ($30\text{ m}\times 250\text{ mm}\times 0.25\text{ mm}$). The mass spectra were recorded under an electron impact ionization voltage of 70 eV . The gas chromatograph was operated in the split less injection mode. The oven temperature was programmed from $60\text{ }^\circ\text{C}$ (1 min) to $220\text{ }^\circ\text{C}$ (1 min) at a rate of $20\text{ }^\circ\text{C min}^{-1}$ and then to $280\text{ }^\circ\text{C}$ (4 min) at a rate of $5\text{ }^\circ\text{C min}^{-1}$. The MSD was used in the single ion-monitoring mode (SIM) at m/z 149 and 163. The identification and quantification of target compounds was based on the relative retention time, the presence of target ions and their relative abundance. The target ion was m/z 149 for DBP, BBP and DEHP and m/z 163 for DMP. Linearity was investigated in the range $0.25\text{--}2.5\text{ }\mu\text{g mL}^{-1}$. The linear dynamic range for the investigated phthalates by GC-MS was $0.25\text{--}50\text{ }\mu\text{g mL}^{-1}$. The limit of detection (LOD) and limit of quantitation (LOQ) for each phthalate were calculated from six replicated measurements of a low concentration spiked standard solution according to the Analytical Detection Limit Guidance from the Wisconsin Department of Natural Resources.²⁵

The laboratory contamination was monitored with blank samples obtained from Milli-Q water treated in the same manner as the milk samples.

Extraction procedures

Fourteen extraction procedures were examined. Each entailed different conditions (type of extractant, extraction time, agitation and settling). Two solvent mixtures were studied for extraction, acetone/*n*-hexane at a 1:1 volume ratio and methanol/*n*-hexane at a 1:3 volume ratio. The salting out effect was examined using acetonitrile as the extraction agent with the addition of NaCl to saturation. The liquid-liquid extractions for these three systems were performed by adding a volume of the extraction agents to a volume of sample in a 2:1 ratio, followed by vigorously hand shaking for 1 h and left standing for 24 h. In extraction methods using ethyl acetate, *n*-hexane, acetonitrile, acetone, dichloromethane, dichloroethane, trichloroethylene and trichloroethane, the volume ratio of the extraction agent to a milk sample was 2:1, agitation was performed in an ultrasonic bath for 1 h and hand-shaking for 1 h. The extractions with extractants soluble in the feed solution, *i.e.*, acetone and alcohols (ethanol, methanol and 2-propanol), the volume ratio of extractant to sample was also 1:2, agitation in an ultrasonic bath for 1 h and standing overnight at room temperature were applied.

RESULTS AND DISCUSSION

GC-MS acquisition

A chromatogram of the investigated phthalates is given in Fig. S-2 of the Supplementary material. The four phthalates were separated using the selected chromatographic conditions. The chromatogram shows that the separation of the phthalates (using the optimized conditions) occurred within a running time of 20 min and that GC-MS method is well suited for the simultaneous determination of the 4 phthalates. For the considered range of phthalate concentrations, $0.25\text{--}2.50\text{ }\mu\text{g mL}^{-1}$, the response of the mass-selective detector was linear. The correlation coefficients (R^2) ranged from 0.990 to 0.999. The limits of detection (LOD) values, calculated according to the Winefordner and Long criterion,²⁶ were $0.01\text{--}0.04\text{ }\mu\text{g mL}^{-1}$. The precision of the GC-MS method, expressed as the relative standard deviation (RSD , $n = 3$), was found to be in the range 1.7–4.9 %.

The retention times, selected masses and the scan start times for each phthalate studied by GC–MS are listed in Table I.

TABLE I. Target ions, retention times and scan start times for the investigated phthalates determined by GC–MS; target ions observed in SIM are shown in bold

Phthalate	<i>m/z</i>	Retention time, min	Scan start time, min
DMP	163 , 194	8.03	7.80
DBP	149 , 150, 223, 205	11.57	11.20
BBP	149 , 91, 206, 238	16.02	15.50
DEHP	149 , 167, 279, 150	18.39	17.90

Optimization of extraction procedure

The choice of the optimum extraction solvent for separation was determined from a consideration of several criteria: high boiling point and a low vapor pressure in order to reduce the risk of evaporation, high selectivity that enables fewer stages to be used, insolubility of solvent for prevention of solvent losses, good chromatographic behavior, and high partitioning coefficient of the analyte. Based on these considerations, several extraction solvents and mixture of solvents were investigated. As milk forms stable emulsions with the majority of solvents, all the investigated extractants were characterized by the appearance of extract and raffinate, the possibility to define the phase boundary, the possibility to perform phase separation, clearness of the extracts and formation of emulsions. Among the investigated solvents and solvent systems, *n*-hexane presented the best extractant because it gave a homogenous and clear extract with precipitated raffinate phase, thus a well-defined interfacial boundary and the possibility to separate the phases (Table II).

Agitation of samples with extractants enhanced the extraction efficiency and reduced the extraction time for reaching the equilibrium. In this study, stirring, shaking and ultrasonic treatment were investigated for the extraction of the phthalates from nine milk-based samples. Too vigorous agitation was avoided since it produced stable emulsions without visible phase boundary and the possibility of phase separation. In order to achieve effective phase separation, shaking of the samples and extractants was chosen as the best agitation method.

The extraction time to obtain higher peak areas of phthalates relative to internal standard peak area was investigated in the range of 10 to 30 min. An extraction time of 15 min was selected for extraction since the systems reached the steady state during this period.

The addition of an inorganic salt into a mixture of milk and a water-miscible organic solvent, such as acetonitrile, caused separation of the solvent from the mixture and the formation of a two-phase system. The results revealed that salt addition, although providing for a well-defined interfacial boundary, was not a satisfac-

TABLE II. Extraction systems studied for phthalate extraction from milk-based samples

Extractant	Appearance of:		Interfacial boundary	Phase separation
	Extract	Raffinate		
Acetone: <i>n</i> -hexane 1000 mL diluted milk sample was mixed with 10 mL acetone and 10 mL <i>n</i> -hexane, shaken for 30 min and repeated for extract enrichment. After settling overnight, the <i>n</i> -hexane/acetone phase was taken. The enriched extract was evaporated to dryness and re-dissolved in <i>n</i> -hexane.	Heterogeneous, creaming	Yellow, opaque	Not defined	—
Acetonitrile:NaCl 1000 mL diluted milk sample was mixed with 20 mL acetonitrile, 20 g sodium chloride, shaken for 30 min and repeated for extract enrichment. After settling overnight, the <i>n</i> -hexane/acetone phase was taken. The enriched extract was evaporated to dryness and redissolved in <i>n</i> -hexane.	Homogenous, clear	Precipitate	Well defined	—
Methanol: <i>n</i> -hexane 1000 mL diluted milk sample was mixed with 5 mL methanol and 15 mL <i>n</i> -hexane, shaken for 30 min and repeated for extract enrichment. After settling overnight, the <i>n</i> -hexane/acetone phase was taken. The enriched extract was evaporated to dryness and redissolved in <i>n</i> -hexane.	Heterogeneous, opaque	Voluminous precipitate	Not defined	—
Acetonitrile 1000 mL diluted milk sample was mixed with 20 mL acetonitrile. Agitation: ultrasonic bath for 1 h and hand shaking for 1 h. Extract phase submitted to new sample volume for enrichment with a final extract to solvent volume ratio of 1:50. Settling overnight. The combined extract was evaporated to dryness and redissolved in <i>n</i> -hexane.	Heterogeneous, yellow	Voluminous precipitate	Not defined	—
Ethyl acetate The same procedure as for acetonitrile	Homogenous, clear	Coalescence with creaming	Well defined	+
Cyclohexane The same procedure as for acetonitrile	Homogenous, clear	Foaming, precipitate	Well defined	+
<i>n</i> -Hexane The same procedure as for acetonitrile	Homogenous, clear	Precipitate	Well defined	+
Dichloromethane The same procedure as for acetonitrile	Heterogeneous, opaque	Precipitate	Well defined	+

TABLE II. Continued

Extractant	Appearance of		Interfacial boundary	Phase separation
	Extract	Raffinate		
Trichloroethane	Heterogeneous, opaque	Precipitate	Well defined	+
The same procedure as for acetonitrile				
Dichloroethane	Heterogeneous, opaque	Precipitate	Well defined	+
The same procedure as for acetonitrile				
Extractants soluble in feed solution	Appearance of extract and raffinate		Interfacial boundary	Phase separation
Methanol	Heterogeneous, voluminous precipitate,		Not defined	-
Ethanol				-
2-Propanol	flocculation			-
Acetone				-

tory method due to low phase separation and adhesion of milk globules on the wall of the separation funnel.

Based on literature data, the effect of the sample to solvent ratio on the total extracted phthalates from milk products was found to be the best at the 1:20 level. Various amounts of a mixture of solvents were used in order to determine the optimum quantity of the extracting solvent, based on the appearance of extract, phase boundary and possibility of phase separation.²⁷

This work showed that due to dilution of milk samples, the satisfactory ratio of solvent to sample volume was found to be at the 1:50 level, when the extract phase is several times submitted to a new sample volume, leading to better concentration of analyte and reduction in solvent consumption. In this way, enrichment of the extract phase with phthalates could be achieved by repeating the extraction procedure.

The study showed that the influence of milk type was not a critical factor in the determination of an adequate extraction procedure. All the observed effects for optimization of the extraction procedure were more or less the same for all six investigated samples of dairy products. Based on all the obtained results and observations during optimization of the extraction procedure, the parameters that provided the most efficient phthalate extraction were: ratio of sample volume to solvent volume, 1:2; the procedure of enrichment of the extract phase by submitting the extract to a new sample volume, to obtain a final extract to sample ratio 1:50, leading also to a reduction in solvent consumption; shaking as agitation method in order to avoid the formation of stable emulsions and an extraction time in the range 15 to 30 min.

Phthalate analysis in standard n-hexane solutions

Phthalates were identified by GC-MS in the full scan mode and quantified in the SIM mode. Linear calibration curves for the phthalates dissolved in *n*-hexane were obtained in the concentration range 0.25–2.50 µg mL⁻¹. The linearity range

and respective correlation coefficients (R^2) calculated in the range 0.25–2.50 $\mu\text{g mL}^{-1}$, the LOD and the LOQ values for each phthalate investigated in this study and determined by GC–MS (in SIM mode) are reported in Table III. The R^2 values for all the phthalates in the linear range were above 0.990. The LOD and LOQ values of each phthalate analyzed in this study were adequate for estimating such compounds in milk samples: the LOD values ranged between 0.01 and 0.04 $\mu\text{g mL}^{-1}$ whereas LOQ values ranged between 0.05 and 0.12 $\mu\text{g mL}^{-1}$ with RSD values between 1.7–4.9 %. These values were determined according to the Knoll definition,²⁸ i.e., an analyte concentration that produced a chromatographic peak equal to three times (LOD) and seven times (LOQ) the standard deviation of the baseline noise. In comparison with other extraction methods, this method provided comparable LOD and LOQ values.^{11,19}

TABLE III. Linearity range and the respective values of correlation coefficients (R^2), LOD and LOQ values, and repeatability (RSD) of each phthalate; linearity range: 0.25–2.50 $\mu\text{g mL}^{-1}$

Phthalate	R^2	$LOD / \mu\text{g mL}^{-1}$	$LOQ / \mu\text{g mL}^{-1}$	$RSD / \%$
DMP	0.999	0.04	0.12	4.9
DBP	0.999	0.01	0.05	1.7
BBP	0.992	0.02	0.08	2.4
DEHP	0.990	0.04	0.12	3.6

Phthalate analysis in matrix extracts

Validation of the phthalate quantification method in milk samples, considering the possible matrix effect, was performed with successive milk dilution. The high percentage of fat in milk may affect on the one hand the extraction efficiency of the phthalates and the analytical sensitivity, precision and stability of the response of the chromatographic system on the other. Therefore, for an estimation of the correlation of the milk fat content with the recovery for each phthalate, milk samples with different level of dilution were spiked and examined. For an estimation of the analytical sensitivity, the slopes of the curves obtained for diluted milk samples spiked with phthalates were examined and compared to the slopes of the calibration curves of phthalate standards in *n*-hexane.

As expected, higher phthalate recoveries were obtained by diluting the milk samples in water, whereby the recovery efficiency was improved by 60–80 %, compared to a dilution of 50 vol. % (Table IV). The low recovery rate (only 10 %) for the sample with 50 % milk content was expected due to the hydrophobic nature of phthalates, which are more soluble in milk fat globules giving lower distribution ratio between the extract and the milk sample. The recovery of phthalates was the highest for water samples (without any milk), which is in accordance with previous investigations performed with commercial bottled water samples.^{29,30}

TABLE IV. Phthalates recoveries (%) from spiked diluted milk samples with 3 ppb of each phthalate

Milk content, vol. %	DMP	DBP	BBP	DEHP
0	14.00	75.00	125.00	135.00
0.5	10.82	62.30	89.51	73.61
2	7.10	60.86	92.34	69.22
3	10.12	61.78	90.18	68.00
6	13.10	54.14	72.41	65.00
10	13.10	41.72	57.24	71.03
15	13.83	34.04	46.81	60.00
30	13.33	25.45	37.27	45.00
50	11.76	4.41	8.66	10.95

The lowest recovery values were for DMP which is the phthalate with the lowest molar mass, only one carbon atom in hydrocarbon side chain and with even 10^3 times higher water solubility than the rest of investigated phthalates. Generally, higher recovery is observed for the high-molecular weight phthalates ($\log K_{ow} = 7.6$ for DEHP), while low-molecular weight phthalates are more water-soluble relatively hydrophilic and thus the recovery decreases ($\log K_{ow} = 1.5$ for DMP). The same trend is observed for lower spike phthalate concentration of 3 ppb (Table IV) and for higher spike phthalate concentration of 6 ppb, as shown in Fig. 1.

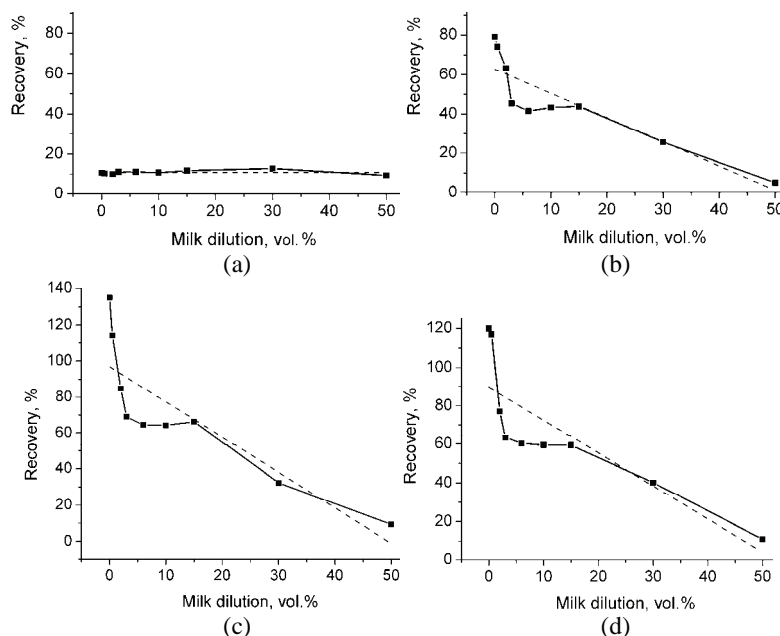


Fig. 1. Recoveries (average values) for the determination of phthalates in water dissolved milk samples spiked with $6 \mu\text{g ml}^{-1}$ of each phthalate: a) DMP, b) DBP, c) BBP and d) DEHP.

The analytical sensitivity of diluted milk samples spiked with phthalates were examined and compared to the calibration phthalate standards in *n*-hexane regarding the slopes of the obtained standard curves (Fig. 2).

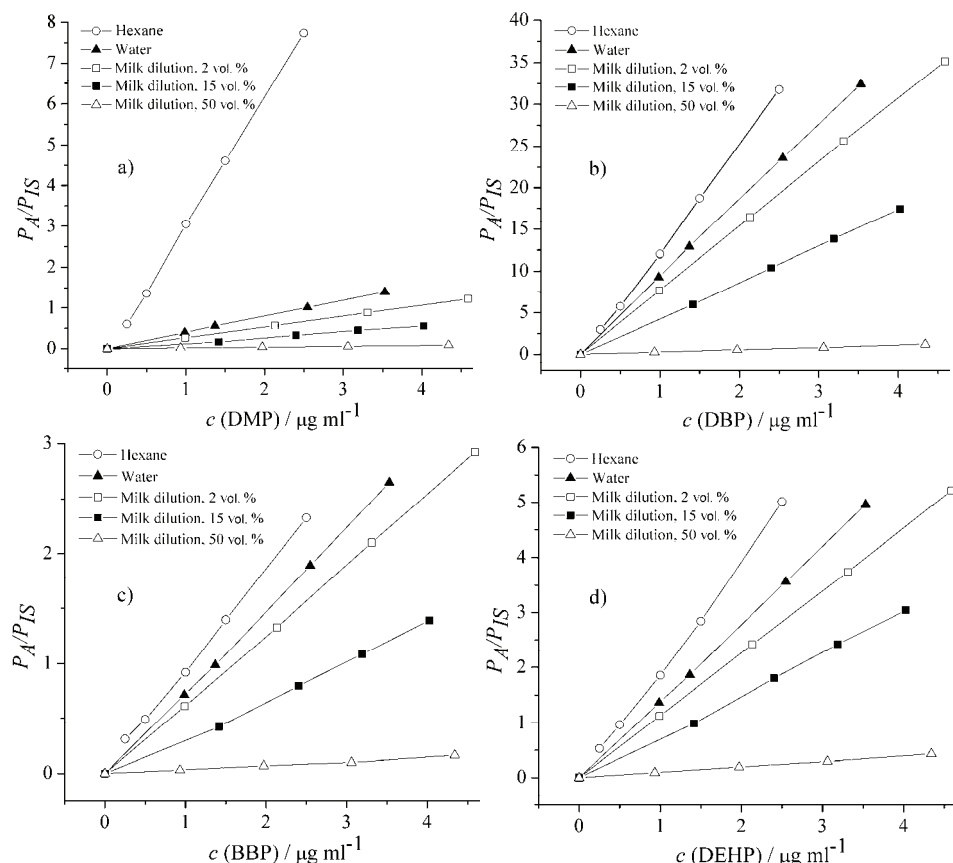


Fig. 2. The slopes of the curves for each phthalate prepared in *n*-hexane and milk matrix: a) DMP, b) DBP, c) BBP and d) DEHP. P_A and P_{IS} presents the values for chromatogram peak are of analyte and internal standard.

The concentrations of phthalates analyzed in the matrix extracts were in general lower than in *n*-hexane, showing a negative matrix effect that made for a less stable response of the chromatographic system and lower analytical sensitivity and precision.

The values of the slopes of the curve, obtained by linear regression and tabulated in Table V, show that the response and precision were the lowest for the milk sample with the highest fat content and for DMP as the most water soluble phthalate. This suggested a strategy for the elimination of matrix effect, *i.e.*,

dilution of the milk extract, especially for more hydrophobic phthalates such as the majority of commonly used phthalates.

TABLE V. Slopes of the curve obtained from solvent (*n*-hexane) and matrix (water and diluted milk samples)

Phthalate	<i>n</i> -Hexane	Water	Milk content, vol. %		
			2	15	50
DBP	12.8829	9.17614	7.6756	4.3494	0.28192
DEHP	1.9924	1.4067	1.135	0.7638	0.099
BBP	0.905	0.75284	0.6380	0.3490	0.0371
DMP	3.1800	0.39551	0.2669	0.14242	0.02068

CONCLUSIONS

The method of extraction of phthalates from milk samples by *n*-hexane was shown to be a simple and effective procedure. The validation results of the method were satisfactory, since the recovery data and relative standard deviation values indicated good method accuracy and precision ($R^2 > 0.990$) for phthalates when evaluated in a milk matrix. An increase in the recovery of less polar phthalates in matrix milk standards by matrix dilution was observed. Recovery for hydrophilic phthalates, such as DMP, was not changed by matrix dilution and was continuously low for the investigated method. The same trend for influence of matrix dilution on phthalate recovery was observed at two phthalate spiking levels. Elimination of the matrix effect by dilution of the milk extract, especially for more hydrophobic phthalates such as the majority of commonly used phthalates, was shown to be a satisfactory method.

SUPPLEMENTARY MATERIAL

The chemical structures of the four studied phthalates, GC-MS chromatogram of a standard solution containing phthalates and physicochemical properties of the four studied phthalate esters are available electronically from <http://www.shd.org.rs/JSCS/>, or from the corresponding author on request.

Acknowledgments. Financial support for this investigation from Ministry of Education, Science and Technological Development of the Republic Serbia, Project TR 31060, is gratefully acknowledged.

ИЗВОД

ЕВАЛУАЦИЈА МЕТОДЕ ЕКСТРАКЦИЈЕ ФТАЛАТА ИЗ МЛЕКА У ЗАВИСНОСТИ ОД
САДРЖАЈА МАСТИ У МЛЕКУ

ДАНИЦА С. МИЛОЈКОВИЋ¹, ДАРКО Х. АНЂЕЛКОВИЋ¹, ГОРДАНА М. КОЦИЋ² И ТАТЈАНА Д. АНЂЕЛКОВИЋ¹

¹Природно-математички факултет, Универзитет у Нишу, Вишеградска 33, 18000 Ниш и

²Медицински факултет, Универзитет у Нишу, Булевар гр Зорана Ђинђића 81, 18000 Ниш

У циљу одређивања диметил-фталата (DMP), ди-*n*-бутил-фталата (DBP), бензил бутил-фталата (BBP) и ди-(2-етилхексил)-фталата (DEHP) у шест различитих узорака млека упоређени су резултати добијени течно-течном екстракцијом куплованом са

гасном хроматографијом—масеном спектрометријом. Извршена је оптимизација екстракционих фактора: припрема узорака, врста и запремина органског растварача, ефекат исољавања и мешања и време екстракције. Одабрани су базни максимуми испитиваних фталата (m/z 149 за DBP, BBP и DEHP и m/z 163 за DMP) за даље истраживање. Снимање је извршено у моду мониторинга изабраног јона. Калибрациона права је линеарна у опсегу 0,25 до 2,50 $\mu\text{g mL}^{-1}$ са израчунатим LOD вредностима између 0,01 и 0,04 $\mu\text{g mL}^{-1}$ и LOQ вредностима између 0,05 μg и 0,12 $\mu\text{g mL}^{-1}$, са RSD између 1,7 и 4,9 %. Истраживање је показало раст измереног аналита ("recovery") за мање поларне фталате разблаживањем матрикса млека. "Recovery" за хидрофилне фталате, као што је ДМП, се не мења разблаживањем матрикса млека и константантно је низак за испитивану методу. Две концентрације унутрашњег стандарда ("spike"), тестиране ради испитивања утицаја разблажења млека на "recovery" фталата, показују исти тренд.

(Примљено 4. децембра 2014, ревидирано 26. фебруара, прихваћено 19. марта 2015)

REFERENCES

1. D. Cadogan, *Plast. Addit. Cmpd.* **4** (2002) 28
2. European Commission IP/99/829, *Ban of phthalates in childcare articles and toys*, 1999
3. R. H. Waring, R. M. Harris, *Maturitas* **68** (2011) 111
4. Department of Health and Human Services Centers for Disease Control and Prevention, *Third National Report on Human Exposure to Environmental Chemicals*, 2005
5. World Health Organization: Guidelines for Drinking Water Quality, 2008
6. X.-L. Cao, *Compr. Rev. Food. Sci. F.* **9** (2010) 21
7. European Food Safety Authority, *Opinion of the scientific panel on food additives, flavouring, processing aids and material in contact with food on a request from the Commission related to dibutyl phthalate (DBP) for use in food contact materials*, EFSA J. **242** (2005) 1
8. European Food Safety Authority, *Opinion of the scientific panel on food additives, flavouring, processing aids and material in contact with food on a request from the Commission related to butylbenzyl phthalate (BBP) for use in food contact materials*, EFSA J. **241** (2005) 1
9. European Food Safety Authority, *Opinion of the scientific panel on food additives, flavouring, processing aids and material in contact with food on a request from the Commission related to bis(2-ethylhexyl) phthalate (DEHP) for use in food contact materials*, EFSA J. **243** (2005) 1
10. O. Ballesteros, A. Zafra, A. Navalon, J. L. Vilchez, *J. Chromatogr. A* **1121** (2006) 154
11. A. Penalver, E. Pocurull, F. Borrull, R. M. Marce, *J. Chromatogr. A* **872** (2000) 191
12. N. Kayali, F. Tamayo, L. Polo-Diez, *Talanta* **69** (2006) 1095
13. K. Kato, M. J. Silva, J. W. Brock, J. A. Reidy, N. A. Malek, C. C. Hodge, H. Nakazawa, L. L. Needham, D. B. Barr, *J. Anal. Toxicol.* **27** (2003) 284
14. G. Mortensen, K. Main, A.-M. Andersson, H. Leffers, N. Skakkebak, *Anal. Bioanal. Chem.* **382** (2005) 1084
15. J. Zhu, S. Phillips, Y.-L. Feng, X. Yang, *Environ. Sci. Technol.* **40** (2006) 5276
16. M. Kim, S. J. Yun, G.-S. Chung, *Food. Addit. Contam.* **26** (2009) 134
17. M. A. Farajzadeh, D. Djozan, M. R. Afshar, M. J. Norouzi, *J. Sep. Sci.* **35** (2012) 742
18. H. Fromme, L. Gruber, E. Seckin, U. Raab, S. Zimmermann, M. Kiranoglu, M. Schlummer, U. Schewgler, S. Smolic, W. Volk, *Environ. Int.* **37** (2011) 715
19. B. Cavaliere, B. Macchione, G. Sindona, A. Tagarelli, *J. Chromatogr. A* **1205** (2008) 137
20. J. D. Carrillo, C. Salazar, C. Moreta, M. T. Tena, *J. Chromatogr. A* **1164** (2007) 248

21. N. Casajuana, S. Lacorte, *J. Agr. Food. Chem.* **52** (2004) 3702
22. Y. Tsumura, S. Ishimitsu, I. Saito, H. Sakai, Y. Kobayashi, Y. Tonogai, *Food. Addit. Contam.* **18** (2001) 449.
23. A. Fankhauser-Noti, K. Grob, *Anal. Chim. Acta* **582** (2007) 353
24. Z. Guo, S. Wang, D. Wei, M. Wang, H. Zhang, P. Gai, J. Duan, *Meat Sci.* **84** (2010) 484
25. Wisconsin Department of Natural Resources Laboratory Certification Program: Analytical Detection Limit Guidance & Laboratory Guide for Determining Method Detection Limits (1996) <http://dnr.wi.gov/regulations/labcert/documents/guidance/-lodguide.pdf>
26. G. L. Long, J. D. Winefordner, *Anal. Chem.* **55** (1983) 712A
27. T. Perez-Palacios, J. Ruiz, I. M. Ferreira, C. Petisca, T. Antequera, *Meat. Sci.* **91** (2012) 369
28. J. K. Knoll, *J. Chromatogr. Sci.* **23** (1985) 422
29. D. Milojković, T. Andelković, G. Kocić, in *Proceedings of 12th International Conference on Fundamental and Applied Aspects of Physical Chemistry*, Belgrade, Serbia, 2014, p. 925
30. D. Milojković, D. Andelković, T. Andelković, R. Nikolić, G. Kocić, N. Stojiljković, in *Proceedings of 51st Meeting of the Serbian Chemical Society*, Niš, Serbia, 2014, p. 78.

SUPPLEMENTARY MATERIAL TO
**Evaluation of a method for phthalate extraction from milk
related to the milk dilution ratio**

DANICA S. MILOJKOVIĆ¹, DARKO H. ANĐELKOVIĆ¹, GORDANA M. KOĆIĆ²
and TATJANA D. ANĐELKOVIĆ^{1*}

¹Faculty of Sciences and Mathematics, University of Niš, Višegradska 33, 18000 Niš, Serbia

and ²Faculty of Medicine, University of Niš, Bulevar dr Zorana Đindjića 81, 18000 Niš, Serbia

J. Serb. Chem. Soc. 80 (8) (2015) 983–996

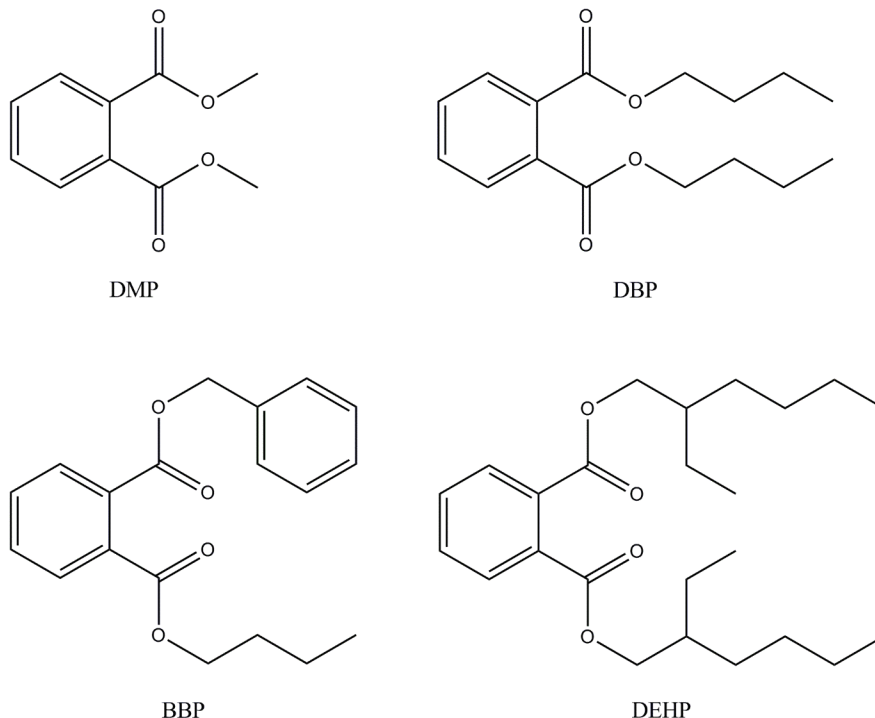
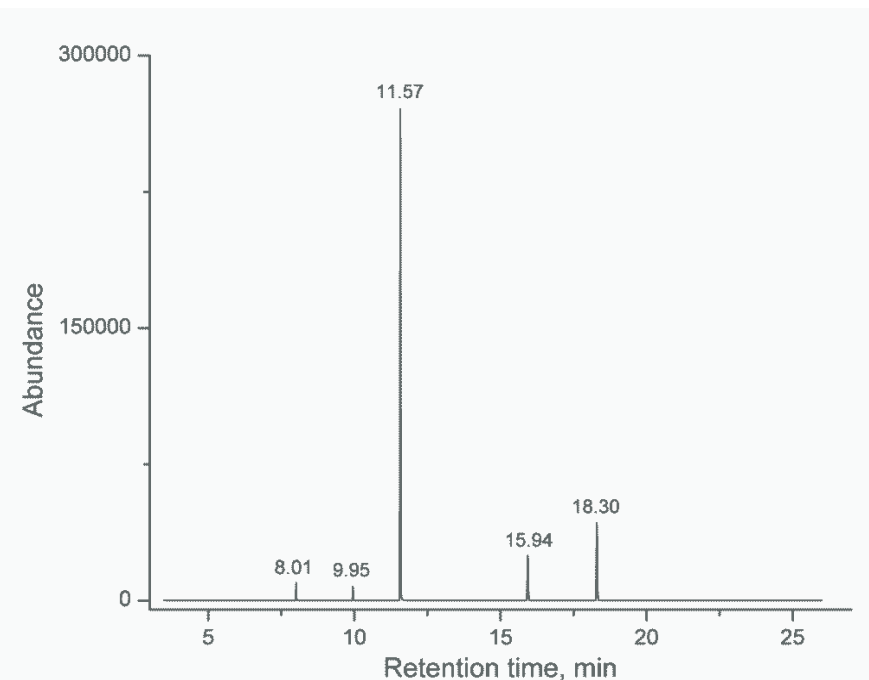


Fig. S-1. The chemical structures of the four studied phthalates.

*Corresponding author. E-mail: tatjanaan@gmail.com

TABLE S-I. Physicochemical properties of the four studied phthalate esters

Name	Acronym	CAS number	Molecular weight, g mol ⁻¹	Boiling point, °C	Water solubility at 25 °C, mg L ⁻¹	log K _{ow} 25 °C
Dimethyl phthalate	DMP	131-11-3	194.18	282	4200	1.5
Di- <i>n</i> -butyl phthalate	DBP	84-74-2	278.35	340	11.2	4.6
Benzyl butyl phthalate	BBP	85-68-7	312.36	370	2.7	4.7
Di-(2-ethylhexyl) phthalate	DEHP	117-81-7	390.56	386	3e ⁻³	7.6

Fig. S-2. GC-MS chromatogram of a standard solution containing the phthalates: DMP, DBP, BBP and DEHP each at a concentration of 0.25 µg mL⁻¹.



QTAIM investigation of a dipyrazol-1-ylmethane derivative and its Zn(II) complexes (ZnLX_2 , X = Cl, Br or I)

MARYAM DEHESTANI and LEILA ZEIDABADINEJAD*

Department of Chemistry, Shahid Bahonar University of Kerman, 76169 Kerman, Iran

(Received 24 February, revised 27 March, accepted 31 March 2015)

Abstract: Topological analyses of the electron density were performed on the bis(pyrazol-1-yl)methane derivative 9-(4-(di-1*H*-pyrazol-1-ylmethyl)phenyl)-9*H*-carbazole (**L**) and its zinc(II) complexes: ZnLCl_2 (**1**), ZnLBr_2 (**2**) and ZnLI_2 (**3**) using the quantum theory of atoms in molecules (QTAIM) at the B3PW91/6-31g(d) theoretical level. The topological parameters derived from the Bader theory were also analyzed; these are characteristics of Zn-bond critical points and of ring critical points. The calculated structural parameters were the frontier molecular orbital energies, the highest occupied molecular orbital energy (E_{HOMO}), the lowest unoccupied molecular orbital energy (E_{LUMO}), hardness (η), softness (S), the absolute electronegativity (χ), the electrophilicity index (ω) and the fractions of electrons transferred (ΔN) from ZnLX_2 complexes to **L**. Numerous correlations and dependencies between the energy terms of the symmetry adapted perturbation theory approach (SAPT), geometrical, topological and energetic parameters were detected and are described.

Keywords: ZnLX_2 ; charge transfer; bond critical point; SAPT.

INTRODUCTION

The coordination chemistry of di/poly-pyrazolylmethane has seen significant development during the past few years.^{1,2} One of the current interesting topics is to rationally design and synthesize supramolecular structures based on di/poly-pyrazolylmethane units, which are capable of multiple binding modes and have the potential to participate in important non-covalent interactions that direct their self-assembly into remarkable architectures.³ Compared with coordination bonds, non-covalent forces are weaker, but they are common and play critical roles in the formation of supramolecular structures due to their significant contribution to the self-assembly process.^{4–6} More studies focused on the weak non-covalent forces in the design and synthesis of supramolecular structures. Herein, the

*Corresponding author. E-mail: lzeidabadi@yahoo.com
doi: 10.2298/JSC150224027Z

dipyrazol-1-ylmethane derivative 9-(4-(di-1*H*-pyrazol-1-ylmethyl)phenyl)-9*H*-carbazole (**L**) and its zinc(II) complexes: ZnLCl₂ (**1**), ZnLBr₂ (**2**) and ZnLI₂ (**3**) are reported. The ligand **L**, ZnLBr₂ and ZnLI₂ were synthesized by Wang *et al.*⁷ In the solid state, each compound showed extensive non-covalent interactions, including weak hydrogen bonds and C···H···π interactions that organize the molecules into 2D and 3D structures. It could be stated that such interactions are common not only in the present compounds but also in a large number of known polypyrazolylborate and polypyrazolylmethane compounds.

QTAIM,⁸ the chemical bonds in both isolated species and molecular crystals can be classified and quantified in terms of features of the bond critical points in the electron density, both theoretically and experimentally. The variety of the atomic interactions can be approximately divided into shared (or covalent) interactions, intermediate (partially covalent) interactions and closed-shell (van der Waals, ionic, metal, *etc.*) interactions.^{9–11} The fundamental differences between the two limiting extremes in the interactions, *i.e.*, closed-shell interactions and shared ones, are the electron density features at the bond critical point. These are the value of electron density, ρ_b , and the sign of the Laplacian of the electron density, $\nabla^2\rho_b$, as well as the energy density $H_{e,b} = G_b + V_b$, where V_b and G_b are the potential and kinetic energy densities, respectively.^{10,11} Shared interactions exhibit $\rho_b \geq 0.14$ au, $\nabla^2\rho_b < 0$ and $H_b < 0$, while closed-shell interactions show $\rho_b \leq 0.05$ au, $\nabla^2\rho_b > 0$ and $H_b > 0$. In the intermediate region, $\nabla^2\rho_b(r) > 0$ and $H_b(r) < 0$.

The term non-covalent interaction may be ambiguous since covalency is attributed not only to typical chemical bonds. It is also connected with the hydrogen bond and with the other interactions, such as halogen or dihydrogen bonds. Covalency is usually attributed to charge transfer and polarization interaction energy contributions. It seems that there are meaningful differences between the interaction mentioned above, such as ionic bond and covalent bonds. The goal of this study was to apply density functional theory (DFT) calculations¹² and the QTAIM theory¹³ to analyze the properties of the N···Zn–X bonds in ZnLCl₂, ZnLBr₂ and ZnLI₂. The latter gives direct information on the presence and type of chemical bonds in these structures.

COMPUTATIONAL DETAILS

All calculations, including optimizations were performed with Gaussian 03 sets of code¹³ using the B3PW91/6-31G(d) level of theory without any symmetry restraints. Quantum chemical calculations of **L** based on density functional theory was performed at the B3PW91/6-31G(d) level and calculations of complexes **1–3** were realized with B3PW91/6-31G(d) for the C, H, N, Cl, Br and I atoms and the LANL2DZ basis set for the Zn atoms.

QTAIM was also applied, and the characteristics of the bond critical points (BCPs) and ring critical points (RCPs) were analyzed in terms of the following properties: the electron density at the critical point, its Laplacian and the total electron energy density at the critical point. For the latter, its components were also investigated: the potential electron energy

density and the kinetic electron energy density. The following relations are well known if all terms are expressed in atomic units:

$$\frac{1}{4} \nabla^2 \rho_b = 2G_b + V_b \quad (1)$$

$$H_{e,b} = G_b + V_b \quad (2)$$

The symmetry adapted perturbation theory (SAPT) approach was applied to deepen the understanding of the nature of the interactions¹⁴ for complexes **1–3**. The MOLPRO package¹⁵ was used to perform the calculations. SAPT is a well-established approach to calculate the interaction energy of two closed-shell moieties, whereby the interaction energy is obtained directly as the sum of defined contributions. Thus, it is different from the commonly applied approaches in which the binding energy is calculated as the difference between the energy of the complex and the sum of the energies of the monomers. In the SAPT approach, the interaction energy consists of the following terms: the first-order electrostatics $E_{\text{elst}}^{(1)}$, the second-order induction $E_{\text{ind}}^{(2)}$ and dispersion $E_{\text{disp}}^{(2)}$ energies, and their exchange counterparts: first-order exchange $E_{\text{exch}}^{(1)}$, second-order exchange–induction $E_{\text{exch-ind}}^{(2)}$ and exchange–dispersion $E_{\text{exch-disp}}^{(2)}$. The SAPT method up to the second order gives the main part of the interaction energy. The SAPT2 interaction energy is calculated according to Eq. (3):

$$E_{\text{int}}^{\text{SAPT2}} = E_{\text{elst}}^{(1)} + E_{\text{ind}}^{(2)} + E_{\text{disp}}^{(2)} + E_{\text{exch}}^{(1)} + E_{\text{exch-ind}}^{(2)} + E_{\text{exch-disp}}^{(2)} + \delta E_{\text{HF}} \quad (3)$$

RESULTS AND DISCUSSION

Structure of the ligand

Ligand L crystallizes in the monoclinic space group P2₁, selected bond distances and angles are listed in Table I. The molecular structure of L and its 1D linear chain are shown in Fig. 1. The dihedral angles between the carbazole ring and the central phenyl unit are 44.3° in molecule **a** and 46.9° in molecule **b**. In molecule **a**, the dihedral angles of the central phenyl unit and the pyrazole rings (R1, R2) are 71.4 and 80.4°, respectively. The dihedral angle of the two pyrazole rings (R1, R2) is 54.9°. In molecule **b**, the dihedral angles of the central phenyl unit and the pyrazole rings (R3, R4) are 71.8 and 80.0°, respectively. The dihedral angle of the two pyrazole rings (R3, R4) is 55.5°. There is no extended conjugation among the carbazole, phenyl and pyrazole rings.

In the molecular structure of complexes **1–3**, the Zn(II) ion is four coordinated by two nitrogen atoms of the pyrazolyl groups (L) and two halogen ions to form a distorted tetrahedral geometry. The two pyrazole groups linked to Zn(II) lead to changes in the structure of the ligand. In the structure of ZnLCl₂, shown in Fig. 2, the dihedral angles between the carbazole ring and the phenyl unit, between the phenyl unit and the pyrazole rings, and between the two pyrazole rings are 60, 78 and 77, and 52°, respectively. The dihedral angles between the carbazole ring and the phenyl unit, and between the phenyl unit and pyrazole rings are larger than those of the free ligand are. However, the dihedral angle of the two pyrazole rings is smaller than that observed for the free ligand, indicating that

TABLE I. Calculated geometry parameters of L, ZnLCl₂, ZnLBr₂ and ZnLi₂

Cmpd.	Bond length, Å		Bond angle, °
L	N1–N3	1.3411	N3–N1–C1 120.45
	N2–N4	1.3442	N4–N2–C1 121.36
	N1–C1	1.4546, (1.451) ⁹	N1–C1–H1 104.77
	N2–C1	1.4453, (1.455) ⁹	N2–C1–H1 106.38
	C1–C2	1.5112, (1.523) ⁹	N1–C1–N2 110.65, (110.7) ⁹
	C1–H1	1.1064	C2–C1–H1 108.59
	N1–N3	1.3474	N3–N1–C1 110.73
Complex 1	N2–N4	1.3479	N4–N2–C1 110.73
	N1–C1	1.4544	N1–C1–H1 104.76
	N2–C1	1.4447	N2–C1–H1 106.31
	C1–C2	1.5110	N1–C1–N2 110.73
	C1–H1	1.1019	C2–C1–H1 108.64
	Zn–Cl1	2.2091	N3–Zn–N4 86.97
	Zn–Cl2	2.1960	N3–Zn–Cl1 105.77
	Zn–N3	2.0848	N3–Zn–Cl2 112.71
	Zn–N4	2.0779	N4–Zn–Cl1 104.73
	N1–N3	1.3466	N3–N1–C1 120.95
Complex 2	N2–N4	1.3478	N4–N2–C1 120.87
	N1–C1	1.4545	N1–C1–H1 104.75
	N2–C1	1.4447	N2–C1–H1 106.31
	C1–C2	1.5109	N1–C1–N2 110.72
	C1–H1	1.1019	C2–C1–H1 108.65
	Zn–Br1	2.3033, (2.364) ⁹	N3–Zn–N4 86.76, (89.29) ⁹
	Zn–Br2	2.2993, (2.355) ⁹	N3–Zn–Br1 106.08, (109.6) ⁹
	Zn–N3	2.1019, (2.071) ⁹	N3–Zn–Br2 110.89, (120.4) ⁹
	Zn–N4	2.1007, (2.064) ⁹	N4–Zn–Br1 104.15, (108.0) ⁹
	N1–N3	1.3913	N3–N1–C1 120.27
Complex 3	N2–N4	1.3895	N4–N2–C1 120.54
	N1–C1	1.4545	N1–C1–H1 104.75
	N2–C1	1.4447	N2–C1–H1 106.31
	C1–H1	1.1019	C2–C1–H1 108.65
	Zn–I1	2.5109, (2.550) ⁹	N3–Zn–N4 91.57, (88.74) ⁹
	Zn–I2	2.4882, (2.533) ⁹	N3–Zn–I1 106.39, (108.3) ⁹
	Zn–N3	1.9468, (2.057) ⁹	N3–Zn–I2 116.78, (115.1) ⁹
	Zn–N4	1.9448, (2.050) ⁹	N4–Zn–I1 108.28, (109.1) ⁹

the planarity of ligand in complex 1 is worse than that for the free ligand. The Zn–N3 and Zn–N5 bond lengths are 2.0848 and 2.0779 Å, respectively. The bond distances of Zn–Cl1 and Zn–Cl2 are 2.2091 and 2.1960 Å, respectively. In complexes 2 and 3, the changes in the structure of ligand are similar to that of complex 1. The planarity of coordinated ligand is also worse than that of the free ligand. The corresponding angles and bond lengths for complexes 2 and 3 are listed in Table I and displayed in Figs. 3 and 4.

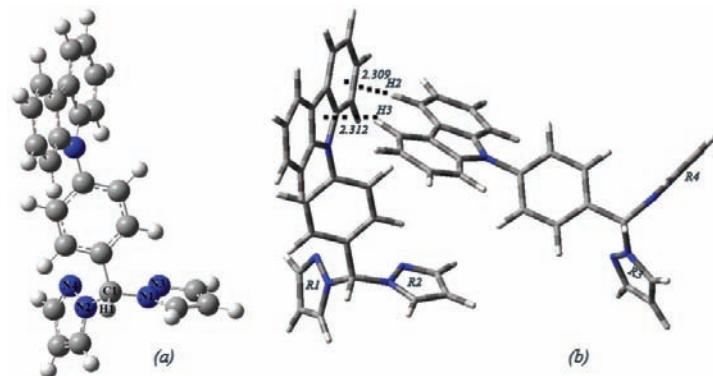


Fig. 1. a) The molecular structure of L and b) the 1D linear chain of ligand L. The bond lengths are in Å.

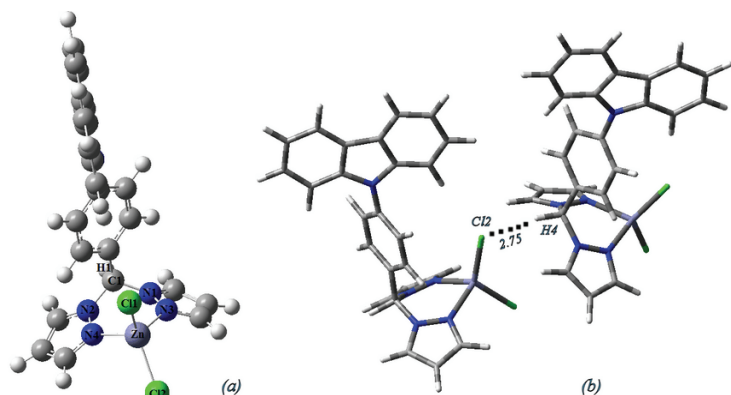


Fig. 2. a) The molecular structure of complex 1 and b) the 1D structure of complex 1 showing the weak C–H···Cl bond in Å.

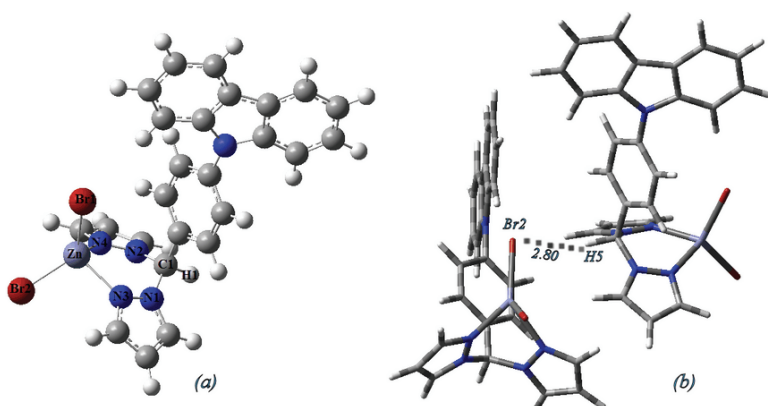


Fig. 3. a) The molecular structure of complex 2 and b) the 1D structure of complex 2 showing the weak C–H···Br bond in Å.

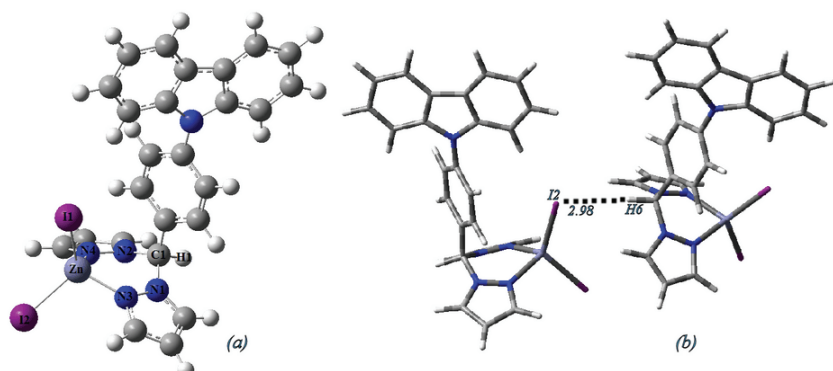


Fig. 4. a) The molecular structure of complex **3** and b) the 1D structure of complex **3** showing the weak C—H···I bond in Å.

Global reactivity descriptors

A large part of theoretical chemistry related to reactivity is based on the concept of frontier molecular orbitals (FMO), especially the lowest unoccupied molecular orbital (LUMO) and the highest occupied molecular orbital (HOMO). The interaction between these orbitals often allows a good description of the reactivity of reactions. The FMO theory says that the attack of an electrophilic species will occur where there is more density of the HOMO, whereas the attack of a nucleophilic species will occur in a region with a higher density of the LUMO. Parr and coworkers demonstrated that nearly all the frontier molecular theory could be rationalized from the DFT.¹⁶

The μ and molecular η for an N -electron system with total energy E_t and external potential $V(\vec{r})$ are defined respectively, as the first and second derivatives of the energy with respect to N :^{17,18}

$$\mu = \left[\frac{\partial E}{\partial N} \right]_{V(\vec{r})} = -\chi \quad (4)$$

and

$$\eta = \frac{1}{2} \left[\frac{\partial^2 E}{\partial N^2} \right]_{V(\vec{r})} = \frac{1}{2} \left[\frac{\partial \mu}{\partial N} \right] \quad (5)$$

where χ (eV) in Eq. (4) is the electronegativity. In numerical applications, μ and η are calculated using of the difference approximation:

$$\mu = -\frac{1}{2} (IP + EA) \quad (6)$$

$$\eta = \frac{1}{2} (IP - EA) \quad (7)$$

The vertical ionization potential (IP) and the electron affinity (E_A) can be obtained from the energy of the neutral, anionic, and the cationic species at the geometry of the corresponding N electron neutral species, as follows:

$$IP = [E(N-1) - E(N)] \quad (8)$$

$$E_A = [E(N) - E(N+1)] \quad (9)$$

Equations (6) and (7) can be simplified using the Koopmans theorem,¹² which approximates the electronic affinity and the ionization potential to the negative of the LUMO and HOMO energy, respectively.

$$\mu = -\frac{1}{2}(E_{\text{LUMO}} + E_{\text{HOMO}}) \quad (10)$$

$$\eta = \frac{1}{2}(E_{\text{LUMO}} - E_{\text{HOMO}}) \quad (11)$$

The electrophilicity index (ω) and global softness (S) are defined as follows:

$$\omega = \frac{\mu^2}{2\eta} \quad (12)$$

$$S = 1/\eta \quad (13)$$

According to Parr *et al.*,¹⁸ ω is a global reactivity index similar to the chemical hardness and chemical potential. This new reactivity index measures the stabilization in energy when the system reserves additional electronic charge (ΔN). The direction of the charge transfer is determined by the electronic chemical potential of the molecule because an electrophile is a chemical species capable of accepting electrons from the environment; its energy must decrease upon accepting an electronic charge. Thus, its electronic chemical potential must be negative.

The calculated values of E_{HOMO} , E_{LUMO} , χ , μ , η , S and ω for L and its complexes are listed in Table II.

In a reaction between two molecules, species can act as a nucleophile, which has a lower value of the electrophilicity index. The values of the electrophilicity index show that ZnCl_2 , ZnBr_2 and ZnI_2 are good nucleophiles; hence, these nucleophiles can attack the ligand L. Electrophilic charge transfer (ECT)¹⁹ is explained as the difference between the ΔN_{max} values of the interacting molecules. Considering two molecules A (L) and B (ZnCl_2 , ZnBr_2 and ZnI_2) approaching each other, two cases exist, *i*) $ECT > 0$, charge flow from B to A, *ii*) $ECT < 0$, charge flow from A to B. The ECT is calculated as follows:

$$ECT = (\Delta N_{\text{max}})_A - (\Delta N_{\text{max}})_B \quad (14)$$

where $(\Delta N_{\text{max}})_A = \mu_A / \eta_A$ and $(\Delta N_{\text{max}})_B = \mu_B / \eta_B$.

TABLE II. Calculated E_{HOMO} , E_{LUMO} , χ , μ , η , S and ω (in eV) for L, ZnCl_2 , ZnBr_2 and ZnI_2

Molecule	E_{HOMO} / eV	E_{LUMO} / eV	χ / eV	μ / eV	η / eV	S / eV	ω / eV
L	-0.1999	-0.0271	0.1135	-0.1135	0.0864	0.0432	0.0746
ZnCl_2	-0.3093	-0.1360	0.2226	-0.2226	0.0867	0.0433	0.2858
ZnBr_2	-0.2877	-0.1224	0.2051	-0.2051	0.0826	0.0413	0.2546
ZnI_2	-0.2699	-0.0678	0.1678	-0.1678	0.1010	0.0505	0.1394

The ECT was calculated as 1.253, 1.169 and 0.347 for complexes **1–3**, respectively. These results show that electrons are transferred from ZnX_2 to L. Therefore, the L was treated as an electron acceptor and, hence, ZnX_2 was treated as an electron donor. Thus, L has electrophilic behavior because the value of chemical potential is low. As shown in Table II, the high value of chemical potential and low value of electrophilicity index for these complexes **1–3** favor their nucleophilic behavior.

Local reactivity descriptors

The Fukui function (FF)^{16,20} or frontier function (f_k^+ , f_k^-) measures changes in electron number (removing electrons from the HOMO or adding electrons to LUMO, respectively) in chemical reactions and has been used to predict the reactivity of sites in a molecule. This function is a local density functional descriptor that is calculated using the proposed procedure based on a finite difference method.²¹

In this work, the two functions f^+ and f^- were used to determine electrophilic and nucleophilic attack, respectively. These functions can be given by:

$$f_k^+ = q_k^{(N+1)} - q_k^{(N)} \quad \text{for molecule } k \text{ as an electrophile}$$

$$f_k^- = q_k^{(N)} - q_k^{(N-1)} \quad \text{for molecule } k \text{ as a nucleophile}$$

where the parameters $q_k^{(N)}$, $q_k^{(N-1)}$ and $q_k^{(N+1)}$ are the charges of molecule k calculated in the systems N , $N-1$ and $N+1$ electrons, respectively, at the optimized geometry of the molecule with N electrons. In the past few years, the condensed Fukui functions have been used to explain the regioselectivity in chemical reactions.²² It is a tool that allows the prediction of which electron or moiety of a molecule will display more or less nucleophilic or electrophilic character. Electrophilic reactivity descriptors f_k^+ and nucleophilic reactivity descriptors f_k^- for all molecules are listed in Table III. The maximum values of the nucleophilic reactivity descriptors at Zn indicate that these sites are more prone to electro-

TABLE III. Selected reactivity descriptors indexes of ZnCl_2 , ZnBr_2 and ZnI_2

Molecule	Atom	$q(N)$	$q(N-1)$	$q(N+1)$	f_k^+	f_k^-
ZnCl_2	Zn	1.1269	1.2494	0.4060	-0.7208	-0.1226
ZnBr_2	Zn	0.9693	1.0814	0.2835	-0.6858	-0.1121
ZnI_2	Zn	0.7296	0.7651	0.0554	-0.6742	-0.0356

philic attack in the ZnCl_2 molecule. Thus, it can be stated that the Zn atom attacked the N atom of L corresponding in all complexes.

Relationship between geometrical and topological parameters

The calculations performed on the wide spectrum of related species enabled a deeper insight into the characteristics of intramolecular interactions to be obtained. Here, mainly relationships between the bond length and the characteristics of the corresponding bond critical point are considered. For the systems analyzed herein, a pseudo-ring containing the $\text{N}3\cdots\text{Zn}\cdots\text{N}4$ intramolecular bond is created and hence, an RCP also exist in complexes **1–3**. The geometrical and topological parameters of these interactions are presented in Table IV. Briefly summarizing, the greater is the electron density at the RCP of an intramolecular bond, the stronger is the interaction and the shorter is the bond. The $\text{Zn}\cdots\text{N}$ bond lengths are 2.2091, 2.3033 and 2.5109 Å for complexes **1–3**, respectively. The values of $\nabla^2\rho_b$ for complexes **1–3** are –0.0201, –0.0388 and –0.0579 au, respectively. As can be seen, the bond length is shorter and the value of $\nabla^2\rho_b$ higher in ZnLCl_2 than in the other complexes. Relatively, the values of the $\nabla^2\rho_b$, and

TABLE IV. Topological properties (in au) of the charge density at the bond critical point of L, ZnLCl_2 , ZnLBr_2 , and ZnLI_2 , $\rho(r)$, $\nabla^2\rho(r)$, and G_b , V_b , $H_{e,b}$ and $|V_b|/G_b$

Molecule	Bond	ρ_b	$\nabla^2\rho(r)$	G_b	V_b	$H_{e,b}$	$ V_b /G_b$
L	N1–C1	0.2772	0.2120	0.1352	0.3472	–0.2120	2.568
	N2–C1	0.2713	0.2030	0.1334	–0.4700	–0.3366	3.523
	C1–H1	0.2744	0.2350	0.0331	–0.3011	–0.2680	9.0967
	N1–N3	0.3748	0.1782	0.2132	–0.6046	–0.3914	2.8358
ZnLCl_2	N1–C1	0.2741	0.2070	0.1514	–0.5097	–0.3583	3.3666
	N2–C1	0.2688	0.1998	0.1413	–0.4823	–0.3410	3.4133
	N1–N3	0.3703	0.1768	0.2027	–0.5822	–0.3795	2.8722
	Zn–Cl1	0.0793	–0.0201	0.0829	–0.1157	–0.0328	1.395
	Zn–Cl2	0.0810	–0.0207	0.0849	–0.1192	–0.0343	1.4040
	Zn–N3	0.0722	–0.0620	0.0878	–0.1135	–0.0257	1.2927
	Zn–N4	0.0712	–0.0617	0.0866	–0.1114	–0.0248	1.2863
	N1–C1	0.2688	0.1998	0.1413	–0.4825	–0.3412	3.4147
ZnLBr_2	N2–C1	0.2741	0.2073	0.3580	–0.5088	–0.1508	1.4212
	N1–N3	0.3711	0.1775	0.2033	–0.5842	–0.3809	2.8735
	Zn–Br1	0.0782	–0.0388	0.0722	–0.1056	–0.3340	1.4620
	Zn–Br2	0.0779	–0.0393	0.0725	–0.1056	–0.3310	1.4566
	Zn–N3	0.0684	–0.0596	0.0822	–0.1047	–0.0225	1.2737
	Zn–N4	0.0683	–0.0593	0.0818	–0.1043	–0.0225	1.2751
	N1–C1	0.2379	0.0848	0.1232	–0.3313	–0.2081	2.6891
ZnLI_2	N2–C1	0.2427	0.0888	0.1276	–0.3441	–0.2165	2.6967
	N1–N3	0.2994	0.1065	0.1660	–0.4385	–0.2725	2.6416
	Zn–I1	0.0559	–0.0579	0.0587	–0.0596	–0.0009	1.0153
	Zn–I2	0.0538	–0.0563	0.0564	–0.0565	–0.0001	1.0018
	Zn–N3	0.0878	–0.1533	0.1571	–0.1608	–0.0037	1.0236
	Zn–N4	0.0882	–0.1538	0.1578	–0.1616	–0.0038	1.0241

$H_{e,b}$, also the values of $1 < |V_b|/G_b < 2$ indicate that the Zn–X (X = Cl, Br and I) and the Zn–N interactions in all complexes have a significant partially covalent component. For the N1–C1, N2–C1, C1–H1 and N1–N3 interactions, the values of the Laplacian are positive, which may mean that the ionic bond could not be classified as very strong one because all $H_{e,b}$ values are negative, which may indicate that such interactions are rather strong. With reducing electronegativity of the X atom connected to Zn(II), the bond strength decreases.

The SAPT calculations

The SAPT applied here seems to be a proper approach to analyze the closed-shell interactions. It was mentioned previously that the nucleophilic attack of Zn atom of ZnX_2 (X = Cl, Br and I) molecules on the ligand L leads to the formation of complexes **1–3**. The SAPT2 interaction energy as well as the interaction energy terms in Eq. (3) are given in Table V. If the attractive (negative) terms of the interaction energy are considered, the induction one, $E_{\text{ind}}^{(2)}$, seems to be the most important, followed by the electrostatic term, $E_{\text{elst}}^{(1)}$, and the dispersive term. However, the induction and dispersive terms are strongly damped by their exchange counterparts, $E_{\text{exch-ind}}^{(2)}$ and $E_{\text{exch-disp}}^{(2)}$, respectively. In the case of the induction interaction energy, it is reduced by 70–82 % while for the dispersive energy, its reduction is of 29–30 %. On the other hand, the first order electrostatic energy is outweighed by the first order exchange energy. This shows the role of the induction energy in spite of the fact that the latter one is strongly reduced by its counterpart. There are other observations; the absolute value of the dispersive energy is greater for the complex ZnLCl_2 than for the complexes ZnLBr_2 and ZnLI_2 , even if the exchange counterpart of the dispersion energy is taken into account. However all interaction energy terms are interrelated and thus for stronger interaction and consequently shorter intermolecular distance, the absolute values of all interaction energy terms increase.

TABLE V. SAPT interaction energies for the ZnLI_2 , ZnLBr_2 and ZnLCl_2 complexes

Energy term, au	ZnLI_2	ZnLBr_2	ZnLCl_2
$E_{\text{elst}}^{(1)}$	−9595.54	−10084.66	−10205.6
$E_{\text{ind}}^{(2)}$	11217.12	11786.44	11927.80
$E_{\text{disp}}^{(2)}$	−18535.24	−19475.99	−19709.57
$E_{\text{exch}}^{(1)}$	−3216.07	−3403.57	−3444.39
$E_{\text{exch-ind}}^{(2)}$	14696.23	15442.13	15627.33
$E_{\text{exch-disp}}^{(2)}$	959.7	1008.46	1020.56
δE_{HF}	−1524.66	−1575.72	−1594.07
$E_{\text{int}}^{\text{SAPT2}}$	−5998.46	−6302.91	−6378.50

CONCLUSIONS

The complexes of ligand L and the different non-covalent interactions were considered herein. It was found that for all interactions in which the Zn atom acts as a nucleophile, a relationship between the $Zn \cdots N$ distance and the Laplacian of electron density at the corresponding bond critical point exists. This indicates a region of partially covalent bonds where the Laplacian is negative and the electron density is lower of 0.15 au. Electrophilic charge transfer confirms that the electrons are transferred from the ZnX_2 to the ligand L; thus, the corresponding ligand can be treated as an electron acceptor. The results of Fukui functions indicate Zn atom attack on the N atom of the ligand. The SAPT approach was also applied to analyze interactions in the zinc complexes. It was found that the induction energy is the most important attractive interaction energy term for the studied complexes, followed by electrostatic and dispersive terms. This means that for such strong interactions, the electron density shift is very important for the process of complexation but also that electrostatic interactions steer the arrangement of sub-units in the complexes.

ИЗВОД

QTAIM ИСПИТИВАЊЕ ДЕРИВАТА ДИПИРАЗОЛ-1-ИЛМЕТАНА И ОДГОВАРАЈУЋИХ
 $Zn(II)$ КОМПЛЕКСА ($ZnLX_2$, $X = Cl, Br$ ИЛИ I)

MARYAM DEHESTANI¹ и LEILA ZEIDABADINEJAD¹

Department of Chemistry, Shahid Bahonar University of Kerman, 76169 Kerman, Iran

Применом квантне теорије атома у молекулама (QTAIM) на В3PW91/6-31g(d) нивоу теорије урађена је тополошка анализа електронске густине 9-(4-(ди-1Н-пиразол-1-илметил)фенил)-9Н-карбазола (L) и одговарајућих цинк(II) комплекса: $ZnLCl_2$ (**1**), $ZnLBr_2$ (**2**) и $ZnLI_2$ (**3**). Анализирани су тополошки параметри добијени применом Бадерове теорије који су карактеристични за критичне тачке координованог цинка и ароматичног прстена. Израчунати су следећи структурни параметри: енергија највише попуњене молекулске орбитале (E_{HOMO}), енергија најниже непопуњене молекулске орбитале (E_{LUMO}), тврди (η) и меки (S) карактер, апсолутна електронегативност (χ), индекс електрофилности (ω) и расподела електрона у комплексу $ZnLX_2$ (ΔN). Описане су корелације између енергије добијене применом SAPT теорије (симетријски прилагођена пертурбациона теорија), геометријских, тополошких и енергетских параметара.

(Примљено 24. фебруара, ревидирано 27. марта, прихваћено 31. марта 2015)

REFERENCES

1. S. Trofimenco, *Chem. Rev.* **93** (1993) 943
2. J. Xia, Z.-J. Zhang, W. Shi, J.-F. Wei, P. Cheng, *Cryst. Growth Des.* **10** (2010) 2323
3. D. L. Reger, R. P. Watson, M. D. Smith, P. J. Pellechia, *Organometallics* **1544** (2005) 24
4. F. Jin, F.-X. Zhou, X.-F. Yang, L.-H. Cheng, Y.-Y. Duan, H.-P. Zhou, L. Kong, F.-Y. Hao, J.-Y. Wu, Y.-P. Tian, *Polyhedron* **43** (2012) 1
5. C. B. Aakeröy, M. Fasulo, N. Schultheiss, J. Desper, C. Moore, *J. Am. Chem. Soc.* **129** (2007) 13772

6. M. Tuikka, M. Niskanen, P. Hirva, K. Rissanen, A. Valkonen, M. Haukka, *Chem. Commun.* **47** (2011) 3427
7. S.-C. Wang, Y.-C. Zhang, F. Jin, W.-D. Liu, H.-P. Zhou, J.-Y. Wu, Y.-P. Tian, *Synth. React. Inorg., Met.-Org. Nano-Met. Chem.* **45** (2015) 639
8. R.F. Bader, *Atoms in molecules*, Wiley Online Library, 1990
9. A. Ranganathan, G. Kulkarni, C. Rao, *J. Phys. Chem., A* **107** (2003) 6073
10. T.-H. Tang, E. Deretey, S. Knak Jensen, I. G. Csizmadia, *Eur. Phys. J., D* **37** (2006) 217
11. P. M. Dominiak, E. Grech, G. Barr, S. Teat, P. Mallinson, K. Woźniak, *Chem. Eur. J.* **9** (2003) 963
12. R. G. Parr, W. Yang, *Density-functional theory of atoms and molecules*, Oxford University Press, New York, 1989, p. 220
13. Gaussian 09, Revision D.01, Gaussian, Inc., Wallingford, CT, 2008
14. B. Jeziorski, R. Moszynski, K. Szalewicz, *Chem. Rev.* **94** (1994) 1887
15. H. J. Werner, P. Knowles, *MOLPRO*, University of Birmingham, 2012
16. R. G. Parr, W. Yang, *J. Am. Chem. Soc.* **106** (1984) 4049
17. P. Geerlings, F. De Proft, W. Langenaeker, *Chem. Rev.* **103** (2003) 1793
18. R. G. Parr, L. V. Szentpaly, S. Liu, *J. Am. Chem. Soc.* **121** (1999) 1922
19. J. Padmanabhan, R. Parthasarathi, V. Subramanian, P. Chattaraj, *J. Phys. Chem., A* **111** (2007) 1358
20. K. Senthilkumar, M. Ramaswamy, P. Kolandaivel, *J. Quantum Chem.* **81** (2001) 4
21. W. Yang, W. J. Mortier, *J. Am. Chem. Soc.* **108** (1986) 5708
22. G. F. Lehr, R. G. Lawler, *J. Am. Chem. Soc.* **106** (1984) 4048.



Multicenter Wiener indices and their applications

IVAN GUTMAN^{1,2*}, BORIS FURTULA^{1#} and XUELIANG LI³

¹Faculty of Science, University of Kragujevac, P. O. Box 60, 34000 Kragujevac, Serbia,

²State University of Novi Pazar, Novi Pazar, Serbia and ³Center for Combinatorics,
Nankai University, Tianjin, 300071, China

(Received 26 January, revised 12 February, accepted 13 February 2015)

Abstract: The Wiener index W could be viewed as a molecular structure descriptor composed of increments representing interactions between pairs of atoms. A generalization of the W are the Steiner–Wiener indices W_k , $k = 3, 4, \dots$. In the quantity W_k , interactions between k -tuples of atoms play a role, based on the concept of the Steiner distance. It is shown that the term $W + \lambda W_k$ provides an approximation for the boiling points of alkanes better than W itself. The best such approximation is obtained for $k = 7$.

Keywords: Wiener index; multicenter Wiener index; Steiner distance; Steiner–Wiener index; molecular graph.

INTRODUCTION

The Wiener index (W) is one of the oldest and most examined graph-based molecular structure descriptors. Details on its mathematical properties and chemical applications are given in reviews,^{1–5} recent research papers,^{6–9} and the references cited therein. On the occasion of the fiftieth anniversary of the Wiener index, three special journal issues were published.^{10–12} Additional historical data on W can be found in a survey.¹³

The Wiener index is defined in the following manner. Let G be a molecular graph and v_1, v_2, \dots, v_n be its vertices. The distance between the vertices v_i and v_j , denoted by $d(v_i, v_j)$, is the number of edges in (= the length of) the shortest path that connects v_i and v_j . Then:

$$W = W(G) = \sum_{i < j} d(v_i, v_j) \quad (1)$$

with the summation embracing all pairs of vertices (v_i, v_j) of the molecular graph G .

* Corresponding author. E-mail: gutman@kg.ac.rs

Serbian Chemical Society member.

doi: 10.2298/JSC150126015G

Bearing in mind that each vertex of the molecular graph represents an atom of the underlying molecule,¹⁴ the quantity W , defined by means of Eq. (1), may be viewed as a sum of structural increments representing pairs of atoms, *i.e.*, two-center interatomic interactions.

From this point of view, one could think of three-center, four-center, *etc.* interactions that would lead to the following evident multicenter extension of the Wiener-index concept:

$$W_3 = W_3(G) = \sum_{i < j < k} d(v_i, v_j, v_k) \quad (2)$$

$$W_4 = W_4(G) = \sum_{i < j < k < l} d(v_i, v_j, v_k, v_l) \quad (3)$$

$$W_5 = W_5(G) = \sum_{i < j < k < l < m} d(v_i, v_j, v_k, v_l, v_m) \quad (4)$$

etc. In formulas (2)–(4), the meaning of the three-, four-, five-vertex distances requires clarification. In fact, a long time ago, Chartrand *et al.* introduced such a multi-vertex distance into graph theory,¹⁵ which was eventually much studied under the name “Steiner distance”.¹⁶ Its definition is given in the subsequent section.

The multicenter Wiener-type indices based on the Steiner distance will be referred to as “Steiner–Wiener indices” and are defined in the subsequent section. The present work is aimed at establishing their chemical applicability.

STEINER DISTANCE AND STEINER–WIENER INDEX

Let G be a connected graph with n vertices. Let $S = \{v_{i_1}, v_{i_2}, \dots, v_{i_k}\}$ be a set of k distinct vertices of G . Then the Steiner tree, $T(S)$, is a tree (= connected acyclic graph) that is a subgraph of G , containing all vertices of S , and possessing a minimal number of edges. The number of edges of $T(S)$ is the Steiner distance of the vertices $v_{i_1}, v_{i_2}, \dots, v_{i_k}$. For details on the Steiner-distance concept, see elsewhere.^{17,18}

For $k = 2, 3, \dots, n$, the k -th Steiner–Wiener index of the (molecular) graph G is defined as:

$$W_k = W_k(G) = \sum_S d(v_{i_1}, v_{i_2}, \dots, v_{i_k}) \quad (5)$$

where the summation goes over all k -element subsets $S = \{v_{i_1}, v_{i_2}, \dots, v_{i_k}\}$ of the vertex set of G .

Steiner–Wiener indices, W_k , were recently considered,¹⁹ and their basic mathematical properties determined. Some of these are the following:

1. $W_2(G)$ coincides with the ordinary Wiener index $W(G)$, Eq. (1).
2. Eqs. (2), (3), and (4) are special cases of Eq. (5), for $k = 3$, $k = 4$ and $k = 5$, respectively.
3. For a graph G with n vertices, if $k = n$, then $W_k(G) = n - 1$.
4. For a graph G with n vertices, if $k > n$, then $W_k(G) = 0$.

For a tree T , and for all $k = 2, 3, \dots, n$:

$$W_k(T) = \sum_e \sum_{i=1}^{k-1} \binom{n_1(e)}{i} \binom{n_2(e)}{k-i} \quad (6)$$

where $n_1(e)$ and $n_2(e)$ are the number of vertices lying on the two sides of the edge e , and where the first summation goes over all edges of T . For all edges e of the tree T , $n_1(e) + n_2(e) = n$.

Note that for $k = 2$, formula (6) reduces to the expression (7), discovered by Wiener himself as early as in 1947.^{7,14,20}

$$W(T) = \sum_e n_1(e)n_2(e) \quad (7)$$

STEINER-WIENER INDICES AND BOILING POINTS OF ALKANES

The first chemical application of the Wiener index was its usage for the prediction of the normal boiling points of alkanes.²⁰ Eventually, correlations with boiling points became a standard test for the quality of topological indices.^{21–24} In view of this, this physico-chemical parameter is also used in these studies of the Steiner–Wiener indices.

The well known²³ plot of the normal boiling points *vs.* the Wiener index is reproduced in Fig. 1. The curve passing through the data-points is of the form:

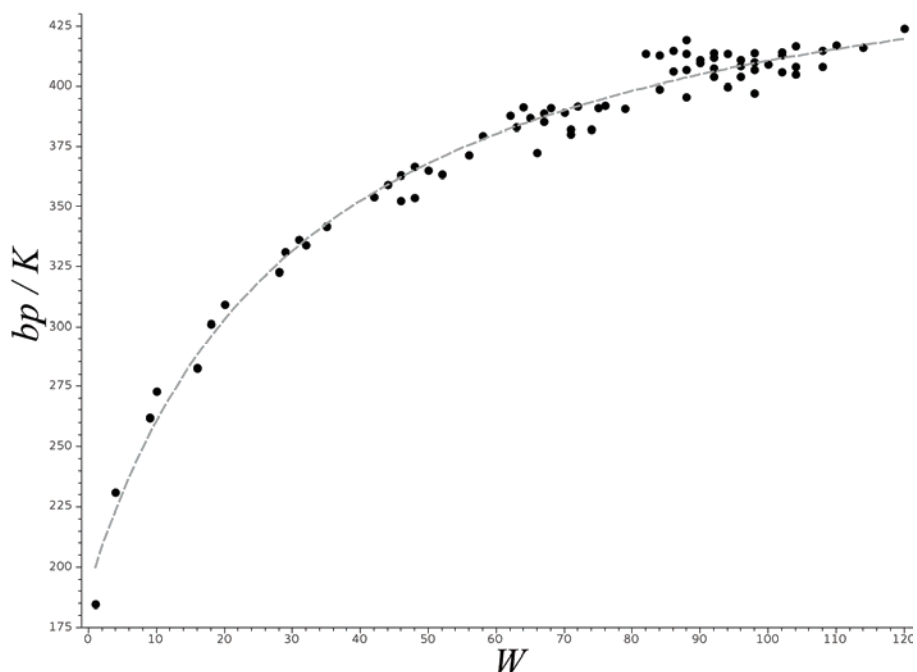


Fig. 1. Correlation between normal boiling points (bp / K) and Wiener index (W) for the set of all isomeric alkanes with 2 to 9 carbon atoms (74 compounds).²⁵ The curve passing through the data-points is specified by Eq. (8). Statistical data pertaining to this correlation are found in Tables I and II, for $k = 2$.

$$bp \approx bp_{\text{calc}}(W^*) = \frac{a + bW^*}{1 + cW^*} \quad (8)$$

where $W^* = W$ and where a , b and c are fitting parameters. The correlation between the experimental and calculated boiling points (*i.e.*, between bp and bp_{calc} , *cf.* Eq. (8)), is shown in Fig. 2.

TABLE I. Fitting parameters in formulas (8) and (9), for $k = 2, 3, \dots, 9$. The (a, b, c) -values were obtained by means of the scaled Levenberg–Marquardt algorithm.²⁶ The λ -values are those for which the respective correlation coefficients are maximal, *cf.* Fig. 3. The parameters for the best approximation are indicated by boldface

k	a	b	c	λ
2	191.328	15.104	0.031	–
3	192.480	14.547	0.031	0.023
4	193.704	14.820	0.032	0.044
5	191.287	16.476	0.037	0.063
6	186.764	18.773	0.043	0.127
7	181.255	21.421	0.049	0.392
8	180.547	20.834	0.047	0.802
9	187.788	16.790	0.036	1.400

TABLE II. Statistical data for the correlations between boiling points and the topological indices $W^* = W + \lambda W_k$, $k = 2, 3, \dots, 9$; R = correlation coefficient, ARE = average relative error (in %), MRE = maximal observed relative error (in %). The data for the best approximation are indicated by boldface. For details, see Eqs. (8) and (9) and the text

k	R	ARE	MRE
2	0.98954	1.45	8.42
3	0.98957	1.45	8.83
4	0.99018	1.41	9.46
5	0.99135	1.33	8.58
6	0.99256	1.23	6.80
7	0.99323	1.18	4.63
8	0.99273	1.23	4.19
9	0.99149	1.33	6.98

The most obvious idea for testing the Steiner–Wiener indices would be to set $W^* = W_k$ into Eq. (8). This, however, did not yield any improvement, and thus had to be abandoned. A better option was to modify the Wiener index as:

$$W^* = W + \lambda W_k \quad (9)$$

and use the variable W^* in combination with Eq. (8). For each fixed choice of k , $k = 3, 4, \dots, 8$, the parameter λ was varied, and its value determined to maximize the correlation coefficient for the linear correlation between bp and $bp_{\text{calc}}(W^*)$. In all the studied cases, an optimal value for λ exists at which the correlation coefficients attain a maximum; a characteristic example is shown in Fig. 3.

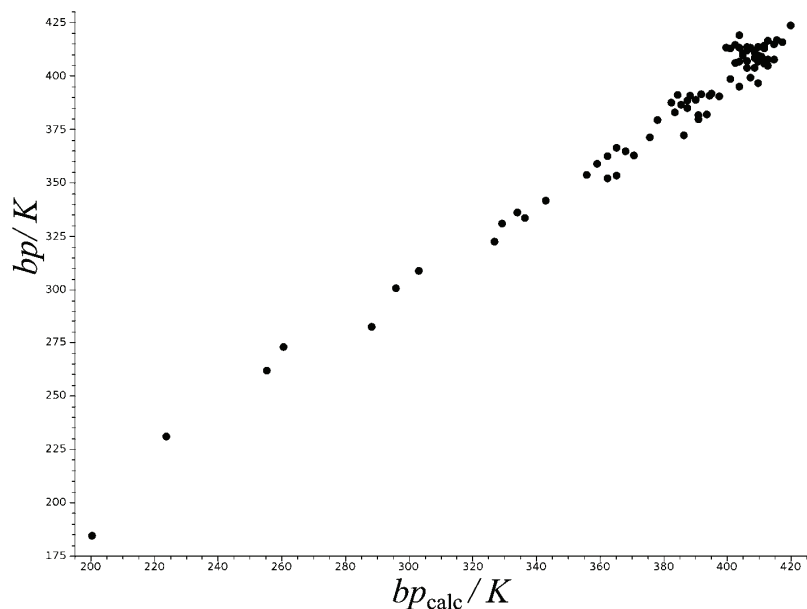


Fig. 2. Correlation between the calculated boiling points (bp_{calc} , according to Eq. (8), $W^* = W$) and the experimental boiling points (bp) for the same compounds as in Fig. 1. Statistical data pertaining to this correlation are found in Tables I and II, for $k = 2$.

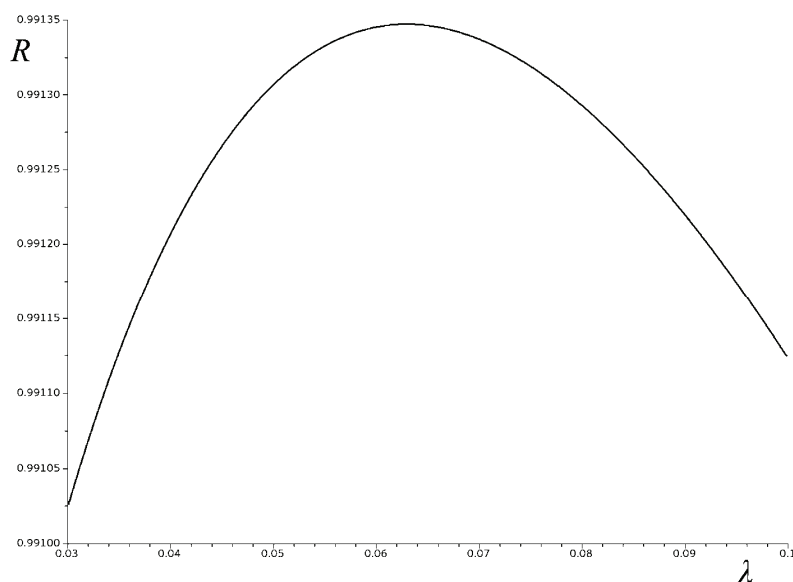


Fig. 3. The λ -dependence of the correlation coefficient R for the correlation between bp and bp_{calc} for the case $k = 5$. The maximum is attained at $\lambda = 0.063$, cf. Table I.

The results thus obtained are presented in Tables I and II, and in Figs. 4 and 5.

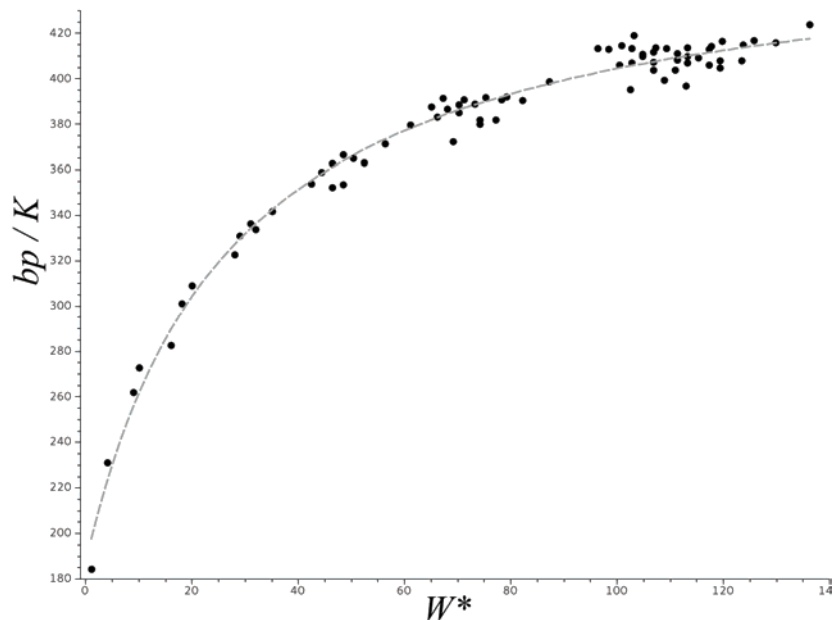


Fig. 4. Normal boiling points (bp / K) vs. $W + \lambda W_7$ for the same alkanes as in Fig. 1. As the data in Tables I and II show, the choice $k = 7$ provides the best agreement between bp and bp_{calc} , cf. Eqs. (8) and (9).

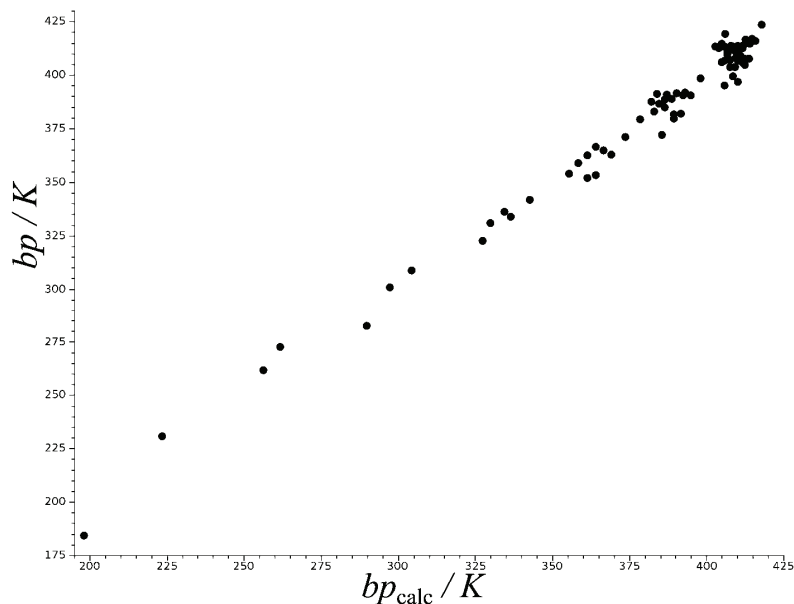


Fig. 5. The best correlation between bp and bp_{calc} , was obtained by Eqs. (8) and (9) for $k = 7$. Statistical data pertaining to this correlation are to be found in Tables I and II.

DISCUSSION AND CONCLUDING REMARKS

Viewing at the Wiener index as a structure descriptor based on two-center interatomic interactions, it could be expected that the next-important structural feature would be three-center interactions. In the case of Steiner–Wiener index applied to alkanes, this certainly cannot be the case, since for trees the following identity holds:

$$W_3(T) = \frac{n-2}{2} W(T) \quad (10)$$

Therefore, W_3 contains the exactly same structural information as the ordinary Wiener index, W .

Relation (10) is deduced from Eq. (6) as follows. For $k=3$, Eq. (6) has the form:

$$W_3(T) = \sum_e \left[\binom{n_1(e)}{1} \binom{n_2(e)}{2} + \binom{n_1(e)}{2} \binom{n_2(e)}{1} \right]$$

which, bearing in mind that $n_1(e) + n_2(e) = n$, is transformed into:

$$\begin{aligned} W_3(T) &= \sum_e \left[n_1(e) \frac{n_2(e)[n_2(e)-1]}{2} + n_2(e) \frac{n_1(e)[n_1(e)-1]}{2} \right] \\ &= \sum_e n_1(e) n_2(e) \frac{n_1(e) + n_2(e) - 2}{2} = \frac{n-2}{2} \sum_e n_1(e) n_2(e) \end{aligned}$$

Formula (10) is now obtained from Eq. (7).

The calculations fully agree with the above argument: The accuracies of the models for $k=2$ and $k=3$ were the same, see Table I.

If $k > 3$, because of the very large number of k -tuples of vertices, the calculation of the Steiner–Wiener index W_k based on its definition (5) becomes extremely cumbersome. In the case of acyclic systems (such as the molecular graphs of alkanes), instead of Eq. (5), the calculations could be realized using Eq. (6), which is significantly easier. In fact, by means of Eq. (6) any Steiner–Wiener index W_k could be calculated just as easily as the ordinary Wiener index W .

The fact that the accuracy of the approximations based on the indices $W^* = W + \lambda W$ increases with k , and reaches its maximum at $k=7$, is somewhat unexpected. It may be that this is a statistics-based artifact of the considered models. Nevertheless, this phenomenon deserves further examination.

The results of the present study may be considered from a pessimistic and from an optimistic point of view. A pessimist would say that there is very little difference between the Figs. 1 and 4, as well as between Figs. 2 and 5. An optimist would point to the fact that the average and maximal errors of the best

model (based on $W + \lambda W_7$) are, respectively, by 20 and 50 % smaller than those of the starting model (based solely on W). In view of this, it may be concluded that by adding multicenter distance-contributions to the Wiener index, its applicability to model physicochemical properties of alkanes is improved, but only to a limited extent.

ИЗВОД
ВИШЕЦЕНТРИЧНИ ВИНЕРОВИ ИНДЕКСИ И ЊИХОВЕ ПРИМЕНЕ

ИВАН ГУТМАН^{1,2}, БОРИС ФУРТУЛА¹ и XUELIANG LI³

¹Природно-математички факултет Универзитета у Крајеву, ²Државни универзитет у Новом Пазару и ³Center for Combinatorics, Nankai University, Tianjin, China

Винеров индекс W се може посматрати као молекулски структурни дескриптор састављен од сабирача који репрезентују интеракције између парова атома. Једна генерализација Винеровог индекса су Штајнер–Винерови индекси W_k , $k = 3, 4, \dots$ У индексу W_k се води рачуна о интеракцијама k атома, заснованих на појму Штајнеровог растојања. Показано је да формула $W + \lambda W_k$ омогућава апроксимативно израчунавање тачке кључња алкана боље него сам Винеров индекс. Најбоља таква апроксимација је за $k = 7$.

(Примљено 26. јануара, ревидирано 12. фебруара, прихваћено 13. фебруара 2015)

REFERENCES

1. I. Gutman, Y. N. Yeh, S. L. Lee, Y. L. Luo, *Indian J. Chem., A* **32** (1993) 651
2. S. Nikolić, N. Trinajstić, Z. Mihalić, *Croat. Chim. Acta* **68** (1995) 105
3. D. H. Rouvray, in *Topology in Chemistry – Discrete Mathematics of Molecules*, D. H. Rouvray, R. B. King, Eds., Horwood, Chichester, 2002, p. 16
4. K. Xu, M. Liu, K. C. Das, I. Gutman, B. Furtula, *MATCH Commun. Math. Comput. Chem.* **71** (2014) 461
5. M. Liu, B. Liu, *MATCH Commun. Math. Comput. Chem.* **69** (2013) 491
6. A. Hamzeh, S. Hosseini-Zadeh, A. R. Ashrafi, *MATCH Commun. Math. Comput. Chem.* **69** (2013) 47
7. R. Škrekovski, I. Gutman, *MATCH Commun. Math. Comput. Chem.* **72** (2014) 295
8. H. Lin, *MATCH Commun. Math. Comput. Chem.* **72** (2014) 783
9. K. Hrinakova, M. Knor, R. Škrekovski, A. Tepeh, *MATCH Commun. Math. Comput. Chem.* **72** (2014) 791
10. *50th Anniversary of the Wiener Index*, I. Gutman, S. Klavžar, B. Mohar, Eds., *Discr. Appl. Math.* **80** (1997), pp. 1–113
11. *Fifty Years of the Wiener Index*, I. Gutman, S. Klavžar, B. Mohar, Eds., *MATCH Commun. Math. Comput. Chem.* **35** (1997), pp. 1–259
12. *Fifty Years of the Wiener Index*, I. Gutman, Ed., *J. Serb. Chem. Soc.* **62** (1997), pp. 185–294
13. D. H. Rouvray, in *Topology in Chemistry – Discrete Mathematics of Molecules*, D. H. Rouvray, R. B. King, Eds., Horwood, Chichester, 2002, p. 1
14. I. Gutman, O. E. Polansky, *Mathematical Concepts in Organic Chemistry*, Springer, Berlin, Germany, 1986
15. G. Chartrand, O. R. Oellermann, S. Tian, H. B. Zou, *Časopis Pest. Mat.* **114** (1989) 399
16. Jakob Steiner (1795–1863), Swiss mathematician

17. F. K. Hwang, D. S. Richards, P. Winter, *The Steiner Tree Problem*, North-Holland, Amsterdam, 1992
18. W. Goddard, O. R. Oellermann, in: *Structural Analysis of Complex Networks*, M. Dehmer, Ed., Birkhäuser, Dordrecht, 2011, pp. 49–72
19. X. Li, Y. Mao, I. Gutman, *Discuss. Math. Graph Theory*, in press
20. H. Wiener, *J. Am. Chem. Soc.* **69** (1947) 17
21. D. H. Rouvray, *J. Comput. Chem.* **8** (1987) 470
22. P. G. Seybold, M. May, U. A. Bagal, *J. Chem. Educ.* **64** (1987) 575
23. Z. Mihalić, N. Trinajstić, *J. Chem. Educ.* **69** (1992) 701
24. G. Rücker, C. Rücker, *J. Chem. Inf. Comput. Sci.* **39** (1999) 788
25. R. L. Brown, S. E. Stein, in: *NIST Standard Reference Database No. 69*, P. J. Linstrom, W. G. Mallard, Eds., Gaithersburg, MD, 2014, <http://webbook.nist.gov>
26. J. Nocedal, S. J. Wright, *Numerical Optimization*, Springer, New York, 2006.



Dynamics of cetyltrimethylammonium bromide-mediated reaction of phenylsulfinylacetic acid with Cr(VI): Treatment of pseudo-phase models

PERUMAL SUBRAMANIAM^{1*} and NATESAN THAMIL SELVI²

¹Research Department of Chemistry, Aditanar College of Arts and Science, Tiruchendur-628 216, Tamil Nadu, India and ²Govindammal Aditanar College for Women, Tiruchendur-628 215, Tamil Nadu, India

(Received 19 September, revised 28 December, accepted 31 December 2014)

Abstract: The influence of cetyltrimethylammonium bromide, CTAB, on the oxidative decarboxylation of phenylsulfinylacetic acid, PSAA, and several *meta*- and *para*-substituted PSAs by Cr(VI) was investigated in 95 % H₂O–5 % CH₃CN medium. The rate profile displayed a peculiar trend with an initial rate increase at low CTAB followed by sharp rate inhibition at higher CTAB concentrations. The initial rate acceleration could be explained by strong binding of SO₄²⁻ on the positively charged micellar surface. The specific partitioning of PSAA in the micellar phase by hydrophobic interaction and the oxidizing species HCrO₃⁺ in aqueous phase by electrostatic repulsion accounted for the rate retardation at higher CTAB concentrations. The Hammett plot with different substituted PSAs showed excellent correlation affording negative ρ value, which supports the proposed mechanism involving the intermediate formation of sulfonium cation. The obtained ρ value in CTAB medium was found to be slightly lower than that in aqueous medium. Quantitative analysis of the rate data for the inhibition shown by CTAB was performed using the Menger–Portnoy and the Piszkevicz pseudo-phase models. The binding constant for PSAA with micelles was evaluated from the Piszkevicz cooperative model.

Keywords: phenylsulfinylacetic acid; Cr(VI); CTAB micellar effect; Hammett correlation; Piszkevicz cooperative model.

INTRODUCTION

Surfactants and their micellar aggregates exhibit widespread applications in chemical, biochemical, pharmaceutical and industrial fields. Cationic surfactants are useful as antifungal, antibacterial and antiseptic agents and have attracted much attention with reference to their interaction with DNA and lipids.¹ The

*Corresponding author. E-mail: subramaniam.perumal@gmail.com
doi: 10.2298/JSC140916001S

fascinating feature of aqueous surfactant solution is their self-organization into micelles above the critical micellar concentration, *cmc*. This leads to micellar aggregates having an architecture in which the hydrophobic groups of surfactants occupy the interior while the hydrophilic head groups at the surface are in contact with bulk water. In the case of ionic micelles, the interface is charged giving rise to an electrical double layer with a potential difference up to hundred of millivolts between the micellar pseudo-phase and water. Thus, the electrostatic potential and polarity prevailing in the interior of the aggregate differ from those of the bulk aqueous phase.

The redox processes in micellar media are considered as models to obtain insight into the dynamics and mechanistic paths of several redox processes occurring in complex biological systems.^{2–5} Micellar systems were used in a number of studies, including oxidation reactions, due to their effectiveness in altering the rate of the reactions by their inherent characteristics of their surface activity.^{6–11} Micelles act as nano reactors that may drastically modulate the reactivity of entrapped reactants. The importance of micelles arise from the fact that micelle catalyzed reactions resemble enzyme catalyzed reactions in several aspects.¹² The investigation of coupled systems composed of electron transfer and micelle-forming surfactant may contribute in a unique way to the understanding of the redox processes. Ionic micelles typically catalyze the reactions of a reactive counter ion with hydrophobic substrates that bind to the micelles.^{13–16} For bimolecular reactions, inhibition arises from the incorporation of one reactant into the micellar pseudo-phase and exclusion of the other from it.

Although there are several reports in the literature on the investigation of micellar effects on the redox reactions of organic sulfur compounds,^{16–21} the corresponding study on sulfur-containing carboxylic acids is limited. Even though phenylsulfinylacetic acid (PSAA) shows a wide range of synthetic utility, no reports are available in the literature on the oxidation of PSAA except a few recent works.^{22–25} Hence, this investigation of the redox reaction between PSAA and Cr(VI) in the presence of cationic surfactant cetyltrimethylammonium bromide (CTAB) is of great interest. The substituent and micellar effects are highlighted and the rate data in the presence of CTAB were subjected to Menger-Portnoy and Piszkiewicz kinetic pseudo-phase models.

EXPERIMENTAL

Preparation of phenylmercaptoacetic acids

Phenylmercaptoacetic acids, the precursors used for the synthesis of the PSAAs, were prepared from the corresponding thiophenols.^{26,27} The appropriate amount of thiophenol (0.05 mol) dissolved in 10 mL of 20 % sodium hydroxide solution was mixed with 4.7 g of chloroacetic acid dissolved in 10 mL of water without allowing the temperature to rise and then the mixture was heated in an oil bath at 120–130 °C for 5 h. The solution was cooled, acidified with 50 % HCl and the phenylmercaptoacetic acid obtained as solid was recrystallized from

water. The melting points of phenylmercaptoacetic acids were determined and checked with the corresponding literature values.²⁸

Preparation of phenylsulfinylacetic acids

PSAAs and ten *meta*- and *para*-substituted PSAAs were prepared by the controlled oxidation of the corresponding phenylmercaptoacetic acids using 30 % H₂O₂.²⁹ The temperature was maintained at 40 °C and the reaction mixture was stirred until all the H₂O₂ had been consumed. At the end of the reaction, a clear and colorless syrupy liquid was obtained which was kept overnight. After evaporation of water under reduced pressure, a white solid was obtained. The solid was digested with hot benzene for a few minutes and then recrystallized. For the recrystallization of *para*- and *meta*-methyl PSAAs, CHCl₃-petroleum ether (1:1) mixture was used, while ethyl acetate-benzene (1:1) solvent mixture was used for the recrystallization of PSAA and the other *meta*- and *para*-substituted PSAAs. The recrystallized PSAAs were dried and their melting points were determined and compared with the corresponding literature values.²⁸ The purity was also checked by LC-MS. The recrystallized samples were stored in a vacuum desiccator and used for kinetic studies.

Kinetic measurements

All the kinetic runs were performed under pseudo-first-order conditions by maintaining a large excess of PSAA over the concentration of Cr(VI). The progress of the reaction in CTAB medium was monitored by following the rate of decrease of [Cr(VI)] spectrophotometrically at 360 nm. In order to avoid solubility problems, the reaction was conducted in a 95 % water-5 % CH₃CN medium. Several researchers used similar solvent systems to study the micellar effect in the oxidation of organic sulfides.^{17,21,30-32} As the reaction mixture in the presence of CTAB produced turbidity with perchloric acid, in order to circumvent the solubility problem, sulfuric acid and potassium sulfate were used to maintain the H⁺ concentration and ionic strength, respectively.

RESULTS AND DISCUSSION

Effect of reactants on the reaction rate

The kinetic study at different initial concentrations of reactants, [Cr(VI)], [PSAA] and [H⁺], at fixed concentrations of the other substances showed first-order dependence on Cr(VI), PSAA and H⁺. The constancy of the pseudo-first-order rate constant values with increasing concentration of Cr(VI) in the presence of CTAB (Table I) and excellent linear plots of log [Cr(VI)] against time are in agreement with the first-order dependence of the reaction on the Cr(VI) concentration. The observed trend of the constant *k*₁ with varying Cr(VI) con-

TABLE I. Effect of the Cr(VI) and PSAA concentrations on the rate of the CTAB-mediated reaction. [H⁺] = 0.50 mol dm⁻³, [CTAB] = 5.0×10⁻² mol dm⁻³, *I* = 0.65 mol dm⁻³

[PSAA] / 10 ⁻² mol dm ⁻³	[Cr(VI)] / 10 ⁻⁴ mol dm ⁻³	<i>k</i> ₁ / 10 ⁻⁵ s ⁻¹	<i>k</i> ₂ / 10 ⁻³ mol ⁻¹ dm ³ s ⁻¹
3.0	5.0	3.16±0.01	1.05±0.03
5.0	5.0	6.03±0.01	1.21±0.02
7.0	5.0	7.86±0.01	1.12±0.01
10	5.0	11.6±0.02	1.16±0.02
5.0	3.0	6.31±0.01	1.26±0.02
5.0	7.0	6.15±0.02	1.23±0.04

centrations is contradictory with that of the reaction in the absence of micelles, where a negative effect with concentration of Cr(VI) was registered.²³ The observed constancy of the k_1 values in the CTAB-mediated reaction indicates that dimer formation was prevented by the surfactant molecules.

The unit-order dependence on PSAA was evidenced by the unit slope of the double logarithmic plot of k_1 vs. [PSAA] and invariant second-order rate constant values at different PSAA concentrations (Table I). The first-order dependence with respect to H⁺ in the presence of CTAB is assessed from the unit slope of the log–log plot of k_1 vs. [H⁺] and the constant values of $k_1/[H^+]$ (Table II).

TABLE II. Effect of the H⁺ concentration and temperature on the rate of the reaction; [PSAA] = 5.0×10^{-2} mol dm⁻³, [Cr(VI)] = 5.0×10^{-4} mol dm⁻³, [CTAB] = 5.0×10^{-2} mol dm⁻³, solvent: 95 % H₂O–5 % CH₃CN (V/V)

[H ⁺] / mol dm ⁻³	$k_1^a \times 10^5$ s ⁻¹	$k_1 \times 10^4/[H^+]$ mol ⁻¹ dm ³ s ⁻¹	t °C	$k_2^b \times 10^4$ mol ⁻¹ dm ³ s ⁻¹
0.25	2.64±0.02	1.06±0.08	20	3.61±0.03
0.35	3.65±0.01	1.04±0.03	25	7.20±0.01
0.50	6.03±0.01	1.20±0.02	30	12.1±0.02
0.75	7.84±0.02	1.12±0.03	35	18.2±0.03

$$\Delta H = 80.0 \pm 3.25 \text{ kJ mol}^{-1}$$

$$\Delta S = -37.3 \pm 11.3 \text{ J mol}^{-1} \text{ K}^{-1}$$

$$^a I = 0.80 \text{ mol dm}^{-3}; ^b I = 0.65 \text{ mol dm}^{-3}, [\text{H}^+] = 0.50 \text{ mol dm}^{-3}$$

Effect of temperature and activation parameters

In order to evaluate the activation parameters, the reaction in CTAB medium was performed at four different temperatures, *viz.*, 20, 25, 30 and 35 °C. The second-order rate constants, k_2 and the activation parameters, ΔS and ΔH were evaluated respectively from the intercept and slope of the Eyring plot of $\log k_2/T$ vs. $1/T$ and are presented in Table II. The value of the entropy of activation is useful for the interpretation of the structure of transition state. A comparison of ΔS with that of the reaction in aqueous medium ($\Delta S = -24.5 \text{ J mol}^{-1} \text{ K}^{-1}$) shows that the reactant molecules tend to associate in a well-structured activated state in the micellar medium with less degrees of freedom.

Effect of variation of the CTAB concentration

In order to explore the role of the CTAB surfactant micelles on the reaction rate, the reaction was studied as a function of the CTAB concentration at constant concentrations of Cr(VI), PSAA and H⁺ at 30 °C. The effect of the surfactant CTAB on the rate of the reaction and the calculated pseudo-first-order rate constants are presented in Table III. The variation of the CTAB concentration showed two distinct effects on the rate of the reaction, *i.e.*, an initial increase in rate up to 0.5×10^{-2} mol dm⁻³ followed by a steady downward trend. There was a well-defined maximum in the rate profile at 0.5×10^{-2} mol dm⁻³ of CTAB.

TABLE III. Effect of the CTAB concentration on the rate of the reaction. $[PSAA] = 5.0 \times 10^{-2}$ mol dm $^{-3}$, $[Cr(VI)] = 5.0 \times 10^{-4}$ mol dm $^{-3}$, $[H^+] = 0.50$ mol dm $^{-3}$, solvent: 95 % H₂O–5 % CH₃CN (V/V), $I = 0.65$ mol dm $^{-3}$

$[CTAB] / 10^{-2}$ mol dm $^{-3}$	$k_1 / 10^{-5}$ s $^{-1}$
0	8.35±0.02
0.10	8.72±0.01
0.25	9.37±0.02
0.50	10.9±0.04
0.75	10.2±0.07
1.0	10.0±0.02
2.0	8.22±0.04
3.0	7.13±0.03
5.0	6.03±0.01
7.0	4.93±0.02
9.0	3.82±0.02
10	3.31±0.05
12	2.50±0.03

Substituent effect

The study of the influence of substituents on the rate of a reaction often provides insight into the nature of the transition state and mechanism. To probe the reaction mechanism in the cationic micellar medium, the substituent effect was studied with several *meta*- and *para*-substituted PSAs at 30 °C in the presence of CTAB. The investigation showed that the rate of the reaction was accelerated by electron-donating groups and retarded by electron-withdrawing groups present in the phenyl ring of PSAs. This indicates that electron-donating substituents enhance the nucleophilicity of the sulfur and facilitate the attack by the oxidizing species in the rate-determining step. A Hammett plot (Fig. 1) drawn for the kinetic data (Table IV) obtained in CTAB medium at 30 °C shows excel-

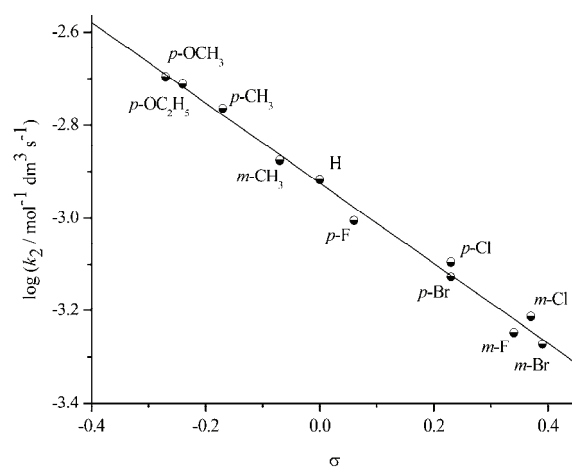


Fig. 1. Hammett plot for CTAB mediated reaction at 30 °C; $\rho = -0.864 \pm 0.03$; $r = 0.996$.

lent correlation with the σ values affording negative ρ value (-0.864), which is lower in magnitude than that of the reaction in the absence of CTAB. This showed that the reaction in CTAB micellar medium was less sensitive to substituent effects, which is against the Reactivity–Selectivity Principle. However, the obtained ρ value is comparable with that of the reaction in the presence of sodium dodecyl sulfate (SDS).²⁵ The observed negative reaction constant supports the generation of an electron deficient sulfur center in the transition state and the linear relationship proves the operation of same mechanism in all the substituted PSAs.

TABLE IV. Second-order rate constants for the reactions of substituted PSAs with Cr(VI) in CTAB medium; $[X\text{-PSAA}] = 3.0 \times 10^{-2}$ mol dm $^{-3}$, $[\text{Cr(VI)}] = 5.0 \times 10^{-4}$ mol dm $^{-3}$, $[\text{H}^+] = 0.50$ mol dm $^{-3}$, $I = 0.65$ mol dm $^{-3}$, $T = 30^\circ\text{C}$

Cmpd. No.	X	$k_2 / 10^{-4}$ mol $^{-1}$ dm 3 s $^{-1}$	$k_2^{\text{CTAB}}/k_2^{\text{aq.}}$
1	<i>m</i> -Br	5.35 ± 0.10	0.054
2	<i>m</i> -Cl	6.12 ± 0.05	0.059
3	<i>m</i> -F	5.66 ± 0.04	0.046
4	<i>p</i> -Cl	8.04 ± 0.02	0.047
5	<i>p</i> -Br	7.47 ± 0.02	0.041
6	<i>p</i> -F	9.88 ± 0.01	0.041
7	H	12.1 ± 0.02	0.039
8	<i>m</i> -CH ₃	13.3 ± 0.03	0.032
9	<i>p</i> -CH ₃	17.2 ± 0.02	0.032
10	<i>p</i> -OC ₂ H ₅	19.4 ± 0.05	0.033
11	<i>p</i> -OCH ₃	20.1 ± 0.02	0.029

Product analysis

The organic product of the reaction was identified from LC-MS and FT-IR spectral studies as (methylsulfonyl)benzene. The recorded LC-MS spectrogram shows that the product eluted at a retention time of 1.829 min ionized in the atmospheric pressure chemical ionization (APCI) (+) mode at *m/z* 157 with a relative abundance of 86 %, which corresponds to the mass of methyl phenyl sulfone (*m/z* = 156). The IR spectrum of the product showed strong absorptions for the symmetric and asymmetric stretching vibrations of the >SO₂ group at 1148 and 1290 cm $^{-1}$, respectively. The final product of Cr(VI) was identified as Cr(III) from the absorption spectrum of the reaction mixture after completion of the reaction, which displayed two absorption peaks in the region 410 and 580 nm (Fig. 2) corresponding to the d-d transitions of Cr(III). This finding is in contradiction with the results observed in the reaction without micelles when a blue shift was observed in the absorption peaks of Cr(III).²³ It was assumed that in the absence of CTAB, Cr(III) formed a complex with the organic product, methyl phenyl sulfone. In a CTAB micellar medium, methyl phenyl sulfone may be solubilized deep in the micelle by hydrophobic interaction while the Cr(III) ion

existed in the aqueous phase as the result of electrostatic repulsion. Thus, the methyl phenyl sulfone became inaccessible for complexation with and hence there was no shift in the characteristic peaks of the Cr(III) ion in the absorption spectrum of the product.

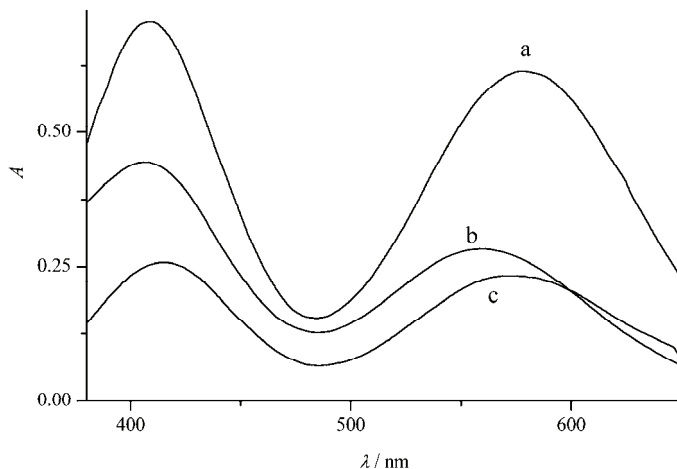


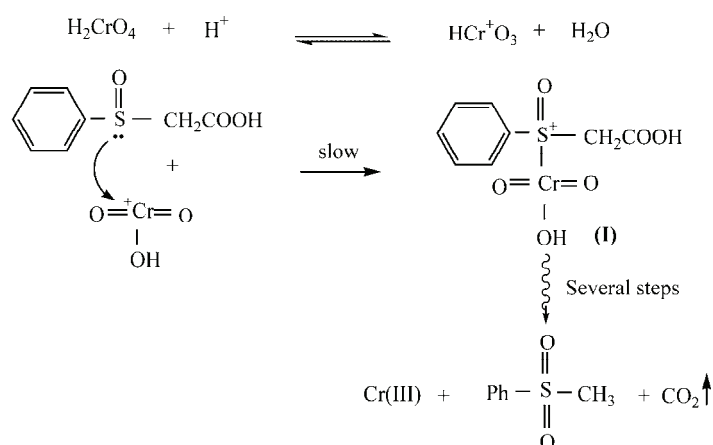
Fig. 2. Absorption spectrum of: a) free Cr(III) ion, b) the reaction mixture in CTAB after completion and c) the reaction mixture without CTAB after completion.

Reaction mechanism in micellar media

The kinetic results reveal that the redox reaction of PSAA and Cr(VI) follows the rate law:

$$-\frac{d[\text{Cr(VI)}]}{dt} = k[\text{PSAA}][\text{H}^+][\text{Cr(VI)}] \quad (1)$$

From the kinetic evidence, it is clear that the redox reaction between PSAA and Cr(VI) in CTAB micelle follows unit-order with respect to Cr(VI), PSAA and H⁺, as observed in the absence of micelles. Based on these kinetic observations, the substituent effect and the formation of methyl phenyl sulfone as the product, it is concluded that the same reaction mechanism as in aqueous medium,²³ was operative in CTAB micellar medium (Scheme 1). Scheme 1 satisfactorily explains the retardation effect observed in cationic micellar medium. The positive charge on the cationic micelle, CTAB prevents the approach of the protonated species of Cr(VI) and also disfavors the formation of positively charged sulfonium ion intermediate (**I**) in the rate determining step by coulombic forces. The observed micellar effect thus favors the proposed mechanism involving the formation of positively charged sulfonium ion intermediate because of nucleophilic attack of sulfur atom of PSAA on Cr of HCrO₃⁺.



Scheme 1. Mechanism of oxidative decarboxylation of phenylsulfinylacetic acid.

To afford spectral evidence for the mechanism of the reaction of PSAA with Cr(VI) in micellar media, the reaction mixture in the presence of CTAB was scanned in the UV–Vis region at different time intervals (Fig. 3). The UV–Vis absorption spectra of the reaction mixture in CTAB micellar medium displayed a similar pattern of absorption peaks to that in the absence of micelles, which may be taken as positive evidence for the existence of the same type of intermediate both in the aqueous and micelle-mediated reactions. The change in the absorption spectra of Cr(VI) with PSAA, the significant hyperchromic shift and the widen-

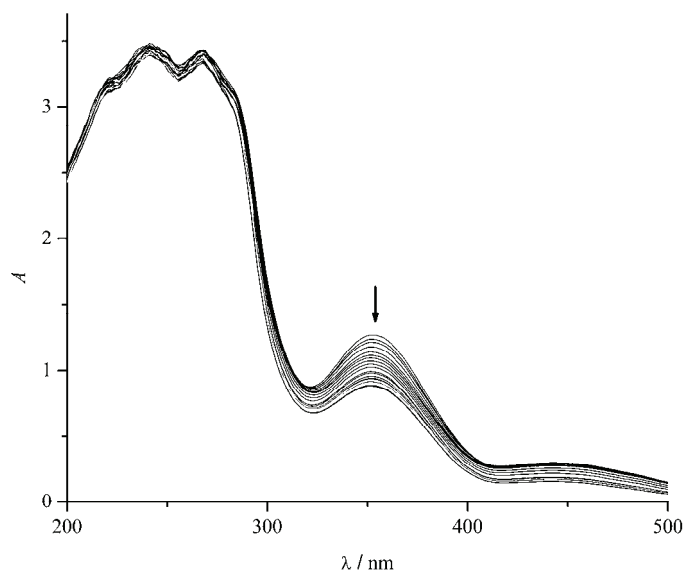


Fig. 3. Variation of absorbance of the reaction mixture with time. $[\text{PSAA}] = 5.0 \times 10^{-2} \text{ mol dm}^{-3}$, $[\text{Cr(VI)}] = 5.0 \times 10^{-4} \text{ mol dm}^{-3}$, $[\text{H}^+] = 0.50 \text{ mol dm}^{-3}$, $[\text{CTAB}] = 5.0 \times 10^{-2} \text{ mol dm}^{-3}$.

ing of the peak in the region 200 to 300 nm for the reaction mixture (Fig. 3) also confirmed the existence of the Cr(VI)-PSAA complex (**I**) having a direct S-Cr bond, as in the case of the reaction in the absence of CTAB.

The UV-Vis absorption spectrum of Cr(VI) in CTAB medium showed a hyperchromic shift in the region of 200 to 300 nm and a hypochromic shift near 350 nm. Furthermore, a red shift of the wavelength from 351 to 360 nm was observed in the spectrum of Cr(VI) in CTAB medium, which indicates that the absorption spectrum of Cr(VI) was affected by the surfactant CTAB (Fig. 4). Although this spectrum appears to be similar to the one in SDS medium,²⁵ a notable difference in SDS medium was the observation of hyperchromic shifts in both the peaks of Cr(VI). The similarity of absorption spectra of the reaction mixture in both SDS and CTAB media demonstrated the involvement of the same transition state intermediate in both cases.

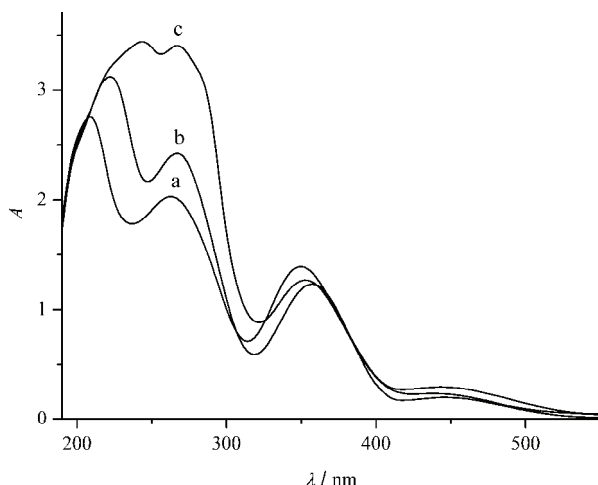


Fig. 4. Absorption spectra of: a) Cr(VI), b) Cr(VI) in CTAB and c) reaction mixture; [PSAA] = 5.0×10^{-2} mol dm⁻³, [Cr(VI)] = 5.0×10^{-4} mol dm⁻³, [H⁺] = 0.50 mol dm⁻³, [CTAB] = 5.0×10^{-2} mol dm⁻³.

Interpretation of the micellar effect

The effect of ionic micelles on the reaction rate of bimolecular reactions is mainly due to the association or incorporation of reactants through electrostatic or hydrophobic interactions within the small volume of the self-assemblies.¹² In the present cationic micellar medium, the positively charged head groups of CTAB prevented the approach of the oxidizing species HCrO₃⁺ by electrostatic repulsion and so the oxidizing species remained in aqueous phase. The other reactant PSAA that is neutral preferably partitioned in the micellar pseudo-phase of CTAB by hydrophobic interaction, and hence, became unavailable for the reaction with HCrO₃⁺ in aqueous phase. Thus, the overall retarding effect ob-

erved with increasing CTAB concentration above 0.5×10^{-2} mol dm $^{-3}$ was due to preferential partitioning of PSAA and HCrO $_3^+$ in the micellar pseudo-phase and aqueous medium, respectively, followed by a decrease in stoichiometric concentration of both reactants in both the phases. Consequently, the reaction rate in both aqueous and micellar phases decreased that led to an overall rate retardation. Moreover, during the course of the reaction, a positive charge developed on the sulfur due to electron transfer from the sulfur atom of PSAA to Cr(VI), which was prevented at higher concentrations of CTAB.

The increase in rate constant at low concentrations of CTAB up to 0.5×10^{-2} mol dm $^{-3}$ is interesting and this may be due to a specific salt effect. As sulfuric acid and potassium sulfate are used, respectively, to maintain the H $^+$ concentration and ionic strength in the CTAB medium, the reaction mixture contained excess of SO 4^{2-} . The trend of binding efficiency of counter ions with micelles follows the Hofmeister series.³³ As SO 4^{2-} is positioned in the place of higher order in the Hofmeister series, the SO 4^{2-} has a high probability of binding with the positively charged CTAB. It was shown that strong binding of SO 4^{2-} to the micellar surface of cetyltrimethylammonium ion yields micelle properties which differ considerably from those with other counter ions.³⁴ Among the homologous of CTAX surfactants, X = Cl $^-$, Br $^-$, SO 4^{2-} , CTA sulfate is the only one that exhibits a positive enthalpy of micellization as a result of the strong and specific affinity of SO 4^{2-} for the micelle interface.³⁵ Furthermore, the micelle size and reactivity of CTAB aggregates were found to be affected by divalent counter ions, such as SO 4^{2-} , as a result of strong binding.^{36,37}

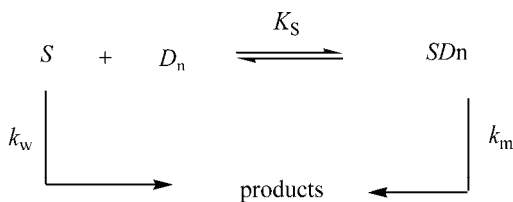
Based on these facts, it is assumed that complete neutralization of the positive charges on the CTAB micellar surface may occur at low concentrations of CTAB, *i.e.*, up to 0.5×10^{-2} mol dm $^{-3}$, as a result of strong binding of SO 4^{2-} . Under such condition, inclusion of HCrO $_3^+$ into CTAB micellar phase is possible. Thus, the accelerating effect observed in the region of low concentrations of CTAB may be due to increasing stoichiometric concentrations of both reactants in micellar phase, which favors the formation of the sulfonium ion intermediate. It is worth mentioning here that Kabir-ud-Din *et al.*³⁸ observed a substantial decrease in rate in the oxidation of oxalic acid by Cr(VI) in CTAB medium in the presence of added salt, Na $_2$ SO 4 . They explained the result based on the strong binding of SO 4^{2-} to CTAB, which prevents the inclusion of the reactive species HCrO 4^- .

Treatment of pseudo-phase models

Various models have been proposed to describe the variation of reaction rate in the presence of micelles. Among them, the pseudo-phase model is the most commonly used model to interpret the catalytic/inhibitory activity of micelles and to calculate binding parameters.

Menger–Portnoy model

The observed rate inhibition in the CTAB medium could be analyzed by considering the distribution pattern of reactants between the micellar and aqueous phases by application of the pseudo-phase kinetic model proposed by Menger and Portnoy and its modified forms.^{39–42} This model considers the partitioning of the substrate between the aqueous and micellar pseudo-phases as given in Scheme 2 proposed by Menger and Portnoy.³⁹



Scheme 2. Menger–Portnoy model.

From Scheme 2, the observed rate constant, k_ψ , is given by:

$$k_\psi = \frac{k_w + k_m K_S [D_n]}{1 + K_S [D_n]} \quad (2)$$

where D_n , S and SD_n represent micellar surfactant, free substrate and associated substrate, respectively, and k_w and k_m are the pseudo-first-order rate constants in aqueous and micellar phases, respectively, K_S is the binding constant of the substrate with the surfactant and $[D_n]$ is the concentration of the micellar surfactant, which is related to the stoichiometric concentration of the surfactant, $[D]_T$ and critical micelle concentration, cmc as $[D_n] = [D]_T - cmc$. The cmc value of CTAB was taken from the literature as 9.2×10^{-4} mol dm⁻³.^{43,44} The applicability of Menger–Portnoy model (Scheme 2) for the observed inhibitory effect of CTAB in the oxidative decarboxylation of PSAA was tested by modifying Eq. (2) as:

$$\frac{1}{(k_w - k_\psi)} = \frac{1}{(k_w - k_m)} + \frac{1}{(k_w - k_m) K_S [D_n]} \quad (3)$$

The modified Eq. (3) was successfully applied to various micellar inhibition reactions by different researchers.^{45–47} Using the rate data, the values of $1/(k_w - k_\psi)$ were plotted against $1/[D_n]$ in the concentration range 2.0×10^{-2} – 12×10^{-2} mol dm⁻³. The Menger–Portnoy model is applicable to micellar inhibition only if the plot of $1/(k_w - k_\psi)$ vs. $1/[D_n]$ is linear with a positive slope and intercept.⁴⁸ In the present case, although the plot of $1/(k_w - k_\psi)$ vs. $1/[D_n]$ was linear, the plot afforded a negative intercept, showing its inadequacy to explain the micellar effect.

According to Rajasekaran *et al.*,⁴⁹ as double reciprocal plot is involved in this model, there exists some uncertainty in the intercept. In order to remove this uncertainty, they modified Eq. (3) to:

$$(k_\psi - k_w) = -\frac{(k_\psi - k_w)}{K_S[D_n]} + (k_m - k_w) \quad (4)$$

The plot of $(k_\psi - k_w)$ vs. $(k_\psi - k_w)/[D_n]$ should be linear and from the slope and intercept of the plot, the rate constant for the micellar phase, k_m , and the substrate-micelle binding constant, K_S could be evaluated. However, for the present reaction, the plot of $(k_\psi - k_w)$ vs. $(k_\psi - k_w)/[D_n]$ was non-linear (Fig. 5), which indicates the inapplicability of the Menger-Portnoy model to the inhibition of this reaction by CTAB.

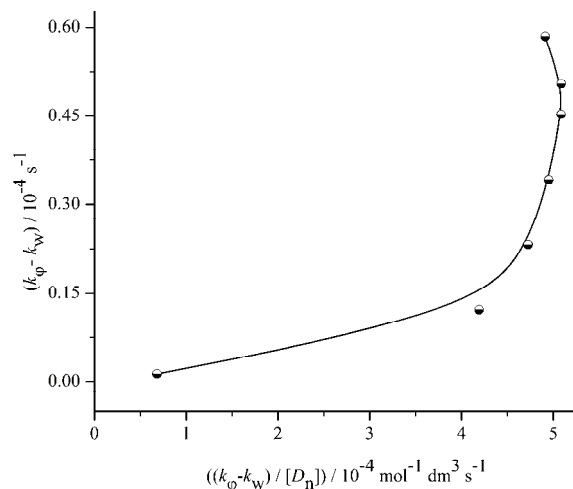


Fig. 5. Validity of Menger-Portnoy model.

Piszkevicz cooperative model

Many micellar reactions were also explained by the cooperative model developed by Piszkevicz,⁵⁰⁻⁵² which is analogous to the Hill model applied to enzyme-catalyzed reactions. This model was developed for micelle-catalyzed reactions showing a maximum rate followed by inhibition, as was observed in the present case. This model relates the cooperativity between a neutral species of the reaction and a surfactant to form the reactive micelles, as in Scheme 3 that was proposed by Piszkevicz.⁵⁰

From Scheme 3, the observed rate constant, k_ψ could be expressed as a function of the concentration of surfactant:

$$k_\psi = \frac{k_m[D]^n + K_D k_w}{K_D + [D]^n} \quad (5)$$

Equation (5) can be rearranged to:

$$\log \frac{(k_\psi - k_w)}{(k_m - k_\psi)} = n \log[D] - \log K_D \quad (6)$$

where, k_m is the rate constant at maximum surfactant concentration within the given range and $k_m \approx 0$ if the reaction is inhibited by surfactant.^{19,49,53} n is the index of cooperativity that is a measure of the association of additional surfactant molecules to an aggregate in the whole surfactant concentration range, K_D is the dissociation constant of micellized substrate back to its free components and its inverse is K that is the association constant of the micelle–substrate complex. The advantage of the Eq. (6) is that it does not require knowledge of the *cmc* value of the surfactant used. Although Eq. (6) is generally used for micelle-catalyzed reactions, it was also applied to micellar inhibition reactions with certain modifications.^{19,54–57}

Since CTAB retards the rate to a significant extent at high concentrations, it is assumed that the incorporation of positively charged oxidizing species, HCrO_3^+ into the positively charged micelle is negligible. Thus at higher CTAB concentrations, HCrO_3^+ is mainly solubilized in the aqueous phase and hence, it is presumed that $k_m \approx 0$. Under these conditions, Eq. (6) becomes:

$$\log \frac{(k_w - k_\psi)}{k_\psi} = n \log[D] - \log K_D \quad (7)$$

In the present reaction, the plot of $\log [(k_w - k_\psi)/k_\psi]$ vs. $\log [\text{CTAB}]$ was found to be linear (Fig. 6, $r = 0.996$) in the rate retardation region of CTAB, 3.0×10^{-2} – 12×10^{-2} mol dm⁻³. The linearity of the plot obtained with the micelle support the positive cooperativity between PSAA and micelles to form reactive micelles, which indicates that the PSAA molecules are included into the micellar phase. The Piszkeiwicz parameters, n and K_D determined, respectively, from the slope and intercept of the linear plot were $n = 1.86$ and $K_D = 9.11 \times 10^{-3}$. The association constant, K computed from the reciprocal of K_D was 109.82, which

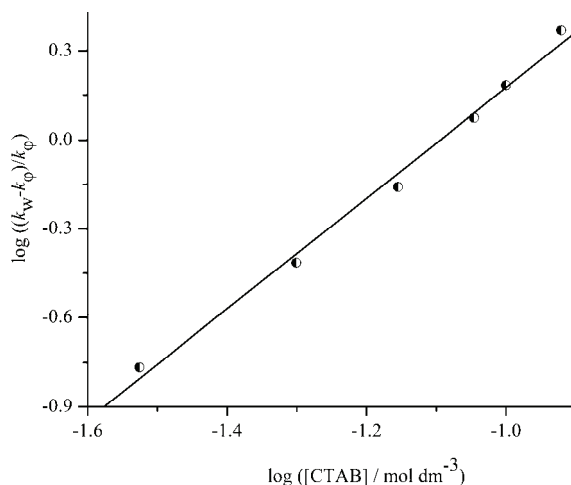


Fig. 6. Applicability of Piszkeiwicz cooperative model.

indicates binding of PSAA to the micelles. The value of n greater than unity indicates positive cooperativity, *i.e.*, the binding of the first molecule of the substrate makes it easier for subsequent molecules to bind. Furthermore, the value of n is far less than the aggregation number (20 to 100) of the surfactants, which indicates the formation of catalytically productive sub-micellar aggregates.³⁸

CONCLUSIONS

The CTAB mediated redox reaction of PSAA with Cr(VI) displayed two different effects, an initial increase in the rate constant followed by a sharp decrease with increasing concentration of CTAB. The observed trends of the rate constant were explained in terms of specific binding of SO_4^{2-} on the micellar surface and interactions such as electrostatic and hydrophobic. The kinetic data were treated for micellar effects with the Menger–Portnoy and Piszkeiwicz pseudo-phase models. The results obtained from the kinetic studies were better fitted with the Piszkeiwicz model and hence, the binding constant for PSAA with CTAB micelles was evaluated using this model.

ИЗВОД
ДИНАМИКА РЕАКЦИЈЕ ФЕНИЛСУЛФИНИЛАЦЕТАТНЕ КИСЕЛИНЕ СА Cr(VI)
У ПРИСУСТВУ ЦЕТИЛТРИМЕТИЛАМОНИЈУМ-БРОМИДА: ТРЕТМАН
ПСЕУДО-ФАЗНИМ МОДЕЛИМА

PERUMAL SUBRAMANIAM¹ и NATESAN THAMIL SELVI²

¹Research Department of Chemistry, Aditanar College of Arts and Science, Tiruchendur-628 216, Tamil Nadu, India и ²Govindammal Aditanar College for Women, Tiruchendur-628 215, Tamil Nadu, India

Утицај цетилtrimетиламонијум бромида (CTAB) на оксидативну декарбоксилацију фенилсулфинилацетатне киселине (PSAA) и неколико *мей-а-* и *йара-*супституисаних фенилсулфинилацетатних киселина (PSAA-а) са Cr(VI) је испитиван у раствору 95 % H_2O -5% CH_3CN . Почетна брзина реакције расте при малим [CTAB], а затим долази до наглог пада брзине реакције при већим [CTAB]. Раствор почетне брзине може бити објашњен јаком везом између SO_4^{2-} и позитивно наелектрисане мицеларне површине. Специфична расподела PSAA у мицеларној фази услед хидрофобних интеракција, односно оксидујуће врсте HCrO_3^+ у воденој фази услед електростатичког одбијања, доводе до успоравања брзине при већим [CTAB]. Hammett дијаграм са различитим супституисаним PSAA-а је показао одличну корелацију негативне вредности ρ што подржава предложени механизам који укључује формирање интермедијера сулфонијум катиона. Добијена вредност ρ у CTAB средини је нешто нижа у поређењу са вредношћу добијеном за водену средину. Квантитативна анализа података за инхибицију брзине реакције од стране CTAB је урађена применом Menger–Portnoy и Piszkeiwicz псевдо-фазног модела. Константа везивања PSAA за мицелу је одређена на основу Piszkeiwicz кооперативног модела.

(Примљено 19. септембра, ревидирано 28. децембра, прихваћено 31. децембра 2014)

REFERENCES

1. S. Moulik, P. Dutta, D. K. Chatteraj, S. P. Moulik, *Colloids Surfaces* **11** (1998) 1
2. S. Mahiuddin, O. Zech, S. Raith, D. Touraud, W. Kunz, *Langmuir* **25** (2009) 12516

3. J. B. Engberts, J. Kevelam, *Curr. Opin. Colloid Interface Sci.* **1** (1996) 779
4. D. V. Tulumello, C. M. Deber, *Biochemistry* **48** (2009) 12096
5. A. Basu, B. Saha, *Am. J. Anal. Chem.* **1** (2010) 25
6. F. Sanchez, M. L. Moya, R. Jimenez, C. H. Gomez, M. C. Carmona, C. P. Lopez, *J. Chem. Soc. Faraday Trans.* **93** (1997) 1281
7. J. Panda, G. P. Panigrahi, *J. Indian Chem. Soc.* **79** (2002) 58
8. Kabir-ud-Din, M. Bano, I. A. Khan, *Ind. J. Chem., A* **42** (2003) 998
9. A. H. Gemeay, I. A. Mansour, G. R. Sharkaway, B. A. Zaki, *J. Colloid Interface Sci.* **263** (2003) 228
10. C. A Bunton, *Catal. Rev. – Sci. Eng.* **20** (1979) 1
11. F. Jing, X. Q. An, W. G. Shen, *J. Mol. Catal., B* **24** (2003) 53
12. J. H. Fendler, E. J. Fendler, *Catalysis in Micellar and Macromolecular Systems*, Academic Press, New York, 1975
13. C. J. Drummond, F. Griesser, *J. Colloid Interface Sci.* **281** (1989) 127
14. S. Otto, J. B. F. N. Engberts, J. C. T. Kwak, *J. Am. Chem. Soc.* **120** (1998) 9517
15. K. Manabe, Y. Mori, T. Wakabayashi, S. Nagayama, S. Kobayashi, *J. Am. Chem. Soc.* **122** (2000) 7202
16. A. K. Das, *Coord. Chem. Rev.* **248** (2004) 81
17. B. Sankararaj, S. Rajagopal, K. Pitchumani, *Indian J. Chem., A* **34** (1995) 440
18. A. K. Das, S. K. Mondal, D. Kar, M. Das, *J. Chem. Res.* (1998) 574
19. A. K. Das, S. K. Mondal, D. Kar, M. Das, *Int. J. Chem. Kinet.* **33** (2001) 173
20. S. Balakumar, P. Thanasekaran, E. Rajkumar, K. John Adaikalasamy, S. Rajagopal, R. Ramaraj, T. Rajendran, B. Manimaran, K. L. Lu, *Org. Biomol. Chem.* **4** (2006) 352
21. J. R. Bosco Bharathy, T. K. Ganesan, E. Rajkumar, S. Rajagopal, B. Manimaran, T. Rajendran, K. L. Lu, *Tetrahedron* **61** (2005) 4679
22. P. Subramaniam, N. Thamil Selvi, *Am. J. Anal. Chem.* **4** (2013) 20
23. P. Subramaniam, N. Thamil Selvi, S. Sugirtha Devi, *J. Korean Chem. Soc.* **58** (2014) 17
24. P. Subramaniam, S. Sugirtha Devi, S. Anbarasan, *J. Mol. Catal., A* **390** (2014) 159
25. P. Subramaniam, N. Thamil Selvi, *Int. J. Adv. Sci. Tech. Res.* **4** (2014) 418
26. D. J. Pasto, R. Kent, *J. Org. Chem.* **30** (1965) 2684
27. C. Srinivasan, P. Subramaniam, *J. Chem. Soc. Perkin Trans. 2* (1990) 1061
28. W. J. Kenney, J. A. Walsh, D. A. Davenport, *J. Am. Chem. Soc.* **83** (1961) 4019
29. D. Walker, J. Leib, *Can. J. Chem.* **40** (1962) 1242
30. R. Bacaloglu, A. Blasko, C. A. Bunton, H. J. Foroudian, *J. Phys. Org. Chem.* **5** (1992) 171
31. A. Blasko, C. A. Bunton, S. Wright, *J. Phys. Chem.* **97** (1993) 5435
32. C. A. Bunton, H. J. Foroudian, A. Kumar, *J. Chem. Soc. Perkin Trans. 2* (1995) 33
33. C. Oelschlaeger, P. Suwita, N. Willenbacher, *Langmuir* **26** (2010) 7045
34. O. Soderman, *Curr. Opin. Colloid Interface Sci.* **9** (2004) 154
35. E. Feitosa, M. R. S. Brazolin, R. M. Zumstein Georgetto Naal, M. P. Freire de Moraes Del Lama, J. R. Lopes, W. Loh, M. Vasilescu, *J. Colloids Interface Sci.* **299** (2006) 883
36. V. K. Aswal, P. S. Goyal, *Chem. Phys. Lett.* **364** (2002) 44
37. B. Yogeve, B. C. R. Guillaume, J. H. Fendler, *Langmuir* **7** (1991) 623
38. Kabir-ud-Din, K. Hartani, Z. Khan, *Colloids Surfaces, A* **193** (2001) 1
39. F. M. Menger, C. E. Portnoy, *J. Am. Chem. Soc.* **89** (1967) 4698
40. C. A. Bunton, *Catal. Rev. Sci. Eng.* **20** (1979) 1
41. C. A. Bunton, *J. Mol. Liq.* **72** (1997) 231
42. S. Vera, E. Rodenas, *Tetrahedron* **42** (1986) 143

43. P. Balakumar, S. Balakumar, P. Subramaniam, *Der Chem. Sin.* **3** (2012) 959
44. H. C. Gao, R. X. Zhu, X. Y. Yang, S. Z. Mao, S. Zhao, J. Y. Yu, R. Y. Du, *J. Colloids Interface Sci.* **273** (2004) 626
45. R. Shukla, S. K. Upadhyay, *Indian J. Chem., A* **46** (2007) 1116
46. R. Swain, G. P. Panigrahi, *Indian J. Chem., A* **40** (2001) 1191
47. Kabir-ud-Din, K. Hartani, *Transit. Met. Chem.* **25** (2000) 478
48. K. Ramakrishna, P. Syamala, P. V. Subba Rao, *Indian J. Chem., A* **39** (2000) 639
49. K. Rajasekaran, A. Sarathi, S. Ramalakshmi, *J. Chem. Sci.* **120** (2008) 475
50. D. Piszkiewicz, *J. Am. Chem. Soc.* **98** (1976) 3053
51. D. Piszkiewicz, *J. Am. Chem. Soc.* **99** (1977) 7695
52. D. Piszkiewicz, *J. Am. Chem. Soc.* **99** (1977) 1550
53. B. Samiey, F. Ashoori, *Act Chim. Slov.* **58** (2011) 223
54. G. P. Panigrahi, B. P. Sahu, *J. Ind. Chem. Soc.* **68** (1991) 239
55. N. C. Sarada, I. A. K. Reddy, *J. Ind. Chem. Soc.* **70** (1993) 35
56. K. K. Ghosh, S. K. Kar, *J. Ind. Chem. Soc.* **75** (1998) 39
57. A. K. Das, A. Roy, B. Saha, *Transit. Met. Chem.* **26** (2001) 630.



Voltammetric and theoretical studies of the electrochemical behavior of cephalosporins at a mercury electrode

KATARINA NIKOLIĆ[#], MARA M. ALEKSIĆ^{*#}, VERA KAPETANOVIĆ
and DANICA AGBABA[#]

Faculty of Pharmacy, University of Belgrade, Vojvode Stepe 450, 11000 Belgrade, Serbia

(Received 29 January, revised 23 February, accepted 26 February 2015)

Abstract: The adsorption and electroreduction behavior of cefpodoxime proxetil, cefotaxime, desacetylcefotaxime, cefetamet, ceftriaxone, ceftazidime, and cefuroxime axetil at a mercury electrode surface were studied using cyclic (CV), differential pulse (DPV) and adsorptive stripping differential pulse (AdSDPV) voltammetry. The quantitative structure property relationship (QSPR) study of the seven cephalosporins adsorption at the mercury electrode was based on density functional theory DFT-B3LYP/6-31G(d,p) calculations of molecular orbitals, partial charges and electron densities of the analytes. The DFT-parameters and QSPR model explain well the process of adsorption of the examined cephalosporins. The QSPR study defined that cephalosporins with lower electron density on the nitrogen atom of the N–O bond, higher number of hydrogen bond-accepting groups, and higher principal moment of inertia should express high adsorption on the mercury electrode.

Keywords: cephalosporins; AdSDPV; CV; DFT; QSPR; computational electrochemistry.

INTRODUCTION

Cephalosporins are semi-synthetic β -lactam antibiotics similar to penicillins, but with a broader spectrum of antibacterial properties and a higher resistance to β -lactamase.¹

These compounds contain a β -lactam/dihydrothiazine moiety bearing different substituents at the C3 and C7 position. Methoxyimino cephalosporins are reducible at a mercury electrode and therefore present electrochemically a very important class of antibiotics. This characteristic enables the application of electroanalytical techniques for the sensitive determination of methoxyimino cephalosporins. These cephalosporins were extensively studied at a mercury elec-

* Corresponding author. E-mail: mara@pharmacy.bg.ac.rs

[#] Serbian Chemical Society member.

doi: 10.2298/JSC150129019N

trode, the mechanism of methoxyimino reduction at the mercury electrode was established and voltammetric methods based on the adsorptive accumulation of cephalosporins at the mercury electrode were developed.^{2–6} Regardless of the high sensitivity of the determination in pharmaceutical formulations, this method still could not be used for the determination of cephalosporins in a biological matrix. Apart from the reduction at mercury electrode, methoxyimino cephalosporins may be reduced or oxidized at different solid electrodes that may be specially modified and activated.^{7–12} These determinations appeared to be less sensitive than at a mercury electrode.^{7–12} Since the process of the reduction of methoxyimino cephalosporins is associated with adsorption at the electrode surface, adsorptive stripping voltammetry was successfully applied for their quantitative determination as a highly selective and precise electroanalytical technique.^{13–15}

The application of adsorptive stripping method enabled the determination of low concentrations of cephalosporins *in vivo* from biological samples, such as urine, serum or cerebrospinal fluid.^{13–15} The mechanism of reduction of the methoxyimino cephalosporins, such as cefpodoxime proxetil (CPDX-PR), cefotaxime (CTX), desacetylcefotaxime (DCTX) and cefetamet (CET), at a mercury electrode was established and reported in previous papers.^{16–20} The Methoxyimino group in cephalosporin molecules undergoes reduction at mercury electrodes yielding well-defined polarographic waves and voltammetric peaks, over a wide pH interval from 2 to 12.^{16–20}

Based on previous findings,^{16–20} the voltammetric study is now extended to include structurally closely related cephalosporins, *i.e.*, ceftriaxone (CRO), ceftazidime (CAZ) and cefuroxime axetil (CXM).

In this work, adsorptive techniques were applied for a study of the electro-reduction behavior and for the quantitative determination of ceftriaxone, ceftazidime, and cefuroxime axetil. The experimental results of the group of seven methoxyimino cephalosporins were further used in a quantum chemical study. The theoretical study was used to describe the adsorption mechanism at the mercury electrode surface and to predict the electrochemical adsorption at mercury electrode of related cephalosporins.

To the best of our knowledge, there is no scientific report either about the study of the electrochemical behavior of cephalosporins or a quantum chemical study of their electrochemical adsorption mechanism on a mercury electrode.

EXPERIMENTAL

Reagents and chemicals

Cephalosporins (CEF) were from Sigma and all chemicals were of analytical grade quality. Britton–Robinson (BR) universal buffer was prepared from stock solutions of 0.04 mol dm⁻³ boric, orthophosphoric and acetic acids with the appropriate volumes of 0.2 mol dm⁻³ NaOH.

Apparatus

The voltammetric measurements were performed with an Amel 433-A computerized polarographic analyzer. A three-electrode system was employed with a hanging mercury dropping electrode (HMDE), an Ag/AgCl reference electrode and a Pt-auxiliary electrode. All potentials in the paper are expressed *vs.* Ag/AgCl. Adsorptive stripping differential pulse voltammetry (AdSDPV) was performed under the following conditions: scan speed 200 mV s⁻¹, pulse amplitude 100 mV, pulse width 20 ms, from 0 to -1.6 V. After recording the base-line, when a fresh mercury drop has been formed, voltammograms were recorded after a certain time of adsorptive accumulation at selected accumulation potential and selected pH, in a stirred solution (300 rpm). The accumulation period in a stirred solution was followed by a 10 s settling period to allow for quiescence of the solution and uniform distribution of the deposited substance on the surface of the mercury drop. When the differential pulse voltammetry (DPV) mode was used, the following parameters were applied: pulse repetition 100 ms, pulse amplitude 25 mV and pulse width 20 mV. The cyclic voltammograms (CV) were recorded at a scan rate ranging from 5 to 100 mV s⁻¹.

A Radiometer pH meter, PHM 220, with a combined pH electrode Radiometer GK2401B, was used and appropriate standard buffer solutions.

Solutions preparations

A stock solution (S₀) of 1×10⁻⁴ mol dm⁻³ of CEF was prepared by dissolving an accurate mass of CEF in redistilled water, and stored in freezer. More dilute solutions were prepared daily from the stock solution.

Procedures

A 15 mL aliquot of the corresponding supporting electrolyte solution (BR buffer only) or 13.5 mL aliquot of the corresponding supporting electrolyte solution (BR buffer) and 1.5 mL of S₀ was placed in the voltammetric cell, and deaerated for 10 min with high purity nitrogen and voltammograms were recorded.

Computational methods

The experimentally determined slope ($\Delta i_p/\Delta \nu$) and the computed molecular parameters of the examined cephalosporins were used to build QSPR models and to examine electrochemical adsorption and electroreduction mechanism of the cephalosporins.

Calculation of the pK_a values and a selection of the dominant molecules/ions species at the experimental pH 2.0–3.5 (Fig. 1), were performed for all the analyzed compounds using the Marvin 5.5.1.0 program.²¹ The minimum energy conformations of the analyzed compounds were obtained by the CS Gaussian 98 program^{22,23} using the B3LYP/3-21G basis set.^{24–26}

The molecular refractivity (MR), the partition coefficient (Clog P), the distribution coefficient (log D at pH 1.5, 2.5, and 4.0), the radius, the principal moment of inertia (PMI), the Connolly accessible area (SAS), the Connolly molecular area (MS), the molecular surface area (MSA), the polar surface area (PSA), the hydrogen bond donors (HBD) and the hydrogen bond acceptors (HBA) were computed for the optimized molecular models using the MarvinSketch 5.1.5.0²¹ and the Chem3D Ultra 7.0.0²² programs.

The CS Gaussian 98 program²³ using the B3LYP hybrid functional that included the 6-31G basis set (B3LYP/6-31G(d,p))^{24–26} was applied for the computation of the molecular parameters, *i.e.*, the energies of the highest occupied molecular orbital (*HOMO*) and the lowest unoccupied molecular orbital (*LUMO*), the chemical potential (μ), electronegativity (χ), hardness (η), global softness (S), electrophilicity index (ω) and the dipole moment.

The calculated molecular descriptors were used for the development of the QSPR model using partial least square (PLS) regression.²⁷

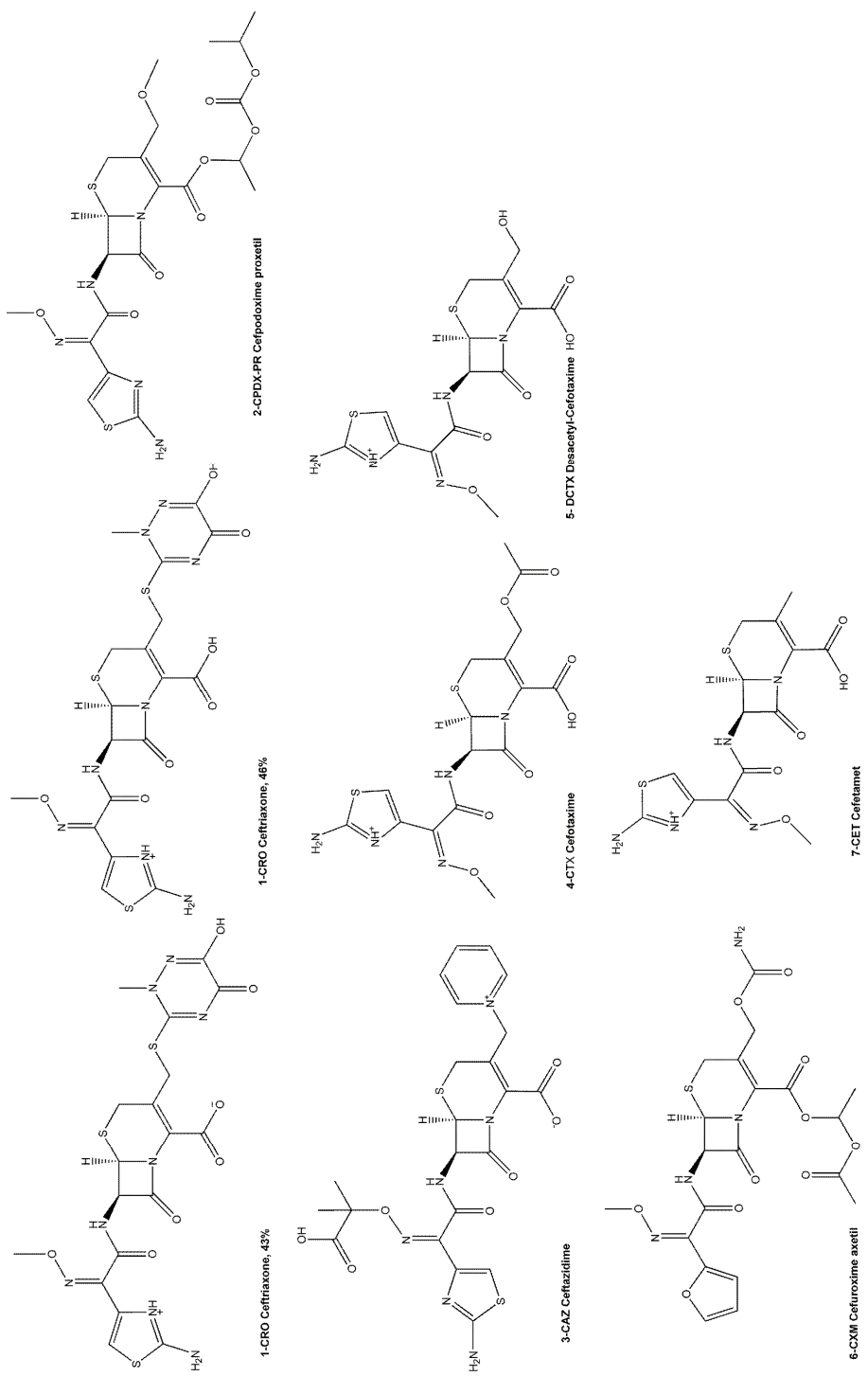


Fig. 1. Dominant forms of the cephalosporins at the analytical pH 2.0–3.5.

The QSPR study was realized using the soft independent modeling of class analogy SIMCA P+ 12.0 program,²⁸ for the PLS regression analysis. In QSPR modeling, a summary of the importance of every variable (X_k) for both \mathbf{Y} and \mathbf{X} matrices is described by the variable importance in the projection (VIP_k) parameter. The X variables with a VIP value larger than 1 are the most relevant for explaining the regression model, while the X variables with a VIP value below 1 have a smaller influence on the regression model.²⁷

Validations of the *PLS* regression models were performed by the leave-one-out cross-validation (LOO-CV) method. The predictive power of the model is determined by the Q^2 value, which is the cross-validated version of R^2 , and the root mean square error of prediction ($RMSEP$). The model was fitted to the data leaving one data point out. The elaborated PLS model then predicts the left-out data point. This procedure was repeated until all data points had been left out, which results in a number of parallel models. The difference between the observed and the predicted values in the left-out data point ($e_{(i)}$) were calculated for each model and used for the calculation of the prediction error ($RMSEP$).

In this setting, the predicted sum of squares ($PRESS$), $RMSEP$ and $Q^2(Y)$ were defined as:

$$PRESS = \sum_{i=1}^n e_{(i)}^2 \quad (1)$$

$$RMSEP = \sqrt{(PRESS / n)} \quad (2)$$

$$Q^2 = 1 - (PRESS / SSTo) \quad (3)$$

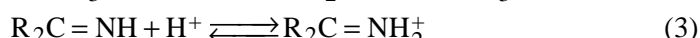
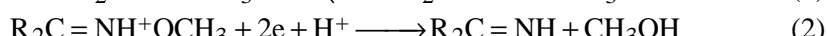
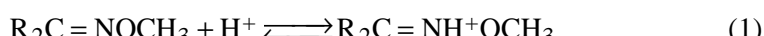
where $SSTo$ is the variation, sum of squares (total).

Models with $Q^2 \geq 0.5$ could be considered as having good predictive capabilities.²⁷

The quality of the PLSR models was estimated using such parameters as $RMSEP$, Q^2 , and the correlation coefficients observed vs. predicted (r^2 (Obs vs. Pred)).²⁷

RESULTS AND DISCUSSION

The mechanism of the reduction of methoxyimino group involves two steps.^{29–31} First, the nitrogen of the N–OCH₃ group is protonated (1), then the N–O bond is cleaved (2), yielding an imine that was then protonated (3) and reduced to the corresponding amine (4):



The specificity of this reduction is evidenced by the appearance of only one well-defined voltammetric peak (I) in acid and neutral media, while in slightly alkaline medium, splitting of this peak occurs, and two peaks are obtained (II and III). Peak I represents the overall reduction of the oxime group that involves transfer of four electrons yielding an amine. As the rate of protonation of oxime decreases with increasing pH, the reduction peak decreases, and above certain pH value, the reduction occurs in two steps corresponding to oxime reduction to the imine, and imine reduction to amine, respectively. This separation into two two-

-electron processes is caused by differences in position and rate of establishment of acid–base equilibrium resulting in the protonation of the oxime and imino group,³² *i.e.* their pK_a values.

In more alkaline solutions, at $\text{pH} > 10$, a new peak (IV) appeared at a more negative potential, $E \approx -1.5$ V (Fig. 2) due to the reduction of the unprotonated form. In addition, all the cephalosporins underwent a two-electron reduction of the unsaturated C=C bond of the dihydrothiazine ring. This reduction occurred in an acid medium at potentials very close to that of hydrogen ion reduction and therefore was not convenient for analytical investigations.

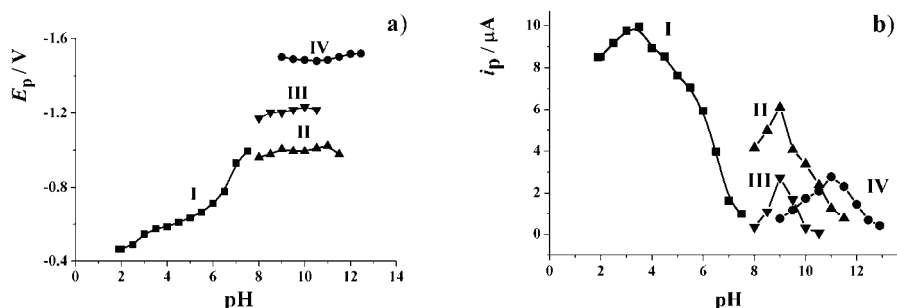


Fig. 2. Graphically presented pH influence on the DPV peak: a) potential and b) current of 1×10^{-5} mol dm⁻³ CPDX-PR in BR buffer.¹⁸

A plot of the obtained peak potentials as a function of pH (Fig. 2a) shows several linear segments with varying $dE_p/d\text{pH}$ slopes, which indicates a varying number of protons transferred before the potential determining electron transfer. The slopes, $dE_p/d\text{pH}$, obtained by curve fitting were as follows: 0.058 V pH⁻¹ at pH 2–6, 0.189 V pH⁻¹ at pH 6–7.5 for peak I; 0.026 V pH⁻¹ at pH 8–10 for peak II; 0.029 V pH⁻¹ at pH 8–10 for peak III and ≈ 0 V pH⁻¹ at pH > 9 for peak IV. The slope of 58 mV obtained for peak I at pH < 6 suggested the same number of electrons and protons involved in the electrode process, while the slope of 26–29 mV obtained for peaks II and III suggested fewer protons involved, (protons:electrons = 1:2). Decrease in the slope at pH > 8 indicates the pH region in which the pre-protonation becomes too slow relative to diffusion. The peak potential of peak IV is pH-independent, which is in accordance to theory in the case of the reduction of unprotonated species.

According to the peak current–pH dependence (Fig. 2b), it is evident that all peaks show a maxima at a certain pH value. The maximum of the i_p vs. pH curve indicates pronounced adsorption at the given pH. All the investigated cephalosporins showed DPV current maximum of peak I at a pH of around 3.

The mechanism of the reaction of methoxyiminocephalosporins at a mercury electrode^{16–20} confirmed that the reduction of cephalosporins was mostly complicated by the effects of adsorption at the electrode surface. The conjugated

acids of these compounds were adsorbed at the electrode surface at potentials between 0.0 and 0.2 V, and desorbed between -1.0 and -1.2 V. Previous polarographic experiments proved that the reduced form was less strongly adsorbed than the oxidized one,³³ while the unprotonated form of cephalosporins, which was reduced at pH ≥ 10, showed no adsorption.^{5,32,33} These experiments confirmed that the adsorption prevails in an acid medium.^{5,32,33} The symmetrical shape of the voltammetric peaks of cefpodoxime, cefotaxime, desacetylcefotaxime and cefetamet, as well as the pronounced maxima of the curves presenting the current intensity vs. pH, indicated strong adsorption of these compounds at the mercury surface. The linear dependence of the voltammetric peak current on the scan rate, i_p vs. v , is also characteristic for adsorption-controlled processes (Fig. 3), and a higher slope was obtained when the adsorption was more pronounced.

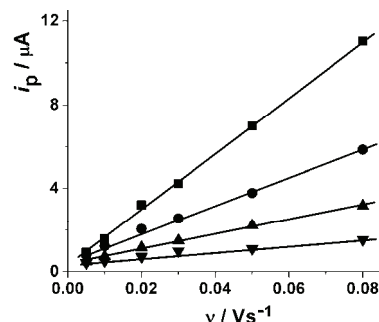


Fig. 3. Effect of the scan rate on the peak current for 1×10^{-5} mol dm⁻³ ceftriaxone (■), cefpodoxime proxetil (●), ceftazidime (▲) and cefuroxime axetil (▼) in BR buffer solutions.

Thus, the electrochemical adsorption of CRO, CPDX-PR, CAZ, CTX, DCTX, CXM and CET on the mercury electrode (Table I) was monitored by measuring the slopes ($\Delta i_p / \Delta v$).

TABLE I. Experimentally obtained slopes ($\Delta i_p / \Delta v$) for the investigated cephalosporins

Compound	pH	Slope ($\Delta i_p / \Delta v$) / $\mu\text{A V}^{-1} \text{s}$
Ceftriaxone (+/-, +)	3.0	134.07
Cefpodoxime proxetil	3.5	65.80 ¹⁸
Ceftazidime	3.0	35.56
Cefotaxime	2.8	17.40 ^{16,19}
Desacetylcefotaxime	2.8	16.30 ¹⁶
Cefuroxime axetil	3.0	14.43
Cefetamet	2.0	13.70 ¹⁷

In addition, the regression equations for $\log i_p = f(\log v)$ were calculated for all the investigated cephalosporins. Some of them are listed below:

- ceftriaxone (pH 3.0): $\log i_p = 0.898 \log v + 2.016$ ($r = 0.9988$)
- cefpodoxime proxetil (pH 3.5): $\log i_p = 0.706 \log v + 1.510$ ($r = 0.9970$)
- ceftazidime (pH 3.0): $\log i_p = 0.682 \log v + 1.232$ ($r = 0.9986$)
- cefuroxime axetil (pH 2.8): $\log i_p = 0.561 \log v + 0.742$ ($r = 0.9961$).

The corresponding slopes (higher than the theoretical value of 0.5 for a diffusion controlled process but lower than 1.0 for a process controlled only by adsorption) confirmed the influence of adsorption in acid solutions at mercury surface. According to the obtained slopes, the most pronounced adsorption was observed for ceftriaxone, and it decreased in the same order as already established with the $\Delta i_p/\Delta v$ values.

The differences observed between the investigated compounds are the consequence of specific adsorption and different orientation of these molecules at the mercury surface. It was established that the adsorption was more pronounced when the C7 substituent was more bulky. Since all these compounds possess a 2-aminothiazole ring at C7, it could be assumed that this ring plays a great role in adsorption on the mercury surface. The presence of the NH_3^+ group of the aminothiazole ring in an acid medium creates electrostatic forces with the mercury surface in the negative potential range and thus contributes to the adsorption. Finally, electron donor atoms, such as nitrogen and oxygen, in the side chain, increase the electron density of the thiazole ring and enhance the adsorption of methoxyimino cephalosporins.

Although the substituent in C2 and C3 position shows less contribution to the adsorption than the C7 substituent, the presence of different structures causes the differences in the adsorption characteristics. Therefore, the more complex structures of CRO, CPDX-PR, CAZ and CTX compared to those of DCTX, CXM and CET could generally explain the more strongly pronounced adsorption of the molecules in the first group.

Further, a quantum chemical and QSPR study of CRO, CPDX-PR, CAZ, CTX, DCTX, CXM and CET adsorption at the mercury electrode was performed to investigate the adsorption mechanism of the cephalosporins and to create a model for the prediction of the electrochemical adsorption for related compounds.

In the QSPR study, the experimentally determined slope ($\Delta i_p/\Delta v$), obtained using the CV technique on a mercury electrode, were used as dependent variables, while the computed molecular parameters (*MR*, $\log D$, *SAS*, *MS*, *MSA*, *PSA*, *HBD*, *HBA*, *HOMO*, *LUMO*, chemical potential (μ), electronegativity (χ), hardness (η), global softness (S), electrophilicity index (ω) and dipole moment) of the examined compounds were used as independent variables. The density functional theory (DFT)-based reactivity descriptors (*HOMO*, *LUMO*, μ , χ , η , S and ω) were successfully used in many previous studies^{34–43} for the interpretation of various reaction mechanisms.

Descriptors with the highest *VIP* and coefficient values were selected for building the QSPR model (Fig. 4A). The optimal combination of the most relevant descriptors (*HBA*, electron density on the nitrogen of the N–O bond ($ED_{(N)}$), *PMIY*, *HBA–HBD*, *PSA*, *MR*, *Clog P*, diameter, and ovality for building

the QSPR models was chosen based on the R^2 , Q^2 and $RMSEP$ values of the obtained PLS models.

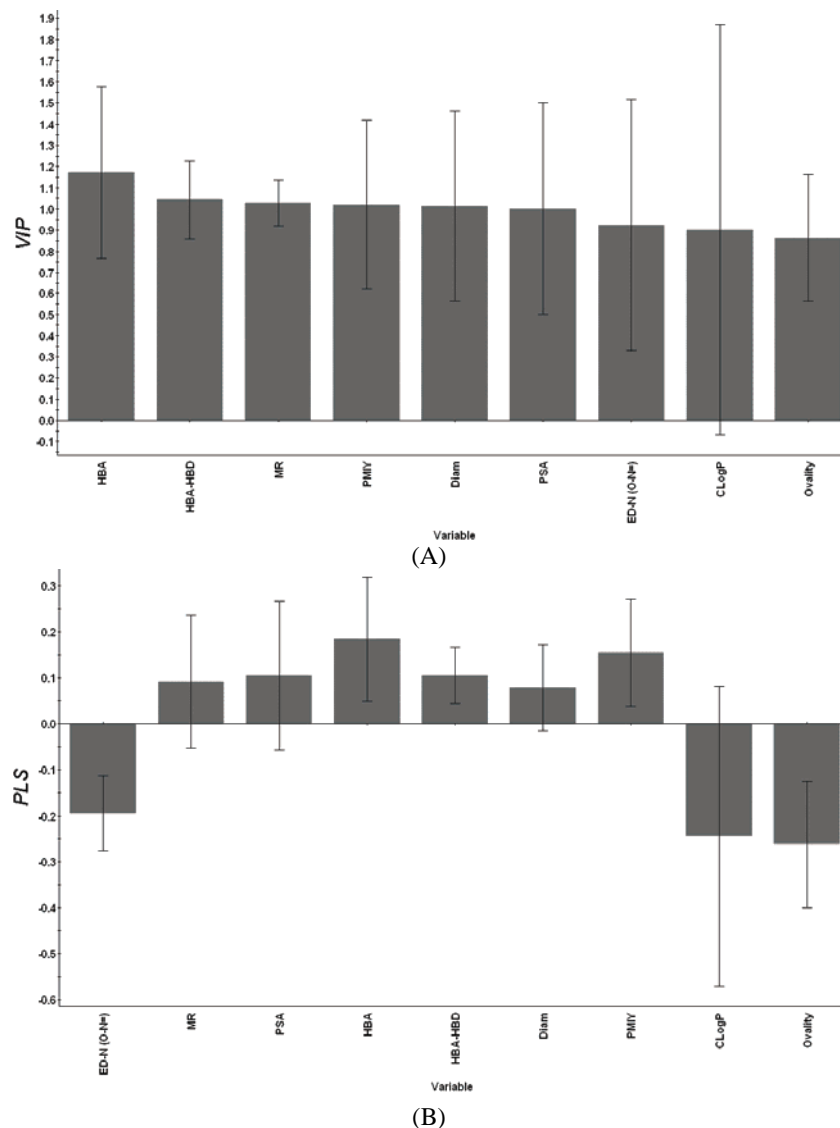


Fig. 4. A) VIP plot and B) coefficient plot of the developed QSPR model.

The coefficient plot (Fig. 4B) of the developed QSPR model indicated a negative correlation between the $ED_{(N)}$, $Clog\text{ }P$ and ovality parameters and adsorption on the surface of a mercury electrode (Table II). Therefore, the cephalosporins with lower electron density on the nitrogen atom of the N–O bond

TABLE II. Molecular descriptors of electrochemical adsorption of the cephalosporins on a mercury electrode (slope, $\Delta i_p/\Delta v$), selected in the QSPR study. Observed and QSPR-predicted electrochemical adsorption on a mercury electrode (slope, $\Delta i_p/\Delta v$)

Compound	<i>HBA</i>	<i>ED_(N)</i> (6-31(d,p))	<i>B3LYP-</i> (6-31(d,p))	<i>PM_Y</i>	<i>HB_{A-HBD}</i>	<i>PSA</i>	<i>MR</i>	<i>Clog P</i>	Diameter	Ovality	Slope, $\Delta i_p/\Delta v$ $\mu\text{A V}^{-1}\text{s}$	Predicted slope, $\Delta i_p/\Delta v$ $\mu\text{A V}^{-1}$
Ceftriaxone (+/-, +)	16.76	5.36609	12996.80	11.52	213.72	145.60	-1.278550	18	1.55442	134.07	123.61	
Cefpodoxime	13.62	5.37192	13530.30	10.24	180.97	131.36	0.800662	18	1.58462	65.80 ¹⁸	63.3864	
proxel												
Ceftazidime	14.23	5.38056	9143.53	9.46	192.83	143.88	0.426563	17	1.59622	35.56	57.8674	
Cefotaxime	12.56	5.46491	8521.44	8.12	175.12	116.30	0.1444262	15	1.62029	17.40 ^{16,19}	14.6256	
Desacetyl- -cefotaxime	11.59	5.46569	6983.57	6.18	169.05	107.15	-0.773237	13	1.54477	16.30 ⁶	26.9867	
Cefuroxime axetil	12.00	5.44607	10327.80	9.00	189.06	117.03	0.654200	15	1.67265	14.43	6.22526	
Cefetanet	10.13	5.39467	6356.62	5.26	148.82	105.37	0.862763	12	1.54172	13.70 ⁷	4.55847	
<i>R</i> ²	0.926									<i>RMSEP</i>	11.248	
<i>Q</i> ²	0.725									<i>r</i> ² , Obs vs. Pred	0.962	

lower lipophilicity should express high adsorption on a mercury electrode. The coefficient plot (Fig. 4B) also indicated a positive correlation between the *MR*, *PSA*, *HBA*, *HBA-HBD*, *PMIY* and diameter parameters and adsorption on the surface of a mercury electrode and hence, cephalosporins with higher *PSA*, *MR*, diameter and *PMIY* values and a higher number of hydrogen bond accepting groups should have a high adsorption on a mercury electrode.

The QSPR-model with the two significant components, $R^2 = 0.926$ and $Q^2 = 0.725$, with the lowest *RMSEP* (11.248) and the highest r^2 value (Obs vs. Pred; 0.962), was selected for further study (Table II). The obtained statistical parameters of the QSPR model indicated to a good prognostic capacity of the developed QSPR model.

Prediction of the slope ($\Delta i_p/\Delta v$) using the developed PLS-QSPR-model, could be applied to the other related cephalosporins.

Molecular models of cephalosporins (Fig. 5) confirmed essential influence of electron densities and charge of nitrogen for their adsorption on the mercury electrode surface.

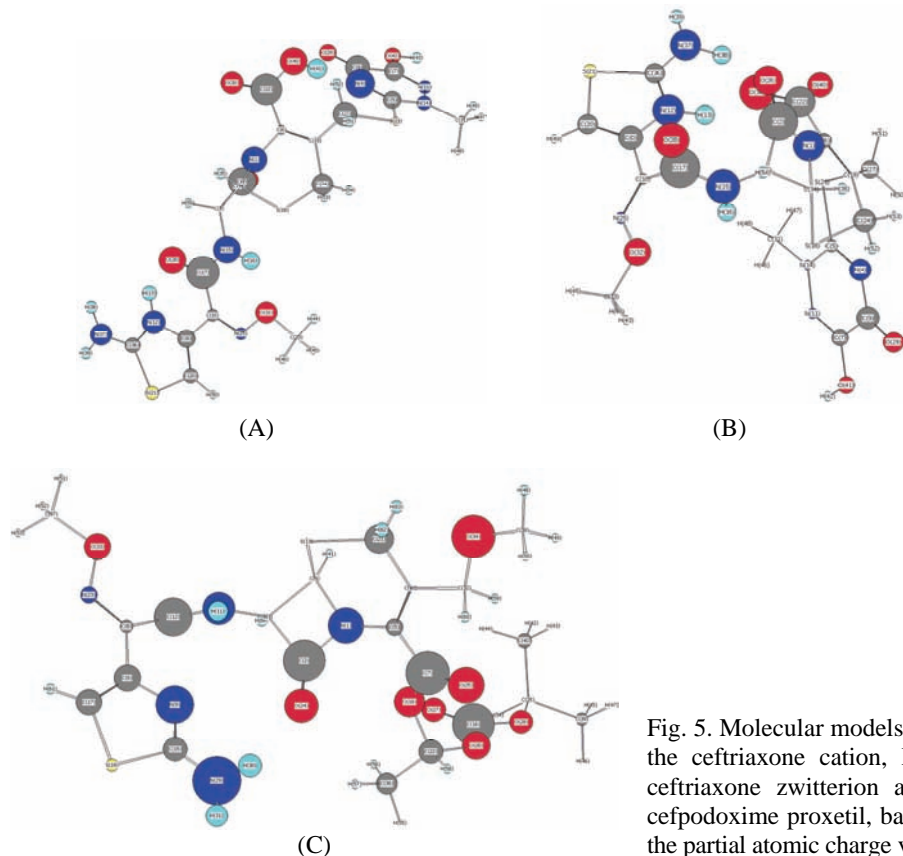


Fig. 5. Molecular models of: A) the ceftriaxone cation, B) the ceftriaxone zwitterion and C) cefpodoxime proxetil, based on the partial atomic charge values.

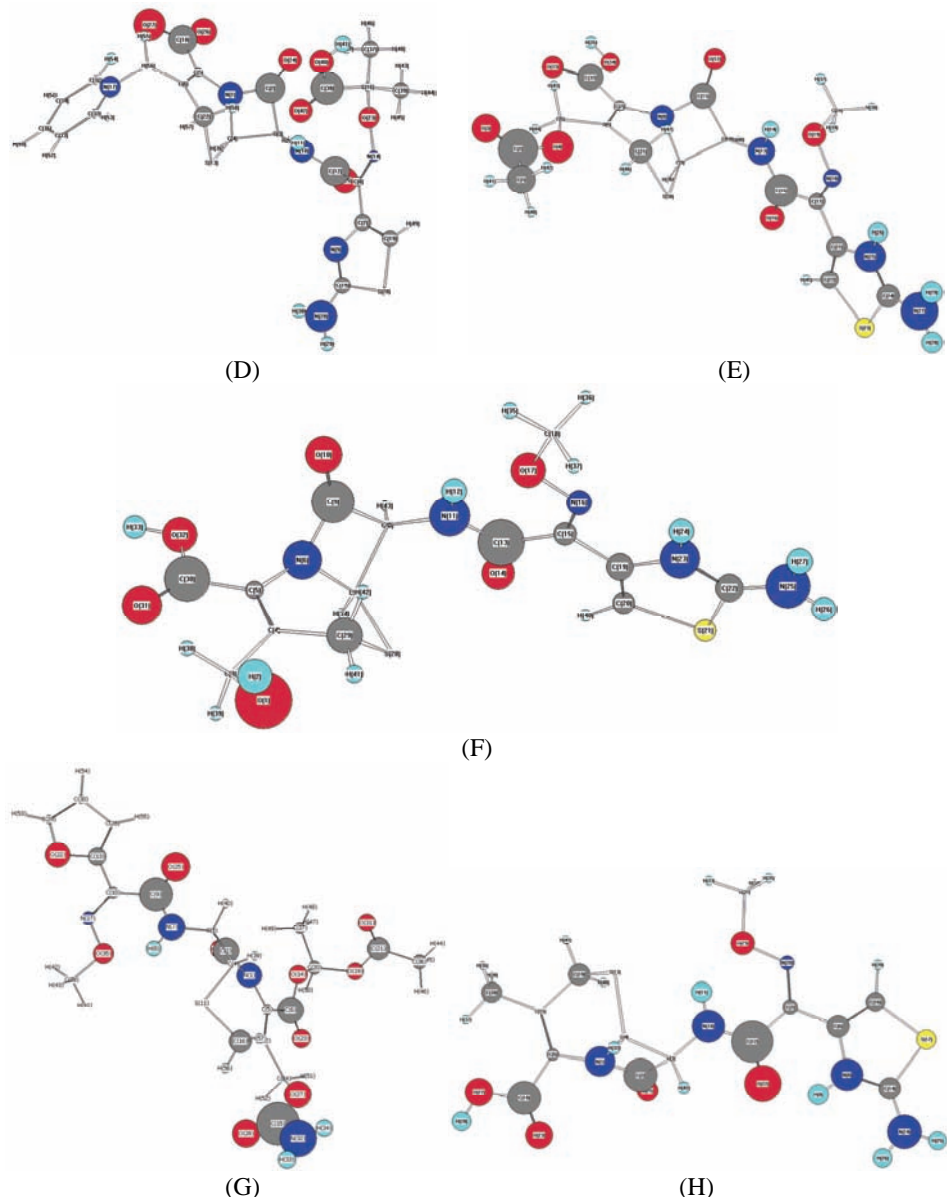


Fig. 5. (Continued) Molecular models of: D) ceftazidime, E) cefotaxime, F) desacetylcefotaxime, G) cefuroxime-axetil and H) cefetamet, based on the partial atomic charge values.

CONCLUSIONS

A previous voltammetric study of the electroreduction behavior and adsorption of methoxyimino cephalosporins (cefpodoxime proxetil, cefotaxime, desacetylcefotaxime and cefetamet) on a mercury electrode surface has been ext-

ended to structurally related cephalosporins (ceftriaxone, ceftazidime, and cefuroxime axetile). The density functional theory and QSPR studies were used to explain the adsorption mechanism at a mercury electrode surface and to predict the electrochemical adsorption at a mercury electrode of the related cephalosporins. The QSPR study selected the *HBA*, the electron density on the nitrogen of the N–O bond ($ED_{(N)}$), PMI_Y , *HBA–HBD*, *PSA*, *MR*, *Clog P*, diameter and ovality parameters as the most significant molecular determinants for the electrochemical adsorption of cephalosporins on a mercury electrode.

The developed QSPR model indicated a negative correlation between the $ED_{(N)}$, $C \log P$, and ovality parameters and adsorption, and a positive correlation between the *MR*, *PSA*, *HBA*, *HBA–HBD*, PMI_Y and diameter parameters and adsorption on the surface of a mercury electrode. Therefore, cephalosporins with lower electron density on the nitrogen atom of the N–O bond, lower lipophilicity, a higher principal moment of inertia and higher number of hydrogen bond accepting groups should express high adsorption on a mercury electrode. Prediction of the electrochemical adsorption using the developed QSPR model could be a very helpful tool for use in future cephalosporins studies. The presented study is first reported theoretical investigation of the electrochemical behaviors of cephalosporins.

Acknowledgments. This work was supported by the Ministry of Education, Science and Technological Development of the Republic of Serbia, Contract No. 172033.

ИЗВОД

ВОЛТАМЕТРИЈСКО И ТЕОРИЈСКО ПРОУЧАВАЊЕ ПОНАШАЊА ЦЕФАЛОСПОРИНА НА ЖИВИНОЈ ЕЛЕКТРОДИ

КАТАРИНА НИКОЛИЋ, МАРА М. АЛЕКСИЋ, ВЕРА КАПЕТАНОВИЋ и ДАНИЦА АГБАБА

Фармацеутички факултет, Универзитет у Београду, Војводе Степе 450, 11000 Београд

Применом цикличне (CV), диференцијално-пулсне (DPV) и адсорптивне "stripping" диференцијално-пулсне (AdSDPV) волтаметрије испитано је електрохемијско понашање и адсорпција цефподоксим-проксетила, цефотаксима, дезацетил-цефотаксима, цефетамета, цефтриаксона, цефтазидима и цефуроксим-аксетила на површини живине електроде. Студија квантитативних односа структуре и особина (QSPR) је коришћена за испитивање адсорпције седам цефалоспорина на живиној електроди. Применом теорије функционала густине DFT-B3LYP/6-31G(d,p) су израчунате енергије молекулских орбитала, парцијално наелектрисање и електронске густине испитиваних аналита, које су употребљене као молекулски параметри у QSPR студији. Помоћу изабраних DFT-параметара и QSPR модела је објашњен процес адсорпције испитиваних цефалоспорина. Резултати QSPR анализе показали су да већу адсорпцију на живи покazuју цефалоспорини са нижим наелектрисањем на сумпору тиазинског дела молекула, мањом електронском густином на атому азота N–O везе, већим бројем група које граде водоничне везе и већим главним моментом инерције.

(Примљено 29. јануара, ревидирано 23. фебруара, прихваћено 26. фебруара 2015)

REFERENCES

1. J. M. Beale Jr., in *Wilson and Gisvold's Textbook of Organic Medicinal and Pharmaceutical Chemistry*, 12th ed., J. M. Beale, Jr., J. H. Block, Eds., Lippincott, Williams & Wilkins, Philadelphia, PA, 2011, p. 278
2. N. A. El-Maali, A. M. M. Ali, M. A. Ghandoor, *Electroanalysis* **5** (1993) 599
3. G. Bernacca, L. Nucci, F. Pergola, *Electroanalysis* **6** (1994) 327
4. B. Ogorevc, V. Hudnik, S. Gomiscek, Z. Fresenius, *Anal. Chem.* **330** (1988) 59
5. A. G. Fogg, N. M. Fayad, C. Burgess, A. McGlynn, *Anal. Chim. Acta* **108** (1979) 205
6. S. Altinoz, A. Temizer, *J. Pharm. Sci.* **79** (1990) 351
7. M. Avramov-Ivić, V. Kapetanović, M. Aleksić, P. Zuman, *J. Serb. Chem. Soc.* **65** (2000) 47
8. B. Dogan, A. Golcu, M. Dolaz, S. A. Ozkan, *Curr. Pharm. Anal.* **5** (2009) 197
9. P. Nigam, S. Mohan, S. Kundu, R. Prakash, *Talanta* **77** (2009) 1436
10. S. A. Ozkan, B. Uslu, P. Zuman, *Anal. Chim. Acta* **457** (2002) 265
11. S. Majdi, A. Jabbari, H. Heli, H. Yadegari, A. A. Moosavi-Movahedi, S. Haghgoo, *J. Solid State Electrochem.* **13** (2009) 407
12. N. Yilmaz, I. Biryol, *J. Pharm. Biomed. Anal.* **17** (1998) 1335
13. S. R. El-Shaboury, G. A. Saleh, F. A. Mohamed, A. H. Rageh, *J. Pharm. Biomed. Anal.* **45** (2007) 1
14. Q. Xu, A. J. Yuan, R. Zhang, X. Bian, D. Chen, X. Hu, *Curr. Pharm. Anal.* **5** (2009) 144
15. S. A. Özkan, B. Uslu, H. Y. Aboul-Enein, *Crit. Rev. Anal. Chem.* **33** (2003) 155
16. M. M. Aleksić, V. Kapetanović, J. Atanacković, B. Jocić, M. Zečević, *Talanta* **77** (2008) 131
17. M. M. Aleksić, Lj. Milovanović, V. Kapetanović, *J. Pharm. Biomed. Anal.* **32** (2003) 957
18. M. M. Aleksić, M. Ilić, V. Kapetanović, *J. Pharm. Biomed. Anal.* **36** (2004) 899
19. M. M. Aleksić, V. Kapetanović, *J. Electroanal. Chem.* **593** (2006) 258
20. P. Zuman, V. Kapetanović, M. M. Aleksić, *Anal. Lett.* **33** (2000) 2821
21. MarvinSketch 5.5.1.0 program, ChemAxon, Budapest, Hungary, www.chemaxon.com/products.html (accessed July, 2011)
22. CS Chem3D Ultra 7.0 (Property Picker ActiveX Control), Cambridge Soft Corporation, 2001, <http://www.cambridgesoft.com/>
23. Gaussian 98 (Revision A.7), Gaussian, Inc., Pittsburgh, PA, 1998
24. A. D. Becke, *J. Chem. Phys.* **98** (1993), 5648
25. C. Lee, W. Yang, R. G. Parr, *Phys. Rev., B* **37** (1988) 785
26. C. C. J. Roothaan, *Rev. Mod. Phys.* **23** (1951) 69
27. L. Eriksson, E. Johansson, N. Kettaneh-Wold, J. Trygg, C. Wikstrom, S. Wold, *Multi-and Megavariate Data Analysis. Basic Principles and Applications I*, 2nd ed., Umetrics Academy, Umeå, 2006, p. 63–101
28. SIMCA P+ program, version 12.0, Umetrics AB, Umeå, 2008
29. M. M. Aleksić, V. Kapetanović, P. Zuman, *Collect. Czech. Chem. Commun.* **69** (2004) 1429
30. M. M. Aleksić, V. Kapetanović, P. Zuman, *Collect. Czech. Chem. Commun.* **66** (2001) 1005
31. M. Erceg, V. Kapetanović, D. Sužnjević, D. Dumanović, *Microchem. J.* **57** (1997) 73
32. V. Kapetanović, M. M. Aleksić, P. Zuman, *J. Electroanal. Chem.* **507** (2001) 263
33. V. Kapetanović, M. M. Aleksić, M. Erceg, D. Veselinović, *Farmaco* **55** (2000) 13
34. R. G. Parr, W. Yang, *Density-Functional Theory of Atoms and Molecules*, Oxford University Press, New York, 1989, pp. 47–70

35. R. P. Iczkowski, J. L. Margrave, *J. Am. Chem. Soc.* **83** (1961) 3547
36. R. G. Parr, R .G. Pearson, *J. Am. Chem. Soc.* **105** (1983) 7521
37. A. Ponti, *J. Phys. Chem., A* **104** (2000) 8843
38. G. Molteni, A. Ponti, *Chem.-Eur. J.* **9** (2003) 2770
39. P. Geerlings, F. De Proft, W. Langenaeker, *Chem. Rev.* **103** (2003) 1793
40. T. Mineva, T. Heine, *J. Phys. Chem. A* **108** (2004) 11086
41. R. G. Parr, L. V. Szentpály, S. Liu, *J. Am. Chem. Soc.* **121** (1999) 1922
42. M. Huang, A. Maynard, J. A. Turpin, L. Graham, G. M. Janini, D. G. Covell, W. G. Rice, *J. Med. Chem.* **41** (1998) 1371
43. A. T. Maynard, M. Huang, W. G. Rice, D. G. Covell, *Proc. Natl. Acad. Sci. USA* **95** (1998) 11578.



Analysis of alcohol dehydrogenase inhibitors from *Desmodium styracifolium* using centrifugal ultrafiltration coupled with HPLC-MS

LIANGLIANG LIU¹, MIAO CHEN¹ and XIAOQING CHEN^{1,2*}

¹Institute of Bast Fiber Crops, Chinese Academy of Agricultural Sciences, Changsha 410205, China and ²School of Chemistry and Chemical Engineering, Central South University, Changsha 410083, China

(Received 19 September, revised 16 December 2014, accepted 9 March 2015)

Abstract: Alcohol dehydrogenase (ADH) inhibitors play an important role in the treatment of human methanol or ethylene glycol poisoning and the suppression of acetaldehyde accumulation in alcoholics. In this study, centrifugal ultrafiltration coupled with high performance liquid chromatography-mass spectrometry (HPLC-MS) was utilized to screen and identify ADH inhibitors from an ethyl acetate extract of *Desmodium styracifolium* (Osb.) Merr. The experimental conditions of the centrifugal ultrafiltration were optimized. Under the optimum conditions (ADH concentration: 37.5 µg mL⁻¹, incubation time: 90 min, pH 7.0 and temperature: 15 °C), formononetin and aromadendrin were successfully screened and identified from the ethyl acetate extract of *D. styracifolium*. The screening result was verified by ADH inhibition assays. The IC_{50} values of formononetin and aromadendrin were 70.8 and 84.7 µg mL⁻¹, which were in accordance with their degrees of binding. Aromadendrin was for the first time reported to have inhibitory activity on ADH. This method provides an effective way to screen active compounds from natural products.

Keywords: alcohol dehydrogenases; aromadendrin; centrifugal ultrafiltration; *Desmodium styracifolium*; formononetin.

INTRODUCTION

Nowadays, natural products have become the primary source for chemical and pharmaceutical research because of their long history in clinical practice and reliable therapeutic efficacy.^{1,2} In the last thirty years, 46 % of the new chemical entities approved as drugs by the US Food and Drug Administration were relevant to natural products.³ However, the chemical composition of natural products is complex. Compared to the numerous compounds existing in natural pro-

*Corresponding author. E-mail: xqchen@csu.edu.cn
doi: 10.2298/JSC140919023L

ducts, the numbers and contents of active compounds are relatively low. The conventional procedures for screening active compounds in natural products are laborious and time-consuming.⁴ Accordingly, numerous screening methods were developed, such as cell membrane chromatography, ultrafiltration and equilibrium dialysis.^{5–7}

Centrifugal ultrafiltration is a rapid method using centrifugation force and a semi-permeable membrane to retain high molecular weight solutes.^{8,9} Compounds with a molecular weight higher than the nominal molecular weight cut-off of the membrane would be retained, while low molecular weight compounds could pass through the membrane.^{10,11} Based on this principle, when an extract of natural products was incubated with some enzyme, the active compounds in the natural products would bind to the enzyme and be trapped by the membrane together with enzyme. Combined with high performance liquid chromatography–mass spectrometry (HPLC–MS) analysis, active compounds could be identified by comparing the chromatograms before and after centrifugal ultrafiltration. Therefore, centrifugal ultrafiltration coupled with HPLC–MS could become a simple and powerful tool for discovering active compounds from natural products,^{12,13} and many examples have been performed by this method to screen enzyme inhibitors and ligands.^{14–19} These studies showed that the screening could be accomplished rapidly and the crude samples could be analyzed without further purification.

Alcohol dehydrogenases (ADH) catalyzes the oxidation of alcohols with the reduction of nicotinamide adenine dinucleotide (NAD^+) in many organisms.²⁰ In the human body, ADH is also involved in the oxidation of methanol to formaldehyde and ethylene glycol to glycolic and oxalic acids.^{21,22} However, the existence of formaldehyde or glycolic acid is harmful to humans. ADH inhibitors hinder the metabolisms of methanol and ethylene glycol, and, consequently, could be used in the therapies of human methanol and ethylene glycol poisonings.^{23,24} Moreover, ADH inhibitors could suppress acetaldehyde accumulation in alcoholics.²⁵ *Desmodium styracifolium* (Osb.) Merr. is known in China for its heat-clearing and diuretic properties. It is also an important Chinese medicine for the treatments of renal stones and cardio-cerebrovascular disease. The experiments showed that the ethyl acetate extract of *D. styracifolium* showed inhibition on ADH. However, the related detail research is still inadequate.

In this study, ADH inhibitors from *D. styracifolium* were analyzed by centrifugal ultrafiltration coupled with HPLC–MS. The experimental conditions, including enzyme concentration, incubation time, pH and temperature, were investigated and optimized. Two ADH inhibitors were identified under the optimum conditions. Experiment results proved this method could screen and analyze ADH inhibitors without the purification of natural samples and the screening results were reliable.

EXPERIMENTAL

Materials

Dried *Desmodium styracifolium* (Osb.) Merr. was purchased from Beijing Tongrentang Co., Ltd. (Changsha, China). Alcohol dehydrogenase (ADH) was acquired from Sigma-Aldrich Chemicals (St. Louis, MO, USA). Nicotinamide adenine dinucleotide (NAD^+) was obtained from F. Hoffmann-La Roche Ltd. (Basel, Switzerland). Acetonitrile, methanol and acetic acid used for HPLC were chromatographic grade and obtained from Tedia Company Inc. (Fairfield, OH, USA). Ultrapure water (18.2 M Ω resistivity) was obtained from a Milli-Q water purification system (Millipore, Bedford, MA, USA). The other chemicals were analytical grade. Formononetin and aromadendrin were isolated and characterized from *D. styracifolium* in the laboratory and their structures were identified by UV, MS and NMR.²⁶ Their purities were determined to be over 95 % by normalization of the peak areas detected by HPLC-DAD-MS/MS.

Preparation of Desmodium styracifolium extract

Dried *D. styracifolium* (30.00 g) was suspended in 300 mL of ethanol (95 %,) and reflux extracted at 85 °C for 3 h. After cooled at room temperature, the solvent was removed with vacuum rotary evaporation. Then the residue (1.25 g) was dissolved in 150 mL of water and extracted successively with equal volumes of petroleum ether, ethyl acetate and *n*-butanol. The evaporated ethyl acetate extract (0.19 g) was dissolved in 150 mL of water, filtered through a 0.45 µm membrane (Acrodisc® Syringe Filter, Pall, Port Washington, NY, USA) and stored at 4 °C for further experiments.

Screening of ADH inhibitors by centrifugal ultrafiltration

A mixture of *D. styracifolium* extract (100 µL, 0.5 mg mL⁻¹) and ADH solution (100 µL, 37.5 µg mL⁻¹) was incubated at 15 °C for 90 min. After incubation, the mixture was poured into a centrifugal ultrafiltration device (Nanosep MF Centrifugal Devices, ≤10 kDa, Pall, Port Washington, NY, USA) and centrifuged at 7000 rpm for 30 min at room temperature. The control experiments were performed under the same conditions using denatured enzyme instead of active enzyme. The filtrates were directly analyzed by HPLC-MS without dilution. All the binding assays were performed in triplicate.

HPLC-MS analysis

HPLC was performed on an Acquity™ UPLC system (Waters, Milford, MA, USA) with a cooled autosampler and column oven enabling temperature control of the analytical column. A reversed phase SunFire™ C₁₈ (250 mm×4.6 mm i.d., 5 µm, Waters, Milford, MA, USA) column was employed for the analysis. The chromatographic separation was realized using a mixture of solvents, acetonitrile (A) and water containing 0.4 % acetic acid (B). The gradient program for the *D. styracifolium* extract was as follows: 22–33 % A (0–10 min) and 33–40 % A (10–20 min). The flow rate was 1.0 mL min⁻¹ and the column temperature was 25 °C. The detection wavelength was set at 254 nm and the injection volume was 20 µL. Triple-quadrupole mass detection was performed on a Micromass® Quattro Micro™ API mass spectrometer (Waters Corp., Milford, MA, USA) with an electrospray ionization (ESI) interface. The ESI source was set in the negative ionization mode. The following settings were applied to the instrument: capillary voltage, 3.00 kV; cone voltage, 40.0 V; extractor voltage, 3.00 V; source temperature, 120 °C; desolvation temperature, 400 °C; desolvation gas flow rate, 750 L h⁻¹; cone gas flow rate, 50 L h⁻¹ and dwell time, 0.05 s. Nitrogen was used as the desolvation and cone gas. Mass detection was performed in the full scan mode for *m/z* in the range 160–800.

All collected data were acquired and processed using MassLynx™ NT 4.1 software with QuanLynx™ program (Waters Corp., Milford, MA, USA).

Enzyme activity assay

A mixture of ethanol (500 µL), NAD⁺ (500 µL, 1 mg mL⁻¹) and phosphate buffer solution (1000 µL, pH 7.0, 0.2 M, PBS) were used as the substrate. To initiate the reaction, 10 µL of ADH (37.5 µg mL⁻¹) was added to the substrate at 15 °C. After incubation for 5 min, the increase in absorbance at 340 nm was measured using an UV–Vis spectrophotometer (UV-2450, Shimadzu, Kyoto, Japan). One unit of ADH activity was defined as the amount of enzyme that reduced 1 nmol of NAD⁺ per minute under the assay conditions.

When the inhibition of ADH activity was studied, 1000 µL of *D. styracifolium* extract with different concentrations were used instead of PBS. The substrate was incubated for 5 min at 15 °C before the addition of 10 µL of ADH (37.5 µg mL⁻¹). The mixture was incubated for 5 min and the increase in absorbance at 340 nm was measured. The percentage inhibition, *I%*, of the ADH activity was calculated using Eq. (1).

$$I\% = 1 - 100 \left(\frac{\Delta A_1}{\Delta A_0} \right) \quad (1)$$

where ΔA_0 is the increase in absorbance at 340 nm and ΔA_1 is the increase in absorbance at 340 nm in the presence of *D. styracifolium* extract. All experiments were conducted in triplicate under the same conditions and the results were obtained as the average of the corresponding experimental values.

Optimization of the screening conditions

The effect of ADH concentration on the screening was evaluated using different concentrations of ADH (12.5, 25.0, 37.5 and 50.0 µg mL⁻¹). Various incubation times (10, 60, 90 and 120 min) were also studied to determine the appropriate incubation time for the assays. To acquire the optimum pH and temperature for screening, the experiments were conducted at different pH value from 5.0 to 9.0 and temperatures in the range from 5 to 45 °C. All experiments were conducted in triplicate and the results were obtained as the average of the corresponding experimental values. The binding strength of compounds to ADH was defined as the binding degree, *BD%*, which can be calculated using Eq. (2):

$$BD\% = 1 - 100 \left(\frac{Ab}{Aa} \right) \quad (2)$$

where *Aa* and *Ab* are the peak areas of a compound in the HPLC chromatograms incubated with denatured and active ADH, respectively.

RESULTS AND DISCUSSION

Optimization of HPLC analysis

The separation of each compound in the extracts of natural products is a challenge for HPLC analysis. Acid in the mobile phase could reduce peak tailing and increase the signal.²⁷ Therefore, different mobile phases with different flow rates, detection wavelengths and column temperatures were utilized to optimize the HPLC conditions for the analysis of the *D. styracifolium* extract. The results showed that the optimum chromatographic separation was achieved using a mix-

ture of solvents, acetonitrile (A) and water containing 0.4 % acetic acid (B). A gradient program was operated as follows: 22–33 % A (0–10 min) and 33–40 % A (10–20 min). The flow rate was 1.0 mL min⁻¹ and the column temperature was 25 °C. The detection wavelength was set at 254 nm and the injection volume was 20 µL. All constituents could reach baseline separation and a relatively short analysis time was achieved. Chromatograms obtained under these conditions are shown in Fig. 1.

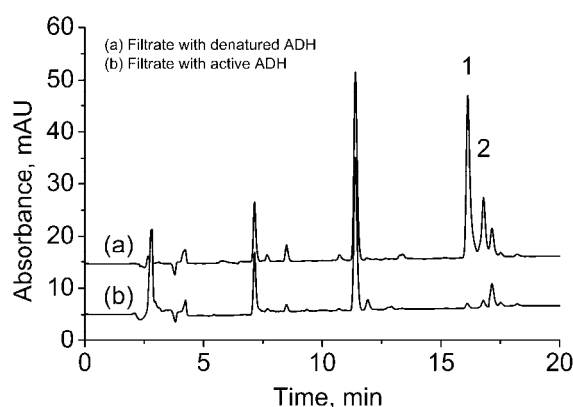


Fig. 1. The chromatograms of filtrates incubated with denatured (a) and active (b) ADH.

Optimization of the screening conditions

Effect of ADH concentration. Different concentrations of ADH (12.5, 25.0, 37.5 and 50.0 µg mL⁻¹) were incubated with *D. styracifolium* extract to investigate the effect of the ADH concentration on binding degree. The chromatograms of filtrates incubated with different concentrations of ADH are shown in Fig. 2A. The peaks of compounds 1 and 2 decreased with increasing ADH concentration. When the concentration of ADH was higher than 37.5 µg mL⁻¹, the

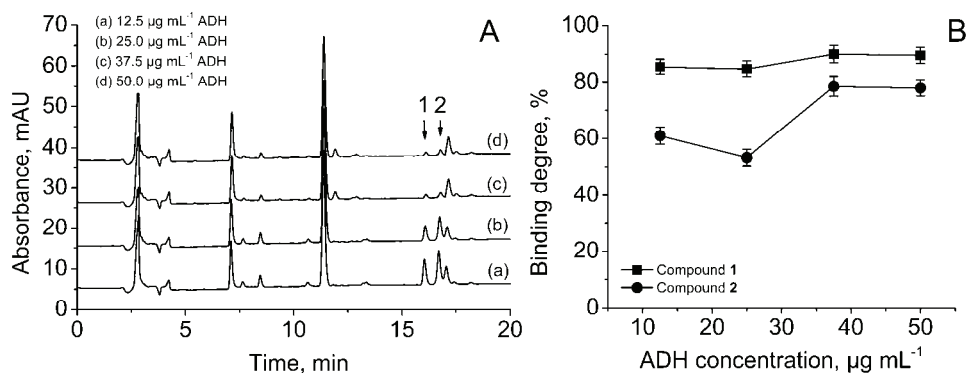


Fig. 2. A) The chromatograms of the filtrates incubated with different concentrations of ADH; B) the effect of the ADH concentration on the binding degrees.

binding degrees remained unchanged (Fig. 2B). As superfluous enzyme is wasteful and would increase the cost of the experiment, an ADH concentration of 37.5 $\mu\text{g mL}^{-1}$ was considered optimal.

Effect of incubation time. A sufficient period was necessary to achieve ligand–enzyme equilibrium. Hence, different incubation periods ranging from 10 to 120 min were studied to investigate the effect of time on the binding degree. The binding degrees of compounds **1** and **2** at different incubation times were calculated and are shown in Fig. 3A. The binding degrees of compounds **1** and **2** became the highest when the incubation time reached 90 min, and did not increase on prolongation of the incubation time. The results manifested that 90 min incubation time was sufficient in screening experiments.

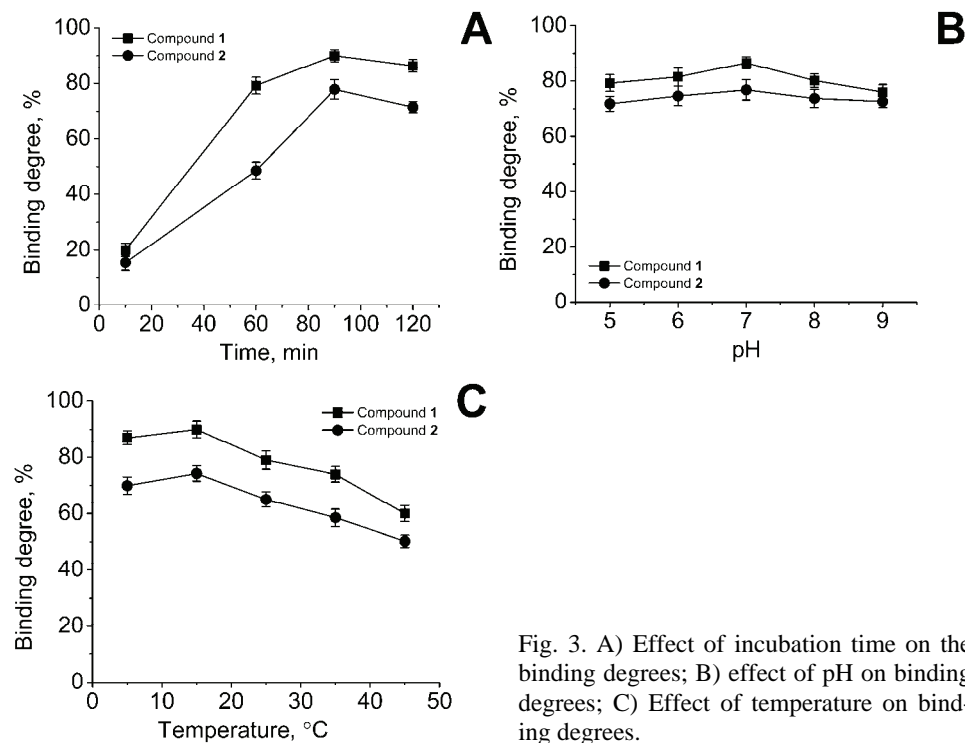


Fig. 3. A) Effect of incubation time on the binding degrees; B) effect of pH on binding degrees; C) Effect of temperature on binding degrees.

Effect of pH. The pH value affects the status of an enzyme and its activity. The effect of pH on the binding degree was studied at different pH values ranging from 5.0 to 9.0. As shown in Fig. 3B, the maximum binding degrees of compounds **1** and **2** were obtained at pH 7.0. As reported in the literatures, ADH showed optimum activity at pH 7.0, which was in accordance with the obtained experiment results.²⁸ Therefore, the screening pH value was set at 7.0.

Effect of temperature. The effect of temperature on binding degree was investigated and the results are shown in Fig. 3C. It was found that the highest binding degrees were achieved at 15 °C. The enzyme is thermally sensitive in general and its activity would decrease in a high temperature environment.²⁹ Thus, the temperature was set at 15 °C in order to maintain the enzyme active during the experiments.

Screening and identification of ADH inhibitors

The ethyl acetate part of the *D. styracifolium* extract showed ADH inhibition with an IC_{50} value of 36.2 µg mL⁻¹, while the IC_{50} values of the petroleum ether and *n*-butanol parts were greater than 500 µg mL⁻¹. These results suggested that there were compounds that inhibited ADH in the ethyl acetate part of the *D. styracifolium* extract. Therefore, the ethyl acetate part of the *D. styracifolium* extract was selected as the screening sample and was analyzed by centrifugal ultrafiltration combined with HPLC-MS.

Screening experiments with denatured ADH were performed to exclude the possibility of nonspecific adsorption between the compounds and enzyme. The chromatograms of the filtrates incubated with denatured and active ADH are seen in Fig. 1. Two compounds marked as **1** and **2** clearly showed decreases in peak

TABLE I. The identification, UV, and MS characteristics of compounds in *D. styracifolium*

Peak	Formula	UV (λ_{max} / nm)	Proposed ion	Structural assignment	Ref.
1	C ₁₆ H ₁₂ O ₄	248.3	[M+H] ⁺ 269	Formononetin	30
2	C ₁₅ H ₁₂ O ₆	225.3	[M+H] ⁺ 289	Aromadendrin	31

areas after centrifugal ultrafiltration with active ADH. The chemical structure of these two compounds was identified according to their UV and HPLC-MS spectroscopic data. According to previous reports, the data shown in Table I were in agreement with literature values.^{30,31} Therefore, these two compounds were identified as formononetin and aromadendrin. Their chemical structures are shown in Fig. 4. The screening results indicated formononetin and aromadendrin had potential inhibitory activities on ADH.

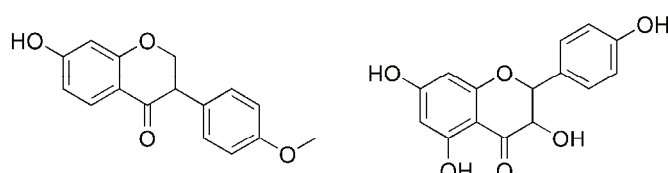


Fig. 4. Chemical structures of the screened compounds.

Inhibition analysis of the screened compounds

In order to confirm the screening results, the inhibitory activities of authentic formononetin and aromadendrin were analyzed. The authentic samples of formononetin and aromadendrin exhibited inhibitory activities on ADH, and their IC_{50} values were 70.8 and 84.7 $\mu\text{g mL}^{-1}$, respectively. In addition, the binding degrees of formononetin and aromadendrin under the optimum conditions were 90.0 % and 86.5 %, respectively. These results showed that the compound with high binding degree had the lower IC_{50} value. The binding degree could indicate not only the potential inhibitory activity of compound, but also the degree of inhibition. Based on current literature, the inhibitory activity of formononetin on ADH has been reported,³² while, the inhibitory activity of aromadendrin on ADH is reported herein for the first time. This demonstrated that screening utilizing centrifugal ultrafiltration combined with HPLC-MS was effective and conclusive.

CONCLUSIONS

A facile screening method based on centrifugal ultrafiltration combined with HPLC-MS was established for analyzing ADH inhibitors from *D. styracifolium*. The experimental conditions were optimized. Finally, formononetin and aromadendrin were screened, identified and analyzed as ADH inhibitors. This method proved to be rapid and effective for the identification of active compounds in natural products.

Acknowledgements. This work was financially supported by the National Natural Science Foundation of China (21175155), Key Project of Philosophy and Social Sciences Research, Ministry of Education, PRC (No. 13JZD0016, Research on Institutional Building of Ecological Civilization), the Specialized Research Fund for the Doctoral Program of Higher Education of China (20130162110017) and the Hunan Provincial Innovation Foundation for Postgraduates (CX2012B119).

ИЗВОД

АНАЛИЗА ИНХИБИТОРА АЛКОХОЛНЕ ДЕХИДРОГЕНАЗЕ ИЗ *Desmodium styracifolium*
ПРИМЕНОМ ЦЕНТРИФУГАЛНЕ УЛТРАФИЛТРАЦИЈЕ СПРЕГНУТЕ СА HPLC-MS

LIANGLIANG LIU¹, MIAO CHEN¹ и XIAOQING CHEN^{1,2}

¹*Institute of Bast Fiber Crops, Chinese Academy of Agricultural Sciences, Changsha 410205, China* и ²*School of Chemistry and Chemical Engineering, Central South University, Changsha 410083, China*

Инхибитори алкохол дехидрогеназе (ADH) имају значајну улогу у третирању тро-вања метанолом и етиленгликолом и супресији акумулације ацеталдехида код алкохоличара. У овом раду, центрифугална ултрафилтрација је спречнута са високоефикасном течном хроматографијом–масеном спектрометријом (HPLC-MS), ради скрининга и идентификације ADH инхибитора из етилацетатног екстракта *Desmodium styracifolium* (Osb.) Merr. Оптимизовани су услови центрифугалне ултрафилтрације. При оптималним условима (концентрација ADH: 37,5 $\mu\text{g mL}^{-1}$, време инкубације: 90 min, pH 7,0 и температура: 15 °C), формононетин и аромадендрин су успешно идентификовани из

етилацетатног екстракта *D. styracifolium*. Резултати скрининга су верификовани тестом ADH инхибиције. Вредности IC_{50} за формононетин и аромадендрин су биле 70,8 и 84,7 $\mu\text{g mL}^{-1}$, што је сагласно са афинитетом везивања ових једињења. Инхибиторна активност на ADH је први пут публикована за аромадендрин. Ова метода обезбеђује ефикасан начин за скрининг активних једињења у природним производима.

(Примљено 19. септембра, ревидирано 16. децембра 2014, прихваћено 9. марта 2015)

REFERENCES

- J. Rey-Ladino, A. G. Ross, A. W. Cripps, D. P. McManus, R. Quinn, *Vaccine* **29** (2011) 6464
- H. S. Kang, S. F. Brady, *Angew. Chem. Int. Edit.* **52** (2013) 11063
- D. J. Newman, G. M. Cragg, *J. Nat. Prod.* **75** (2012) 311
- G. M. Cragg, D. J. Newman, *BBA – Gen. Subjects* **1830** (2013) 3670
- X. Wang, H. Sun, A. Zhang, G. Jiao, W. Sun, Y. Yuan, *Analyst* **136** (2011) 5068
- Y. Yan, Y. Hao, S. Hu, X. Chen, X. Bai, *J. Chromatogr., A* **1322** (2013) 8
- C. J. Henrich, J. A. Beutler, *Nat. Prod. Rep.* **30** (2013) 1284
- J. H. Xie, M. Y. Shen, S. P. Nie, Q. Zhao, C. Li, M. Y. Xie, *Carbohyd. Polym.* **101** (2014) 479
- K. Inoue, S. Nitta, T. Hino, H. Oka, *J. Chromatogr., B* **877** (2009) 461
- H. Yu, Y. Zhang, X. Sun, J. Liu, H. Zhang, *Chem. Eng. J.* **237** (2014) 322
- E. E. Borujeni, A. L. Zydney, *Biotechniques* **53** (2012) 49
- L. Liu, S. Shi, X. Chen, M. Peng, *J. Chromatogr., B* **932** (2013) 19
- L. Zhang, Z. Q. Zhang, W. C. Dong, S. J. Jing, J. F. Zhang, Y. Jiang, *J. Chromatogr., A* **1318** (2013) 265
- J. Shi, X. Y. Zhang, Z. J. Ma, M. Zhang, F. Sun, *Molecules* **15** (2010) 3556
- L. Ma, Z. F. Wang, L. N. Chen, F. R. Song, Z. Q. Liu, S. Y. Liu, *Chem. J. Chin. U.* **34** (2013) 331 (in Chinese)
- Y. Liu, S. Liu, Z. Q. Liu, *J. Chromatogr., B* **923** (2013) 48
- S. Y. Shi, M. J. Peng, Y. P. Zhang, S. Peng, *Anal. Bioanal. Chem.* **405** (2013) 42133
- H. B. Zhu, S. Liu, C. Y. Wang, Z. Q. Liu, F. R. Song, *Chem. J. Chin. U.* **34** (2013) 1635 (in Chinese)
- C. F. Zhao, Y. Q. Liu, D. L. Cong, H. Zhang, J. J. Yu, Y. Jiang, X. Y. Cui, J. M. Sun, *Biomed. Chromatogr.* **27** (2013) 1621
- E. Hamnevik, C. Blikstad, S. Norrehed, M. Widersten, *J. Mol. Catal., B* **99** (2014) 68
- S. L. MacAllister, J. Choi, L. Dedina, P. J. O'Brien, *Chem-Biol. Interact.* **191** (2011) 308
- M. J. Burns, A. Graudins, C. K. Aaron, K. McMartin, J. Brent, *Ann. Emerg. Med.* **30** (1997) 829
- S. L. Lee, H. T. Shih, Y. C. Chi, Y. P. Li, S. J. Yin, *Chem-Biol. Interact.* **191** (2011) 26
- F. J. Baud, M. Galliot, A. Astier, D. V. Bien, R. Garnier, J. Likforman, C. Bismuth, *New Engl. J. Med.* **319** (1988) 97
- K. Inoue, Y. Kera, T. Kiriyama, S. Komura, *Jpn. J. Pharmacol.* **38** (1985) 43
- W. Su, Q. Liu, Q. Yang, J. G. Yu, X. Q. Chen, *J. Sep. Sci.* **36** (2013) 3338
- D. V. McCalley, *J. Chromatogr., A* **1075** (2005) 57
- S. Xu, Y. Lu, Z. Jiang, H. Wu, *J. Mol. Catal., B* **43** (2006) 68
- G. Martelli, C. Folli, L. Visai, M. Daglia, D. Ferrari, *Process Biochem.* **49** (2014) 154
- W. M. Keung, *Alcoholism: Clin. Exp. Res.* **17** (1993) 1254
- Y. C. Chang, M. G. Nair, R. C. Santell, W. G. Helferich, *J. Agr. Food Chem.* **42** (1994) 1869
- W. H. Tolleson, D. R. Doerge, M. I. Churchwell, M. M. Marques, D. W. Roberts, *J. Agr. Food Chem.* **50** (2002) 4783.



Structural effects of the monomer type on the properties of copolyimides and copolyimide–silica hybrid materials

CANAN KIZILKAYA, MERVE BICEN, SEVİM KARATAS and ATILLA GUNGOR*

Marmara University, Faculty of Science and Letters, Department of Chemistry,
34722, Istanbul, Turkey

(Received 14 October 2014, revised 26 February, accepted 19 March 2015)

Abstract: In this work, the effects of two different diamine monomers containing phosphine oxide on the thermal, mechanical and morphological properties of copolyimides and their hybrid materials were investigated. The gas separation properties of the synthesized copolyimides were also analyzed. The two different diamine monomers containing phosphine oxide were bis(3-aminophenyl)phenylphosphine oxide (BAPO) and bis[4-(3-aminophenoxy)phenyl]phenylphosphine oxide (*m*-BAPO). In the synthesis of the copolyimides, 3,3'-diaminodiphenyl sulfone (3,3'-DDS) was also used as the diamine, as well as 2,2-bis(3,4-dicarboxyphenyl)hexafluoropropane dianhydride (6FDA). Copolyimide films were prepared by thermal imidization. Furthermore, hybrid materials containing 5 % SiO₂ were synthesized by the sol–gel technique. Fourier-transform infrared spectroscopy (FTIR) and nuclear magnetic resonance spectroscopy (NMR) confirmed the expected structures. Dynamic mechanical analysis (DMA) demonstrated that the *m*-BAPO-based copolyimides had lower glass transition temperatures (T_g) than the BAPO-based ones. The thermal decomposition temperature of the *m*-BAPO-containing copolyimide without silica was shifted to a higher value. The moduli and strength values of the BAPO diamine-containing copolyimide and its hybrid were higher than those of the *m*-BAPO-containing materials. Contact angle measurements showed their hydrophobicity. Scanning electron microscope (SEM) analysis showed the dispersion of the silica particles in the copolyimides. These copolyimides may be used in the coating industry. The CO₂ permeability and the perm-selectivity were the highest, among the other values found in this study, when the *m*-BAPO-containing copolyimide in the absence of silica was used. The gas permeabilities obtained from this work were in the decreasing order: $P_{\text{CO}_2} > P_{\text{O}_2} > P_{\text{N}_2}$.

Keywords: copolyamic acid; inorganic compound; sol–gel; imidization; hydrophobic nature; permeation.

*Corresponding author. E-mail: atillag_1@yahoo.com
doi: 10.2298/JSC141014029K

INTRODUCTION

Polyimides (PIs) exhibit outstanding characteristics such as high tensile modulus, high thermal stability and solvent resistance. They find applications ranging from aerospace,¹ microelectronic devices, and the coating industry to separation membrane technologies.²

The thermal and mechanical properties of PIs can be further improved by the introduction of silica into the PI matrix, forming hybrid organic–inorganic materials. These materials can be prepared utilizing the sol–gel process to form silica in a polyamic acid solution. Films are formed from the solution by solvent casting.³ The silica nanoparticles are formed in the PI matrix *via* hydrolysis and polycondensation of organic silanes.⁴

The unique characteristics of fluorine, such as high electronegativity, low polarity, low cohesive and surface free energy, gave rise to attempts to fluorinate PIs in 1972. Since then, fluorine-containing diamines and dianhydrides have been introduced to prepare fluorinated PIs. However, fluorinated PIs have drawbacks, such as poor adhesion and low mechanical strength. Phosphine oxide-containing polyimides, which show excellent adhesive properties with excellent thermal stability, enabled fluorinated PIs to exhibit improved properties.⁵ Much research has been performed on PIs to investigate the relationship between chemical structure and gas transport properties. 2,2-Bis(3,4-dicarboxyphenyl)hexafluoropropane dianhydride (6FDA)-based PIs show high gas permeability. The presence of the bulky $-\text{C}(\text{CF}_3)_2-$ group provides restricted intrasegmental mobility and stiffened backbones. Moreover, some of 6FDA-based PIs were employed to fabricate high performance membranes.⁶

In the present work, the effects of two different diamine monomers containing phosphine oxide on the thermal, mechanical and morphological properties of copolyimides and their hybrid materials were investigated. The gas separation properties of the synthesized copolyimides were also analyzed. The two diamine monomers with phosphine oxide were bis(3-aminophenyl)phenylphosphine oxide (BAPO) and bis[4-(3-aminophenoxy)phenyl]phenylphosphine oxide (*m*-BAPO). In the synthesis of the copolyimides, 3,3'-diaminodiphenyl sulfone (3,3'-DDS) was also used as the diamine, as well as 2,2-bis(3,4-dicarboxyphenyl)hexafluoropropane dianhydride (6FDA). Copolyimide films were prepared by thermal imidization. Furthermore, hybrid materials containing 5 % SiO_2 were synthesized by the sol–gel technique.

EXPERIMENTAL

Materials

The dianhydride monomer, 2,2-bis(3,4-dicarboxyphenyl)hexafluoropropane dianhydride (6FDA, >99 %) was purchased from Aldrich and used as received. 3,3'-Diaminodiphenyl sulfone (3,3'-DDS), phenylphosphonic dichloride (98 %), *N*-methyl-2-pyrrolidone (NMP) and dimethylacetamide (DMAc) were obtained from Merck. NMP and DMAc were dried over

phosphorus pentoxide (P_2O_5) and freshly distilled under vacuum before use. 1-Bromo-4-fluorobenzene (99 %), Mg powder (99.9 %), anhydrous potassium carbonate (K_2CO_3 , 99.9 %) and 3-aminophenol were provided by Aldrich and used as received. Tetrahydrofuran (THF) was freshly distilled under nitrogen over sodium. Tetraethyl orthosilicate (TEOS) and 3-(glycidyloxy)propyltrimethoxysilane (GPTMS) were purchased from Merck. Some common solvents, such as chloroform, ethanol, methanol and dichloroethane, were used as received.

Synthesis of diamine monomers

In this study, two different diamine monomers (BAPPO and *m*-BAPPO) were synthesized. Bis(3-aminophenyl)phenylphosphine oxide (BAPPO) was synthesized by a three-step reaction as mentioned in the previous work.⁷ First, triphenylphosphine (TPP) was oxidized to triphenylphosphine oxide (TPPO) by treating with H_2O_2 . Then, bis(3-nitrophenyl)phenylphosphine oxide (BNPPO) was prepared by the nitration of TPPO using concentrated nitric acid in the presence of sulfuric acid. Finally, BNPPO was subjected to hydrogenation in a high-pressure reactor (Parr Instrument Co.) to produce BAPPO.

Bis[4-(3-aminophenoxy)phenyl]phenylphosphine oxide (*m*-BAPPO) was synthesized as described in the literature.⁸ First, bis(4-fluorophenyl)phenylphosphine oxide (BFPPO) was synthesized by treating 1-bromo-4-fluorobenzene with phenylphosphonic dichloride in the presence of Mg turnings *via* the Grignard technique. Then, *m*-BAPPO (Scheme S-1 of the Supplementary material to this paper) was prepared by treating 37.23 g (0.118 mol) BFPPO with 26.56 g (0.243 mol) 3-aminophenol in a DMAc/toluene mixture using 40.20 g (0.292 mol) K_2CO_3 as a weak base to form the required aminophenolate nucleophile.

Preparation of copolyamic acid solution

The copolyamic acid solution (PAA) used as a copolyimide precursor was prepared in NMP as follows: the diamine monomers and dried NMP were charged into a three-necked flask equipped with a nitrogen inlet and a condenser. Then, equimolar amount of the dianhydride monomers were incrementally added into the content of the flask. The concentration afforded was 20 %. The reaction mixture was stirred overnight at room temperature to obtain a viscous PAA solution.

In this study, 6FDA-based copolyimides were synthesized from the aromatic diamines 3,3'-DDS, BAPPO and *m*-BAPPO.

Silica sol preparation

Silica sol was prepared by the hydrolysis and condensation of TEOS as follows: TEOS (8.7 g, 0.042 mol), GPTMS (2.25 g, 0.010 mol) and EtOH (2.21 g, 0.048 mol) were charged into a glass vial and then distilled water (1.77 g, 0.098 mol) that had been acidified by adding HCl was slowly dropped into the vial. The mixture was magnetically stirred at room temperature until a clear solution was obtained. Then, the silica sol was kept at room temperature for about 1 h.

Preparation of copolyimide–silica hybrid materials

To obtain the hybrid solution, 5 % silica sol was added dropwise into a PAA solution and stirred continuously at room temperature for 4 h. This preparation procedure is illustrated in Scheme S-2 of the Supplementary material. After thorough stirring, the clear and viscous hybrid solutions were cast onto glass plates using a 30- μ m wire gaged applicator and then thermal imidization was performed stepwise at 80, 100, 150, 200 and 300 °C for 1 h at each temperature. After the imidization was completed, the glass plates were immersed in hot water (90 °C) for 1 h to remove easily the hybrid films from the glass surfaces.

Characterization

The FTIR spectra were recorded on a PerkinElmer Spectrum 100 ATR FTIR spectrophotometer. The NMR spectra were recorded on a Varian 600 MHz spectrometer operating for ^1H -NMR and ^{31}P -NMR using CDCl_3 as the solvent. Thermogravimetric analyses (TGA) of the hybrid free films were performed using a Perkin Elmer thermogravimetric analyzer Pyris 1 TGA model. Samples were run from 30 °C to 750 °C at a heating rate of 10 °C min $^{-1}$ under an air atmosphere. The glass transition temperatures of free films prepared as 10 mm×20 mm samples were obtained from an SII Nanotechnology ExStar 6000 model dynamic mechanical analyzer (DMA). The scans were obtained at a heating rate of 5 °C min $^{-1}$, from 30 to 450 °C. The limiting oxygen index (*LOI*) values of the free hybrid films were measured using a fire testing technology (FTT) type instrument according to ASTM D2863-08. The mechanical properties of the free films were determined by standard tensile stress-strain tests in order to measure the moduli, tensile strength, and elongation at break. Standard tensile stress-strain experiments were performed at room temperature on a Material Testing Machine Z010/TN2S, using a crosshead speed of 5 mm min $^{-1}$. In order to determine the hydrophobic properties of the materials, contact angle measurements were performed with a Kruss (Easy Drop DSA-2) tensiometer, equipped with a camera. Analyses were made at room temperature by means of the sessile drop technique. For each sample, at least four measurements were made, and the average was taken. The measuring liquid was distilled water. To determine the morphological behavior, secondary electron images (SEI) were applied in SEMs. SEM imaging of the films were performed on a Philips XL30 ESEM-FEG/EDAX. The specimens were prepared for SEM by freeze fracturing in liquid nitrogen and applying a gold coating of approximately 300 Å. An SEM-energy-dispersive X-ray spectroscopy (SEM-EDS) spectrum was recorded to verify the presence of silica in the copolyimide–silica hybrid. In addition, a gas permeation analyzer (Brugger GDP-C 2000) was used to measure the pure gas permeability coefficients of the polymeric membranes to O₂, N₂, and CO₂. The pure gas permeability coefficients were measured using the constant volume and variable pressure method. The experiments were performed at 35 °C with atmospheric feed-side pressure. The samples were masked for gas permeation measurement following the technique of the Koros group⁹ with a permeation area of 3.94 cm 2 .

RESULTS AND DISCUSSION

The aim of this study was to investigate the effect of diamine monomers containing phosphine oxide on the thermal, mechanical and morphological properties of copolyimides and their hybrid materials, as well as the gas separation properties. Two different diamine monomers were synthesized (BAPPO and *m*-BAPPO). The BAPPO monomer was synthesized according to a previous study.⁷ The synthesis route for the other monomer (*m*-BAPPO) is illustrated in Scheme S-1 of the Supplementary material. The chemical structure of *m*-BAPPO was identified by FTIR, ^1H -NMR and ^{31}P -NMR spectroscopy.

The FTIR results for *m*-BAPPO (shown in Fig. S-1 of the Supplementary material) displayed aromatic C–H stretching at 3058 cm $^{-1}$, C–H out-of-plane bending at 830 cm $^{-1}$, C–H in-plane bending at 1143 and 1115 cm $^{-1}$, aromatic C–C stretching at 1577 and 1486 cm $^{-1}$, asymmetric C–O–C stretching at 1232

cm^{-1} , P=O stretching at 1170 cm^{-1} , P–aryl stretching at 1436 and 996 cm^{-1} , N–H stretching at $3445, 3324$ and 1594 cm^{-1} , and C–N stretching at 1283 cm^{-1} .

In the $^1\text{H-NMR}$ spectrum (Fig. S-2 of the Supplementary material) of *m*-BAPPO, proton peaks arising from the ether and amino groups were observed up-field because of the shielding effects of the electron-donating ether and amino moieties. As could be seen in Fig. S-2, the protons in the amino groups appeared at 3.4 – 3.8 ppm as a broad peak. In addition, the other proton peaks of *m*-BAPPO were: 7.71 – 7.40 ppm (5H , *m*, O=P–C₆H₅), 6.80 – 7.20 ppm (4H , *m*, O=P–C₆H₄–O–), 6.60 – 6.37 ppm (4H , *m*, –O–C₆H₄–NH₂). As shown in Fig. S-3 of the Supplementary material, the $^{31}\text{P-NMR}$ analysis provided a sharp single peak at 29 ppm for *m*-BAPPO.

In this study, BAPPO–3,3'-DDS/6FDA, *m*-BAPPO–3,3'-DDS/6FDA copolyimides and their hybrids were prepared. The hybrid materials containing the polyamic acid (PAA) solution and silica sol, which was obtained in a sol–gel reaction, were synthesized. TEOS and GPTMS acted as an inorganic networker and a coupling agent, respectively. In addition, HCl acid acted as the acid catalyst for the partial hydrolysis. The compositions of the PI–SiO₂ hybrids are presented in Table I. Hybrid formulations applied on glass plates were cured by stepwise heating at elevated temperatures. The chemical structures of the copolyimides and copolyimide–silica hybrids were shown in Scheme S-3a–d of the Supplementary material. The FTIR spectra of the copolyimides and their hybrid copolyimides containing 5 % silica are shown in Fig. S-4a–d of the Supplementary material. As seen in Fig. S-4, characteristic imide absorptions at 1783 and 1720 cm^{-1} (typical of imide carbonyl asymmetrical and symmetrical stretching, respectively) were present. The peaks at 1363 and 718 cm^{-1} indicated C–N–C stretching and imide ring deformation. Moreover, the peaks at 1203 , 1300 and 1100 cm^{-1} were ascribed to C–F multiple stretching bands. As shown in Figs. S-4b and d, when the inorganic components were introduced into the polyimide matrix, strong absorption bands were observed in the range 1000 to 1100 cm^{-1} and at 423 cm^{-1} . These bands were ascribed to the characteristic Si–O–Si stretching vibration and bending vibration, respectively.^{10,11} The spectra given in Fig.

TABLE I. The composition (mass, g) of copolyimide–silica hybrid films; the PAA solution was 20 wt. %. The PAA solution used in the experiment was 3 g PAA/15 mL solvent. This means that the PAA in solid form was 3 g after removal of the solvent; silica mass: 0.15 g of silica sol was added. Therefore, the silica solution used in the experiment was 0.15 g silica/3 mL solution (5 wt. %); 6FDA mass: 1.777 g; 3,3'-DDS mass: 0.4966 g

Sample	BAPPO	<i>m</i> -BAPPO	Silica sol used
BAPPO–3,3'-DDS/6FDA	0.6160	0	0
<i>m</i> -BAPPO–3,3'-DDS/6FDA	0	0.9850	0
BAPPO–3,3'-DDS/6FDA/SiO ₂	0.6160	0	0.15
<i>m</i> -BAPPO–3,3'-DDS/6FDA/SiO ₂	0	0.9850	0.15

S-4 of the Supplementary material confirmed the formation of the expected structures.

As seen in Tables II and III, thermal properties of the copolyimides and hybrid copolyimides were evaluated by dynamic mechanical analysis (DMA) and thermogravimetric analysis (TGA). The storage modulus (E' , Fig. S-5a–d of the Supplementary material) and $\tan \delta$ (Figs. S-6–S-9 of the Supplementary material) were plotted. The values of the glass transition temperatures of copolyimides and hybrid copolyimides are very important for the determination of the optimum processing and service temperatures at which the polymer preserves its desirable properties.^{12,13} The T_g of the copolyimides increased when silica was introduced into the PI matrix. This result indicated that the coupling agent improved the interaction between the polymer matrix and the inorganic segment, which caused an increased restricting strength of silica on PI and hence an increased T_g of the material. The data were collected by DMA. Due to the flexible etheric linkage of *m*-BAPPO, the obtained T_g values were lower than those of the BAPPO-containing copolyimides and their hybrids. However, BAPPO based copolyimides exhibited higher elongation at break values than those of the *m*-BAPPO-based copolyimides. This result is likely due to the three dimensional geometry of the monomers (BAPPO and *m*-BAPPO). The monomer BAPPO alone is a tetrahedral structure so that the aminophenyl groups are in approximately 110° tetrahedral geometry. Therefore, the amino groups can be in different directions when reacted with the dianhydride. The obtained copolyimide might be an asymmetric structure. On the other hand, the obtained copolyimide might be a symmetric structure (more symmetric than the BAPPO-based one) when the *m*-BAPPO moiety reacted with the dianhydride. The aminophenyl groups of the monomer *m*-BAPPO are in trigonal (approximately 120°) geometry, due to the etheric linkages. Trigonal structures are more symmetric than tetrahedral systems. When the asymmetry exists throughout the molecular structure, the asymmetric structure shows greater elasticity (greater elongation at break). Easier molecular packing properties can be observed in the presence of symmetric structures. Two or three T_g values were obtained due to small amounts of phase separation. This might have been possible, since the reactivities of the diamines (BAPPO, *m*-BAPPO and 3,3'-DDS) are different when they react with the dianhydride (6FDA). The introduction of the inorganic material can also cause phase separation due to differences in the reactivity.

TABLE II. Glass transition temperatures of the copolyimides and hybrid copolyimides

Sample	T_1 / °C	T_2 / °C	T_3 / °C
BAPPO–3,3'-DDS/6FDA	218	272	301
<i>m</i> -BAPPO–3,3'-DDS/6FDA	209	245	–
BAPPO–3,3'-DDS/6FDA/SiO ₂	217	274	323
<i>m</i> -BAPPO–3,3'-DDS/6FDA/SiO ₂	220	257	–

TABLE III. Thermal properties of the copolyimides and hybrid copolyimides

Sample	1 st decomposition temperature, T_1 / °C	2 nd decomposition temperature, T_2 / °C	Char wt. %	LOI wt. %
BAPO-3,3'-DDS/6FDA	319	523	20	46.0
<i>m</i> -BAPO-3,3'-DDS/6FDA	310	537	28	48.0
BAPO-3,3'-DDS/6FDA/SiO ₂	350	525	15	46.7
<i>m</i> -BAPO-3,3'-DDS/6FDA/SiO ₂	330	509	7	47.4

The thermal degradation behaviors of the copolyimides and hybrid copolyimides are summarized in Table III. The polymers exhibited first weight loss at temperatures between 310 and 350 °C, which could probably be attributed to incomplete imidization. The second weight loss started between 509 and 537 °C, which corresponded to the degradation of the polymer. The incorporation of silica into the polyimide matrix may cause the production of SiF_{4(g)} in the presence of -CF₃- present in the 6FDA moiety.¹⁴ The char yields of the copolyimide silica hybrid materials between 7–28 % were found. The thermal decomposition temperature of the hybrids shifted to lower values because of the removal of silica as SiF_{4(g)}. It was found that the thermal decomposition temperature of the *m*-BAPO-containing copolyimide without silica was shifted to a higher value, increasing the char yield.

Moreover, the flame retardant properties of the copolyimide and hybrid copolyimide films were evaluated by measuring their limiting oxygen index (LOI) values. From Table III, it can be seen that the LOI values for the copolyimides were changed only slightly on addition of the silica particles into the PI matrix.

The tensile properties of copolyimide films were examined by stress-strain measurements and the results were summarized in Table IV. The moduli and the strength values of BAPO diamine-containing copolyimide and its hybrids were higher than those of the *m*-BAPO-containing materials. This situation was explained by higher free volume of *m*-BAPO because of the extra phenyl group that resulted in a lowering of the moduli. In other words, the more space the bulky groups take, the lower are the observed moduli. Compared to the neat copolyimides, a decrease in mechanical properties was observed when silica was introduced into the copolyimide matrix. This result may be due to the increased crosslinking density by the formation of an organic–inorganic network structure.

TABLE IV. Physical and mechanical properties of the copolyimides and hybrid copolyimides

Samples	Modulus, GPa, at 40 °C	Tensile strength, MPa	Elongation at break, %	Contact angle θ / °
BAPO-3,3'-DDS/6FDA	3.54	518	3.92	93
<i>m</i> -BAPO-3,3'-DDS/6FDA	3.12	226	1.62	102
BAPO-3,3'-DDS/6FDA/SiO ₂	3.36	267	3.32	97
<i>m</i> -BAPO-3,3'-DDS/6FDA/SiO ₂	2.95	189	1.98	107

Contact angle measurements provide information about the hydrophobicity and hydrophilicity of a material surface. These measurements were performed with drops of distilled water at four different areas on the sample. The averages of these four measurements were calculated. The obtained contact angle values, for each material were given in Table IV. The contact angles had a tendency to increase on addition of silica, demonstrating a more hydrophobic coating surface. The presence of $-C(CF_3)_2-$ also provided for a more hydrophobic surface.

SEM analysis (Fig. S-10a–d of the Supplementary material) exhibited that the silica particles were dispersed in the copolyimide matrix. A microphase separation was observed in the *m*-BAPPO-containing copolyimide–silica hybrid. SEM–energy-dispersive X-ray spectroscopy (SEM–EDS, Fig. S-10e of the Supplementary material) verified the presence of silica in the copolyimide–silica hybrids.

In addition to the thermal, mechanical and morphological studies, the gas permeability coefficients and permselectivity data measured at 35 °C are reported in Table V. The gas permeabilities and permselectivities can be calculated as follows:

$$P = DS \quad (1)$$

$$\alpha_{A/B} = P_A/P_B \quad (2)$$

where P is the permeability coefficient, D is the diffusion coefficient and S is solubility coefficient. α represents the permselectivities of gases A and B.⁶ The order of the kinetic (\AA) diameters of the studied gases is CO_2 , 3.3; O_2 , 3.46 and N_2 , 3.64. The gas permeabilities from this study were in the decreasing order: $P_{\text{CO}_2} > P_{\text{O}_2} > P_{\text{N}_2}$. Thus, the larger is the kinetic diameter of a gas, the lower is its permeability. As seen in Table V, the *m*-BAPPO-containing copolyimide without silica was better than the others in terms of the permeabilities of O_2 and CO_2 , whereas the BAPPO-containing copolyimide in the presence of silica was better than others for the permeability of N_2 . The introduction of silica increased the volume of the copolymer due to the effect of crosslinking so that the N_2 gas, possessing the largest kinetic diameter, could easily diffuse throughout the

TABLE V. Permeability coefficients and permselectivity of the copolyimides and hybrid copolyimides at 35 °C

Sample	Permeability coefficients			Permselectivities	
	P_{O_2} /barrier	P_{N_2} /barrier	P_{CO_2} /barrier	$a_{\text{O}_2/\text{N}_2}$	$a_{\text{CO}_2/\text{N}_2}$
BAPO–3,3'-DDS/6FDA	0.310	0.046	0.365	6.74	7.93
<i>m</i> -BAPO–3,3'-DDS/6FDA	0.405	0.084	1.137	4.82	13.54
BAPO–3,3'-DDS/6FDA/ SiO_2	0.229	0.104	0.232	2.20	2.23
<i>m</i> -BAPO–3,3'-DDS/ 6FDA/ SiO_2	0.165	0.093	0.366	1.78	3.94

BAPPO-containing hybrid matrix. Due to the increased volumes, the selectivities were adversely affected. The reason is that all gases can pass through without determining their diffusion rates in the presence of large volumes. Since CO₂ is a condensable gas, it should have a higher permeability value than those of the other two gases. It is too difficult to obtain the highest permeability as well as the highest selectivity. As seen in Table V, the permeability and permselectivity of CO₂ were the highest among the values for the copolyimides and copolyimide–silica hybrids in this study, when the *m*-BAPPO containing copolyimide in the absence of silica was used.

CONCLUSIONS

In this study, copolyamic acid solutions (PAAs) were obtained by the reaction between *m*-BAPPO or BAPPO, DDS and 6FDA. Copolyimide films were prepared by thermal (bulk) imidization. Hybrid materials containing 5 % SiO₂ were synthesized by the sol–gel technique. The FTIR, ³¹P-NMR and ¹H-NMR spectra confirmed the expected structures. DMA analysis showed that the *m*-BAPPO-based copolyimides had lower T_g values than those of the BAPPO-based copolyimides. T_g of copolyimides increased when silica was introduced into the copolyimide matrix. Thermal analysis showed that in the presence of silica, the weight loss was shifted to lower temperatures because of the removal of silica as SiF_{4(g)}, compared to the neat copolyimide. However, the thermal stability was sufficiently high compared to that of branched-silica hybrid membranes.¹⁵ The LOI results did not change significantly on addition of silica particles into the matrix. Mechanical tests showed a decrease in mechanical properties on introduction of silica into the copolyimide matrix, compared to the neat copolyimides. This result may be due to the increased crosslinking density caused by the formation of organic–inorganic network structures. However, the moduli of the hybrids could be considered good.¹⁶ Contact angle measurements confirmed the hydrophobic nature of the surface of the coating. SEM analyses confirmed that silica particles are able to disperse in the polyimide matrix. These copolyimides with various properties may be used in the coating industry. In addition to the thermal, mechanical and morphological studies, gas permeability coefficients and permselectivity measurements were also performed. The condensable gas (*i.e.*, CO₂) was observed to have higher permeability value than those of other two examined gases (*i.e.*, N₂ and O₂). This could be explained by the plasticization effect. More soluble penetrants induce significant plasticization. The CO₂ permeability and the selectivity were the highest among the values of copolyimides and copolyimide–silica hybrids in this study when the *m*-BAPPO-containing copolyimide in the absence of silica was used. The gas permeabilities obtained from this work were in the decreasing order: $P_{CO_2} > P_{O_2} > P_{N_2}$.

SUPPLEMENTARY MATERIAL

FTIR, ^1H -NMR and ^{31}P -NMR spectra, SEM images, storage moduli and $\tan \delta$ values, as well as the synthesis routes and structures of the samples, are available electronically from <http://www.shd.org.rs/JSCS/>, or from the corresponding author on request.

ИЗВОД

УТИЦАЈ СТРУКТУРЕ МОНОМЕРА НА СВОЈСТВА КОПОЛИИМИДА И
КОПОЛИИМИД/СИЛИЦИЈУМ-ДИОКСИД ХИБРИДНИХ МАТЕРИЈАЛА

CANAN KIZILKAYA, MERVE BICEN, SEVİM KARATAS и ATILLA GUNGOR

Marmara University, Faculty of Science and Letters, Department of Chemistry, 34722, Istanbul, Turkey

У овом раду је приказан утицај структуре мономера, тј. два различита диамина на бази фосфорин-оксида, на термичка, механичка и морфолошка својства синтетисаних кополиимида и њихових хибридних материјала. Поред тога, анализирана је способност синтетисаних кополиимида за раздвајање гасова. Два различита мономера односно диамина на бази фосфор-оксида су коришћена: бис(3-аминофенил)фенилфосфин-оксид (BAPPO) и бис[4-(3-аминофенокси)фенил]фенилфосфорин-оксид (*m*-BAPPO). У синтезама кополиимида 3,3'-диаминодифенил-сулфон (3,3'-DDS) је коришћен као диамин, а такође и 2,2-бис(3,4-дикарбоксифенил)хексафлуорпропан-дианхидрид (6FDA). Кополиимидни филмови су добијени термичком имидизацијом у другом ступњу реакције поликондензације. Хибридни материјали са 5 % SiO_2 су синтетисани користећи сол-гел поступак. Структура синтетисаних кополиимида је потврђена FTIR и NMR спектроскопијом. Динамичка механичка анализа (DMA) је показала да кополииимиди на бази *m*-BAPPO имају ниже температуре остакљивања (T_g) у односу на BAPPO кополиимиде. *m*-BAPPO кополииимиди без SiO_2 испољавају бољу термичку стабилност. Модули и затезна чврстоћа кополиимида на бази BAPPO диамина као и њихових хибридних материјала била је већа у односу на *m*-BAPPO аналогне материјале. Мерења контактних углова су потврдила хидрофобност њихове површине. Скенирајућа електронска микроскопија (SEM) је показала диспергованост силицијум-диоксидних честица у кополиимидној матрици. Синтетисани кополиимидни материјали могу се потенцијално користити у индустрији премаза. Највећу пропустљивост према CO_2 и највећу селективну пропустљивост према гасовима је показао кополиимид на бази *m*-BAPPO без присуства честица SiO_2 . Пропустљивост према гасовима материјала, приказаних у овом раду, следила је опадајући тренд: $P_{\text{CO}_2} > P_{\text{O}_2} > P_{\text{N}_2}$.

(Примљено 14. октобра 2014, ревидирано 26. фебруара, прихваћено 19. марта 2015)

REFERENCES

1. . Y. K. Yang, W. J. Koros, H. B. Hopfenberg, V. T. Stannet, *J. Appl. Polym. Sci.* **31** (1986) 1619
2. D. Hofman, J. Ulbrich, D. Fritsch, D. Paul, *Polymer* **37** (1996) 4773
3. C. Joly, S. Goizet, J. C. Schrotter, J. Sanchez, M. Escoubes, *J. Membr. Sci.* **130** (1997) 63
4. Y. W. Wang, C. T. Yen, W. C. Chen, *Polymer* **46** (2005) 6959
5. K. U. Jeong, J. J. Kim, T. H. Yoon, *Polymer* **42** (2001) 6019
6. L. Wang, Y. Cao, M. Zhou, S. J. Zhou, Q. Yuan, *J. Membr. Sci.* **305** (2007) 338
7. C. Kizilkaya, S. Karataş, N. K. Apohan, A. Güngör, *J. Appl. Polym. Sci.* **115** (2009) 3256
8. A. Gungor, C. Smith, J. M. Wescott, S. Srinivasan, J. E. McGrath, *Polym. Prepr. (Am. Chem. Soc., Div. Polym. Chem.)* **32** (1991) 172
9. T. T. Moore, S. Damle, P. Williams, W. J. Koros, *J. Membr. Sci.* **245** (2004) 227

10. X. Fang, Z. Wang, Z. Yang, L. Gao, Q. Li, M. Ding, *Polymer* **44** (2003) 2641
11. S. Xiao, X. Feng, Y. Robert, M. Huang, *Macromol. Chem. Phys.* **208** (2007) 2665
12. A. Y. Ardashnikov, I. Y. Kardash, A. N. Pravednikov, *Polym. Sci. USSR* **13** (1971) 2092
13. W. Volksen, P. M. Cotts, in *Polyimides: Synthesis, Characterization and Applications*, Vol. 1, K. L. Mittal, Ed., Plenum, New York, 1984, p. 163
14. C. Hibshman, C. J. Cornelius, E. Marand, *J. Membr. Sci.* **211** (2003) 25
15. M. Miki, T. Suzuki, Y. Yamada, *J. Appl. Polym. Sci.* **130** (2013) 54
16. A. C. Lua, Y. Shen, *Chem. Eng. J.* **20** (2013) 441.



SUPPLEMENTARY MATERIAL TO
**Structural effects of the monomer type on the properties of
copolyimides and copolyimide–silica hybrid materials**

CANAN KIZILKAYA, MERVE BICEN, SEVİM KARATAS and ATILLA GUNGOR*

*Marmara University, Faculty of Science and Letters, Department of Chemistry,
34722, Istanbul, Turkey*

J. Serb. Chem. Soc. 80 (8) (2015) 1061–1071

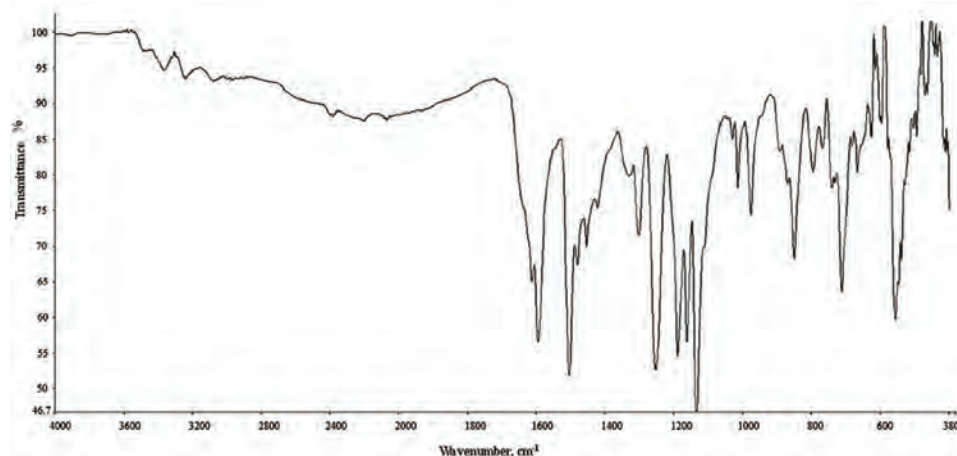


Fig. S-1. FTIR spectrum of bis[4-(3-aminophenoxy)phenyl]phenylphosphine oxide (m-BAPPO).

*Corresponding author. E-mail: atillag_1@yahoo.com

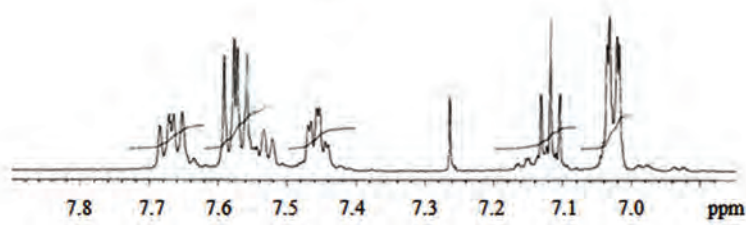
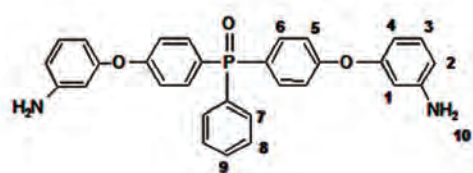
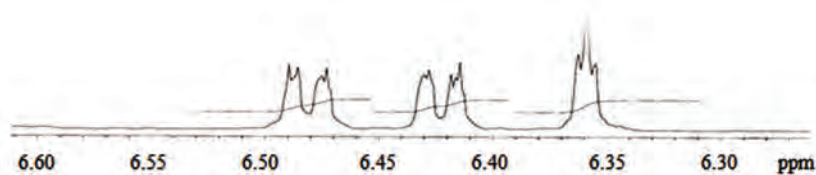


Fig. S-2. ¹H-NMR spectrum of bis[4-(3-aminophenoxy)phenyl]phenylphosphine oxide (*m*-BAPPO).

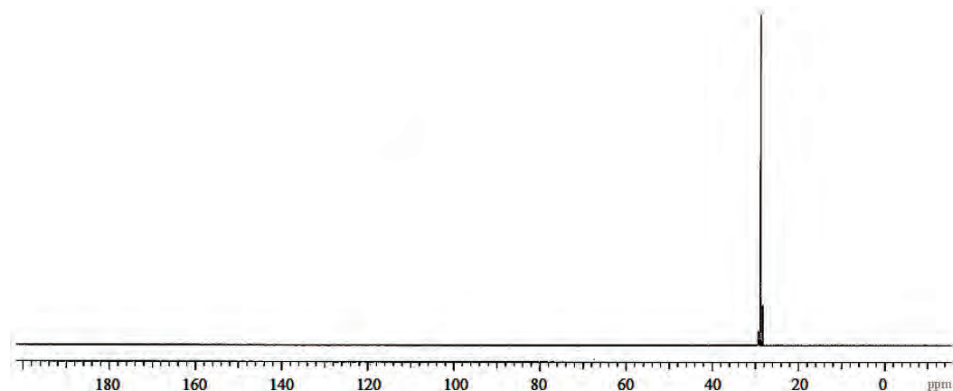


Fig. S-3. ³¹P-NMR spectrum of bis[4-(3-aminophenoxy)phenyl]phenylphosphine oxide (*m*-BAPPO).

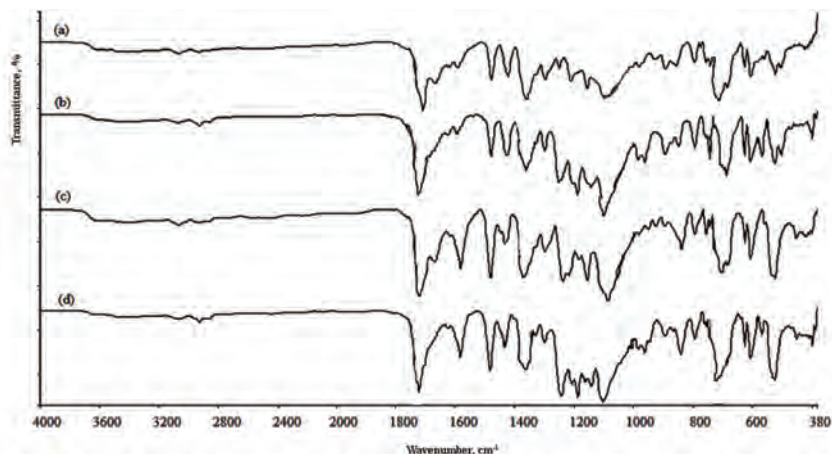


Fig. S-4. FTIR spectrum of: a) BAPOO-3,3'-DDS/6FDA copolyimide; b) BAPOO-3,3'-DDS/6FDA/SiO₂ hybrid copolyimide; c) *m*-BAPOO-3,3'-DDS/6FDA copolyimide; d) *m*-BAPOO-3,3'-DDS/6FDA/SiO₂ hybrid copolyimide.

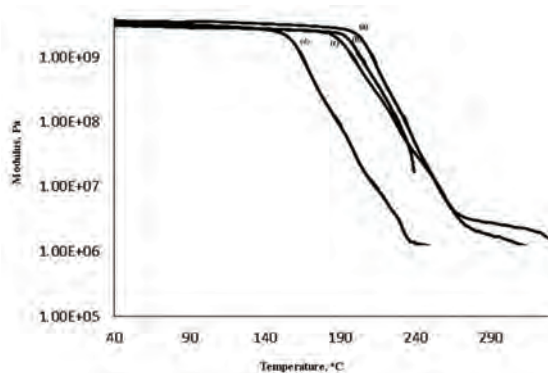


Fig. S-5. Storage (E') modulus of: a) BAPOO-3,3'-DDS/6FDA copolyimide; b) BAPOO-3,3'-DDS/6FDA/SiO₂ hybrid copolyimide; c) *m*-BAPOO-3,3'-DDS/6FDA copolyimide; d) *m*-BAPOO-3,3'-DDS/6FDA/SiO₂ hybrid copolyimide as functions of temperature.

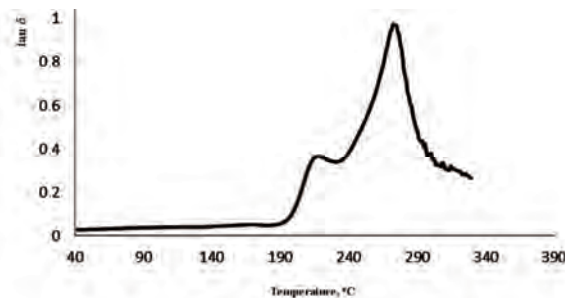


Fig. S-6. The tan δ values of the BAPOO-3,3'-DDS/6FDA copolyimide as a function of temperature.

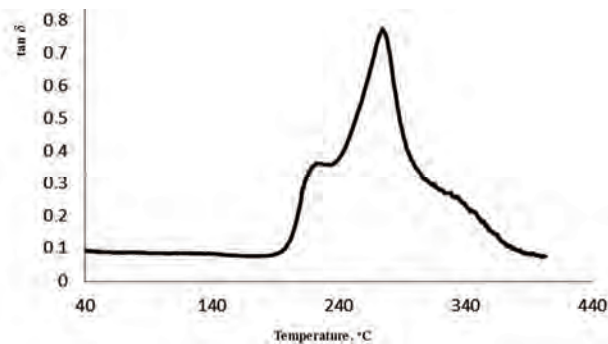


Fig. S-7. The $\tan \delta$ values of the BAPO-3,3'-DDS/6FDA/SiO₂ hybrid copolyimide as a function of temperature.

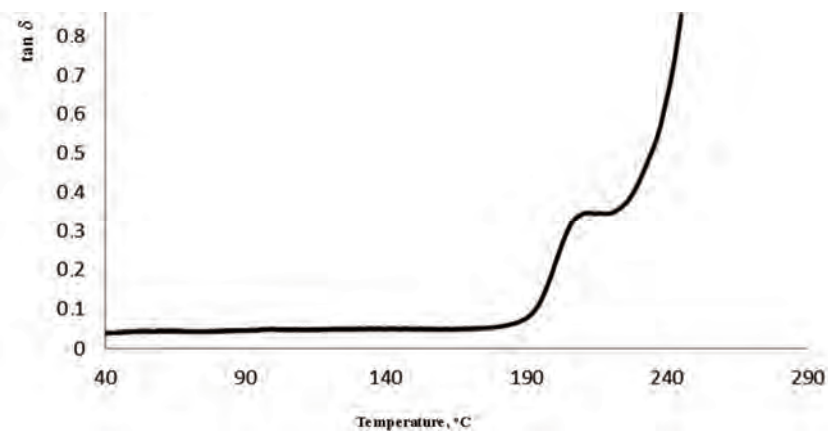


Fig. S-8. The $\tan \delta$ values of the *m*-BAPO-3,3'-DDS/6FDA copolyimide as a function of temperature.

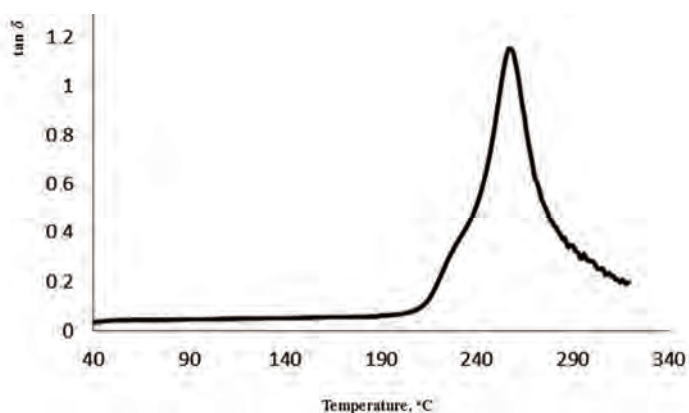


Fig. S-9. The $\tan \delta$ values of the *m*-BAPO-3,3'-DDS/6FDA/SiO₂ hybrid copolyimide as a function of temperature.

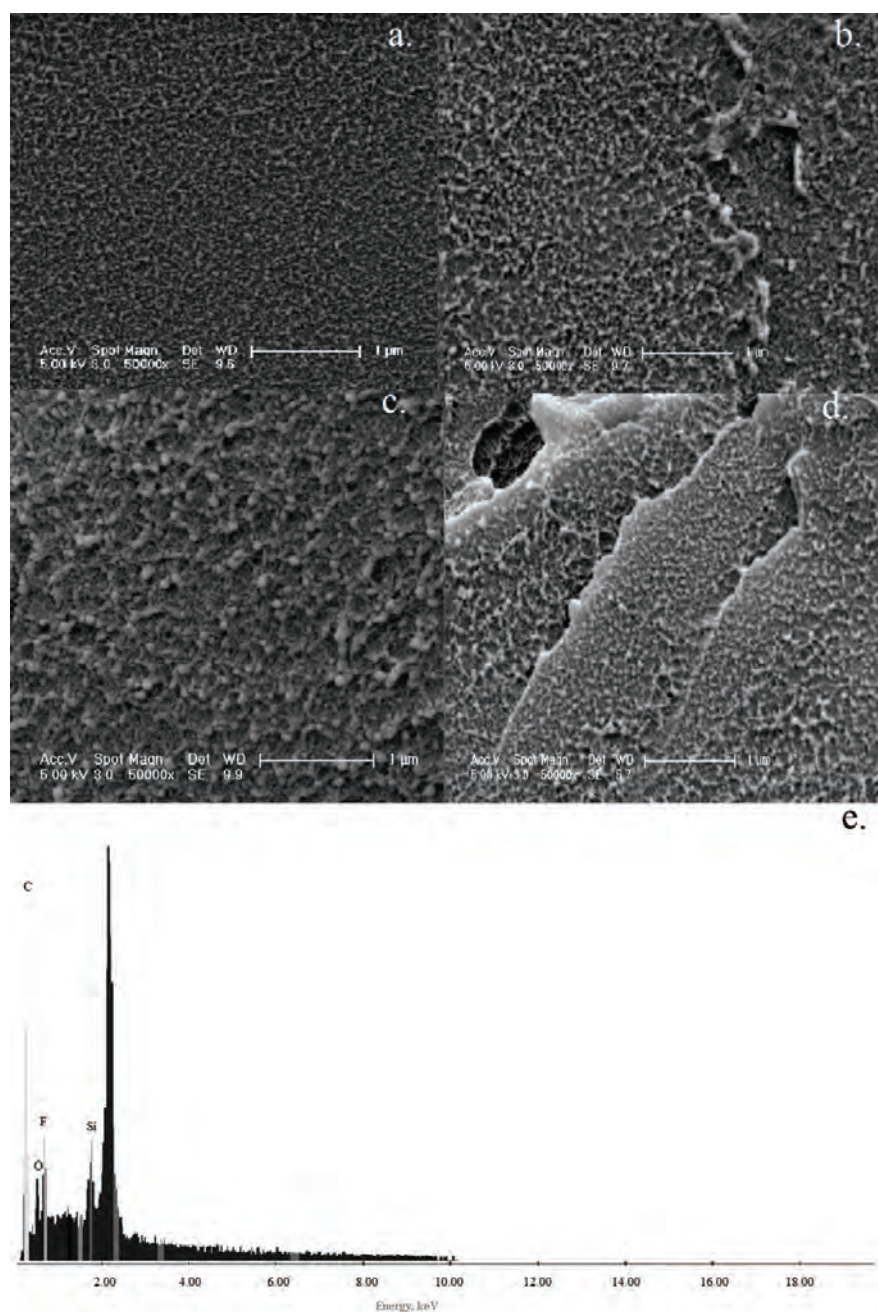
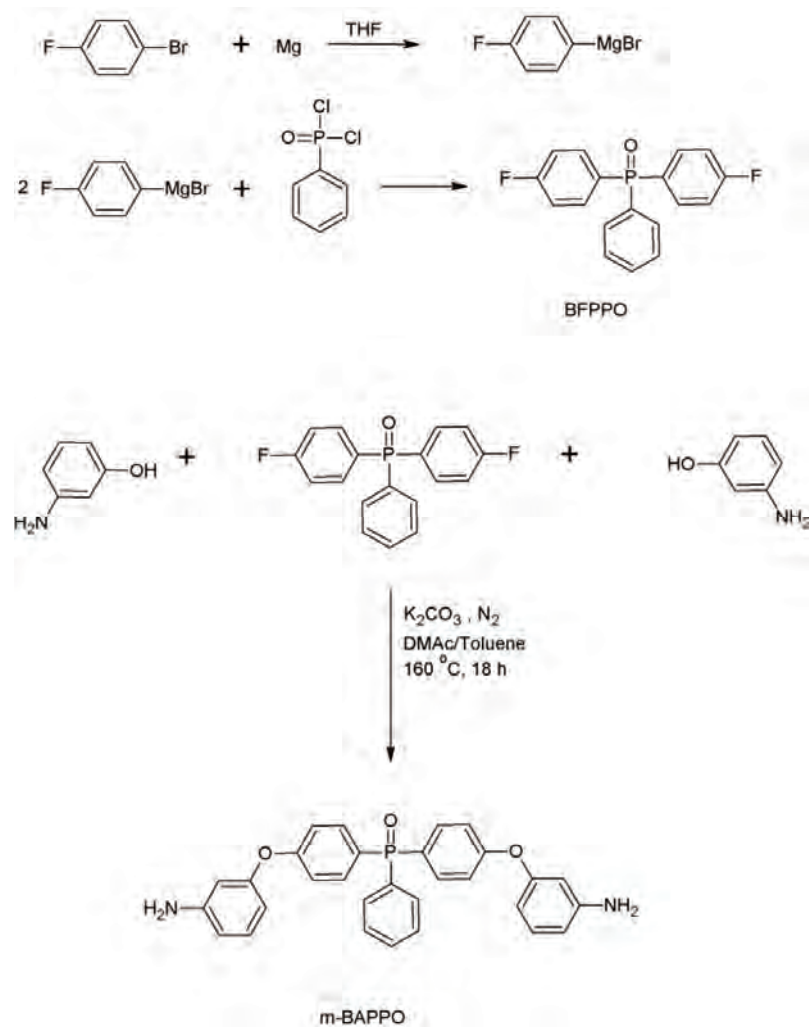
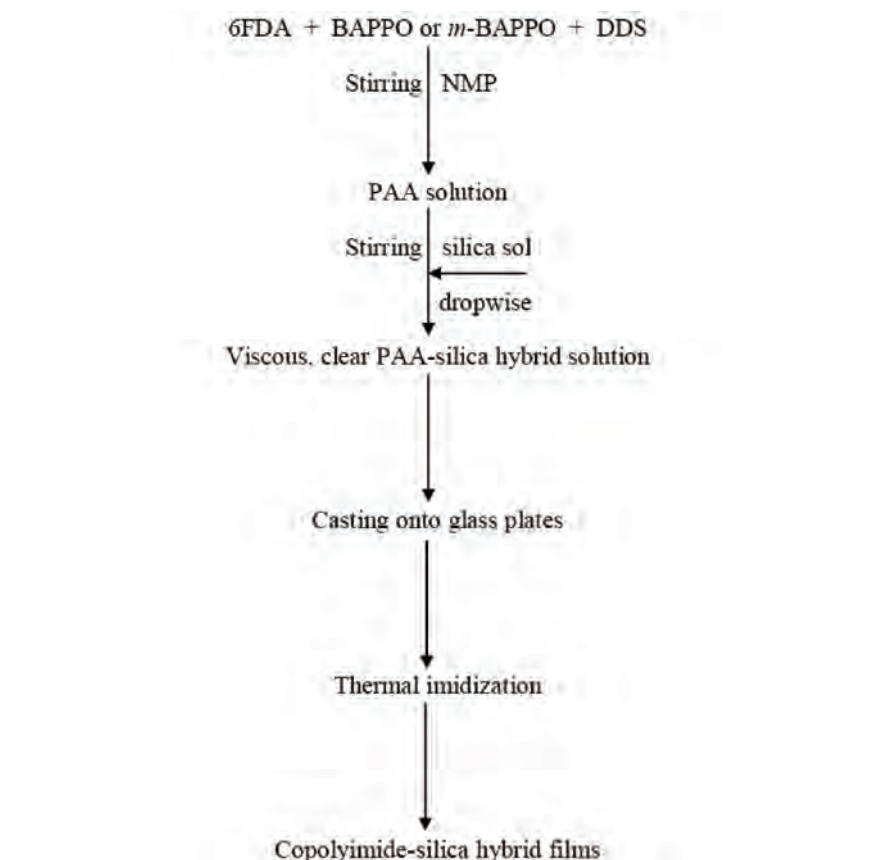


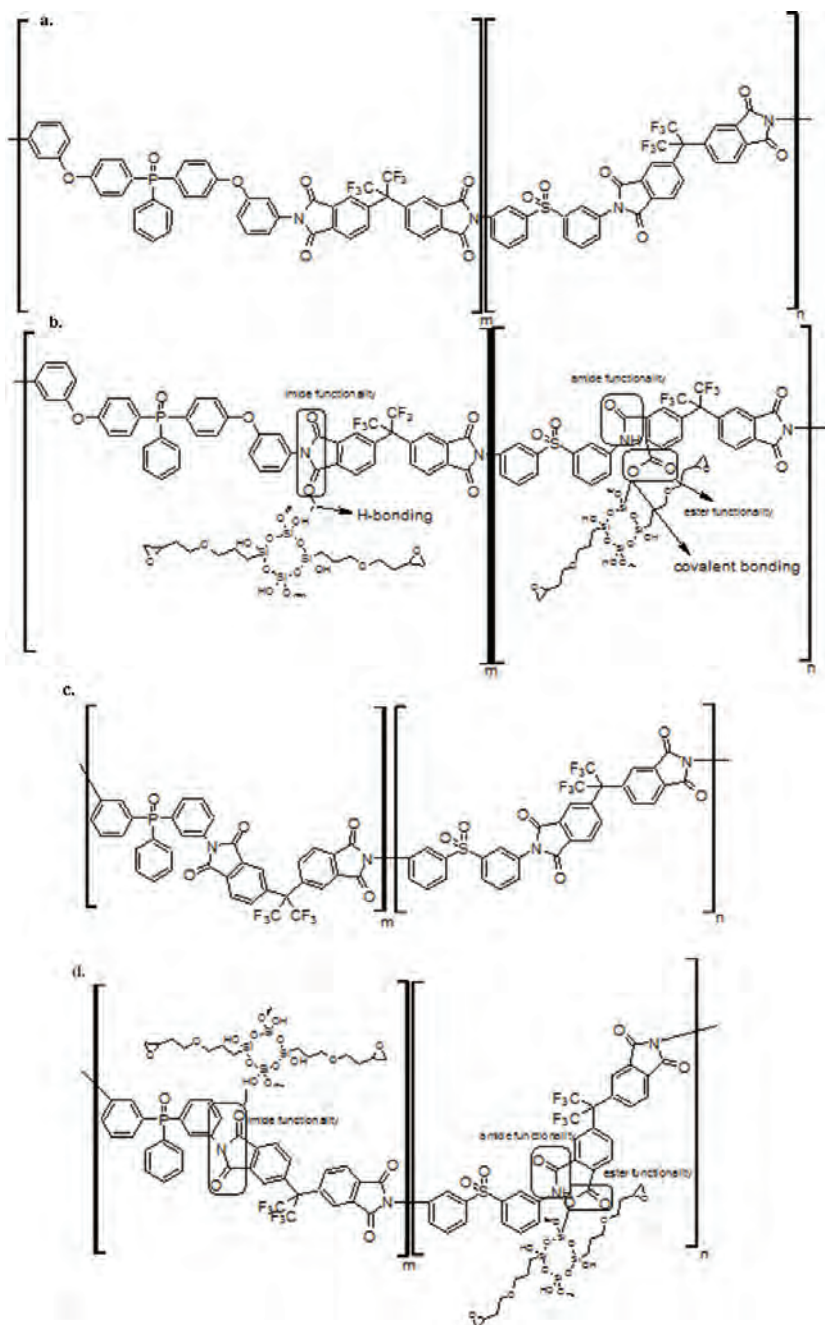
Fig. S-10. SEM image of: a) BAPOO-3,3'-DDS/6FDA copolyimide; b) *m*-BAPOO-3,3'-DDS/6FDA copolyimide; c) BAPOO-3,3'-DDS/6FDA/SiO₂ hybrid copolyimide; d) *m*-BAPOO-3,3'-DDS/6FDA/SiO₂ hybrid copolyimide; e) SEM-EDS image of BAPOO-3,3'-DDS/6FDA/SiO₂ hybrid copolyimide.



Scheme S-1. The synthesis route to bis[4-(3-aminophenoxy)phenyl]phenylphosphine oxide (*m*-BAPPO).



Scheme S-2. Preparation of copolyimide–silica hybrid films (DSS denotes 3,3'-DSS).



Scheme S-3. a and c) The chemical structure of the copolyimides; b and d) the chemical structure of the copolyimide-silica hybrids.



An apparatus proposed for density measurements in compressed liquid regions at pressures of 0.1–60 MPa and temperatures of 288.15–413.15 K

GORICA R. IVANIŠ[#], ALEKSANDAR Ž. TASIĆ*, IVONA R. RADOVIĆ[#], BOJAN D. DJORDJEVIĆ[#], SLOBODAN P. ŠERBANOVIĆ[#] and MIRJANA Lj. KIJEVČANIN[#]

Faculty of Technology and Metallurgy, University of Belgrade, Karnegijeva 4,
11120 Belgrade, Serbia

(Received 27 November 2014, revised 16 March, accepted 17 March 2015)

Abstract: In this work, an apparatus for density measurements in the compressed liquid regions is presented. This installation is based on the use of a DMA HP density measuring cell and a DMA 5000 densimeter (both instruments are products of Anton Paar, Gratz, Austria). Calibration of the DMA HP cell was performed by applying the classical method in which a vacuum, water and *n*-decane were recommended to be used as calibration fluids. To test the capabilities of the set-up, the densities of *n*-hexane, toluene and dichloromethane were measured in the temperature interval 288.15 to 413.15 K and the pressure range 0.1–60 MPa. The obtained results were compared with the corresponding values found in the literature. Depending on the literature selected for comparison (the temperature and pressure ranges available), the average absolute percentage deviations were for *n*-hexane, 0.03–0.10 %; for toluene, 0.04–0.08 % and for dichloromethane, 0.02–0.03 %. A deeper insight into the results of this work showed that most of them were in good agreement with the literature values; higher discrepancies were evidenced in the vicinity of the ends of the temperature and pressure ranges.

Keywords: high pressure; elevated temperature; density; *n*-hexane; toluene; dichloromethane.

INTRODUCTION

It is well known that density represents one of the most important properties of fluids, from both the theoretical and practical points of view.

Namely, accurate density data can help to clarify molecular structure of pure liquid substances and of their mixtures at defined temperatures, pressures and composition. Some essential liquid properties that can be derived from density

* Corresponding author. E-mail: tasic33@gmail.com

[#] Serbian Chemical Society member.

doi: 10.2298/JSC141127026I

measurements are thermomechanical coefficients, such as the isothermal compressibility, κ_T , and the isobaric thermal expansion coefficient, α_p . Based on these properties, the internal pressure, important for studying attractive and repulsive forces present in liquids, can also be determined. By coupling the mentioned isothermal and isobaric properties, κ_T and α_p , and by using the isentropic compressibility κ_S (that is related to the thermodynamic speed of sound), some additional properties can be calculated; in this respect, the isobaric heat capacity and the difference in the isobaric and isothermal heat capacity ($C_p - C_V$) could be mentioned.

From the practical point of view, density data are of utmost importance in the development of new and the testing of existing equations of state; these equations have significant value in the design and operation of production plants in chemical and related process industries.

In our group, over a longer period, some important physical/thermodynamic and transport properties have been investigated; the obtained results were correlated and several modern prediction methods were tested. Mostly, pure non-electrolyte substances and mixtures were investigated, although systems with ionic liquids were also included.^{1–5} These activities were performed under ambient pressure and in the temperature range up to 333.15 K.

In this work, the results of an effort to extend the research to the conditions of elevated temperatures and high pressures are presented. In this respect, the proposed apparatus, based on the principle given by Gardas *et al.*,⁶ was developed and constructed. The classical method of Lagurette *et al.*,⁷ that was recently adjusted by Comuñas *et al.*⁸ for use in broad ranges of temperature and pressure, was chosen for calibration. A vacuum and water were used as calibration fluids, except under conditions where water was no longer in liquid state, when the calibration fluids were vacuum and *n*-decane. The proposed set-up was tested using *n*-hexane, since it was suggested as a model substance for compressed simple liquids.^{9–12} In addition, toluene and dichloromethane were also selected for testing the employed device and the experimental procedure followed.

EXPERIMENTAL

Materials

n-Hexane, *n*-decane and toluene were purchased from Merck with purities of ≥99.0, ≥99 and ≥99.9 mass %, respectively. Sigma–Aldrich supplied dichloromethane with a purity of ≥99.9 mass %.

The purities of the used substances were checked by comparing their measured densities at atmospheric pressure and at various temperatures with the corresponding literature values (Table S-I of the Supplementary material to this paper) and they were in a good agreement, within 0.2, 0.5 and 0.7 kg m^{−3} for *n*-hexane, toluene and dichloromethane, respectively.

Nitrogen 5.0 was provided by Messer Tehnogas, AD, with a purity of >99.999 mass %.

The double deionized Millipore water, provided by Veolia IonPRO-LX MkII system, was used as a calibration fluid. The treated water has a specific conductivity of $2.5 \mu\text{S cm}^{-1}$ and a specific resistance of $18 \text{ M}\Omega \text{ cm}$.

Apparatus – Description of the set-up

The compressed liquid densities at various temperatures and pressures were experimentally studied, employing an Anton Paar DMA HP density-measuring cell for high pressures and temperatures, connected to an Anton Paar DMA 5000 vibrating tube densimeter, as shown schematically in Fig. 1.

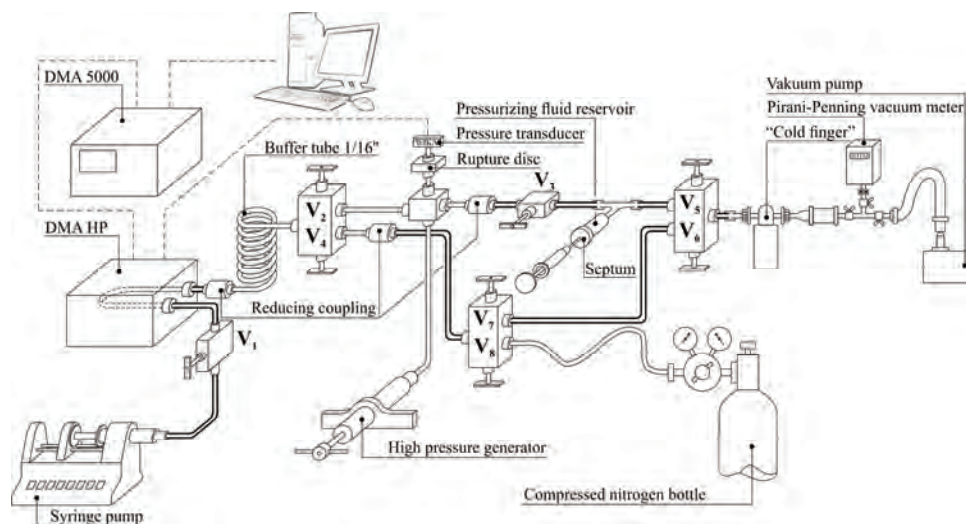


Fig. 1. Scheme of the apparatus for measuring densities at high pressures and elevated temperatures.

As mentioned in the introductory section, the proposed apparatus has been based on the principle proposed by Gardas *et al.*,⁶ although some additional parts of equipment have been brought into the system to construct the set-up.

The apparatus was used in broad ranges of temperature and pressure, varying between 288.15–413.15 K and 0.1–60 MPa, respectively. Each selected temperature was controlled with an integrated Peltier thermostat and the expanded uncertainty (coverage factor $k = 2$) for the temperature was 0.01 K.

A pressure generator, model 50-6-15, from High Pressure Equipment Co. (HiP), was used to adjust and control the pressure in the system; acetone was used as a hydraulic fluid, as proposed in the literature.⁶ The pressure in the system was measured using a pressure transducer WIKA, S-10, Alexander Wiegand GmbH & Co. The transducer was calibrated up to 60 MPa and the expanded uncertainty ($k = 2$) for the pressure was 0.05 MPa.

The period of tube vibration, τ was read on the display of the DMA 5000 densimeter with a digital counter; the vibrating period was displayed to seven significant digits.

All tubing (1/16" and 1/8" O.D.), the high-pressure valves and other high-pressure fittings shown in Fig. 1 are products of HiP Co, USA.

A syringe pump, enabling precise flow control during charging of the sample fluid, was used in order to avoid the formation of micro-bubbles in the capillary tube of the densimeter.

The assembly presented in Fig. 1 incorporates additional pieces of equipment, some of them are mentioned here: the DuoSeal vacuum pump, Welch model 1400, capable to reach an ultimate vacuum down to *ca.* 0.133 Pa (0.001 torr); the vacuum was indicated by a Pirani–Penning instrument; a KGW Isotherm cold trap was situated near the entrance of the pump; in addition, a compressed nitrogen bottle was included in the installation. The stainless steel spiral buffer tube (1/16" O.D. and *ca.* 1.5 m long) guarantees the absence of diffusion of the hydraulic liquid contained in the densimeter cell.⁶

Transferring of the collected data (period of oscillation of U-tube, cell temperature and pressure) from the DMA HP to the DMA 5000 was enabled by connecting the S-BUS interface of the DMA HP and DMA 5000.

The APSoftPrint software program (a Microsoft Excel Add-In) was employed to read out and transfer the measured values to a PC.

Loading of the set-up with the pressurizing fluid

To prepare the apparatus for experimental runs, the pressurizing fluid should be introduced into the appropriate parts: the tubes (and fittings), connecting valves V₂ through V₅ (Fig. 1), and those that join the high-pressure generator (HPG) with the pressure transducer. The HPG must also be filled.

To remove air from the parts of the installation described, the valves V₃ and V₅ are opened, enabling access to the vacuum pump (valve V₂ is closed). After several hours of evacuation, valve V₅ is closed. Then, a Hamilton multilayer silicon rubber septum, being a part of the pressurizing fluid reservoir (not shown in detail in Fig. 1), is penetrated by a needle of a syringe containing degassed acetone. In this way, acetone will occupy the entire evacuated space.

The measurement procedure

Before starting any run, the part of circuit between the syringe pump and valve V₂ (V₂ and V₄ were closed) was cleaned by successive use of ethanol and acetone to remove residues from the previous sample; then dry nitrogen gas was circulated through this part of the system for an appropriate period.

After a slight release of the connection between the buffer tube and the entrance of the valve V₂/V₄, the syringe pump was started, dispensing the sample between the valves V₁ and V₂, until several drops of the fluid had been withdrawn from the apparatus; then the pump was stopped and the mentioned connection tightened again. Since the tubes between the valves V₁ and V₂ were filled with the sample, the valve V₁ was closed. Hence, the sample was introduced into the system by the described operation. Now, when the desired conditions of temperature and pressure in the cell were stable, the vibration period of the U-tube could be determined.

In the present work, isothermal measurements were performed; at each selected isotherm, the pressure was imposed starting from its initial (lowest) value and elevating it towards the maximum value. Hysteresis effects were checked at every isotherm. Then, the temperature of the cell was changed and measurements at a new isotherm were performed.

Calibration

Since the vibrating tube densimeter does not generate directly the density values, it is necessary to calculate the density from the measured period of the oscillation (under a defined temperature *T* and pressure *p*).

Based on the model of the performance of vibrating tube established by Kratky *et al.*,¹³ the period of vibration $\tau(T,p)$ can be related to the sample density $\rho(T,p)$ by a linear function that incorporates two apparatus parameters $A(T,p)$ and $B(T,p)$:

$$\rho(T,p) = A(T,p)\tau^2(T,p) - B(T,p) \quad (1)$$

According to the approach of Lagourette *et al.*,⁷ who hypothetically assumed that the parameter A depends only on temperature while the parameter B remains dependent upon both temperature and pressure, Eq. (1) could be rewritten in the form:

$$\rho(T,p) = A(T)\tau^2(T,p) - B(T,p) \quad (2)$$

Use of this equation considerably simplifies the calibration of the densimeter (*i.e.*, the determination of its parameters $A(T)$ and $B(T,p)$). This method has to be performed by measuring the oscillating period of the evacuated tube over the entire temperature range of interest. In addition, the period of the tube full of the chosen reference fluid, having the certified density, has to be measured over the entire temperature and pressure ranges of the experimental significance. Lagourette *et al.*⁷ performed the calibration using the accurate density values for water of Kell and Whalley¹⁴ in the temperature and pressure ranges 293.15–373.15 K and 0.1–40 MPa, respectively.

Comuñas *et al.*⁸ adjusted the calibration procedure of Lagourette *et al.*⁷ in order to make it suitable for the new equipment (Anton Paar DMA HPM), enabling measurements in broad ranges of temperature and pressures up to 403.15 K and up to 140 MPa, respectively.

Thus, the procedure of Comuñas *et al.*⁸ was employed to calibrate the Anton Paar DMA HP densimeter included in Fig. 1.

In that sense, the period of the oscillation of the evacuated tube was measured over the entire temperature range indicated previously.

For the specific volume of water, Fisher and Dial¹⁵ selected the Tumlirz equation in the form given in the analysis of Eckert:¹⁶

$$V_p = V_\infty + \frac{\lambda}{p_0 + p} \quad (3)$$

where V_p / cm³ g⁻¹ is the specific volume as a function of pressure and temperature; V_∞ / cm³ g⁻¹, λ / bar cm³ g⁻¹ and p_0 / bar, are the pure water parameters. For these parameters, analytical functions were obtained¹⁵ that, in conjunction with Eq. (3), accurately represent the high precision data of Kell and Whalley¹⁷ (within 8 ppm from 273.15–373.15 K and within 15 ppm from 373.15–423.15 K, up to 100 MPa):

$$\begin{aligned} V_\infty &= 0.6980547 - 0.7435626 \times 10^{-3}T + 0.3704258 \times 10^{-4}T^2 - 0.6315724 \times 10^{-6}T^3 + \\ &\quad 0.9829576 \times 10^{-8}T^4 - 0.1197269 \times 10^{-9}T^5 + 0.1005461 \times 10^{-11}T^6 - \\ &\quad 0.5437898 \times 10^{-14}T^7 + 0.169946 \times 10^{-16}T^8 - 0.2295063 \times 10^{-19}T^9 \end{aligned} \quad (4)$$

$$\lambda = 1788.316 + 21.55053T - 0.4695911T^2 + 3.096363 \times 10^{-3}T^3 - 0.7341182 \times 10^{-5}T^4 \quad (5)$$

$$p_0 = 5918.499 + 58.05267T - 1.1253317T^2 + 6.6123869 \times 10^{-3}T^3 - 1.4661625 \times 10^{-5}T^4 \quad (6)$$

Finally, the specific volume values for water, supplied in this way, were recalculated to density. Accordingly:

a) at $0.1 \leq p \leq 60$ MPa and $288.15 \leq T \leq 363.15$ K, calibration of the cell was realized using the data collected as described above and by employing Eq. (7),⁸ obtained by applying Eq. (2):

$$\rho(T, p) = \rho_{\text{water}}(T, p) + \rho_{\text{water}}(T, 0.1 \text{ MPa}) \left[\frac{\tau^2(T, p) - \tau_{\text{water}}^2(T, p)}{\tau_{\text{water}}^2(T, 0.1 \text{ MPa}) - \tau_{\text{vacuum}}^2(T)} \right] \quad (7)$$

here, $\rho_{\text{water}}(T, p)$ is the density of water at T and p ; $\rho_{\text{water}}(T, p)$ represents the period of the oscillation of the vibrating tube full of water at T and p ; $\tau_{\text{vacuum}}(T)$ stands for the period of the evacuated tube at temperature T .

b) At $p = 0.1 \text{ MPa}$ and $T \geq 373.15 \text{ K}$: under these conditions, water is no longer appropriate to be employed as the reference fluid because it exists in the gaseous state. In the present work, *n*-decane was used, as proposed by Comuñas *et al.*⁸ Hence, the data given in the literature¹⁸ was employed; under these circumstances, the following relation was used instead of Eq. (7), as shown in reference:⁸

$$\rho(T, 0.1 \text{ MPa}) = \rho_{n\text{-decane}}(T, 0.1 \text{ MPa}) \left[1 + \frac{\tau^2(T, 0.1 \text{ MPa}) - \tau_{n\text{-decane}}^2(T, 0.1 \text{ MPa})}{\tau_{n\text{-decane}}^2(T, 0.1 \text{ MPa}) - \tau_{\text{vacuum}}^2(T)} \right] \quad (8)$$

c) At $p > 0.1 \text{ MPa}$ and $T \geq 373.15 \text{ K}$, Eq. (9) given by Comuñas *et al.*⁸ was used in the present work:

$$\rho(T, p) = \rho_{\text{water}}(T, p) + \rho_{n\text{-decane}}(T, 0.1 \text{ MPa}) \left[\frac{\tau^2(T, p) - \tau_{\text{water}}^2(T, p)}{\tau_{n\text{-decane}}^2(T, 0.1 \text{ MPa}) - \tau_{\text{vacuum}}^2(T)} \right] \quad (9)$$

By employing the described calibration procedure in the temperature and pressure ranges of interest (288.15–413.15 K and 0.1–60 MPa, respectively), numerous measurements, distributed on 16 isotherms were performed.

The parameters $A(T)$ and $B(T, p)$ of Eq. (2) were determined using Eqs. (10) and (11), respectively, which were clearly presented in the explicit form by Segovia *et al.*:¹⁹

$$A(T) = \frac{\rho_{\text{ref1}}(T, 0.1 \text{ MPa})}{\tau_{\text{ref1}}^2(T, 0.1 \text{ MPa}) - \tau_{\text{vacuum}}^2(T)} \quad (10)$$

$$B(T, p) = \rho_{\text{ref1}}(T, 0.1 \text{ MPa}) \frac{\tau_{\text{ref2}}^2(T, p)}{\tau_{\text{ref1}}^2(T, 0.1 \text{ MPa}) - \tau_{\text{vacuum}}^2(T)} - \rho_{\text{ref2}}(T, p) \quad (11)$$

where ρ_{ref1} and ρ_{ref2} are the densities of reference fluids 1 and 2, respectively, and τ_{ref1} and τ_{ref2} are the oscillation period of the U tube full of reference fluid 1 and 2, respectively. For the interval: $0.1 \leq p \leq 60 \text{ MPa}$ and $288.15 \leq T \leq 363.15 \text{ K}$, both reference fluids are water. At $p = 0.1 \text{ MPa}$ and $T \geq 373.15 \text{ K}$, ref1 and ref2 refer to *n*-decane and at $p > 0.1 \text{ MPa}$ and $T \geq 373.15 \text{ K}$, reference fluid 1 is *n*-decane while reference fluid 2 is water.

As could be seen from Fig. 2a, the values of $A(T)$ decreased linearly with increasing temperature, as expected according to the conclusions of Lagourette *et al.*⁷ In addition, these authors remarked that the ratio of the calibration parameters $A(T)/B(T, p)$ is practically independent of pressure. This observation was appraised by a number of authors who employed various calibration fluid pairs.^{19–21} In each of these cases, it was shown that the ratio $A(T)/B(T, p)$ decreased slightly with increasing pressure. The dependence of the ratio of the calibration parameters on pressure at the selected isotherms chosen in the present work is demonstrated in Fig. 2b.

The calculated expanded uncertainty of the density measurements with a coverage probability of 95 % (coverage factor $k = 2$) is 1.7 kg m^{-3} in the temperature interval 288.15–363.15 K, and 2.7 kg m^{-3} at temperatures 373.15–413.15 K.

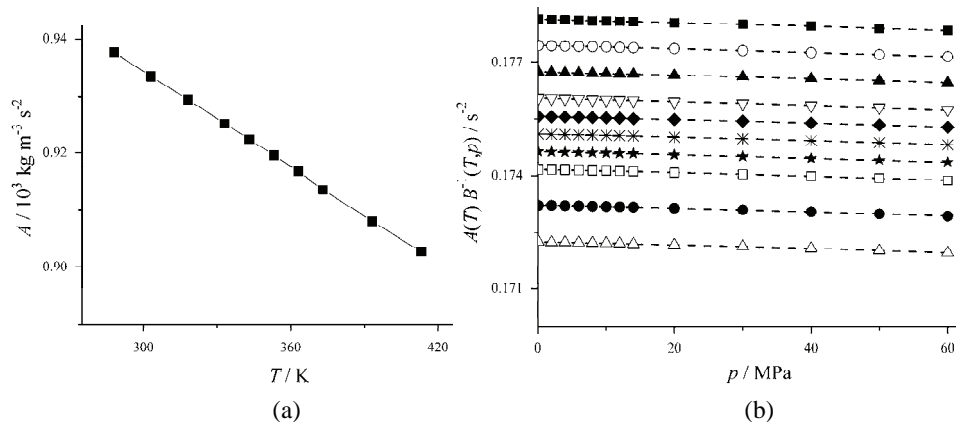


Fig. 2. The calibration parameters: a) dependence of $A(T)$ of the temperature, 288.15–413.15 K, b) the ratio of the $A(T)/B(T,p)$ vs. pressure at different temperatures: (■) 288.15, (○) 303.15, (▲) 318.15, (▽) 333.15, (◆) 343.15, (*) 353.15, (★) 363.15, (□) 373.15, (●) 393.15 and (△) 413.15 K.

The influence of viscosity of the substances on density was also studied. A personal correspondence with the supplier Anton Paar provided the information necessary for the calculation of density correction due to damping effects on the vibrating tube. Assuming that temperature has a greater impact on viscosity than pressure and that the viscosity decreases with increasing temperature, literature data^{22–24} for the viscosity at lower temperatures from the interval of interest in this work were used for the calculation. The calculated differences between the densities presented in this work and those corrected because of the viscosity effect for all three examined substances were under 0.03 kg m^{-3} , which was significantly lower than the calculated value of the expanded uncertainty for density and hence the viscosity influence on density were neglected.

RESULTS AND DISCUSSION

With the intention of checking the quality of the calibration parameters obtained in this study, the densities of *n*-hexane, toluene and dichloromethane, were experimentally determined and compared with some corresponding literature data.

The vibration periods of the U tube within the DMA HP densimeter full of samples, *n*-hexane, toluene or dichloromethane, were measured in the temperature range 288.15–413.15 K, at 16 isotherms, and at pressures up to 60 MPa. The densities of the measured substances were calculated by application of Eqs. (3)–(9) and the obtained values are presented in Tables S-II–IV of the Supplementary material to this paper.

The following criteria, the absolute average percentage deviation (*AAD*), the percentage maximum deviation (*MD*) and the average percentage deviation (*Bias*) were used to evaluate the quality of the agreement of the obtained experimental results with the corresponding literature values:

$$AAD = \frac{100}{N} \sum_{i=1}^N \left| \frac{\rho_i^{\text{exp}} - \rho_i^{\text{lit}}}{\rho_i^{\text{exp}}} \right| \quad (12)$$

$$MD = \max \left(100 \left| \frac{\rho_i^{\text{exp}} - \rho_i^{\text{lit}}}{\rho_i^{\text{exp}}} \right| \right); i = 1, N \quad (13)$$

$$Bias = \frac{100}{N} \sum_{i=1}^N \left(\frac{\rho_i^{\text{exp}} - \rho_i^{\text{lit}}}{\rho_i^{\text{exp}}} \right) \quad (14)$$

where N stands for the number of experimental points, ρ_{exp} denotes the experimental density and ρ_{lit} is the density value from the selected literature.

n-Hexane

The measured data for *n*-hexane (Table S-II) were compared with the densities given in the work of Troncoso *et al.*²⁵ in the temperature range 288.15–313.15 K and at pressures up to 40 MPa. The comparison presented in Fig. 3a shows that the present measurements are in accordance with the tabulated data of Troncoso *et al.* ($AAD = 0.03\%$ (less than 0.2 kg m^{-3}), $MD = 0.09\%$ and $Bias = -0.02\%$). The agreement with the values of Daridon *et al.*²⁶ is moderate in the presented region ($AAD = 0.08\%$ (less than 0.6 kg m^{-3}), $MD = 0.22\%$ and $Bias = -0.08\%$).

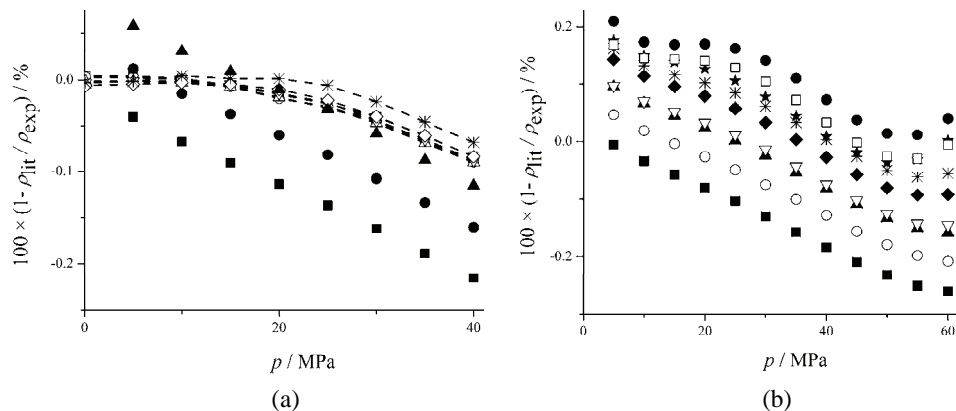


Fig. 3. Comparison of the experimental densities of *n*-hexane with literature values:
a) Troncoso *et al.*:¹¹ (—□—), 288.15, (—○—) 293.15, (—△—) 298.15, (—▽—) 303.15,
(—◇—) 308.15 and (—*—) 313.15 K, and Daridon *et al.*:²⁶ (■) 293.15, (●) 303.15 and (▲)
313.15; b) Daridon *et al.*:²⁶ (■) 293.15, (○) 303.15, (▲) 313.15, (▽) 323.15, (◆) 333.15,
(*) 343.15, (★) 353.15, (□) 363.15 and (●) 373.15 K.

The obtained experimental results were compared with the tabulated data of Daridon *et al.*²⁶ in the temperature interval 293.15–373.15 K and at pressures up

to 60 MPa. The calculated deviations were: $AAD = 0.10\%$ (less than 0.7 kg m^{-3}), $MD = 0.29\%$ and $Bias = -0.01\%$, as shown in Fig. 3b.

In addition, the measurements were compared with the density data of Sanmamed *et al.*²⁷ in the regions: 288.15–323.15 K and up to 60 MPa. The obtained values of the criteria were: $AAD = 0.05\%$ (less than 0.4 kg m^{-3}), $MD = 0.17\%$ and $Bias = -0.04\%$ that could be considered as acceptable.

In conclusion, the density measurements are in very good agreement with those of Troncoso *et al.*²⁵, as well as in accordance with those of Sanmamed *et al.*²⁷. On the other hand, the agreement with the tabulation of Daridon *et al.*,²⁶ which were based on speed of sound measurements, are less good than expected, but should be emphasized that the densities reported in the literature²⁶ belong to a much wider temperature interval.

Toluene

The experimental densities of toluene, given in Table S-III, were compared with those obtained from the equations proposed by Cibulka and Takagi²⁸ over the entire temperature and pressure ranges of interest in the present work. The AAD of the comparison was 0.04% (less than 0.3 kg m^{-3}), the MD was 0.12% and the $Bias$ was -0.04% ; hence, it could be concluded that the results obtained in the present study are in good agreement with those calculated by the procedure proposed in the literature.²⁸ This fact could be noticed by inspecting Fig. 4.

Density data of the present work were also compared with the data calculated from the fit given by Assael *et al.*²⁹ in the temperature range 288.15–373.15 K and up to 60 MPa. The values of the criteria for this comparison were: $AAD = 0.08\%$ (less than 0.7 kg m^{-3}), $MD = 0.15\%$ and $Bias = -0.08\%$. It should be emphasized that the dispersion of the present data corresponded to that given in Fig. 2 of reference.²⁹

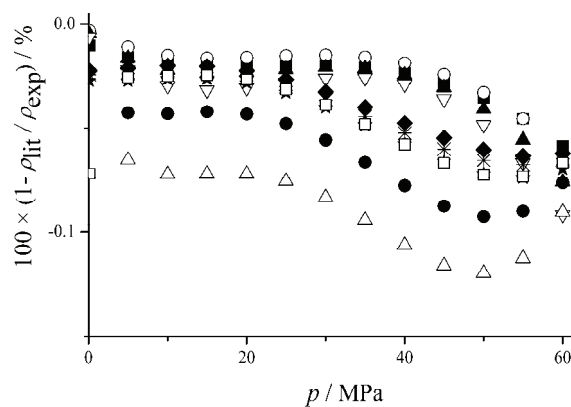


Fig. 4. Comparison of the experimental densities with those obtained using the equation reported by Cibulka *et al.*²⁸ for toluene at various temperatures: (■) 288.15, (○) 303.15, (▲) 318.15, (▽) 333.15, (◆) 343.15, (※) 353.15, (★) 363.15, (□) 373.15, (●) 393.15 and (△) 413.15 K.

In order to assess the obtained densities, an additional comparison was made. Namely, Segovia *et al.*¹⁹ gave a set of density data at various temperatures and pressures (288.15–393.15 K and up to 60 MPa). These data were fitted to the modified Tammann–Tait equation for comparison with the densities given in the present work:

$$\rho = \frac{\rho^{\text{ref}}}{1 - C \ln \left(\frac{B(T) + p}{B(T) + p^{\text{ref}}} \right)} \quad (15)$$

where ρ^{ref} is density at the reference pressure, p^{ref} , which was chosen to be 0.1 MPa. The parameter C was treated as temperature independent and $B(T)$ was obtained using the polynomial expression:

$$B(T) = \sum_{i=0}^2 b_i T^i \quad (16)$$

The values of the individual criteria were: $AAD = 0.05\%$ (less than 0.4 kg m⁻³), $MD = 0.09\%$ and $Bias = -0.04\%$.

By reviewing the values of the criteria mentioned above, it could be noticed that the densities reported herein are in close agreement with the corresponding results appearing in the literature.

Dichloromethane

Gonçalves *et al.*²² presented a correlation for calculating the densities of dichloromethane in broad ranges of temperature and pressure that was used for comparison with the present data measured in the temperature interval 288.15–413.15 K and under pressures of up to 60 MPa (presented in Table S-IV). Deviations between these two density sets were: $AAD = 0.03\%$ (less than 0.4 kg m⁻³), $MD = 0.13\%$ and $Bias = -0.002\%$, indicating good agreement that is visible in Fig. 5.

In the work of Lugo *et al.*,²⁰ a density data set for dichloromethane was presented, covering temperature and pressure ranges of 293.15–353.15 K and 0.1–25 MPa. The present measurements were compared with the density values presented therein; the following deviations were reached: $AAD = 0.03\%$ (less than 0.4 kg m⁻³), $MD = 0.04\%$ and $Bias = -0.03\%$, showing good agreement between the two sets of data.

In addition, the densities of dichloromethane given by Demiriz³⁰ in broad temperature and pressure ranges were employed to assess the densities from the present work. These data³¹ were fitted to the Tammann–Tait equation, according to Eqs. (15) and (16) and in this case p^{ref} was 1 MPa in the ranges: 270–430 K and up to 60 MPa. The densities obtained in the present work agreed quite well

with those estimated using this fit. The deviations achieved were: $AAD = 0.03\%$ (less than 0.5 kg m^{-3}), $MD = 0.30\%$ and $Bias = -0.03\%$.

Values of the criteria given in this section could be considered as good and acceptable compared to those reported by the other authors.

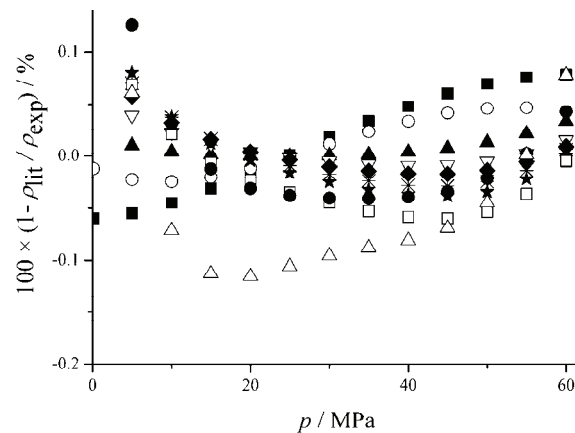


Fig. 5. Comparison of experimental densities with those obtained using the equation reported by Gonçalves *et al.*²⁴ for dichloromethane at various temperatures: (■) 288.15, (○) 303.15, (▲) 318.15, (▽) 333.15, (◆) 343.15, (※) 353.15, (★) 363.15, (□) 373.15, (●) 393.15 and (△) 413.15 K.

CONCLUSIONS

In this work, an apparatus proposed for compressed liquids density measurement over broad ranges of temperature and pressure was described. The Anton Paar DMA HP and Anton Paar 5000 represent the central parts of the set-up. This variable volume apparatus makes use of a buffer tube, as proposed by Gardas *et al.*⁶ The DMA HP was calibrated by applying the method of Comuñas *et al.*⁸ in the temperature and pressure ranges: 288.15 to 413.15 K and 0.1–60 MPa, respectively. The present density measurements for *n*-hexane, toluene and dichloromethane were compared with the corresponding literature values. This assessment showed good quality of the measurements performed. Thus, it could be expected that the recommended apparatus could be reliably applied for measuring the density of a number of other compressed liquids in broad ranges of temperatures and pressures.

SUPPLEMENTARY MATERIAL

The experimental values of the densities of *n*-hexane, toluene and dichloromethane at different temperatures (288.15–413.15 K) and pressures (0.1–60 MPa), as well as at atmospheric pressure, are available electronically from <http://www.shd.org.rs/JSCS/>, or from the corresponding author on request.

Acknowledgements. It is our pleasure to thank Professor Abel Ferreira (Faculdade de Ciências e Tecnologia, Universidade de Coimbra, Portugal) for valuable discussion. Furthermore, we highly appreciate the Anton Paar GmbH, Graz, Austria for donating a DMA HP density-measuring cell to our laboratory, on the occasion of the fortieth anniversary of the vibrating tube densimeter invention. The authors gratefully acknowledge the financial support

received from the Research Fund of Ministry of Education, Science and Technological Development of the Republic of Serbia (project No 172063) and the Faculty of Technology and Metallurgy, University of Belgrade.

ИЗВОД

АПАРАТУРА ПРЕДЛОЖЕНА ЗА МЕРЕЊЕ ГУСТИНА У ОБЛАСТИ КОМПРИМОВАНИХ ТЕЧНОСТИ ОД 0,1 ДО 60 МРа И НА ТЕМПЕРАТУРАМА ОД 288,15 ДО 413,15 К

ГОРИЦА Р. ИВАНИШ, АЛЕКСАНДАР Ж. ТАСИЋ, ИВОНА Р. РАДОВИЋ, БОЈАН Д. ЂОРЂЕВИЋ,
СЛОБОДАН П. ШЕРБАНОВИЋ И МИРЈАНА Љ. КИЈЕВЧАНИН

Технолошко-металуршки факултет у Београду, Карнецијева 4, 11120, Београд

У овом раду је предложена апаратура за мерење густине у области компримованих течности. Инсталација се заснива на коришћењу ћелије за мерење густине DMA HP и густиномера DMA 5000 (произвођач оба производа је Anton Paar, Грац, Аустрија). Калибрација ћелије DMA HP је извршена применом класичне методе која препоручује употребу вакуума, воде и *n*-декана као калибрационих флуида. У циљу провере рада приказане апаратуре мерење су густине *n*-хексана, толуена и дихлорметана у температурном интервалу 288,15 до 413,15 К и опсегу притиска од 0,1 до 60 МРа. Добијени резултати су упоређени са одговарајућим вредностима из литературе. У зависности од одабране литературе, односно опсега температуре и притиска, добијена су следећа средња апсоултна процентуална одступања: за *n*-хексан, 0,03–0,10 %; за толуен, 0,04–0,08 %, а за дихлорметан, 0,02–0,03 %. Детаљнији увид у резултате овог рада показује да је већина њих у доброј сагласности са вредностима из литературе; веће разлике су приметне у близини крајева интервала температуре и притиска.

(Примљено 27. новембра 2014, ревидирано 16. марта, прихваћено 17. марта 2015)

REFERENCES

- M. Lj. Kijevčanin, S. P. Šerbanović, I. R. Radović, B. D. Djordjević, A. Ž. Tasić, *Fluid Phase Equilib.* **251** (2007) 78
- D. M. Bajić, G. R. Ivaniš, Z. Višak, E. M. Živković, S. P. Šerbanović, M. Lj. Kijevčanin, *J. Chem. Thermodyn.* **57** (2013) 510
- M. Lj. Kijevčanin, I. R. Radović, B. D. Djordjević, A. Ž. Tasić, S. P. Šerbanović, *Thermochim. Acta* **525** (2011) 114
- J. M. Vuksanović, G. R. Ivaniš, M. Lj. Kijevčanin, S. P. Šerbanović, Z. P. Višak, M. S. Calado, *Fluid Phase Equilib.* **352** (2013) 100
- A. B. Knežević-Stevanović, S. P. Šerbanović, I. R. Radović, B. D. Djordjević, M. Lj. Kijevčanin, *J. Chem. Eng. Data* **58** (2013) 2932
- R. L. Gardas, I. Johnson, D. M. D. Vaz, I. M. A. Fonseca, A. G. M. Ferreira, *J. Chem. Eng. Data* **52** (2007) 737
- B. Lagourette, C. Boned, H. Saint-Guirons, P. Xans, H. Zhou, *Meas. Sci. Technol.* **3** (1992) 699
- M. J. P. Comuñas, J.-P. Bazile, A. Baylaucq, C. Boned, *J. Chem. Eng. Data* **53** (2008) 986
- S. L. Randzio, J.-P. E. Grolier, J. R. Quint, D. J. Eatough, E. A. Lewis, L. D. Hansen, *Int. J. Thermophys.* **15** (1994) 415
- Ph. Pruzan, *J. Phys. Lett.* **45** (1984) 273
- S. L. Randzio, *Thermochim. Acta* **121** (1987) 463
- Ph. Pruzan, *J. Chem. Thermodyn.* **23** (1991) 247

13. O. Kratky, H. Leopold, H. Stabinger, *Z. Angew. Phys.* **27** (1969) 273
14. G. S. Kell, E. Whalley, *J. Chem. Phys.* **62** (1975) 3496
15. F. H. Fisher, O. E. Dial Jr., Equation of state of pure water and sea water, in Proceedings of the Marine Physical Laboratory of the Scripps Institution of Oceanography, San Diego, CA, USA, 1975, p. 1
16. C. Eckart, *Am. J. Sci.* **256** (1958) 225
17. G. S. Kell, E. Whalley, *Proc. Roy. Soc., A.* **258** (1965) 565
18. *TRC, Thermodynamic Tables*, Texas A & M University, College Station, TX, 1996
19. J. Segovia, O. Fandiño, E. López , L. Lugo, M. C. Martín, J. Fernández, *J. Chem. Thermodyn.* **41** (2009) 632
20. L. Lugo, M. J. P. Comuñas, E. R. López, J. Fernández, *Fluid Phase Equilib.* **186** (2001) 235
21. M. J. P. Comuñas, E. R. Lopez, P. Pires, J. Garcia, J. Fernandez, *Int. J. Thermophys.* **21** (2000) 831
22. F. A. M. M. Gonçalves, C. S. M. F. Costa, J. C. S. Bernardo, I. Johnson, I. M. A. Fonseca, A. G. M. Ferreira, *J. Chem. Thermodyn.* **43** (2011) 105
23. P. Morgado, J. Black, J. B. Lewis, C. R. Iacobella, C. McCabe, L. F. G. Martins, E. J. M. Filipe, *Fluid Phase Equilib.* **358** (2013) 161
24. J. M. Vuksanovic, E. M. Zivkovic, I. R. Radovic, B. D. Djordjevic, S. P. Serbanovic, M. Lj. Kijevcanin, *Fluid Phase Equilib.* **345** (2013) 28
25. J. Troncoso, D. Bessières, C. A. Cerdeiriña, E. Carballo, L. Romaní, *Fluid Phase Equilib.* **208** (2003) 141
26. J. L. Daridon, B. Lagourette, J.-P. E. Grolier, *Int. J. Thermophys.* **19** (1998) 145
27. Y. A. Sanmamed, A. Dopazo-Paz, D. González-Salgado, J. Troncoso, L. Romaní, *J. Chem. Thermodyn.* **41** (2009) 1060
28. I. Cibulka, T. Takagi, *J. Chem. Eng. Data* **44** (1999) 411
29. M. J. Assael, H. M. T. Avelino, N. K. Dalaouti, J. M. N. A. Fareleira, K. R. Harris, *Int. J. Thermophys.* **22** (2001) 789
30. A. M. Demiriz, *PhD Thesis*, University of Bochum, Bochum, Germany, 1986.



SUPPLEMENTARY MATERIAL TO

An apparatus proposed for density measurements in compressed liquid regions at pressures of 0.1–60 MPa and temperatures of 288.15–413.15 K

GORICA R. IVANIŠ[#], ALEKSANDAR Ž. TASIĆ*, IVONA R. RADOVIĆ[#], BOJAN D. DJORDJEVIĆ[#], SLOBODAN P. ŠERBANOVIĆ[#] and MIRJANA Lj. KIJEVČANIN[#]

*Faculty of Technology and Metallurgy, University of Belgrade, Karnegijeva 4,
11120 Belgrade, Serbia*

J. Serb. Chem. Soc. 80 (8) (2015) 1073–1085

TABLE S-I. Comparison of experimental densities with literature data at atmospheric pressure (0.1 MPa) and various temperatures for *n*-hexane, toluene and dichloromethane

Component	T / K	$\rho / \text{kg m}^{-3}$	
		Exp.	Literature
<i>n</i> -Hexane	288.15	664.164	664.03 ¹ , 664.01 ²
	293.15	659.665	659.56 ¹ , 659.49 ²
	298.15	655.134	655.07 ¹ , 654.92 ²
	303.15	650.569	650.53 ¹ , 650.39 ²
	308.15	645.967	645.94 ¹ , 645.75 ²
	313.15	641.330	641.29 ¹ , 641.10 ²
	298.15	862.199	862.1 ³ , 862.5 ⁴
Toluene	308.15	852.848	853.0 ³
	318.15	843.457	843.8 ³
	328.15	834.010	834.5 ³
	293.15	1325.334	1325.67 ⁵ , 1326.35 ⁶
Dichloromethane	303.15	1306.821	1306.99 ⁵

TABLE S-II. Experimental densities, $\rho / \text{kg m}^{-3}$, for *n*-hexane at different temperatures, 288.15–413.15 K and pressures (0.1–60 MPa); $U(\rho) = 1.7 \text{ kg m}^{-3}$ (288.15 $\leq T \leq$ 363.15 K) and 2.7 kg m^{-3} (373.15 $\leq T \leq$ 413.15 K); $U(T) = 0.01 \text{ K}$; $U(p) = 0.05 \text{ MPa}$

p / MPa	T / K							
	288.15	293.15	298.15	303.15	308.15	313.15	318.15	323.15
0.1	664.1	659.6	655.1	650.5	645.9	641.3	636.6	631.8
1	665.0	660.5	656.0	651.5	646.9	642.4	637.7	633.0
5	668.8	664.5	660.1	655.8	651.4	647.0	642.5	638.1
10	673.3	669.2	665.0	660.8	656.6	652.4	648.2	643.9

*Corresponding author. E-mail: tasic33@gmail.com

TABLE S-II. Continued

<i>p</i> / MPa	<i>T</i> / K							
	288.15	293.15	298.15	303.15	308.15	313.15	318.15	323.15
15	677.5	673.6	669.6	665.6	661.5	657.5	653.4	649.4
20	681.6	677.7	673.8	670.0	666.1	662.2	658.3	654.4
25	685.3	681.6	677.8	674.1	670.3	666.6	662.8	659.1
30	688.9	685.3	681.6	678.0	674.3	670.7	667.0	663.4
35	692.3	688.8	685.2	681.7	678.1	674.6	671.0	667.5
40	695.6	692.1	688.7	685.2	681.7	678.3	674.8	671.4
45	698.7	695.3	691.9	688.6	685.2	681.8	678.4	675.0
50	701.8	698.4	695.1	691.8	688.5	685.2	681.9	678.6
55	704.7	701.4	698.2	694.9	691.7	688.5	685.2	682.0
60	707.6	704.4	701.2	698.0	694.8	691.7	688.5	685.4
	328.15	333.15	343.15	353.15	363.15	373.15	393.15	413.15
0.1	627.1	622.3	—	—	—	—	—	—
1	628.3	623.6	613.9	603.8	593.5	583.3	560.8	536.6
5	633.5	629.1	619.8	610.3	600.6	591.0	570.3	548.3
10	639.6	635.4	626.6	617.8	608.7	599.8	581.0	561.3
15	645.3	641.2	632.9	624.6	616.1	607.7	590.4	572.4
20	650.5	646.6	638.6	630.7	622.7	614.8	598.6	582.1
25	655.3	651.6	643.9	636.3	628.7	621.2	605.9	590.4
30	659.8	656.2	648.8	641.4	634.1	626.9	612.3	597.6
35	664.0	660.5	653.4	646.2	639.1	632.2	618.1	604.0
40	667.9	664.5	657.6	650.6	643.8	637.1	623.4	609.8
45	671.7	668.4	661.7	654.9	648.2	641.7	628.4	615.1
50	675.3	672.1	665.5	658.9	652.4	646.1	633.2	620.3
55	678.8	675.7	669.3	663.0	656.5	650.4	638.0	625.6
60	682.3	679.2	673.0	667.0	660.6	654.7	642.9	631.1

TABLE S-III. Experimental densities, ρ / kg m⁻³, for toluene at different temperatures (288.15–413.15 K) and pressures (0.1–60 MPa); $U(\rho) = 1.7$ kg m⁻³ (288.15 K $\leq T \leq$ 363.15 K) and 2.7 kg m⁻³ (373.15 K $\leq T \leq$ 413.15 K); $U(T) = 0.01$ K; $U(p) = 0.05$ MPa

<i>p</i> / MPa	<i>T</i> / K							
	288.15	293.15	298.15	303.15	308.15	313.15	318.15	323.15
0.1	871.4	866.8	862.2	857.5	852.8	848.1	843.4	838.7
1	872.0	867.5	862.8	858.2	853.6	848.9	844.2	839.5
5	874.9	870.4	865.8	861.3	856.7	852.1	847.5	842.9
10	878.3	873.9	869.5	865.0	860.6	856.1	851.6	847.1
15	881.6	877.3	873.0	868.7	864.3	859.9	855.5	851.2
20	884.9	880.7	876.4	872.2	867.9	863.6	859.3	855.1
25	888.0	883.9	879.7	875.6	871.4	867.2	863.0	858.9
30	891.1	887.0	882.9	878.9	874.8	870.7	866.6	862.5
35	894.1	890.1	886.1	882.0	878.0	874.0	870.0	866.0
40	896.9	893.0	889.1	885.1	881.2	877.2	873.3	869.3
45	899.7	895.9	891.9	888.1	884.2	880.3	876.4	872.6
50	902.4	898.6	894.7	890.9	887.1	883.3	879.4	875.6
55	905.0	901.2	897.4	893.6	889.9	886.1	882.3	878.6

TABLE S-III. Continued

<i>p</i> / MPa	<i>T</i> / K							
	288.15	293.15	298.15	303.15	308.15	313.15	318.15	323.15
60	907.5	903.8	900.0	896.3	892.5	888.8	885.1	881.4
	328.15	333.15	343.15	353.15	363.15	373.15	393.15	413.15
0.1	833.9	829.1	819.4	809.6	799.7	789.3	—	—
1	834.7	830.0	820.3	810.6	800.8	790.9	770.4	749.2
5	838.3	833.6	824.3	814.9	805.4	795.8	776.2	755.9
10	842.6	838.1	829.1	820.0	810.9	801.7	782.9	763.6
15	846.7	842.4	833.7	824.9	816.0	807.2	789.1	770.7
20	850.8	846.5	838.1	829.5	820.9	812.3	794.9	777.3
25	854.6	850.5	842.2	833.8	825.5	817.2	800.4	783.4
30	858.4	854.3	846.1	838.0	829.9	821.8	805.4	789.1
35	862.0	858.0	849.9	842.0	834.0	826.1	810.2	794.3
40	865.4	861.5	853.6	845.8	838.0	830.3	814.8	799.3
45	868.7	864.9	857.1	849.4	841.8	834.3	819.1	804.0
50	871.9	868.1	860.5	853.0	845.5	838.1	823.3	808.6
55	874.9	871.1	863.8	856.4	849.1	841.9	827.4	813.0
60	877.7	874.0	867.0	859.8	852.6	845.5	831.4	817.4

TABLE S-IV. Experimental densities, ρ / kg m⁻³, for dichloromethane at different temperatures (288.15–413.15 K) and pressures (0.1–60 MPa); $U(\rho) = 1.7$ kg m⁻³ (288.15 K $\leq T \leq 363.15$ K) and 2.7 kg m⁻³ (373.15 K $\leq T \leq 413.15$ K); $U(T) = 0.01$ K; $U(p) = 0.05$ MPa

<i>p</i> / MPa	<i>T</i> / K							
	288.15	293.15	298.15	303.15	308.15	313.15	318.15	323.15
0.1	1334.5	1325.3	1316.0	1306.8	1297.4	1287.8	—	—
1	1335.6	1326.5	1317.2	1308.1	1298.7	1289.2	1279.7	1270.1
5	1340.6	1331.6	1322.6	1313.6	1304.4	1295.2	1286.0	1276.7
10	1346.6	1337.9	1329.1	1320.3	1311.4	1302.5	1293.6	1284.6
15	1352.5	1344.0	1335.4	1326.8	1318.1	1309.5	1300.8	1292.0
20	1358.3	1349.9	1341.5	1333.1	1324.6	1316.2	1307.7	1299.2
25	1363.8	1355.6	1347.4	1339.1	1330.9	1322.6	1314.3	1306.0
30	1369.2	1361.2	1353.1	1345.0	1337.0	1328.8	1320.7	1312.5
35	1374.4	1366.5	1358.6	1350.7	1342.8	1334.7	1326.7	1318.8
40	1379.5	1371.7	1364.0	1356.2	1348.4	1340.4	1332.6	1324.8
45	1384.3	1376.7	1369.1	1361.5	1353.8	1345.9	1338.3	1330.7
50	1389.1	1381.5	1374.0	1366.5	1359.0	1351.3	1343.8	1336.3
55	1393.6	1386.2	1378.8	1371.4	1364.0	1356.6	1349.2	1341.8
60	1398.0	1390.6	1383.3	1376.0	1368.8	1361.7	1354.4	1347.2
	328.15	333.15	343.15	353.15	363.15	373.15	393.15	413.15
0.1	—	—	—	—	—	—	—	—
1	1260.4	1250.6	1230.7	1210.3	1189.3	1167.4	1122.7	1072.3
5	1267.2	1257.7	1238.5	1218.8	1198.6	1177.7	1135.0	1087.9
10	1275.4	1266.2	1247.7	1228.8	1209.5	1189.7	1149.3	1105.7
15	1283.2	1274.3	1256.3	1238.1	1219.7	1200.8	1162.4	1121.7
20	1290.6	1281.9	1264.6	1247.0	1229.2	1211.1	1174.5	1136.2
25	1297.6	1289.2	1272.3	1255.3	1238.1	1220.6	1185.7	1149.2

TABLE S-IV. Continued

<i>p</i> / MPa	<i>T</i> / K							
	288.15	293.15	298.15	303.15	308.15	313.15	318.15	323.15
30	1304.4	1296.2	1279.7	1263.2	1246.5	1229.6	1196.0	1161.1
35	1310.8	1302.8	1286.8	1270.6	1254.4	1238.0	1205.5	1172.0
40	1317.0	1309.2	1293.5	1277.8	1262.0	1246.0	1214.5	1182.1
45	1323.0	1315.3	1300.0	1284.6	1269.2	1253.5	1223.0	1191.5
50	1328.8	1321.3	1306.3	1291.2	1276.1	1260.8	1231.1	1200.5
55	1334.5	1327.0	1312.3	1297.6	1282.8	1267.9	1238.9	1209.2
60	1340.0	1332.7	1318.3	1303.8	1289.4	1274.9	1246.5	1217.9

REFERENCES

1. J. Troncoso, D. Bessières, C. A. Cerdeiriña, E. Carballo, L. Romaní, *Fluid Phase Equilib.* **208** (2003) 141
2. Y. A. Sanmamed, A. Dopazo-Paz, D. González-Salgado, J. Troncoso, L. Romaní, *J. Chem. Thermodyn.* **41** (2009) 1060
3. L. Morávavková, Z. Wagner, J. Linek, *J. Chem. Thermodyn.* **37** (2005) 658
4. J. Segovia, O. Fandiño, E. López , L. Lugo, M. C. Martín, J. Fernández, *J. Chem. Thermodyn.* **41** (2009) 632
5. L. Lugo, M. J. P. Comuñas, E. R. López, J. Fernández, *Fluid Phase Equilib.* **186** (2001) 235
6. F. A. M. M. Gonçalves, C. S. M. F. Costa, J. C. S. Bernardo, I. Johnson, I. M. A. Fonseca, A. G. M. Ferreira, *J. Chem. Thermodyn.* **43** (2011) 105.



Geochemical investigation as a tool in the determination of the potential hazard for soil contamination (Kremna Basin, Serbia)

TAMARA PERUNOVIĆ¹, KSENIJA STOJANOVIĆ^{1*}, MILICA KAŠANIN-GRUBIN²,
ALEKSANDRA ŠAJNOVIĆ^{2#}, VLADIMIR SIMIĆ³, BRANIMIR JOVANIĆEVIĆ^{1#}
and ILIJA BRČESKI¹

¹University of Belgrade, Faculty of Chemistry, Studentski trg 12–16, 11000 Belgrade, Serbia,

²University of Belgrade, Center of Chemistry, ICTM, Njegoševa 12, 11000 Belgrade, Serbia

and ³University of Belgrade, Faculty of Mining and Geology, Djušina 7,
11000 Belgrade, Serbia

(Received 17 September, revised 31 October, accepted 6 November 2014)

Abstract: The geochemical composition of the soils and underlying sediments in the Kremna Basin was investigated. The aim was to assess whether the observed heavy metal concentrations in the soil samples represent geogenic or anthropogenic contamination. The second objective was to show that geochemical data of underlying sediments should be used as a tool in the determination of the potential hazard for soil contamination. For this purpose, the contents of As, Cr, Cu, Hg, Ni, Pb and Zn of soil samples were compared with standard values, a reference soil sample and local background values of the underlying sediments. The soil samples were unpolluted regarding the contents of As, Hg, Pb and Zn. All samples had higher contents of Cr and Ni, whereas three samples had higher contents of Cu than the limit standard values. Geochemical parameters showed that the higher concentrations of Cr, Cu and Ni in the soils could be attributed to geogenic impact. This conclusion was supported by the Chemical Proxy of Alteration and Chemical Index of Weathering values, which indicated intense weathering of the sediments. The obtained results showed that the Kremna area is under slight to moderate hazard if a land use change would occur, and proved the importance of the geochemical composition of underlying sediments in the interpretation of heavy metal pollution.

Keywords: soils; sediments; geochemistry; heavy metals; pollution; weathering.

*Corresponding author. E-mail: ksenija@chem.bg.ac.rs; xenasyu@yahoo.com
#Serbian Chemical Society member.
doi: 10.2298/JSC170914108P

INTRODUCTION

In natural systems, enrichment and depletion balance each other out. However, anthropogenic influences tend to enrichments in different parts of the system and the distribution function is skewed towards higher values.¹

Heavy metals are one of the serious pollutants in the natural environment due to their toxicity, persistence and bioaccumulation problems.^{2,3} Assessment of the contamination status is regularly based on the Quality Guidelines. Comparison of concentrations of heavy metals measured in samples and contents given by the Quality Guidelines provides data about the level of sample contamination. However, assessment of whether the measured heavy metal concentrations in samples represent geogenic or anthropogenic contamination is difficult based purely on such results. In order to overcome this problem, numerous geochemical parameters have been proposed. These indices are based on comparison of the contents of heavy metals in studied samples and a reference sample. It is very important to choose the most suitable reference sample for the studied area, which can be determined using geochemical or statistical methods.^{1,4}

The geo-accumulation index (I_{geo})⁵ is expressed as follows:

$$I_{geo} = \log_2 \left(\frac{c_n}{1.5B_n} \right) \quad (1)$$

where c_n represents measured concentration of a heavy metal in the sediment or soil sample and B_n is the concentration of an element in the reference sample (background value). The factor 1.5 is incorporated in the equation to account for possible variation in the background data due to lithologic effects. The geo-accumulation index (I_{geo}) scale⁵ consists of seven grades ranging from unpolluted to very strongly polluted:

$I_{geo} < 0$, unpolluted;

$I_{geo} = 0-1$, unpolluted to moderately polluted;

$I_{geo} = 1-2$, moderately polluted;

$I_{geo} = 2-3$, moderately to strongly polluted;

$I_{geo} = 3-4$, strongly polluted;

$I_{geo} = 4-5$, strongly to very strongly polluted;

$I_{geo} > 5$, very strongly polluted.

The pollution load index (PLI) was introduced by Tomlinson *et al.* (1980).⁶

The PLI is calculated using the following equation:

$$PLI = (CF_1 CF_2 CF_3 \dots CF_n)^{1/n} \quad (2)$$

where CF is the contamination factor and n is the number of determined metals.

The contaminant factor CF is defined as:

$$CF = \frac{c_{\text{metal}}}{c_{\text{background}}} \quad (3)$$

where c_{metal} is the concentration of a metal in the sample and $c_{\text{background}}$ represents the background value for the same metal. A $PLI > 1$ implies pollution, whereas $PLI < 1$ indicates no pollution.⁶

The enrichment factor, r is defined as the ratio:⁷

$$r = \frac{c_s - c_{\text{back}}}{c_{\text{back}}} \quad (4)$$

where c_s is the content of metal in the sample, while c_{back} is the concentration of the same metal in the reference sample. Metals with $r > 1$ could be considered as indicators of anthropogenic metal pollution, whereas $r < 1$ indicates no pollution.⁷

The total enrichment factor (R) for each sample averages the enrichment factor (r) values of the all (n) indicator-metals as follow:

$$R = \frac{\sum r}{n} \quad (5)$$

R values exceeding 1.5 indicate high pollution, R values between 1.5 and 1 imply moderate pollution, whereas samples with R values below unity are considered as unpolluted or exposed to low pollution.⁷

Hakanson (1980)⁸ suggested a contamination factor (C_f^i) and the degree of contamination (C_d) to describe the contamination by heavy metals. C_f^i is given by:

$$C_f^i = \frac{\bar{c}_n}{c_{Rn}} \quad (6)$$

where \bar{c}_n is the mean content of a heavy metal in the investigated samples and c_{Rn} is the reference value for a heavy metal.

C_d represents the sum of contamination factors for all analyzed metals and is given by:⁸

$$C_d = \sum C_f^i \quad (7)$$

$C_f^i < 1$ and $C_d < 7$ indicate a low degree of contamination; C_f^i in the range from 1 to 3 and C_d in range from 7 to 14 indicate a moderate degree of contamination; C_f^i in the range from 3 to 6 and C_d in range from 14 to 28 imply a considerable degree of contamination, whereas $C_f^i > 6$ and $C_d > 28$ reflect a very high degree of contamination.⁸

In this study, the geochemical composition of soils and underlying sediments in the Kremna Basin were investigated (Fig. S-1 of the Supplementary material to this paper). This location was chosen, due to its importance as a potential

evaporite (magnesite) deposit and boron occurrence, as well as because of its proximity to the Tara National Park. The aim was to assess whether the observed heavy metal concentrations in the soil samples represent geogenic or anthropogenic impact. The second objective was to show that geochemical data of underlying sediments should be used as a tool in the determination of potential hazard for soil contamination. For this purpose, comparison was performed of the contents of heavy metals (As, Cr, Cu, Hg, Ni, Pb and Zn) of seven soil samples with standard values, a reference soil sample and the local background values of the underlying sediments. The results of the chemical composition of sixty soil samples surrounding the Kremna Basin (Fig. S-1) were used for the calculation of the reference soil sample (Table I). The local background values of the underlying sediments were calculated based on the contents of heavy metals in forty-three sediment samples from the borehole ZLT-2 (depth from 11.5 to 343 m) of the Kremna Basin (Fig. S-1; Table S-I of the Supplementary material to this paper). For assessment of geogenic (natural) and anthropogenic pollution of the soils, numerous geochemical parameters, explained above, were used.

TABLE I. Contents of heavy metals in the reference soil sample (mg kg^{-1}), investigated soil samples and reference standard values

Sample No.	As	Cr	Cu	Hg	Ni	Pb	Zn
The reference soil sample	3.87	89.21	16.76	0.14	423.27	48.10	52.28
1	2.59	365.74	19.84	0.00	1261.02	4.41	53.79
2	2.18	221.15	35.86	0.00	351.81	4.12	39.57
3	2.42	186.64	50.51	0.00	299.66	4.28	92.47
4	2.07	143.91	44.22	0.00	240.50	3.88	59.54
5	2.15	61.083	19.10	0.00	108.10	4.20	49.75
6	2.10	225.59	27.26	0.00	461.76	4.07	51.06
7	2.37	296.07	81.44	0.00	579.69	4.37	54.15
Mean value	2.27	214.31	39.75	0.00	471.79	4.19	57.19
Standards							
RS 88/2010 ⁹	29	100	36	0.3	35	85	140
FBiH 72/09 ¹⁰	15	100	65	1.0	40	80	150
ÖNORM L 1075 ¹¹	20	100	50	1.0	40	100	150

EXPERIMENTAL

The soils were sampled at seven locations (see Supplementary material). From each location, soil samples were taken with a small shovel from a surface area of $40 \text{ cm} \times 40 \text{ cm} \times 10 \text{ cm}$. Each sample originally weighed 2.5 kg. In the laboratory, after removing vegetation and root remains, the samples were air dried at room temperature. Soil samples were then mixed thoroughly and the quartering procedure was used to obtain a representative sample for analyses. The obtained representative samples were gently ground in an agate mortar and finally sieved through a 63- μm sieve.

Sediment samples were dried at 105 °C. In the next step, the samples were successively crushed to 2.36 mm in three stages using a jaw crusher, cone crusher and roller crusher,

respectively. Then, the samples were homogenized. The rough milled fragmented sample was subsequently finely pulverized and sifted through a 63- μm sieve.

About 0.1 g of soil or sediment sample was precisely weighed on an analytical balance. A mixture of 4 cm³ nitric acid (HNO₃, 65 %), 15 cm³ hydrochloric acid (HCl, 37 %), 3 cm³ orthophosphoric acid (H₃PO₄, 85 %) and 1 cm³ hydrofluoric acid (HF, 50 %) was used for digestion of the samples. Digestion was performed in an Advanced Microwave Digestion System (ETHOS 1, Milestone, Italy) using an HPR-1000/10S high pressure segmented rotor. The temperature was controlled with a predetermined power program. The temperature was typically increased to 220 °C in the first 15 min. The temperature of 220 °C was maintained for an additional 20 min. and then cooled down rapidly. The contents of major elements and heavy metals were determined by inductively coupled plasma atomic emission spectrometry (ICP-AES) using a Thermo Scientific iCAP 6500 Duo ICP (Thermo Fisher Scientific, Cambridge, UK) spectrometer equipped with an RACID86 Charge Injector Device (CID) detector, a pneumatic cross-flow type nebulizer, a quartz torch, and an alumina injector, which enabled samples containing HF in a small amount to be detected. The optical system was purged with argon and the Echelle polychromator was thermostated at 38 °C. Two multi-elemental plasma standard solutions (Multi-Element Plasma Standard Solution 4, Specpure®, 1000 $\mu\text{g ml}^{-1}$ and a Semi-Quantitative Standard 1, Specpure®, 10 $\mu\text{g ml}^{-1}$) and two single plasma standard solutions (Silicon, Specpure®, 1000 $\mu\text{g ml}^{-1}$ and Titanium, Specpure®, 1000 $\mu\text{g ml}^{-1}$) certified by Alfa Aesar GmbH & Co KG, Germany, were used to prepare the calibration solutions for the ICP-AES measurements. Two types of blanks were required for the analysis of the prepared samples. The calibration blank was used for establishing the analytical curve and the method blank was used to identify possible contamination resulting from either the reagents (acids) or the equipment used during sample processing. For each run, the samples were prepared in duplicate, and the ICP-AES measurement for each digested sample was performed in triplicate.

RESULTS AND DISCUSSION

Heavy metal content in the reference soil sample

The contents of trace elements in the reference soil sample are given in Table I. The concentrations of all elements in the reference soil sample, with the exception of Ni, were notably lower in comparison to the Serbian Regulation about the program of systematic monitoring of soil quality, indicators for risk assessment of soil degradation and methodology for development of remediation programs, RS 88/2010,⁹ The Bosnian and Herzegovinian Regulation for the determination of permitted quantities of harmful and hazardous substances in the soil and methods of their investigation, FBiH 72/09¹⁰ and the Austrian Standard, ÖNORM L 1075¹¹ values (Table I). The obtained concentration of Ni was higher than all the values given in the considered standard. However, the local background value of 165.69 mg kg⁻¹ for Ni (Table S-I), discussed below, is also higher than the standard values^{10,12–15} (Table S-I), indicating that a high amount of Ni in the reference soil sample is of geogenic origin. Therefore, the reference soil sample could be considered as native and unpolluted and be used for an estimation of the difference between geogenic and anthropogenic impacts in the

investigated soil samples. The elevated content of Ni in the reference unpolluted soil sample (Table I) shows the importance of the mineral and geochemical composition of the underlying sediments, which should be determined prior to any land use change, particularly in areas exposed to intense weathering. Elevated Cr and Ni contents may result from ophiolites (ocean floor on land, which is usually rich in some heavy metals, such as Cr and Ni) occurring in the neighborhood (Dinaric ophiolite belt).¹⁶ The same result was obtained in a recent investigation of sediments from the eastern Posavina region.¹⁷

Heavy metal content in background sediments

The background levels of heavy metals in the underlying sediments were relatively uniformly distributed within borehole ZLT-2, with exception of Cr and Ni, which were generally higher in the lower sedimentary sequence (below 200 m; Table S-I). The contents of almost all heavy metals were lower compared to the limit standard values,^{10,12–15} with exception of Cr and Ni which were higher than the standard values (Table S-I). Elevated contents of Cr and Ni in the sediments are of geogenic origin and originated from the ultrabasic source rocks and serpentinites. According to the relatively uniform distribution of almost all the analyzed trace elements and their relatively low content (Table S-I), it could be concluded that the sediments are unpolluted, derived predominantly from natural sediment sources. Therefore, they could be used as local background levels for soil in this area to estimate the difference between geogenic and anthropogenic impacts, and to assess the enrichment of soil in heavy metals, which originate from the underlying sediments. Despite the relatively low contents of almost all the heavy metals (Table S-I), bearing in mind that the base and the edge of the Kremna Basin consist of ultrabasic rocks, serpentinite and ophiolitic mélange, which are all prone to weathering, the high concentrations of Cr and Ni, and the presence of As, Cu, Hg and Pb in the borehole ZLT-2 could be highly negative to the soil and water quality. This was confirmed by the very high values of the Chemical Proxy of Alteration, *CPA*¹⁸ and the Chemical Index of Weathering, *CIW*^{19,20} (> 80 and > 70 %, respectively), which remain continuously high even up to the depths of 150 m (Table S-I).

Distribution of heavy metals in the soil samples from the Kremna Basin

Relatively thin soil (\approx 40 cm) developed over Miocene sediments in the Kremna Basin. Seven samples at different locations (Fig. S-1) were taken from the surface soil horizon.

The contents of heavy metals in the soils are listed in Table I. Comparison of these results with the limit standard values^{9–11} indicates that all samples have higher contents of Cr (sample 5 being the exception) and Ni (Table I). Moreover, three samples (3, 4 and 7; Table I) show a higher content of Cu than the limit

standard value indicated in the Serbian Regulation about the program of systematic monitoring of soil quality, indicators for risk assessment of soil degradation and methodology for the development of remediation programs, RS 88/2010⁹ (Table I). The contents of the other trace elements were below the standard values^{9–11} (Table I). The obtained results are in a concordance with the observation of Alexander (2013),²¹ that strong weathering of ultramafic rocks and leaching of elements from serpentinites result in high to very high concentrations of Cr, Cu, and Ni in overlying soils, compared to the average data for world soils. The elevated contents of Cr, Cu and Ni (Table I) confirmed the notable influence of the geochemical composition of the underlying sediments on the heavy metal levels in soil.

Determination of geogenic and anthropogenic impact in soils

For more precise estimations of the geogenic and potential anthropogenic impacts on the investigated soil samples, several indices, geo-accumulation index (I_{geo}),⁵ pollution load index (PLI),⁶ enrichment factor (r),⁷ total enrichment factor (R),⁷ contamination factor (C_f^i)⁸ and degree of contamination (C_d)⁸ were used. The values of mentioned indices were calculated related to both, the reference soil sample (Table I) and background sediment levels (borehole ZLT-2; Table S-I). The results are presented in Tables II–V.

TABLE II. Values of geo-accumulation index (I_{geo}) for the investigated soils, related to the reference soil sample and local background sediment level; N.D.: not determined due to concentration of Hg being below detection limit

Soil sample No.	As	Cr	Cu	Hg	Ni	Pb	Zn
I_{geo} , related to the reference soil sample							
1	-1.17	1.45	-0.34	N.D.	0.99	-4.03	-0.54
2	-1.41	0.72	0.51	N.D.	-0.86	-4.13	-0.99
3	-1.26	0.48	1.01	N.D.	-1.08	-4.08	0.24
4	-1.49	0.10	0.81	N.D.	-1.40	-4.22	-0.40
5	-1.43	-1.13	-0.40	N.D.	-2.55	-4.10	-0.66
6	-1.47	0.75	0.12	N.D.	-0.46	-4.15	-0.62
7	-1.29	1.15	1.70	N.D.	-0.13	-4.05	-0.53
Mean value	-1.36	0.50	0.49	N.D.	-0.78	-4.11	-0.50
I_{geo} , related to local background sediment level							
1	-1.74	1.11	0.87	N.D.	2.34	0.21	1.53
2	-1.99	0.38	1.73	N.D.	0.50	0.11	1.09
3	-1.84	0.14	2.22	N.D.	0.27	0.17	2.32
4	-2.07	-0.24	2.03	N.D.	-0.05	0.03	1.68
5	-2.01	-1.47	0.82	N.D.	-1.20	0.14	1.42
6	-2.05	0.41	1.33	N.D.	0.89	0.09	1.46
7	-1.87	0.80	2.91	N.D.	1.22	0.20	1.54
Mean value	-1.94	0.16	1.70	N.D.	0.57	0.14	1.58

The I_{geo} values of the investigated sediments, related to both the reference soil sample and background levels from borehole ZLT-2, are given in Table II. Comparison of the I_{geo} values calculated using the reference soil sample with the geo-accumulation index (I_{geo}) scale⁵ (Table II) showed that the investigated samples were unpolluted regarding As, Hg, Ni, Pb and Zn. Slight enrichment in almost all soil samples, in relation to the reference soil sample, was observed for Cr and Cu (I_{geo} in range 0.1–1.45 and 0.12–1.70, respectively; Table II). The I_{geo} values related to background sediment levels indicated that the investigated soil samples were unpolluted regarding As and Hg. For samples 4 and 5, no pollution with Cr and Ni was detected. Generally, the low mean values of I_{geo} for Cr and Ni (0.16 and 0.57; Table II) imply a geogenic origin of these elements. Slight enrichment was observed for Pb, whereas moderate pollution is noticed for Cu and Zn in all samples, as well as for Cr and Ni in several samples (Table II). These results show the importance of recognition of the biochemical and mineral composition of the underlying sediments for further land usage and prevention of risk for serious soil and water contamination.

TABLE III. Values of pollution load index (*PLI*) for the investigated soils, related to the reference soil sample and local background sediment level

Sample	As	Cr	Cu	Hg	Ni	Pb	Zn
<i>PLI</i> , related to the reference soil sample							
Soil samples	0.58	2.13	2.10	0.00	0.87	0.09	1.06
Mean value				0.98			
<i>PLI</i> , related to local background sediment level							
Soil samples	0.39	1.68	4.89	0.00	2.23	1.65	4.48
Mean value					2.18		

The values of the pollution load index (*PLI*) higher than 1 (Table III) confirmed that the investigated soil samples were enriched in Cr and Cu in comparison to the reference soil sample, whereas no contamination with As, Hg, Ni, Pb and Zn was observed.⁶ On the other hand, the values of *PLI* calculated in relation to the background sediment values showed moderate contamination with Cr and Pb and significant enrichment in Cu, Ni and Zn, whereas pollution with As and Hg was not detected (Table III).⁶

Values of the enrichment factor (r),⁷ calculated using the reference soil sample showed the same result as the I_{geo} and *PLI* values (Table IV). The soil samples were unpolluted regarding As, Hg, Ni, Pb and Zn, whereas slight enrichment was observed of the contents of Cr and Cu in almost all samples (Table IV). In comparison to background sediment levels, significant increases were noticed for Cu and Zn in all samples and for Cr and Ni in a few samples (Table IV). Values of r below 1 indicated no pollution with As, Cr (samples 2–6), Hg and Pb.⁷

TABLE IV. Values of enrichment factor (r) and total enrichment factor (R) for the investigated soils, related to the reference soil sample and local background sediment level

Soil sample No.	As	Cr	Cu	Hg	Ni	Pb	Zn
<i>r</i> , related to the reference soil sample							
1	-0.33	3.10^a	0.18	-1.00	1.98	-0.91	0.03
2	-0.44	1.48	1.14	-1.00	-0.17	-0.91	-0.24
3	-0.38	1.09	2.01	-1.00	-0.29	-0.91	0.77
4	-0.47	0.61	1.64	-1.00	-0.43	-0.92	0.14
5	-0.44	-0.32	0.14	-1.00	-0.74	-0.91	-0.05
6	-0.46	1.53	0.63	-1.00	0.09	-0.92	-0.02
7	-0.39	2.32	3.86	-1.00	0.37	-0.91	0.04
Mean value	-0.41	1.40	1.37	-1.00	0.11	-0.91	0.09
<i>r</i> , related to local background sediment level							
1	-0.55	2.23	1.75	-1.00	6.61	0.74	3.35
2	-0.62	0.95	3.97	-1.00	1.12	0.62	2.20
3	-0.58	0.65	6.00	-1.00	0.81	0.69	6.47
4	-0.64	0.27	5.13	-1.00	0.45	0.53	3.81
5	-0.63	-0.46	1.65	-1.00	-0.35	0.65	3.02
6	-0.64	0.99	2.78	-1.00	1.79	0.60	3.13
7	-0.59	1.62	10.29	-1.00	2.50	0.72	3.38
Mean value	-0.61	0.89	4.51	-1.00	1.85	0.65	3.62
<i>R</i> , related to the reference soil sample							
1					0.68		
2					0.14		
3					0.38		
4					0.10		
5					-0.39		
6					0.14		
7					0.88		
Mean value					0.28		
<i>R</i> , related to local background sediment level							
1					2.35		
2					1.37		
3					2.34		
4					1.59		
5					0.65		
6					1.44		
7					2.98		
Mean value					1.82		

Furthermore, the r values were used for the calculation of the total enrichment factor (R).⁷ The values of R related to the reference soil sample were notably lower than unity, indicating no anthropogenic impact.⁷ However, the R values related to the background sediment level indicated moderate to high enrichment, with the exception of sample 5 (Table IV). This result is primarily caused by sig-

nificantly elevated contents of Cu and Zn in the soil samples in comparison to the underlying sediments.

The values of contamination factor (C_f^i)⁸ in the investigated soil related to the reference soil sample indicated a moderate degree of contamination in Cr and Cu and a slight enhancement in Ni and Zn, whereas no pollution with As, Hg and Pb was observed (Table V). The contamination degree (C_d)⁸ that summarizes all contamination factors for all investigated soil samples reached 7.65, implying a low to moderate enrichment in heavy metals in relation to the reference soil sample (Table V).

TABLE V. Values of contamination factors (C_f^i) and contamination degree (C_d) for the investigated soils, related to the reference soil sample and local background sediment level

Sample	As	Cr	Cu	Hg	Ni	Pb	Zn
C_f^i , related to the reference soil sample							
Soil samples	0.59	2.40	2.37	0.00	1.11	0.09	1.09
Mean value							
					1.09		
C_f^i , related to local background sediment level							
Soil samples	0.39	1.89	5.51	0.00	2.85	1.65	4.62
Mean value							
					2.41		
C_d , related to the reference soil sample							
Soil samples					7.65		
C_d , related to local background sediment level							
Soil samples					16.91		

The contamination factors (C_f^i) related to the background sediment values showed moderate pollution with Cr, Ni and Pb, considerable degrees of pollution by Cu and Zn and no pollution with As and Hg. This resulted in a relatively high value of C_d of 16.91, which indicates a considerable degree of contamination (Table V).⁸

Combining the results of all the mentioned parameters (Tables II–V), which showed very good agreement, it could be concluded that the investigated soil samples were unpolluted in terms of As, Hg, Ni, Pb and Zn, whereas slight enrichments in Cr and Cu were observed in comparison to the reference soil sample. Considering the geological origin and geochemical composition of underlying sediments, which had been exposed to intense weathering, this result is rather related to geogenic than to anthropogenic impacts.

Numerous geochemical parameters calculated in relation to the background values of the underlying sediments also showed very consistent results (Tables II–V). No pollution of the soil samples with As, Hg and Pb were observed. A slight enrichment of the soils in comparison to the underlying sediments was registered for the Cr content. Significant increases in the concentrations of Cu and Zn were detected in all soil samples and of Ni in samples 1 and 7. The ele-

vated content of Ni in these two samples could be attributed to their higher amount of organic matter. Namely, sample 1 was taken from a thin soil layer developed over an outcropping coal layer, while sample 7 was taken from a more developed soil, dark in color, indicating a higher presence of organic matter. Therefore, it could be assumed that in the Kremna Basin, Cu and Zn are the most prone to be readily incorporated into soils as result of weathering and leaching of ultramafic rocks and serpentinites. The obtained results showed the importance of the determination of the mineral and geochemical composition of underlying sediments prior to any land use change in order to prevent potential serious contamination of soil and water.

CONCLUSIONS

Soil samples from the Kremna Basin could be considered as unpolluted regarding the contents of As, Hg, Pb and Zn. All the investigated samples had higher contents of Cr and Ni, whereas three samples showed higher contents of Cu than the limit standard values given by the Serbian Regulation about the program of systematic monitoring of soil quality, indicators for risk assessment of soil degradation and methodology for the development of remediation programs. Values of numerous geochemical parameters calculated in relation to the reference soil sample from this area and background values of the underlying sediments in the Kremna Basin (borehole ZLT-2) indicated that the elevated concentration of Cr and Ni in the analyzed soils could be attributed to geogenic rather than to anthropogenic impact. This conclusion was support by the high values of Chemical Proxy of Alteration (CPA) and Chemical Index of Weathering (CIW), which indicated very intense weathering of the underlying rocks.

Values of the geo-accumulation index (I_{geo}), pollution load index (PLI), enrichment factor (r), total enrichment factor (R), contamination factor (C_f^i) and degree of contamination (C_d), which indicated slight enrichment in Cr and Cu in comparison to the reference soil sample, and significant enrichment in Cu and Zn in comparison to sediment background values, imply that the Kremna area is under slight to moderate hazard risk if a land use change would occur. Physical deterioration and runoff that could easily occur would enhance the chemical weathering of deeper samples (below a depth of 10 m). In this way, heavy metals could get into soil and water. Therefore, erosion control should be mandatory in this area. This study proved that besides topographic characteristics, climatic data, and soil properties, the mineral and geochemical composition of underlying sediments play an important role in the interpretation of the level of geogenic hazard in the investigated area and should be determined prior to any land use change.

Acknowledgements. Investigations within this study were realized in cooperation with the company Rio Tinto–Rio Sava Exploration from Serbia. The study was supported by the Min-

istry of Education, Science and Technological Development of the Republic of Serbia (Projects 176006 and 176016). Dr. Ivan Andelković, Scientific Associate of Innovation Center of the Faculty of Chemistry, University of Belgrade, is greatly acknowledged for the ICP-AES analysis. We are also grateful to the anonymous reviewers for useful comments and suggestions.

ИЗВОД

ГЕОХЕМИЈСКО ИСПИТИВАЊЕ КАО ОСНОВА ЗА УТВРЂИВАЊЕ ПОТЕНЦИЈАЛНОГ РИЗИКА ОД ЗАГАЂИВАЊА ЗЕМЉИШТА (БАСЕН КРЕМНА)

ТАМАРА ПЕРУНОВИЋ¹, КСЕНИЈА СТОЈАНОВИЋ¹, МИЛИЦА КАШАНИН-ГРУВИН², АЛЕКСАНДРА ШАЈНОВИЋ², ВЛАДИМИР СИМИЋ³, БРАНИМИР ЈОВАНЧИЋЕВИЋ¹ и ИЛИЈА БРЧЕСКИ¹

¹Универзитет у Београду, Хемијски факултет, Студентски тир 12–16, 11000 Београд, ²Универзитет у Београду, Центар за хемију, ИХТМ, Његошева 12, 11000 Београд и ³Универзитет у Београду, Рударско-геолошки факултет, Ђушина 7, 11000 Београд

Испитиван је геохемијски састав земљишта и одговарајућих подинских седимената у басену Кремна. Циљ рада је био да се утврди да ли су концентрације тешких метала у узорцима земљишта последица природног или антропогеног загађења. Други циљ рада је био да се покаже да геохемијски подаци о подинским седиментима морају бити разматрани при утврђивању ризика од загађивања земљишта. У ту сврху изведено је поређење садржаја As, Cr, Cu, Hg, Ni, Pb и Zn у земљишту са граничним стандардним вредностима, концентрацијама ових елемената у референтном нативном узорку земљишта и незагађеним подинским седиментима. Узорци земљишта нису контаминирани As, Hg, Pb и Zn. Сви испитивани узорци земљишта имају већи садржај Cr и Ni, док је у три узорка запажен повећан садржај Cu у односу на граничне стандардне вредности. Геохемијски параметри су показали да су повишене концентрације Cr, Cu и Ni у земљишту највероватније последица природног утицаја. Овом закључку у прилог иду вредности хемијског индекса промена и хемијског индекса распадања које указују на интензивно физичко и хемијско распадање седимената. Добијени резултати показују да се подручје Кремне налази под благим до умереним ризиком од било какве промене начина коришћења земљишта, и потврђују значај геохемијског састава подинских седимената при интерпретацији загађивања тешким металима.

(Примљено 17. септембра, ревидирано 31. октобра, прихваћено 6. новембра 2014)

REFERENCES

1. J. Matschullat, R. Ottenstein, C. Reimann, *Environ. Geol.* **39** (2000) 990
2. H. Pekey, *Environ. Monit. Assess.* **123** (2006) 219
3. J. Nouri, A. H. Mahvi, A. Babaei, E. Ahmadpour, *Fluoride* **39** (2006) 321
4. L. Fok, M. R. Peart, J. Chen, *Catena* **101** (2013) 212
5. G. Müller, *Umschan* **79** (1979) 778
6. D. C. Tomlinson, J. G. Wilson, C. R. Harris, D. W. Jeffery, *Helgol. Wiss. Meeresunters.* **33** (1980) 566
7. G. Adami, P. Barbieri, E. Reisenhofer, *Toxicol. Environ. Chem.* **77** (2000) 189
8. L. Hakanson, *Water Res.* **14** (1980) 975
9. http://www.sepa.gov.rs/download/Uredba_o_programu_pracenja_kvaliteta_zemljista.pdf (in Serbian, last accessed October 30, 2014)
10. <http://www.uip-zzh.com/files/zakoni/poljoprivreda/72-09.pdf> (in Serbian, last accessed October 30, 2014)

11. ÖNORM L 1075: *Standard values for inorganic elements in soils under agricultural and horticultural use*, Federal Environment Agency – Austria, 2002
12. <http://www.cis.org.rs/propisi/451?1338287527> (in Serbian, last accessed October 30, 2014)
13. ÖNORM S 2088-2: *Austrian Standards on Contaminated Land Management: Risk assessment for polluted soil concerning impacts on surface environments*, Federal Environment Agency – Austria, 2000
14. https://www.elaw.org/system/files/sediment_summary_table.pdf (last accessed October 30, 2014)
15. *Criteria for the Assessment of Sediment Quality in Quebec and Application Frameworks: Prevention, Dredging and Remediation*, Environment Canada and Ministère du Développement durable, de l'Environnement et des Parcs du Québec, 2007, p. 7, 8
16. K. Ustaszewski, S. M. Schmid, B. Lugović, R. Schuster, U. Schaltegger, D. Bernoulli, L. Hottinger, A. Kounov, B. Fügenschuh, S. Schefer, *Lithos* **108** (2009) 106
17. N. Grba, F. Neubauer, A. Šajnović, K. Stojanović, B. Jovančićević, *J. Serb. Chem. Soc.* **80** (2015) 827
18. B. Buggle, B. Glaser, U. Hambach, N. Gerasimenko, S. Marković, *Quatern. Int.* **240** (2011) 12
19. H. W. Nesbitt, G. M. Young, *Nature* **299** (1982) 715
20. S. M. McLennan, *J. Geol.* **101** (1993) 295
21. E. B. Alexander, *Catena* **116** (2014) 114.



SUPPLEMENTARY MATERIAL TO

Geochemical investigation as a tool in the determination of the potential hazard for soil contamination (Kremna Basin, Serbia)

TAMARA PERUNOVIĆ¹, KSENIJA STOJANOVIĆ^{1*}#, MILICA KAŠANIN-GRUBIN², ALEKSANDRA ŠAJNOVIĆ^{2#}, VLADIMIR SIMIĆ³, BRANIMIR JOVANIĆEVIĆ^{1#} and ILIJA BRČESKI¹

¹University of Belgrade, Faculty of Chemistry, Studentski trg 12–16, 11000 Belgrade, Serbia,

²University of Belgrade, Center of Chemistry, ICTM, Njegoševa 12, 11000 Belgrade, Serbia

and ³University of Belgrade, Faculty of Mining and Geology, Djušina 7, 11000 Belgrade, Serbia

J. Serb. Chem. Soc. 80 (8) (2015) 1087–1099

AREA AND SAMPLING LOCATION

The Kremna Basin covering an area of 15 km² is a lacustrine basin of the Zlatibor complex and is located in southwest Serbia, about 200 km from Belgrade (Fig. S-1). Zlatibor Mountain is one of the largest serpentinite massifs on the Balkan Peninsula and is an ecologically exceptional area with 960 plant species, 280 insect species, 10 amphibians and reptiles, 150 bird species and 54 mammal species.¹

Kremna Basin landscape is hilly–mountainous with pastures, meadows and agriculture as the dominant vegetation type (Fig. S-1). The area is sparsely populated with mountain villages, which are dispersed and mostly isolated. The main water supplies for the villages are springs.

Due to its very interesting geological setting, this basin has been explored for magnesites and borates. During the last few decades, the Kremna Basin was studied for presence of searlesite in the magnesite deposit,² magnesite and dolomite^{3,4} and sepiolite and palygorskite clays.⁵ The total thickness of sediments is about 350 m, and their age is of Lower Miocene, between 19 and 17 Ma.^{6,7}

Obradović and Vasić (2007)⁸ distinguished two main sedimentation series, alluvial and lacustrine, and the latter was further divided into marginal and intrabasinal facies. The alluvial series consists of conglomerates and sandstones containing fragments of ultramafic rock,⁸ while the marginal lacustrine and intrabasinal lacustrine facies consists of carbonate sediments.⁹

*Corresponding author. E-mail: ksenija@chem.bg.ac.rs; xenasyu@yahoo.com

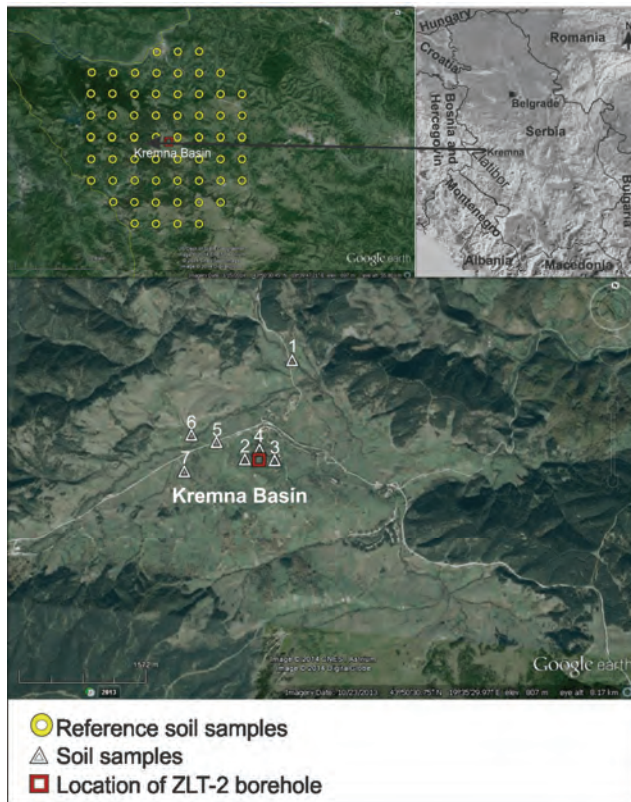


Fig. S-1. Locations in the Kremna Basin, borehole ZLT-2, reference soil samples and soil samples (1–7).

Pedogenic factors influenced the formation of humus silicate soil type on serpentinites in the Zlatibor region.¹⁰ These soils vary in color from black to brown with a dominant silt component and fairly stable aggregates.¹¹ The humus silicate soils in the investigated area are shallow with depth varying between a few cm up to 20–30 cm. Usually only the A–R profile is developed on these soils, but the A–AC–R profile can also really be observed.

There were two main criterions for soil sampling location: proximity to the borehole and outcropping sediments bellow soil. Only seven locations filled one or both of these criterions (Fig. S-1; Table I). Soil sample 1 was taken above the outcropping coal layer about 1.4 km north from the borehole site ZLT-2. At this location, the soil is very thin, up to 10 cm. Samples 2, 3 and 4 were taken in the central part of the basin, close to the location of the borehole ZLT-2. Sample 2 was taken 20 m west from the borehole, sample 3, 30 m east from the borehole, and sample 4 at the borehole site. Sample 5 was taken about 600 m, and sample 6 about 1 km northwest from the borehole site. Both soils are thin and light brown.

Sample 7 was taken about 1 km west from the borehole site and it is darker with more organic matter present.

The reference soil sample (Table I) was determined by a statistical method. The contents of trace elements in the reference soil sample were calculated based on data for sixty soil samples (at depths up to 30 cm) surrounding the Kremna Basin (Fig. S-1), reported by the Agency for Environmental Protection, the Ministry of Energy, Development and Environmental Protection of the Republic of Serbia,¹² using the following approach: for every element the mean ± 2 standard deviation were used to eliminate the top and bottom outlying data.¹³

For studying of the Kremna Basin sediments, 43 core samples (5–10 cm in length) were taken from the ZLT-2 borehole, located in the central part of the Basin (Fig. S-1), at depth from 11.5 to 343 m (Table S-I). The borehole samples were taken for two purposes. The first one was the reconstruction of the origin and geological evolution of the sediments based on the determination of the qualitative mineral composition, content of major and several trace elements, which are important for understanding sedimentation processes, as well as a detailed investigation of the sedimentary organic matter. These results are given in a previous paper.¹⁴ The second purpose of the sampling was to determine background levels of heavy metals in the Kremna Basin. For this purpose, the contents of heavy metals interpreted in this study (As, Cr, Cu, Hg, Ni, Pb and Zn) were determined, whereas the contents of the major elements used for the calculation of the weathering parameters were taken from a previous paper.¹⁴ As was already mentioned, this location was chosen due to its importance as a potential evaporite (magnesite) deposit and boron occurrence, as well as because of its proximity to the Tara National Park. In the ZLT-2 borehole, the Lower Miocene sediments are more than 340 m thick. The borehole ends in weathered serpentinite, which is characterized by the occurrence of rare fragments of serpentinite, sepiolite and small amounts of quartz and dolomite. Background levels of heavy metals in the Kremna Basin sediments were calculated using the same statistical method as for the reference soil sample.¹³

1 TABLE S-I. Contents of heavy metals (mg kg^{-1}) and several major compounds (%) in sediment samples from ZLT-2 borehole of the Kremna
 2 Basin, reference standard values and values of weathering indices

Sample No.	Depth m	Litology	As	Cr	Cu	Hg	Ni	Pb	Zn	Al_2O_3	CaO	Na_2O	P_2O_5	CPA^a %	CIW^b %
1	11.5	Clayey carbonates	18.50	103.77	8.59	0.05	159.86	1.21	9.10	0.94	8.88	0.12	0.01	82.49	70.20
2	13.5	Clayey carbonates	11.90	117.28	12.50	0.03	179.07	0.91	8.07	1.02	22.19	0.09	0.01	87.21	77.33
3	27	Marly dolomite	5.14	103.41	6.55	0.05	119.09	3.12	15.11	3.03	21.58	0.11	0.02	94.33	89.27
4	32	Marly dolomite	3.13	48.42	4.04	0.04	45.29	1.72	10.11	1.87	22.43	0.11	0.01	91.09	83.64
5	42.5	Marlstone	27.07	89.85	9.80	0.06	152.24	2.93	11.11	3.04	37.64	0.07	0.02	96.32	92.89
6	54	Silty Mg-marlstone	79.35	119.56	18.81	0.12	159.83	5.24	26.72	6.80	9.24	0.08	0.01	98.05	96.18
7	55.5	Marly dolomite	30.05	62.73	8.25	0.04	105.64	1.94	11.21	1.97	18.86	0.08	0.03	93.62	88.00
8	64.5	Marly dolomite	6.64	6.88	1.91	0.02	22.62	0.50	4.02	0.61	23.15	0.08	0.01	82.25	69.86
9	70	Marlstone	35.29	105.28	10.67	0.08	114.07	5.03	17.44	6.04	27.70	0.06	0.01	98.35	96.76
10	78	Dolomitic marlstone	34.86	27.66	3.94	0.04	55.58	2.12	8.08	2.09	32.77	0.13	0.01	90.64	82.87
11	80	Dolomitic marlstone	37.89	20.85	4.88	0.07	34.84	1.63	10.16	2.38	36.77	0.11	0.02	92.82	86.60
12	83	Marlstone	35.42	48.88	5.21	0.09	43.27	2.96	17.35	3.31	41.81	0.15	0.04	92.92	86.78
13	96	Marlstone	64.70	90.49	13.12	0.10	136.83	3.66	20.35	3.18	42.84	0.13	0.11	93.60	87.98
14	111	Marlstone	47.50	48.61	7.31	0.08	75.52	2.64	12.18	2.59	36.33	0.14	0.15	91.72	84.70

3 TABLE S-I. Continued

Sample No.	Depth m	Litology	As	Cr	Cu	Hg	Ni	Pb	Zn	Al ₂ O ₃	CaO	Na ₂ O	P ₂ O ₅	CPA ^a %	CIW ^b %
15	113	Marlstone	32.32	265.12	17.74	0.06	156.11	8.97	24.47	5.46	35.35	0.20	0.04	94.21	89.05
16	127	Marlstone	31.41	195.39	18.77	0.07	270.37	6.94	18.36	5.18	38.01	0.25	0.04	92.51	86.06
17	137.5	Marlstone	11.69	55.16	6.35	0.04	72.85	1.91	5.04	1.18	44.58	0.15	0.06	82.58	70.33
18	150	Marlstone	7.78	112.00	10.85	0.06	240.02	3.99	11.25	1.87	32.43	0.16	0.01	87.42	77.66
19	164	Marlstone	8.00	131.69	9.32	0.04	245.54	2.94	8.10	1.82	43.88	0.20	0.12	84.55	73.23
20	185	Dolomitic marlstone	4.55	76.05	7.58	0.03	75.18	1.82	10.11	1.04	29.38	0.23	0.07	73.13	57.65
21	189.5	Dolomitic marlstone	9.06	130.86	9.36	0.04	174.05	2.72	13.09	1.39	26.89	0.22	0.05	79.22	65.59
22	216	Silty Mg-marlstone	3.30	162.47	4.03	0.03	203.59	0.93	5.16	0.31	13.46	0.41	0.01	31.31	18.56
23	219	Marly magnesite	3.04	180.02	4.65	0.02	227.08	1.32	6.07	0.85	5.99	0.29	0.01	63.78	46.82
24	224	Marly dolomite	11.60	323.14	10.27	0.02	440.66	2.77	12.32	1.79	17.10	0.45	0.01	70.62	54.58
25	238	Mg-clay	10.19	87.11	1.80	0.01	261.33	10.40	23.34	4.89	2.36	1.24	0.01	70.54	54.49
26	243.5	Marly magnesite	2.44	138.93	4.97	0.04	189.85	1.12	9.14	0.94	6.29	1.19	0.01	32.58	19.46
27	245	Marly magnesite	4.11	555.53	4.21	0.02	604.73	0.92	8.22	0.73	4.79	0.69	0.01	39.18	24.36
28	248.3	Marly magnesite	1.63	208.73	4.37	0.02	276.49	1.02	6.10	0.66	6.50	2.28	0.01	14.99	8.10
29	255	Marly magnesite	1.83	340.85	3.36	0.02	263.83	0.92	6.10	0.60	4.58	0.70	0.01	34.20	20.63

4 TABLE S-I. Continued

Sample No.	Depth m	Litology	As	Cr	Cu	Hg	Ni	Pb	Zn	Al ₂ O ₃	CaO	Na ₂ O	P ₂ O ₅	CPA ^a %	CIW ^b %
30	258	Silty Mg-marlstone	14.23	1279.03	15.29	0.05	1989.27	4.46	29.74	3.40	6.15	1.71	0.01	54.71	37.66
31	265	Marly magnesite	2.86	223.94	9.51	0.02	346.12	2.35	10.23	1.30	5.84	1.40	0.01	36.04	21.98
32	283	Magnesitic marlstone	2.59	255.57	5.71	0.01	351.32	1.97	9.34	1.35	13.79	1.16	0.01	41.37	26.08
33	286	Magnesitic marlstone	5.24	416.15	7.97	0.03	680.47	2.94	13.63	2.27	11.49	1.56	0.02	46.84	30.58
34	297.5	Magnesitic marlstone	2.91	213.55	39.12	0.08	298.48	3.54	47.86	2.09	9.19	1.53	0.01	45.39	29.36
35	309	Silty Mg-marlstone	6.64	534.03	11.39	0.03	971.31	5.06	27.42	4.62	9.25	2.23	0.02	55.79	38.68
36	317.5	Magnesitic marlstone	7.76	339.77	7.76	0.04	456.86	2.79	13.45	2.19	12.59	1.45	0.01	47.93	31.52
37	324	Silty Mg-marlstone	11.68	712.72	11.89	0.03	802.29	4.63	22.10	3.65	7.70	1.98	0.02	52.87	35.94
38	329	Silty Mg-marlstone	6.92	753.14	13.84	0.04	891.39	4.93	23.06	4.05	10.76	1.83	0.02	57.28	40.13
39	335	Magnesitic marlstone	1.79	36.09	3.38	0.06	195.15	0.42	2.11	0.06	13.48	2.11	0.02	1.79	0.90
40	336	Magnesitic marlstone	1.88	35.78	1.57	0.02	58.46	0.84	3.14	0.28	14.30	2.10	0.02	7.55	3.92
41	340	Mg-clay	9.76	674.94	11.17	0.11	1144.50	0.98	20.60	1.51	2.96	1.90	0.02	32.56	19.45
42	341	Mg-clay	11.94	995.59	11.51	0.13	1705.72	1.74	23.89	2.37	2.93	2.22	0.02	39.38	24.52

5 TABLE S-I. Continued

Sample No.	Depth m	Litology	As	Cr	Cu	Hg	Ni	Pb	Zn	Al ₂ O ₃	CaO	Na ₂ O	P ₂ O ₅	CP ^a %	CIW ^b %
43	343	Mg-clay	1.73	1397.25	27.12	0.13	2420.53	4.00	44.30	4.39	0.68	2.12	0.02	55.73	55.58
Local background values ^c			5.79	113.14	7.21	0.04	165.69	2.54	12.38	1.75	19.12	0.86	0.01	—	—
RS 50/2012 ¹⁸			29	100	36	0.30	35.0	85.0	140	—	—	—	—	—	—
FBiH 72/09 ¹⁹			25	125	100	1.88	62.5	125.0	250	—	—	—	—	—	—
ÖNORM S 2088-2 ²⁰			20	100	100	1.00	60.0	100.0	300	—	—	—	—	—	—
PEL ^d			17	90	108	0.49	—	91.3	271	—	—	—	—	—	—

^aChemical Proxy of Alteration; $CPA = 100Al_2O_3/(Al_2O_3 + Na_2O)$, all oxides are expressed in mole proportions;¹⁵ ^bChemical Index of Weathering; $CIW = 100Al_2O_3/(Al_2O_3 + CaO^* + Na_2O)$, where CaO^* represents Ca in the silicate-bearing minerals only and all oxides are expressed in mole proportions.¹⁶ The procedure for quantification of CaO content of silicate fraction involves subtraction of mole proportion of P_2O_5 from the molar proportion of total CaO. On subtraction, if the “remaining number of moles” is found to be less than the molar proportion of Na_2O , then the “remaining number of moles” is considered as the molar proportion of CaO of silicate fraction. If the “remaining number of moles” is greater than the molar proportion of Na_2O , then the molar proportion of Na_2O is taken as the molar proportion of CaO of silicate fraction;¹⁷ ^cfor every element mean ± 2 standard deviation were used to eliminate the top and bottom outlying data;¹³ ^dProbable Effect Level (*PEL*) characterizes the concentrations of pollutants that may affect the aquatic life^{21,22}

13

REFERENCES

- 14 1. http://www.cajetina.org.rs/sites/default/files/LBAPCajetina_0.pdf (in Serbian, last
15 accessed October 30, 2014)
- 16 2. M. Živković, D. Stojanović, *Vatrostalni materijali* **6** (1976) 3 (In Serbian)
- 17 3. J. Obradović, J. Đurđević-Colson, N. Vasić, A. Radaković, N. Grubin, B. Potkonjak,
18 *Ann. Geol. Penins. Balk.* **56** (1994) 177
- 19 4. J. Obradović, V. Nosik, N. Vasić, N. Grubin, *Zbornik radova Rudarsko-geološkog
20 fakulteta* **57** (1995) 3 (in Serbian)
- 21 5. M. Kovačević, in *Proceedings of the 13th Congress of Yugoslav Geologists*, Herceg
22 Novi, Yugoslavia, 1998, p. 753 (in Serbian)
- 23 6. V. Prysjazhnjuk, V. Kovalenko, N. Krstić, in *Geology and Metallogeny of the Dinarides
24 and the Vardar zone*, S. Karamata, S. Janković, Eds., Academy of Sciences and Arts of
25 the Republic of Srpska, Banja Luka, 2000, p. 219 (in Serbian)
- 26 7. N. Krstić, N. Dumadžanov, J. Olujić, L. Vučanović, J. Janković-Golubović, *Acta
27 Vulcanol.* **13** (2001) 91
- 28 8. J. Obradović, N. Vasić, *Lacustrine Neogene basins in Serbia*, Srpska Akademija nauka i
29 umetnosti, Belgrade, 2007, p. 123 (in Serbian)
- 30 9. J. Obradović, N., J. Đorđević-Colson, N. Grubin, in *Geology of Zlatibor*, M. D. Dimitri-
31 jević, Ed., Geoinstitute, Belgrade, 1996, p. 97
- 32 10. N. S. Miljković, *Fundamentals of soil science*, Prirodno-matematički fakultet, Novi Sad,
33 1996, p. 198 (in Serbian)
- 34 11. D. Tanasijević, N. Pavičević, G. Antonović, Đ. Filipović, Ž. Aleksić, M. Spasojević, *The
35 soil of the Western and Northwestern Serbia*, Institut za proučavanje zemljišta, Beograd,
36 1966, p. 258 (in Serbian)
- 37 12. D. Vidojević, N. Baćanović, B. Dimić, *The report on the status of land in the Republic
38 of Serbia for 2012*, Agencija za zaštitu životne sredine, Ministarstvo energetike, razvoja
39 i zaštite životne sredine Republike Srbije, Belgrade, 2013, pp. 14, 23, 24–28 (in Serbian)
- 40 13. L. Fok, M.R. Peart, J. Chen, *Catena* **101** (2013) 212
- 41 14. T Perunović., K. Stojanović, V. Simić, M. Kašanin-Grubin, A. Šajnović, V. Erić, J.
42 Schwarzbauer, N. Vasić, B. Jovančićević, I. Brčeski, *Ann. Soc. Geol. Pol.* **84** (2014) 185
- 43 15. B. Buggle, B. Glaser, U. Hambach, N. Gerasimenko, S. Marković, *Quatern. Int.* **240**
44 (2011) 12
- 45 16. H.W. Nesbitt, G.M. Young, *Nature* **299** (1982) 715
- 46 17. S.M. McLennan, *J. Geol.* **101** (1993) 295
- 47 18. <http://www.cis.org.rs/propisi/451?1338287527> (in Serbian, last accessed October 30,
48 2014)
- 49 19. <http://www.uip-zzh.com/files/zakoni/poljoprivreda/72-09.pdf> (in Serbian, last accessed
50 October 30, 2014)
- 51 20. *ÖNORM S 2088-2: Austrian Standards on Contaminated Land Management: Risk
52 assessment for polluted soil concerning impacts on surface environments*, Federal
53 Environment Agency – Austria, 2000
- 54 21. https://www.elaw.org/system/files/sediment_summary_table.pdf (last accessed October
55 30, 2014)
- 56 22. *Criteria for the Assessment of Sediment Quality in Quebec and Application Frame-
57 works: Prevention, Dredging and Remediation*, Environment Canada and Ministère du
58 Développement durable, de l'Environnement et des Parcs du Québec, 2007, pp. 7, 8.